Bioinspired Catalytically Active Materials: ATPase Mimics and Artificial Enzymatic Cascade Reactions

Dissertation

zur Erlangung des Grades

“Doktor der Naturwissenschaften“

im Promotionsfach Chemie

am Fachbereich Chemie, Pharmazie und Geowissenschaften

der Johannes Gutenberg-Universität, Mainz

vorgelegt von

Diplom-Chemikerin

Ira Schmid

Mainz, 2018

- D77 –

Mainzer Dissertation

Dekan: [redacted]

Erstgutachter: [redacted]

Zweitgutachter: [redacted]

Tag der Einreichung: 29. Juni 2018

Tag der mündlichen Prüfung: 12. Oktober 2018

Eidesstattliche Erklärung

Die vorliegende Dissertation wurde an der Johannes Gutenberg-Universität Mainz im Institut für Pharmazie und Biochemie zur Erlangung des Grades „Doktor der Naturwissenschaften“ im Fach Chemie angefertigt.

Erstgutachter: [redacted]

Pharmazeutische und Medizinische Chemie

Institut für Pharmazie und Biochemie

Johannes Gutenberg-Universität, Mainz

Zweitgutachter: [redacted]

Institut für Organische Chemie

Johannes Gutenberg-Universität, Mainz

Hiermit versichere ich gemäß §10 Abs. 3d der Promotionsordnung vom 24.07.2007 eidesstattlich:

1. Ich habe die jetzt als Dissertation vorgelegte Arbeit selbst angefertigt und alle benutzten Hilfsmittel (Literatur, Apparaturen, Materialien) in der Arbeit angegeben.
2. Ich habe oder hatte die jetzt als Dissertation vorgelegte Arbeit nicht als Prüfungsarbeit für eine staatliche oder andere wissenschaftliche Prüfung eingereicht.
3. Ich hatte weder die jetzt als Dissertation vorgelegte Arbeit noch Teile davon bei einer anderen Fakultät bzw. einem anderen Fachbereich als Dissertation eingereicht.

Ort, Datum Ira Schmid

Danksagung

Nach vier Jahren geht mit dem Abschluss dieser Arbeit eine interessante, abwechslungsreiche und lehrreiche Zeit zu Ende. Vieles hat in dieser Zeit zum Gelingen meiner Arbeit beigetragen, weshalb ich mich an dieser Stelle ganz herzlich bei folgenden Personen bedanken möchte:

Vielen Dank an meinen Doktorvater [redacted], bei dem ich bereits meine Diplomarbeit anfertigte und der mir im weiteren Verlauf die Möglichkeit gab, in seiner Arbeitsgruppe zu promovieren. Bei der Bearbeitung meines sehr vielseitigen Themas hatte er immer ein offenes Ohr für meine Ideen und Probleme und suchte mit mir nach Lösungen. Er hat mich und meine Projekte immer sehr gefördert und mit ihm konnte ich zahlreiche Auszeichnungen erlangen. Danke für die sehr gute Betreuung, das Vertrauen und die Unterstützung in den letzten vier Jahren!

Ein großes Dankeschön geht an meine Arbeitsgruppe mit der ich viele tolle Stunden verbringen durfte, die mir oft mit Rat und Tat zur Seite stand und mich bei manchen Rückschlägen neu motiviert hat. Danke an [redacted], mit dem ich an unserem gemeinsamen Schreibtisch chemische Probleme aller Art und auch sonstige Fragen diskutieren konnte. Danke an [redacted], die mit ihrer Fröhlichkeit und ihrem riesigen Wissen über Enzymassays zum erfolgreichen Abschluss vieler Projekte beigetragen hat. Danke auch an [redacted], die mit ihrer Hilfsbereitschaft und ihrer immer liebenswerten Art für eine schöne Zusammenarbeit gesorgt hat. Danke an [redacted], der mich mit seinem Wissen über Zellassays und seiner guten Laune sehr unterstützt hat. Vielen Dank an alle Mitarbeiter des Instituts für den freundlichen Umgang und die Unterstützung in all den Jahren.

Besten Dank an all meine Freunde, die ich zum Teil schon sehr lange kenne und die ich während der Zeit meines Studiums und der Promotion kennenlernen durfte. Mit ihnen habe ich zahlreiche, tolle Stunden verbracht, die ich nicht missen möchte.

Ein großes Dankeschön geht an [redacted], die ich bereits seit 22 Jahren kenne und mit der mich eine langjährige Brieffreundschaft verbindet. Meiner Schulfreundin [redacted] danke ich für ihre stets positive, motivierende Art und viele tolle gemeinsame Sporterlebnisse in den letzten fast 20 Jahren. Ebenso meiner ältesten Tennisfreundin [redacted] für die lange Verbundenheit.

Vielen lieben Dank an [redacted], mit der mich unheimlich viel verbindet und mit der ich schon sehr viel erlebt habe in der kurzen Zeit, in der wir uns kennen. Sie hat mit ihrem Verständnis, ihrem offenen Ohr und ihrer analytischen Art viel zum Gelingen meiner Projekte beigetragen.

Des Weiteren danke ich [redacted] für die tollen Gespräche, Diskussionen und die schönen Unternehmungen, die wir zusammen erlebt haben.

Ein großes Dankeschön an meine Freunde aus Studienzeiten: [redacted], [redacted], [redacted], [redacted], [redacted], [redacted] und [redacted] mit denen ich in den letzten fast 10 Jahren eine abwechslungsreiche und lustige Zeit in Mainz erlebt habe. Viele schöne Traditionen wie unser Weihnachtsessen oder das Kanadakochen sind mit euch entstanden. Danke für eure Unterstützung und die Korrekturen meiner Arbeit.

Thank you to my Canadian friends [redacted], [redacted], [redacted] and [redacted] who supported me over the years and helped very much correcting this thesis. I am very happy that our friendship lasted over the ocean and for so many years now.

Ich möchte mich bei meinen Freunden aus dem TSC Mainz ganz herzlich bedanken, mit denen ich in den letzten 10 Jahren viele schöne Stunden beim Tennis verbracht habe, unvergessliche Mannschaftsspiele erlebt habe und die meine ehrenamtliche Arbeit dort sehr unterstützt haben. Vielen Dank an [redacted], [redacted], [redacted], [redacted], [redacted] und [redacted]. Insbesondere möchte ich mich bei [redacted] bedanken, der mir die Möglichkeit gegeben hat, als Trainerin zu arbeiten und über die Jahre ein sehr guter Freund geworden ist. Mit euch allen habe ich wirklich eine wunderschöne Zeit verbracht.

Zum Abschluss möchte ich mich bei meiner Familie ganz herzlich bedanken. Meinen Eltern [redacted] und [redacted] bin ich sehr dankbar, da sie mir all das Erreichte ermöglicht und mich bei meinen Plänen unterstützt haben. Meine Schwester [redacted] ist immer für mich da und hat mir oft geholfen, wo sie nur konnte. Euer Glauben an mich und meine Fähigkeiten haben maßgeblich zum Erfolg dieser Arbeit beigetragen. Vielen Dank!

“Curiosity is the key to problem solving.“

Galileo Galilei

Abstract

Most biochemical reactions in nature are catalyzed by enzymes. These biocatalysts accelerate reaction rates by lowering the activation energy and can carry out different competing and incompatible reactions at the same time. The active site of the enzyme binds to the substrate, catalyzes the reaction and releases the reactions products. The small biocatalysts are distinguished by extraordinary properties and characteristics such as high selectivity, accuracy, and exceptional high catalytic activities. These features make enzymes interesting for various applications in pharma and food industry, agriculture or waste management. However, production of natural enzymes on a large scale remains challenging. Therefore, research aims for artificial methods to mimic the properties and catalytic activities of enzymes.

This thesis focusses on new approaches for the imitation of natural, single enzymes and their cooperation in enzymatic clusters. Natural, soluble enzymes frequently have a hydrophobic core and a hydrophilic shell ensuring their solubility and functionality in complex environments. Inspired by nature, the general principle of core-shell structures is used within this work. A new biopolymer conjugate with attached catalytic moieties is developed to mimic enzymatic functionality. Similar to nature's polypeptide chains, the natural polysaccharide dextran is used as carrier material that allows bioorthogonal attachment of hydrophilic polymers as shielding corona as well as artificial cleavage sites. Such artificial moieties are e.g. supramolecular catalysts which can mimic enzyme-like active sites. Macrocyclic polyamines are known to be highly selective in cleaving adenosine triphosphate (ATP) to its diphosphate (ADP). Cyclic polyamines with functional groups are designed to allow an attachment to the dextran-based backbone. The ATPase-like enzymatic system demonstrates catalytic activity in *in vitro* assays and high biocompatibility. The potential application and performance of the artificial ATPase in complex cellular environment still needs to be evaluated.

In addition, the cooperation of enzymes in molecular machines is mimicked. Molecular machines are multifunctional enzymatic clusters in which enzymes work together to perform complex and demanding transformations. In this thesis, a new access to such multifunctional enzymatic cascade reactions is presented using artificial methods. A catalytically active hexapeptide is conjugated to the surface of cytochrome *c* (Cyt *c*). The combination of the esterase-like activity of the histidine-containing peptide with the peroxidase activity of Cyt *c* results in a biomaterial that performs catalytic cascade reactions within one entity. Additionally, it is possible to transfer the designed approach to other proteins. Further experiments will focus on modifications with several functional entities to implement more complex cascade reactions.

Both developed systems represent promising approaches for the mimicking of enzymes and enzymatic clusters by artificial methods. Further studies will focus on their application possibilities *in vitro* and enhanced multifunctionality.

Zusammenfassung

In der Natur katalysieren Enzyme die meisten biochemischen Reaktionen. Diese Biokatalysatoren beschleunigen Reaktionen, indem sie deren Aktivierungsenergie herabsetzen. Enzyme führen viele konkurrierende Reaktionen durch. In ihrem aktiven Zentrum wird das Substrat gebunden, die Reaktion katalysiert und die Reaktionsprodukte werden freigesetzt. Enzyme zeichnen sich durch außergewöhnliche Eigenschaften wie eine hohe Selektivität, Präzision und hohe katalytische Aktivität aus. Jene Merkmale machen sie für Anwendungen in der Pharma- und Lebensmittelindustrie sowie in der Land- und Abfallwirtschaft besonders interessant. Da die Herstellung von natürlichen Enzymen in großen Mengen allerdings schwierig ist, stellt die Entwicklung künstlicher Methoden zur Nachahmung von enzymatischen Eigenschaften ein sehr interessantes Forschungsfeld dar.

In dieser Arbeit werden neue Herangehensweisen für die Imitation von einzelnen Enzymen und ihrem Zusammenspiel in enzymatischen Clustern beschrieben. Lösliche Enzyme besitzen in der Natur häufig einen eher hydrophoben Kern und eine hydrophile Hülle, die ihre Löslichkeit und Funktionalität gewährleisten. Dieses generelle Prinzip wird in dieser Arbeit verwendet, um ein neuartiges Biopolymerkonjugat mit katalytisch aktiven Komponenten zu entwickeln. Als Trägermaterial wird das natürliche Polysaccharid Dextran verwendet, das durch Modifizierung die gleichzeitige Anbringung einer abschirmenden Korona und von künstlichen, aktiven Zentren ermöglicht. Solche Zentren sind z.B. supramolekulare Strukturen wie macrocyclische Polyamine. Diese Verbindungen, können Adenosintriphosphate (ATP) in Adenosindiphosphate (ADP) spalten. Eine synthetische Modifizierung der Polyamine ermöglicht ihre Anbindung an das Dextran Rückgrat. Das ATPase ähnliche enzymatische System zeigt katalytische Aktivität und eine hohe Biokompatibilität in *in vitro* Experimenten. Zukünftig können weitere Untersuchungen zur Anwendung der künstlichen ATPase in zellulärer Umgebung durchgeführt werden.

Zusätzlich wird die Interaktion von Enzymen in molekularen Maschinen nachgeahmt. Molekulare Maschinen sind Zusammenschlüsse mehrerer Enzyme zu hochkomplexen funktionellen Einheiten. In dieser Arbeit wird eine neue Idee zum Nachbau solcher multifunktionalen Netzwerke, die Kaskadenreaktionen durchführen können, präsentiert. Ein Hexapeptid, das katalytisch aktive Histidine enthält, wird auf die Oberfläche von Cytochrom *c* (Cyt *c*) aufgebracht. Die Kombination der Esterase ähnlichen Aktivität des Peptids mit der Peroxidase Aktivität von Cyt *c* führt zu einem Biomaterial das katalytische Kaskadenreaktionen durchführen kann. Außerdem ist es möglich, das entwickelte System auf andere Proteine zu übertragen. Weitere Experimente sollen die Einführung mehrerer Funktionalitäten ermöglichen und komplexere Kaskadenreaktionen erlauben.

Beide hier entwickelten Systeme stellen vielversprechende Ideen für die Nachahmung von Enzymen und Enzymclustern dar. Zukünftig sollen deren Anwendungsmöglichkeiten *in vitro* und eine verbesserte Multifunktionalität untersucht werden.

Contents

1 Introduction and Basic Concepts

1.1 Enzymes – Multifunctional Catalysts

Structure and Organization

Enzymes are nature's multifunctional biological catalysts. Almost all known enzymes are, with few exceptions, proteins that are formed by the folding of linear peptide chains. These polypeptides consist of the standard 20 amino acids which differ in their side chains in size, charge, shape, hydrophobic or hydrophilic character or in their chemical reactivity.[1] The sequence of amino acids determines the primary structure of proteins and enzymes, respectively.[2] The folding of the main chain to the tertiary structure is a very complex process and devoid of symmetry, however, the distribution of the side chains of amino acids is remarkable. Soluble enzymes that are not attached to cellular components such as membranes have an interior that consists of mainly hydrophobic residues such as leucine, valine or phenylalanine whereas the surface features more hydrophilic residues such as glutamate, lysine and arginine (**Figure 1a**). This distribution is driven by thermodynamic forces to cluster the hydrophobic groups in the core of the enzyme to ensure greater stability of the structure which is mainly associated with noncovalent, hydrophobic intermolecular forces.[3-4] The described architecture protects the catalytically active sites of the enzymes and guarantees their full functionality in complex and demanding biosystems.

Catalytic Activity and Mechanisms

Enzymes are distinguished by an enormous catalytic activity located in their active sites. In comparison to the whole enzyme, the active site represents only a small part of the total volume of the enzyme's structure but provides arrangement of the catalytically active amino acid residues. The active center generates a specific, selective environment such as clefts, crevices or cavities which bind the substrate noncovalently and facilitate the catalysis (**Figure 1a**). The 20 standard amino acids are often not sufficient for carrying out complex chemical reactions at the active site of the enzyme.[5] Therefore lots of enzymes need small molecules, called cofactors, for their catalytic activity. Non-proteinogenic chemical compounds like pyridoxal phosphate, ubiquinone or ascorbic acid assist during catalysis. Cofactors are divided into two groups: metals (inorganic ions) and small organic

compounds, called coenzymes. The latter are often derivatives of vitamins that can be either bound tightly or loosely to the enzyme. If they are bound tightly or even covalently, the coenzyme is called a prosthetic group and cannot dissociate from the enzyme.[6]

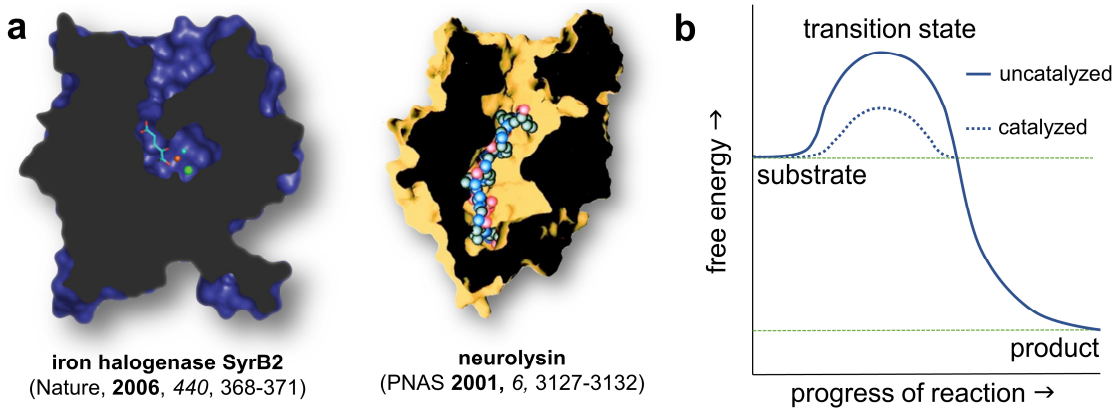

Figure 1: (a) Cross section of enzymes. Nature's multifunctional catalysts provide in their active sides a distinct, often hydrophobic local environment with clefts or cavities for interaction with their substrates. Reprinted with permission from *Blasiak et al.*[7] and *Brown et al.*[8] (b) Comparison of catalyzed and uncatalyzed chemical reaction in energy diagram: enzymes accelerate reactions by lowering the activation energy and facilitate the formation of the transition state.

Enzymes are inevitable for all biochemical transformations since without their presence most reactions cannot occur. They accelerate reactions by factors of as much as a million or more.[1] The setup of enzymes enables their high selectivity and accuracy towards chemical reactions. This property is ensured by their capacity to specifically bind lots of different molecules. Enzymes use all available kinds of intermolecular forces such as hydrogen bonding, dipole or van-der-Waals forces[9] to bring their reaction partners in an optimal orientation for the cleavage or setup of new chemical bonds. Often the catalyzed reactions occur via transition states, which are the highest energy species in reaction pathways. At the same time enzymes facilitate the formation of such transition states and reduce the activation energy of reactions (**Figure 1b**).[10] The bonding of substrate to enzyme enables a catalyzed reaction pathway whose transition state has a lower activation energy than for the comparable reaction without an enzyme.

Enzymes have fundamentally five catalytical mechanisms to form and stabilize a transition state. Mostly they use one or multiple of the following approaches: The first strategy uses bonding energy. Hereby bonding of the transition state to the enzyme is stronger than bonding to substrates or reaction products. The second mechanism is covalent catalysis. At this, amino acid residues, mostly nucleophilic ones like lysines, or enzymatic cofactors like pyridoxal phosphate form covalent bonds to the substrate and generate a transient

intermediate product. The histidine decarboxylase is an example of such a covalent catalysis by forming histamine from histidine using covalent catalysis.[11] A further strategy is general acid-base catalysis. Amino acid residues like histidines act as acids or bases while donating or accepting protons. The acetylcholinesterase (AChE) is an enzyme that uses acid-base catalysis to cleave acetylcholine and some other neurotransmitters.[12] Metal ion catalysis represents the fourth catalytical strategy. In metal complexes or as redox partners, positive metal ions (Zn^{2+}, $Fe^{2+/3+}$, $Cu^{+/2+}$) support the catalysis while stabilizing negative charges or activating water molecules. Carboxypeptidase A, an exopeptidase, uses Zn^{2+} in its active center for the hydrolysis of peptide bonds.[13] The last strategy is catalysis by approximation. By binding two or more substrates in the right orientation and conformation, their spatial position allows for a significantly increased reaction rate. The NMP-Kinases (nucleoside-monophosphate kinase) bring two nucleotides in close proximity to facilitate the transfer of one phosphate group to the other.[14]

Classification of Enzymes

Often enzymes have general names that provide no information about the type of their catalyzed reactions. The name is basically formed by attaching the suffix *-ase* to the substrate they bind and transform.

Table 1: The six main classes of enzymes according to their catalyzed type of reaction with general and specific examples.[1]

enzyme class	type of reaction	examples
oxidoreductases	oxidation-reduction, transfer of oxygen and/or hydrogen atoms or electrons	alcohol dehydrogenase, cytochrome *c* oxidase
transferases	transfer of functional groups like acetyl, methyl or phosphate groups	transaminases, hexokinase
hydrolases	hydrolysis by using water	esterases, pepsin
lyases	non-hydrolytic removal of groups of atoms to form double bonds	aldolase, fumarase
isomerases	rearrangement of groups or atoms within a molecule (intramolecular group transfer)	retinol isomerase tartrate epimerase
ligases	joining of two molecules by forming a new bond and mostly ATP cleavage	synthetases urea carboxylase

In 1964, enzymes were divided into six numbered main classes by the International Union of Biochemistry[15] according to the reaction they catalyze. **Table 1** displays the six major enzyme classes. These groups are further divided into subgroups so that a four-digit number can identify all known enzymes, e.g., the tripeptide aminopeptidase has the number EC 3.4.11.4 where 3 stands for a hydrolase, 4 peptidase, 11 aminopeptidase and 4 for the specific tripeptide aminopeptidase.

Enzyme Kinetics

Terms and calculations that are used in physical chemistry to describe chemical reaction kinetics are transferred to characterize the catalytic activity of enzymes. These methods provide not only information about the catalytic enzymatic rates but also facts about mechanisms of enzyme catalysis, regulation and binding processes.[16]

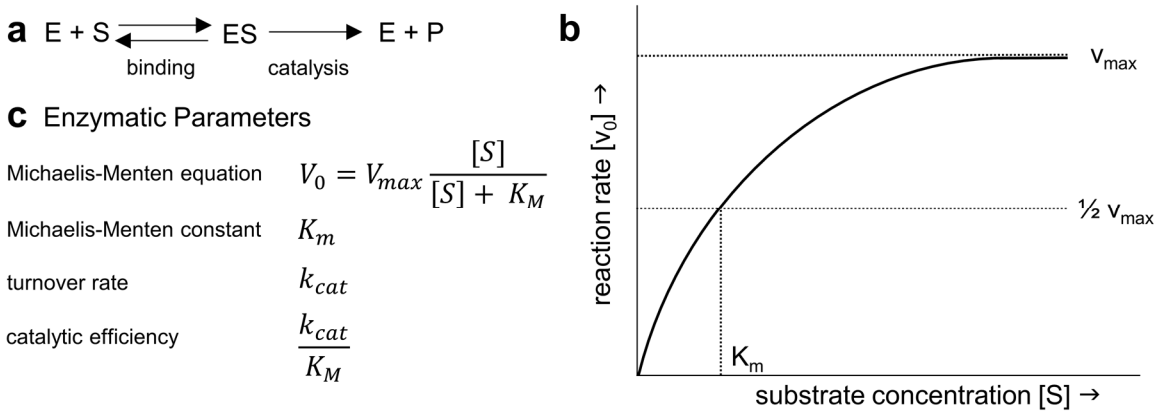

Figure 2: (a) Formation of enzyme-substrate complex and release of product and enzyme. (b) Michaelis-Menten kinetics with saturation curve of an enzyme. v_{max} is maximal velocity which is approached asymptotically. The Michaelis-Menten constant K_M is the substrate concentration at which v_{max} is reached by half. (c) Overview of important enzymatic parameters to describe enzyme kinetics.

In 1913, L. Michaelis and M. Menten[17-18] proposed a simple model to describe enzyme kinetics. They assumed that the enzyme-catalyzed reaction occurs in two stages with a first formation of an enzyme-substrate complex followed by an actual catalysis step which releases the product (**Figure 2a**). In 1924, the model was further used by G. Briggs and J. Haldane who used steady-state assumption[19] to simplify the kinetic equations. Some kinetic parameters[20] will be briefly discussed in the following paragraph but explained in detail once applied. Generally, enzymatic velocity depends on substrate concentration as shown in **Figure 2b**. The maximum speed of a reaction v_{max} can be initially achieved once substrate concentration is high enough to generate a constant rate of product formation. The Michaelis-Menten constant K_M describes the substrate concentration at which the

reaction rate is half of maximum velocity. K_M displays an inverse measurement of substrate's affinity and depends on enzyme and substrate as well as on temperature, pH or ionic strength. A small value for K_M describes a very tight binding to the substrate, a high K_M value, in contrast, a very loose binding. By means of maximal velocity $v_{max,}$ the turnover rate k_{cat} (catalytic rate, rate constant, turnover constant, turnover number) can be calculated. This number describes the number of substrate molecules which can be converted per second to the product at full substrate saturation. The ratio of k_{cat} to K_M is called catalytic efficiency (kinetic efficiency, specificity constant) and combines substrate's affinity of the enzyme with speed of product formation. This parameter allows for comparison of different enzymes because it is defined by two independent parameters.

Potential Application of Enzymes

The possible utilization of enzymes in pharma[21-22], food[23-24], detergent[25] or textile[26] industry attracted huge attention in the last years. Beginning with zymosis which is a process known for over 200 years as alcoholic fermentation and which was fully clarified by L. Pasteur in 1857[27], enzymes are nowadays being used as highly specific biocatalysts which loom large in modern biotechnology.[28] They play an important role in the biogas and bioethanol production as well as in biosensors and biofuel cells. However, modern synthetic chemistry methods advanced enormously in the past years, enzymatic biotransformations still remain the most economic and most cost-effective techniques in many cases. With high turnover numbers and enormous rate accelerations, enzymes are outstanding biocatalysts that can be recovered and reused multiple times. In particular, in the synthesis of enantiomerically pure compounds, which is still a challenge for organic chemists, enzymes have proven superior properties. One example is the synthesis of statins.[29] These compounds inhibit the enzyme HMG-CoA reductase which catalyzes an important step in cholesterol biosynthesis. Statins lower cholesterol level and therefore the probability of morbidity and mortality from coronary heart disease.[30-31] Various statins, like atorvastatin, rosuvastatin or fluvastatin have stereospecific side chains of 3,5-dihydroxy acids which are synthesized enantiomerically pure by lipases, nitrilases or aldolases. But not only isolated enzymes are in the focus of today's research, also immobilized enzymes[32] or association of multiple enzyme complexes[33-34] are in the scope of industrial applications. For example, the second most abundant polysaccharide in nature xylan, a hemicellulose, consisting of mainly D-xyloses can be broken down by

xylanases.[35] The association of multiple xylanases to the "xylanosome" plays an important role in the degradation of hemicelluloses. All linked enzymes interact synergistically with each other and their most important application is as biobleachers in the paper industry as alternatives to toxic chlorine-containing chemicals.

The central focus of today's research lies in improvements of activity, specificity, stability, and multiple functionality of enzymes for various applications. To meet these requirements the development of techniques such as mimicking enzymatic activity or altering their natural catalytic properties is necessary. For mentioned reasons the following two main chapters will focus first on the state of the art of artificial enzyme mimics and specifically on artificial ATPases. Secondly, the attention will be on cooperation of enzymes in clusters and networks, performing cascade reactions. A short overview of nature's models, as well as a literature overview on the last reported synthetic approaches, will be shown.

1.2 Artificial Enzymes

As outlined in the previous chapter, interest in natural enzymes and their outstanding properties is enormous. Viable alternatives are enzyme mimics or artificial enzymes. However, the structural complexity of those biocatalysts is still beyond synthetic ability of modern chemistry. Today only small protein-like structures consisting of around fifty amino acids can be synthesized by solid phase peptide chemistry in a reliable way and with good yields.[36] Side reactions, sequence terminations and problems with maintaining chiral information are main problems occurring during peptide synthesis. Peptides and proteins of greater length need to be prepared by using complex strategies such as chemical ligation methods.[37] Modern biotechnology offers the opportunities for the controlled expression of enzymes with novel and unnatural amino acids. Thus, selective optimization and adaptions can be induced to existing enzymes. However, the upscaling of these techniques is challenging and do not allow for established, routine synthesis. Moreover, prediction of secondary and tertiary structures as well as the resulting properties and functions remains demanding. Hence, mimicking structure and catalytic function of enzymes with help of all tools from chemistry gained huge interest in the last years.

Further advantages of artificial enzymes are not only their easier and more inexpensive preparation procedures but also possibilities to tune and control their structural properties, catalytic efficiencies and their adaption to various, chemical surroundings. The following sections will provide a state of the art of various ideas and concepts for mimicking enzymatic structures and catalytic activities based on non-peptide scaffolds. In the last years, several reviews discussed (nanomaterial-based) artificial enzymes in general.[38-40] The focus in the present thesis is set to the most important and latest results in the field. The overview will start with inorganic materials, then the spectrum will be broadened to bioinspired polymeric and dendritic compounds and end up with supramolecular structures used for enzymatic artificial catalysis. One group of supramolecular catalysts will be highlighted because of their extraordinary catalytic properties and their potential application as artificial ATPases.

1.2.1 Inorganic Materials as Enzyme Mimics

Nanosized enzyme mimics based on inorganic materials have several advantages. Low cost, excellent tolerance to extreme conditions and stability (high temperature, acidity or

organic solvents), a simple separation from reaction mixtures and additional features such as paramagnetic properties are major benefits.[38, 41] Inorganic materials are mostly used in the form of nanoparticles, called "nanozymes". The term was first used in 2004 to describe gold nanoparticles with enzyme-like activity.[42] The gold particles were passivated with a monolayer of 1-sufanyloctane and functionalized by a self-assembling of aza-crown functionalized thiols (**Figure 3a**). These triazacyclononane units were then able to bind transition-metal ions such as Cu^{2+} and Zn^{2+}. If Zn^{2+} is complexed within the aza-crown units particles showed transphosphorylation activity towards 2-hydroxypropyl *p*-nitrophenyl phosphate (HPNP), a model of RNA, releasing the spectrophotometrically measurable *p*-nitrophenol (reaction shown in **Figure 3b**). At that time, Zn^{2+}-based gold particle catalyst represented one of the best catalysts of HPNP. About ten years later, a similar system was published using phenoxyguanidine moieties as end groups of the alkanethiols (**Figure 3b**).[43] In this case, the exact catalytic mechanism was clarified. The guanidine acts in a neutral form as a base and in its protonated form as an acid. Thus, bifunctional catalysis can be achieved within one catalytic system.

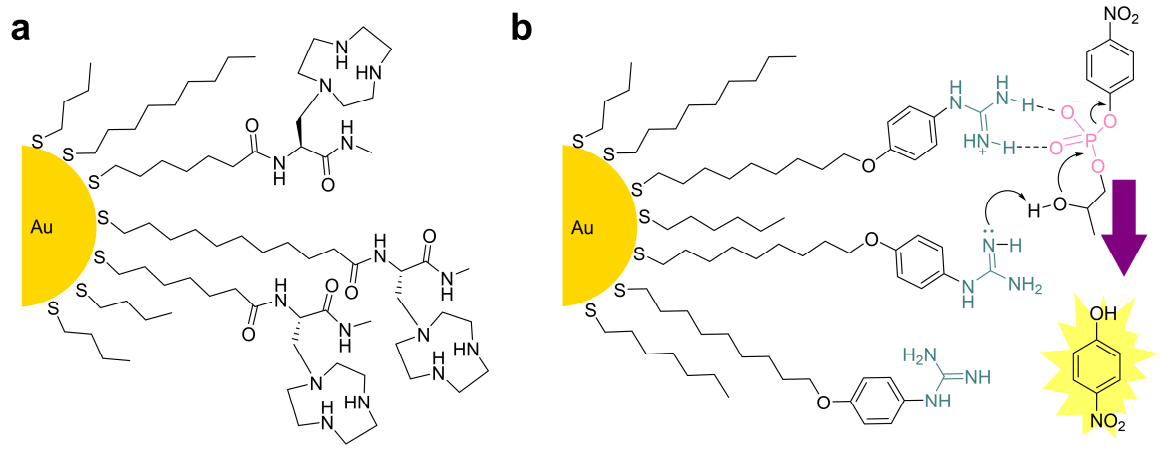

Figure 3: (a) Gold nanoparticles functionalized with selfassembled aza-crown functionalized thiols that can bind Zn^{2+}. The groups on the surface demonstrate transphosphorylation activity towards 2-hydroxypropyl *p*-nitrophenyl phosphate (HPNP), a model of RNA (structure shown in (b), top right corner). Adapted with permission from *Manea et al.*[42] (b) Further developed derivative of (a) and clarification of the exact mechanism of bifunctional catalysis with phenoxyguanidine moieties on the surface of gold nanoparticles towards HPNP. Adapted with permission from *Salvio et al.*[43]

Gold particles in general have a broad field of application,[44] because not only passivated or covered gold particles demonstrate catalytic activity. For water-dispersed gold sol, catalytic activity was observed when used as "naked" gold particles.[45] Gold nanoparticles with a diameter of 3.6 nm were able to catalyze the redox reaction of glucose and air oxygen (O_2) to gluconic acid and H_2O_2 under mild conditions - a reaction which is naturally

carried out by glucose oxidase (GOx). In contrast, nanoparticles of other metals such as Cu, Ag, Pd and Pt showed barely any GOx-like activity.

Other metals such as iron, copper or rare earths are used as artificial enzymes either in combination with gold or alone. For example, a nanocomposite consisting of gold nanoparticles which have a glucose oxidase-like activity, and V_2O_5 nanowires which exhibit intrinsic peroxidase-like activity, was used for the detection of glucose (**Figure 4**).[46] Without using natural enzymes, the system represents a complete inorganic hybrid material with enzymatic, catalytic properties. The cascade reaction which is carried out on the surface of the nanocomposite material is in detail discussed in chapter 1.3.2 (Covalent Linkage of Enzymes).

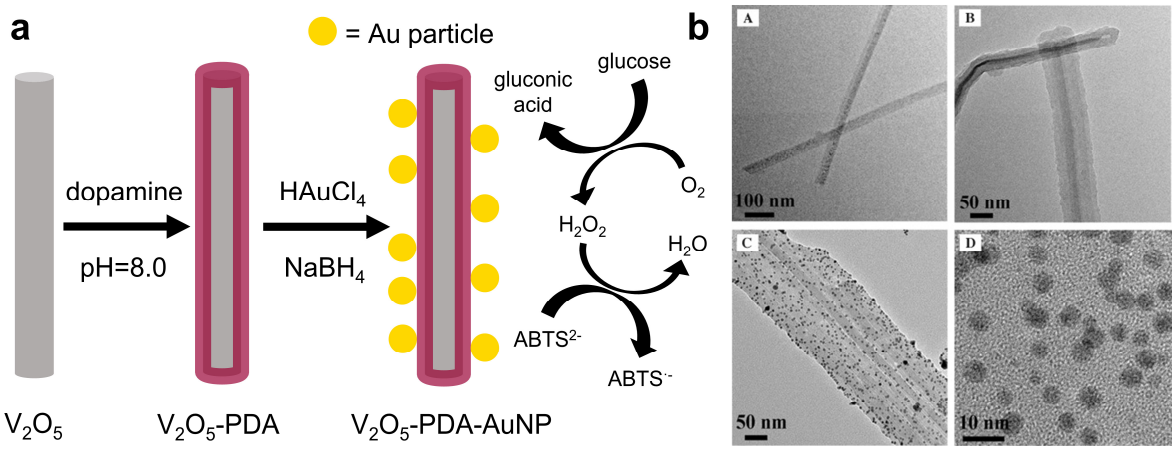

Figure 4: Nanocomposite of gold nanoparticles and vanadium oxide nanowires. (a) Preparation of nanocomposite and catalyzed reaction. Redrawn from *Qu et al.*[46] (b) TEM images of (A) V_2O_5 nanowires (B) V_2O_5-PDA, (C) V_2O_5-PDA-AuNP nanocomposite and detailed picture (D) of Au-NPs on the surface of V_2O_5-PDA. Adapted and reprinted with permission from *Qu et al.*[46]

Vanadium pentoxide nanowires were also used as artificial enzymes for mimicking natural vanadium haloperoxidases.[47] This enzyme prevents bacteria growth on the surface of certain seaweeds and is used to stop biofilm formation on ship hulls which increases hydrodynamic drag and causes increased fuel consumption. The antibacterial behavior can be explained by formation of hypobromous acid (HOBr) during catalysis. Bromide ions (Br^-) are oxidized in presence of hydrogen peroxide (H_2O_2) to hypohalous acid which stops chemical signaling in bacteria. The nanowires have an average length of 300 nm and a width of 20 nm and demonstrated their antibacterial behavior even *in situ*. The catalytic activity of the V_2O_5 wires remained unchanged after mixing with paint formulations for shipping industry.

Another interesting system based on an inorganic material are TiO_2@CeO_x core-shell nanoparticles with an outstanding peroxidase-like catalytic activity.[48] A commercial TiO_2 powder suspension was used and covered with a layer of organometallic CeO_x on the surface. The used technique allowed to tune thickness of the CeO_x layer on the shell and additionally the oxidation state of Ce in either Ce^{3+} or Ce^{4+} which has an influence on catalytic activity. This redox reaction represents a key step in several natural redox enzymes and the ratio between both states is important for the efficiency of artificial enzyme mimics based on that redox pair. Furthermore, if compared to natural enzymes like horseradish peroxidase (HRP) or other artificial enzymes, the TiO_2@CeO_x core-shell nanoparticles display an exceptional performance regarding their MichaelisMenten-constant K_m and v_{max}, the maximal reaction rate.

Laccase mimics are an example of copper-based nanozymes.[49] Laccases are multi copper-containing enzymes that are mainly found in plants, mushrooms and microorganisms. They carry out the coupled reaction of oxidizing phenolic substances and reducing oxygen. The enzyme mimic used guanosine monophosphate (GMP) to coordinate multiple Cu^{2+} ions in a metal-organic framework (MOF) similar to natural laccases. The system demonstrated excellent catalytic activity towards various phenol containing substrates such as hydroquinone, naphthol and catechol.

Iron-based materials such as Fe_3O_4 particles are an additional example. However, particles were long-time considered chemically and biologically inert, in 2007, their intrinsic peroxidase-like activity was discovered.[50] The particles catalyzed the reaction of different typical peroxidase substrates consuming H_2O_2, followed typical Michaelis-Menten kinetics and demonstrated similar behavior to horseradish peroxidase (HRP). Iron oxide materials with enzyme-like activity feature additionally ferromagnetic properties and have to date found many applications in biomedicine and diagnostics (e.g. magnetic resonance imaging, MRI).[51]

Often metal nanoparticles are coated with metal catalysts or conjugated with enzymes, in order to combine the separating power of the magnetic properties with the catalytic activity of the metal surface or the enzyme conjugate.[52] Magnetoferritin nanoparticles were covered with human heavy-chain ferritin as shown in **Figure 5**.[53] These particles that are 4.7 nm in diameter, were used to examine tumor tissue in an imaging technique without using targeting ligands or contrasting agents resulting in good differentiation of malign and benign histoid-specimens. Thereby the protein corona binds to a transferrin

receptor which is overexpressed by tumor cells in colon, human breast and liver cancer. The iron core exhibits its peroxidase-like activity by catalyzing the reaction of di-azo-aminobenzene (DAB), a typical peroxidase substrate, and H_2O_2 which releases a brown dye after the peroxidase-like reaction.

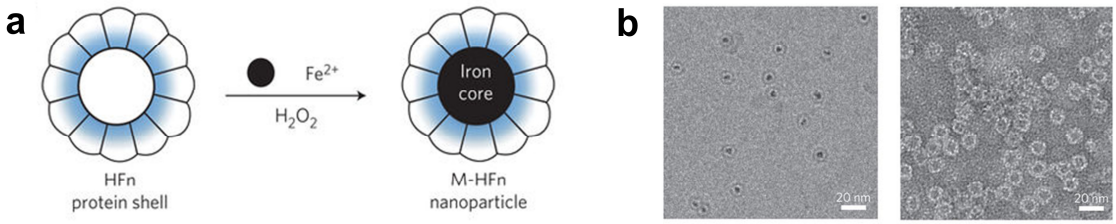

Figure 5: (a) Formation of magnetoferritin nanoparticles by encapsulating iron oxide nanoparticles inside of a recombinant human heavy-chain ferritin (HFn) protein shell. (b) Cryo TEM image of M-HFn nanoparticles (left) and TEM image of HFn protein corona (right). Both figures reprinted with permission from *Fan et al.*[53]

Despite the extraordinary findings and results shown in this section, concerns remain regarding long term accumulation and toxicity effects of inorganic materials, particularly for therapeutic applications.

1.2.2 Polymeric Materials as Enzyme Mimics

Using synthetic polymers, which might be biocompatible and biodegradable, is an alternative to the utilization of inorganic materials. Synthetic polymers have advantageous characteristics compared to inorganic materials regarding their long-term application in biological systems. One big advantage of synthetic materials over biopolymers is the fact that they can be produced on a large and industrial scale.

The preferred utilization of polymers over inorganic materials does not imply full exclusion of metals in structures and setups of artificial enzymes. There are many examples of enzymes with metal ion-mediated catalysis (1.1, subchapter “Catalytic Activity and Mechanisms”) which naturally bind inorganic atoms in their catalytic centers and which self-evidently have to be mimicked as well.

Linear Macromolecules for Biomimetic Catalysis

Considering the setup of enzymes with their folded peptide chains, linear polymers possess certain advantages in order to mimic enzymes. Linear polymer chains can be modified with repeating catalytic centers or binding sites, and high cooperativity can be achieved on macromolecular scaffolds. Examples of such macromolecular scaffolds are poly(*N*-

vinylcaprolactam-*co*-1-vinylimidazole) (PVCL-Vim) and poly(*N*-isopropylacrylamide-*co*-1-vinylimidazole) (PNIPA-Vim), copolymers which exhibited artificial hydrolase activity.[54] The polymers were thermosensitive in water by being soluble at room temperature and undergoing phase transition (aggregation) at higher temperatures >35 °C (lower critical solution temperature, LCST). The imidazoles within the polymer chains demonstrated catalytic activity in the hydrolysis of *p*-nitrophenyl acetate. It was observed that the reaction rate does not follow typical *Arrhenius*-type behavior which describes an exponential increase of the reaction rate with increasing temperature. Instead, in the interval of 35-45 °C (above the aggregation temperature) the growth was faster than exponential and above 45 °C the rate decreased again. This behavior is often observed if copolymers aggregate in aqueous solution. The temperature of aggregation precedes the temperature of rapid growth of reaction rate which is associated with adsorption of surface active substrate at the contact area of aggregates and the increase in concentration of catalytically active imidazole groups on the surface areas. The observed behavior has some similarity to natural enzymatic catalysis where substrate is first bound to the catalytic site of the enzyme forming a relatively stable complex (Michaelis-Menten enzyme-substrate complex, ES, **Figure 2a**).

A combinatorial approach based on polyallylamine polymers was reported for phosphatase-like catalysis.[55] Eight functional carboxylic acids were randomly reacted with the amines of the polyallylamine resulting in amide bonds. Each potential polymeric catalyst differed in nature and number of its functional groups. The catalysis of these functionalized polymers was investigated in the presence of either Mg^{2+}, Zn^{2+} or Fe^{3+} cations towards a phosphodiester resulting in 30,000-fold enhanced phosphatase activity compared to a natural catalytic antibody for that reaction. The group further improved that combinatorial system to carry out elimination reactions based on poly-allylamine-modified polymers.[56]

In 2009, *Breslow et al.* reported an artificial transaminase based on polyvinylimidazoles.[57] 4-Vinylimidazole and copolymers with 1-dodecyl-4-vinylimidazole were used to trans-aminate pyruvic acid to alanine, phenylpyruvic acid to phenylalanine, and indole-3-pyruvic acid to tryptophan in water at pH 7.5 and 20 °C using pyridoxamines carrying hydrophobic side chains as coenzyme mimics. The best enzyme mimic demonstrated substrate selectivity in water and accelerated the transamination of

indole-3-pyruvic acid by a factor of four million, relative to the rate for the uncatalyzed reaction.

Dendrimers as Artificial Enzymes

Inspired by the globular shape of enzymes, chemists tried to synthesize macromolecules not only as linear chains but rather as three-dimensional structures. Dendrimers are such regular branched, tree-like macromolecules. Growing from a core with repetitive units in a radial symmetry and branching, dendrimers form spherical structures (**Figure 6a**). First dendrimers were synthesized in 1978[58] in divergent synthesis methods. Hereby, the dendrimer is assembled from a multifunctional core which extends outwards in the respective generation. In the 1990s, first dendrimers were synthesized with convergent methods.[59] This technique describes their building from small molecules which end up at the surface of the sphere and the ongoing reactions proceed inward. In 1995, their first use as catalysts was published and the term "dendrizyme" was introduced in a literature review.[60] Dendrimers can be either carrying the catalytic active site as a single copy within their core or in multiple copies at the dendritic surface. In the first case, catalysis within the core is often compared to the pocket of the enzyme where the transformations take place. Dendrimers provide a favorable local microenvironment for catalysis in the core and selectivity effects of the dendritic shell. They possess overall shielding properties in complex surroundings, e.g. cell plasma. In the second case, the attachment of multiple catalysts to the end of the branches leads often to cooperativity effects.

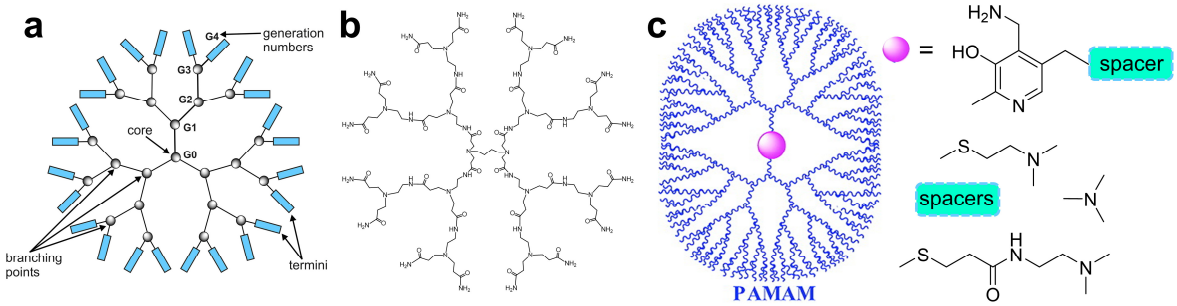

Figure 6: (a) Dendritic structure with a tree-like macromolecule starting from a core (G0) with growing branches (generations). Reprinted from *Lukin* (*creative commons).* (b) PAMAM (poly(amidoamine)) dendrimer structure (c) PAMAM dendrimer with pyridoxamine unit in the core for transamination reactions and various spacer units to optimize the transamination reaction rates. Reprinted with permission from *Liu et al.*[61]

The mimic of thiamine-diphosphate-dependent enzyme pyruvate oxidase was one of the first dendrimer-based artificial enzymes. It was created by introducing dendritic branches

on thiazoliocyclophanes.[62] The so-called dendrophane promotes an aldehyde to ester oxidation supported by a flavin cofactor. However, the reaction was two orders of magnitude slower than with the parent cyclophane.

One widely used dendrimer is the PAMAM (poly(amidoamine)) dendrimer (**Figure 6b**).[63] An artificial transaminase model was created by locating one single pyridoxamine unit in the core of water-soluble PAMAM dendrimer (**Figure 6c**).[61] The structure and size of this enzyme model was tuned to obtain great transamination rates for the synthesis of alanine and phenylalanine from pyruvic and phenolpyruvic acid. In fact, the reaction rate was1000-fold rate enhanced compared to pyridoxamine alone. PAMAM-based dendrimers were over time further refined for applications in demanding and complex systems.[64] Hemin, an iron–porphyrin complex that can mimic the catalytic properties of horseradish peroxidase (HRP), was encapsulated within the dendrimer. By adding a zwitterionic shell consisting of primary amines and carboxyl groups the enzyme-like system was able to operate in biological medium. The mimic was highly water-soluble, pH-sensitive and biocompatible while retaining its catalytic activity.

An artificial peroxidase for the oxidation of aromatic compounds in non-aqueous media was created by a dendritic porphyrin.[65] The core composed of a porphyrin group with the catalytic iron center was surrounded by a dendritic, branched network of 3,5-dihydroxy benzyl alcohol up to G4 size. The dendrimer demonstrated outstanding catalytic properties in the oxidation of 2,6-dimethoxyphenol and 3,4-dimethoxybenzyl(veratryl) alcohol with the oxidation substrate *m*-chloroperoxybenzoic acid. Compared to the natural enzyme lignin peroxidase which carries out the same reaction, the enzyme mimic displayed a higher reduction potential and full functionality in organic solvents.

An alternative to inorganic dendritic catalysts are end-group functionalized poly(propylenimine) dendrimers (PPI-dendrimers) containing multiple catalysts in form of imidazole groups on their surface.[66] An esterase-like activity with general acid/base mechanism was described for the hydrolysis of 2,4-dinitrophenyl acetate in water. A cooperative effect was investigated by increasing the number density on the surface of the dendrimer by increasing the dendrimer generation and thereby decreasing the distance between functional imidazole groups however not resulting in enhanced activity.

Imidazole groups in histidines as catalytic cores were also used by *Reymond et al.* in peptide-based dendrimers.[67-69] His group reported several examples of catalytically active

dendrimers.[70-71] Peptide dendrimers with the repeating unit of Dap-His-Ser (Dap= diamino propionic acid, His=histidine, Ser=serine)[72] which displayed a strong dendritic effect for the catalysis of 8-acyloxypyrene 1,3,6-trisulfonates performed with enzyme-like kinetics in aqueous medium.[73] The enzyme-like activity was specific for this kind of ester (substrate specificity), the substrate binding investigations demonstrated that three histidines optimally bound one substrate and multiple catalytic turnovers were possible. Based on these results, the first dendrimers with protease reactivity were reported by *Reymond et al.*[74] Proteolysis of proteins and peptides is essential to their biological function and thus an important feature to artificial enzymes as well. Trypsin and chymotrypsin reactive sequence motifs were used as cleavage sites. Control over proteolysis was gained by topology of dendrimers by placing different numbers of amino acids between the branching points. Dendrimers with two or three amino acids between the branching points were readily cleaved, in contrast to dendrimers with only one amino acid as spacer molecule which showed sometimes complete resistance to proteolysis.

The main restrictions of dendrimers are their synthetic difficulty and the limited size availability.[75] For these reasons, the scientific research on dendrimers is declining after reaching its zenith in the middle of the new millennium (around 2005). Therefore, most cited literature describing the state of the art of enzyme-like dendrimers was published during that time.

Star Polymers as Containers for Catalysis

Star polymers represent an alternative readily accessible class of branched materials.[76] In contrast to dendrimers, they contain one central core which radiates multiple linear arms, synthesized by chain growth polymerization techniques. Within these linear arms, no branching is observed. Star polymers share similar advantages with dendrimers but they feature additional benefits such as efficient preparation, straight forward synthesis, a larger number of terminal groups[77] and low intrinsic viscosities.[78] In most studies, a star polymer is synthesized by either an “arms-first” or a “core-first” method. Star polymers have been recently reviewed[79] and a few outstanding examples will be presented in here.

Inspired by nature, *Fréchet et al.* explored the use of star polymers to combine normally incompatible catalysts in one-pot sequential reactions.[80] They encapsulated both acidic, represented by *para*-toluenesulfonic acid (PTSA), and alkaline groups, represented by 4-(dialkylamino)pyridine, within well-defined core-shell structure of the star polymers.

The star polymers were synthesized in the arm first approach by radical polymerization. In the chemical cascade reaction, an acid-catalyzed acetal hydrolysis and a nucleophilic amine-catalyzed Baylis–Hillman reaction were carried out. Both reactions are normally incompatible but due to site segregation within the star polymer cores, sequential catalysis is possible.

The same group used the combination of multiple, otherwise incompatible catalysts for asymmetric cascade reactions that involve iminium, enamine, and H-bonding catalysis.[81] The strategy allowed straightforward access to all possible stereoisomers of the cascade product individually by proper choice of catalyst chirality. With this enzyme-like catalysis, it was possible to generate cascade products with multiple chiral centers.

Rodionov et al. described the synthesis of a family of polymer catalysts from modular star polymers with "clickable" cores.[82] The hydrophobic core was formed by polystyrene with azide functional groups which was surrounded by water-soluble PEG arms (**Figure 7**).

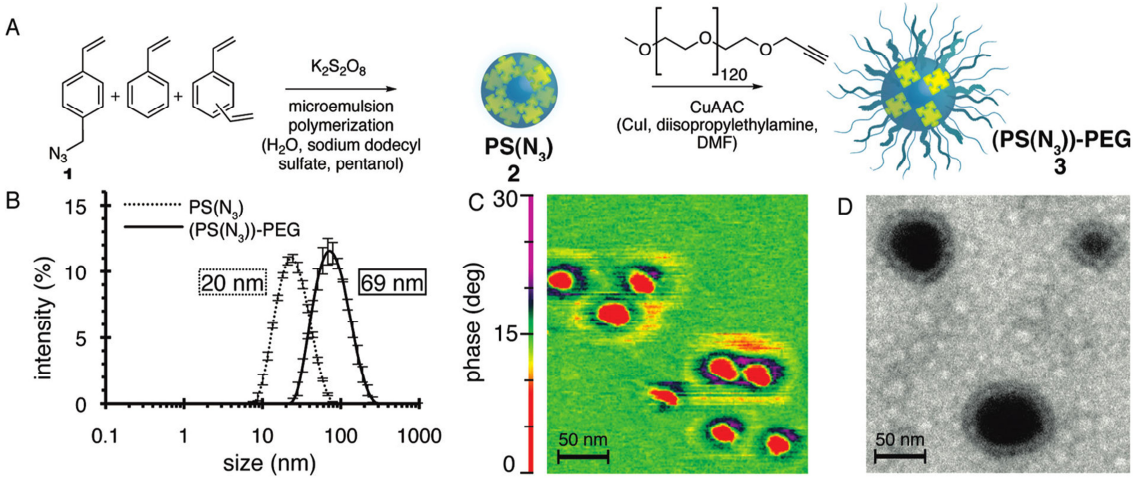

Figure 7: (A) Synthesis of (PS(N_3))-PEG star polymer with microemulsion polymerization followed by Cu-promoted click chemistry with PEG. (B) DLS data for (PS(N_3)) and (PS(N_3))-PEG in water. (C) AFM phase image of (PS(N_3))-PEG. (D) TEM image of (PS(N_3))-PEG stained with sodium phosphotungstate. Reprinted with permission from *Rodionov et al.*[82]

The azide-containing core provided a facile functionalization with various alkyne-containing payloads such as large hydrophobic groups like pyrenes (used to determine the number of reactive azide groups), organocatalysts, metal complexes or dyes like Nile Red. The catalytic activity of the material was investigated by using a model *Knoevenagel* condensation reaction between benzaldehyde and ethyl cyanoacetate in water. The reaction did not occur uncatalyzed at room temperature and was superior compared to catalysis with a linear PEG-modified catalyst. Moreover, the catalyst was recycled multiple times with no loss in activity. A similar approach as described in the previous paragraph

for acid/base site isolation was used here by combining an acid catalyst with an amine catalyst. Hydrolysis of dimethyl benzaldehyde was first carried out by the proline-modified polymer star, followed by *Knoevenagel* condensation of benzaldehyde with ethyl cyanoacetate by PTSA-modified (PS(N_3))-PEG.

Using star polymers as polymer catalysts containing ruthenium complexes are one further alternative. Stars were used for the oxidation reaction of alcohols to ketones.[83] The metal catalysts were directly encapsulated during metal-catalyzed star synthesis in living radical polymerization (ATRP). Synthesis of this star polymer started with the Ru-catalyzed ($RuCl_2(PPh_3)_3$) ATRP reaction of methyl methacrylate (MMA). When monomer conversion reached 90%, a mixture of ethylene glycol dimethylacrylate (EGDMA) and diphenyl-4-styrylphosphine (serving as the cross-linker and ligand for Ru(II), respectively) was added to yield phosphine core-functionalized star polymers. During polymerization, pure Ru metal was encapsulated into the core via ligand exchange. The resulting Ru(II)-functionalized star efficiently catalyzed the oxidation of a 1-phenylethanol to acetophenone.

Single-Chain Nanoparticles as Catalytic Devices

Single-chain nanoparticles (SCNP) are linear polymer chains which collapse or fold into architecturally defined nanostructures.[84] Their application as catalytic nanoreactors has been recently reviewed.[85-86] Four examples of catalytically active SCNPs will be presented here, showing the wide field of application of these structures as enzyme mimics.

A random copolymer consisting of *N*,*N*-dimethylaminoethyl methacrylate (DMAEMA) and 4-methyl-(7-(methacryloyl)oxy-ethyl-oxy)coumarin (CMA) was synthesized which was then cross-linked by the intrachain photodimerization of the coumarin groups (**Figure 8**).[87] The photoinduced cycloaddition reaction under λ=310 nm irradiation led to the collapse of single polymer chains and to formation of SCNPs.

The SCNPs were used as a nanoreactor to *in situ* synthesize colloidal gold nanoparticles without any additional reductants. In tetrahydrofuran (THF) the kinetics of AuNP formation were sensitive to the polymer chain conformation and mobility which are determined by the degree of photodimerization within the coumarin groups. This provides the possibility to optically tune kinetics of AuNP formation and having influence on the catalytic activity of this artificial enzyme.

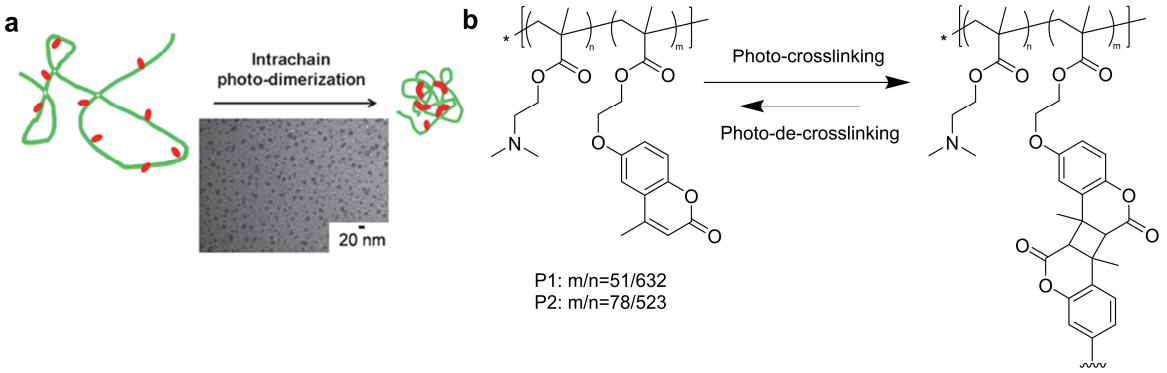

Figure 8: (a) Schematic illustration of SCNP formation by intrachain photodimerization of coumarin groups (orange dots). photo-crosslinking. Reprinted with permission from *He et al.*[87] (b) Chemical structure of *N,N*-dimethylaminoethyl methacrylate (DMAEMA) and 4-methyl-(7-(methacryloyl)oxy-ethyl-oxy)coumarin (CMA) random copolymer with different CMA rates and reversible photo-crosslinking reaction activated by UV light. Adapted from *He et al.*[87]

An aldol reaction in water with Michaelis-Menten kinetics was carried out by an L-proline functionalized, catalytic polymer based on a methacrylate random copolymer (**Figure 9**).[88] The helical terpolymer (polymer composed of three different monomers) consists of 10% benzene-1,3,5-tricarboxamide (BTA) units which introduced a structural compartment to the polymer that allowed a helical stack assembly. 85% of the polymer were oligo(ethylene glycol) units that ensured water-compatibility of the polymer. The remaining 5% were catalytic units of L-proline. This catalyst catalyzed a wide range of C-C bond forming reactions but its activity in water was very poor due to a lack of hydrophobic shielding.

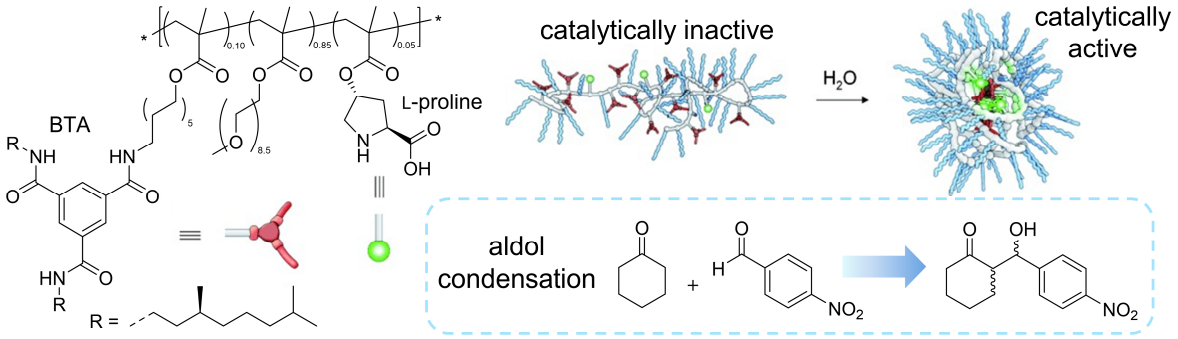

Figure 9: Methacrylate random copolymer functionalized with catalytic active L-proline (green dot) moieties. The helical terpolymer formed by the structural element benzene-1,3,5-tricarboxamide (BTA) entity (red y-shape) carried out the aldol condensation of cyclohexanone and *p*-nitrobenzaldehyde. Only in its folded conformation, the SCNP was catalytically active because of the hydrophobic pockets that were formed around the L-proline centers. Reprinted and modified with permission from *Huerta et al.*[88]

The folding of the polymer provided a new environment for catalysis formed by the hydrophobic pockets of L-proline and thus generating a catalytically active polymer with a similar behavior comparable to an enzyme.

Based on this helical terpolymeric system, catalytically active SCNPs were recently tested for their biological compatibility and application in complex cellular environments.[89] As catalytic sites, a porphyrin-based structure was attached to the polymer for the photocatalytic generation of singlet oxygen from molecular oxygen within the cell. For an application in extracellular space, organometallic loaded SCNPs with Cu^{+} and Pd^{2+} demonstrated an efficient depropargylation of protected rhodamine. The described system was able to perform and remain its functionality in living cells and thus provides a platform for artificial enzyme mimics performing *in vivo*.

Introduction of inorganic complexes to SCNPs is one possibility to mimic metalloenzymes. In 2015, a tunable synthetic [FeFe] hydrogenase mimic was reported by using click chemistry to conjugate a single diiron cluster to a methyl methacrylate (MMA)/anthracene methylmethacrylate (AMMA) copolymer.[90] SCNPs were formed after irradiation of the polymer at λ=310 nm by an intrachain [4πs+4πs] cycloaddition reaction. The iron complexes were conjugated with their introduced allyl or propargyl functional group via thiol-ene/thiol-yne click chemistry to the polymeric scaffold. This hydrogenase-mimic has potential to catalyze the production of H_2.

Other metalloenzyme-mimicking SCNPs are imidazole-functionalized copolymers of P(MMA-*co*HPMA), poly(methyl methacrylate-*co*-3-imidazolyl-2-hydroxypropyl methacrylate), that were used for a selective hydroxylation reaction of phenol.[91] Copper ions were coordinated by imidazole groups to drive the self-folding of the random copolymer. SCNPs demonstrated a selectivity for the hydroxylation reaction of phenol to catechol over >80% with high turnover frequencies.

Overall, the impact of SCNPs lies especially in the defined construction of a polymeric pocket around the catalytic active cores for substrate recognition and catalysis. Thus, they are very well mimicking the catalytic pockets of enzymes. Main drawbacks and concerns remain regarding the random polymer synthesis, in other words the variation of the individual polymer chains in composition and length. Also large scale production of SCNPs remains challenging.

1.2.3 Supramolecular Structures as Enzyme Mimics

A third, already widely investigated strategy for artificial enzymes are supramolecular-based structures. Supramolecular chemistry describes molecular interaction between host and guest. The basis of these binding events are non-covalent interactions such as hydrogen bonds, coulomb-, and π-stacking forces as well as charge-transfer interactions. The literature reveals a vast number of supramolecular catalysts either as small molecules or as nanomaterials such as micelles, host-guest polymers or supramolecular coordinated polymers for diverse applications (**Figure 10a**).[92-97] Herein, only a few outstanding examples and most important results will be shown, before in particular focusing on one specific group of supramolecular catalysts which are important for this thesis.

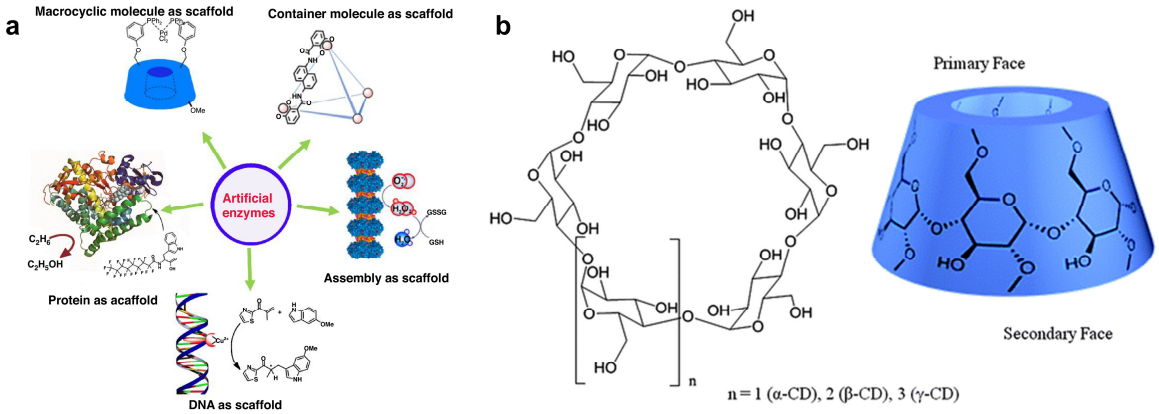

Figure 10: (a) Different approaches for the design of artificial enzymes based on supramolecular scaffolds. Reprinted with permission from *Wang et al.*[93] (b) Chemical and three-dimensional cavity structure of cyclodextrins with 6-8 monomeric saccharide units. Reprinted with permission from *Zhou et al.*[98]

Enzymes utilize supramolecular interactions to form powerful complexes with substrates and ligands. However, study of enzymes and proteins is often challenging due to their intricacy. Furthermore, the study of non-covalent interactions and their impact is crucial to the understanding and imitation of enzyme-substrate interactions. Hence, a perfect way to understand and mimic these effects are small bioorganic model systems and coordination assemblies.[94, 96] Popular supramolecular materials include already preformed macrocycles and container molecules like calixarenes, cyclodextrins, cucurbiturils and crown ethers.[97] Cavity forming entities seem in particular suitable to mimic substrate specific pockets of enzymes. They allow a substrate preorganization and accelerate chemical transformations. Cyclodextrins (CD) (**Figure 10b**) represent a class of 6-8 membered oligo-saccharide rings that form catalytic macrocycles and features a conical cavity that is essentially hydrophobic in nature. So far, they are the most popular and

successful scaffolds for the creation of enzyme mimics and models.[99] The inner diameter of the cavity varies from 0.5-1 nm, has a depth of about 0.8 nm and the oligosaccharide rings are even catalytically active without catalytic moieties.[100-101] Compared to synthetic cavity species like calixarenes or synthetic macrocycles, cyclodextrins have the advantage that they have a readily available geometry. The sugar hydroxyl groups can be used to attach other catalytic and functional groups. *Ronald Breslow* performed pioneering work in this field by publishing in 1970 the first artificial enzyme approach by combining a metal catalytic group with the hydrophobic binding cavity of a modified-cyclodextrin.[102] Over the years, he published several modifications of cyclodextrins for enzyme-like catalysis such as a model for ribonuclease[103] with β-cyclodextrinyl-bisimidazoles or the chlorination of anisole, catalyzed by α-cyclodextrin which delivers the chlorine.[104]

More recent literature describes a cyclodextrin dimer catalyst with a metallo-phenanthroline linking group that complexes Zn^{2+} ions.[105] The diesterase-like activity of the dimer was investigated towards 4-nitrophenyl acetate and bis(4-nitrophenyl) phosphate (BNPP) which is often used as a DNA model compound (**Figure 11**). The cyclodextrin dimer demonstrated a high catalytic efficiency and the hydrophobic interactions between catalyst and substrate were figured out to play an important role in catalytic hydrolysis.

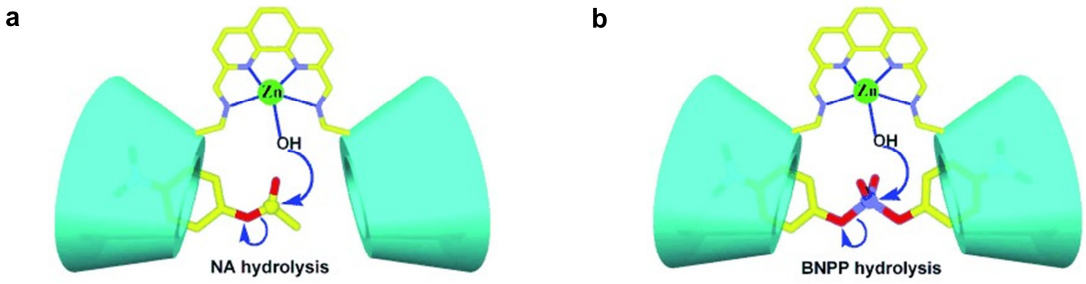

Figure 11: Cyclodextrin dimer connected with a metallophenanthroline linking group that catalyzes the hydrolysis of 4-nitrophenyl acetate and BNPP, a DNA model compound. Reprinted with permission from *Zhou et al.*[105]

The supramolecular oxidation of aromatic amines and benzylic alcohols in the presence of hydrogen peroxide was carried out by a bridged cyclodextrin derivative.[106-107] The cyclodextrin consists of a core of either α- or β-CD with dihydroxyacetone attached to the primary rim through ester bonds. At neutral pH and ambient temperature, the CDs mediate the conversion of H_2O_2, which is bound to the ketone and forms a hydroperoxide adduct, and the benzylic alcohols, which is bound in the hydrophobic cavity, with an extraordinary reaction rate (k_{cat}/k_{uncat} = 60000).

Cyclodextrins are not only used as small molecules, they are often attached to polymeric scaffolds to recreate the size and complexity of natural enzymes. For example, *Zhang et al.* synthesized a star-shaped polymer with a *β*-CD core as a molecular recognition moiety and multiple poly(*N*-isopropylacrylamide) (PNIPAAm) arms.[108] The CD core was modified with 2-bromo-isobutyric bromide to obtain a fourfold modified CD core (4-Br-*β*-CD) which was then used as the starting point for ATRP-mediated polymerization with PNIPAA. This part of the system served as the guest for supramolecular interaction with an adamantane-modified PEG. The self-assembling system with its thermoresponsive properties of the PNIPAAm arms was further used in a slightly modified variant as a mimic of both superoxide dismutase (SOD) and glutathione peroxidase (GPx) (**Figure 12**).[109]

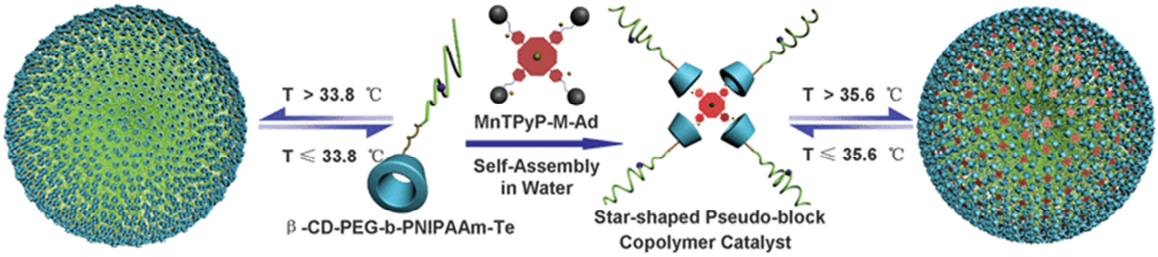

Figure 12: Preparation of enzyme model with superoxide dismutase (SOD) and glutathione peroxidase (GPx) activity. The system is based on a star-shaped polymer which networks with a porphyrin core by supramolecular interactions. The whole system is distinguished by its temperature sensitivity. Reprinted with permission from *Yu et al.*[109]

The enzyme mimic used a Mn(III) porphyrin, Mn(III)*meso*-tetra[1-(1-adamantyl methyl ketone)-4-pyridyl] porphyrin (MnTPyP-M-Ad), as the supramolecular linker in the core of the polymer star as well as efficient active site for the SOD-like enzyme. The temperature responsive block copolymer (*β*-CD-PEG-*b*-PNIPAAm-Te) with incorporated tellurium moieties in the PNIPAAm chain was utilized as GPx active sites. The system demonstrated stable SOD-like activity and high GPx catalytic efficiency with temperature sensitivity. The highest GPx activity was achieved close to body temperature.[109]

Supramolecular chemistry is of course not limited to the interactions of small and low-molecular-weight molecules. Equally, the already described systems from the previous chapters can be studied under the aspects of supramolecular interactions. Examples for such supramolecular interactions in nanometer-sized objects are reported in the literature. Capsules[110], micelles, vesicles, nanotubes[111] or the already described dendrimers[112]were used as scaffolds.[113-114] For example, an artificial nuclease, based on a DNA scaffold was reported.[115] The enzyme model system was based on a tetra cationic pyridylimine metallosupramolecular cylinder which bound strongly to DNA (**Figure 13a**).

The cylinder is a dinuclear double-helical metallosupramolecular scaffold that was assembled by copper(I) centers (**Figure 13b** and **Figure 13c**). In the presence of peroxide, the cleavage of DNA plasmid was observed. The cleavage occurred as a double-stranded cleavage at the same site which can so far not be explained in detail.

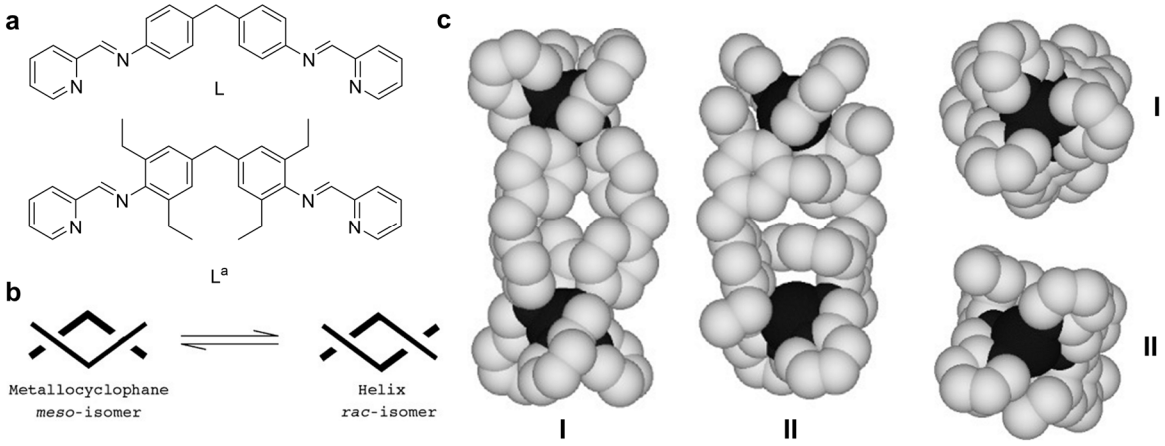

Figure 13: (a) Tetra cationic pyridylimine-based ligands for the formation of metallosupramolecular cylinders. (b) Possible conformations of cylinders in a metallocyclophane or helicate formation. (c) Models for iron(II) cylinder $[Fe_2(L_3)]^{4+}$ (I) and copper(I) cylinder $[Cu_2(L^a)_2]^{2+}$ (II). This cylinder binds strongly to DNA and acts in the presence of peroxide as a nuclease. Reprinted and adapted with permission from *Childs et al.*[115]

Another DNA-based artificial enzyme is a hybrid catalyst of salmon testes DNA and an iron (III) complex of cationic *meso*-tetrakis(*N*-alkylpyridyl)porphyrin.[116] The system was used for carbene-transfer reactions in water under mild conditions featuring especially a large DNA-induced rate acceleration. The system was utilized for the catalytic enantioselective cyclopropanation of styrene derivatives. Corresponding cyclopropanation products were obtained in high stereochemical yields.

A different recently reported approach used tetrahedral cages for the catalysis of a bimolecular aza-Prins cyclization with the unexpected feature of a 1,5-hydride transfer (**Figure 14**).[117-118] The tetrahedral cage was formed by metal coordination of Ga^{3+} in which naphthalene spacers served as ligands. The generated host molecule was highly anionic and hydrophobic, which favors the entrapment of cationic compounds. The synthetic cocatalyst enhanced the reaction rate of the bimolecular reaction of a factor of seven and represented a rare example of high divergence in product selectivity.

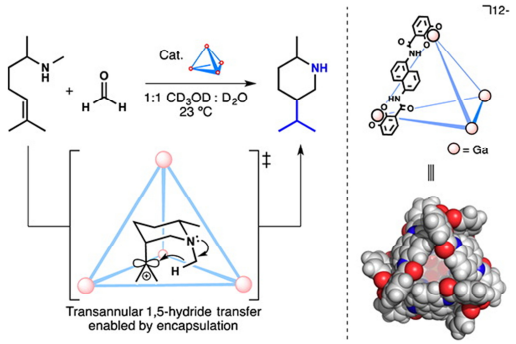

Figure 14: Tetrahedral cage of an organometallic complex formed by Ga^{3+} and naphthalene spacers. The host molecule served as an ideal environment for a biomolecular aza-Prins cyclization which featured a 1,5-hydride transfer reaction. Reprinted with permission from *Kaphan et al.*[117]

The described examples demonstrate the wide application of supramolecular catalysis in varying contexts. The focus in the following part will be now on one specific supramolecular catalyst which has a possible direct application in cells.

ATPase Mimics as Supramolecular Catalysts

Macrocyclic polyamines are one specific group of supramolecular catalysts which are able to act as artificial ATPases. ATPases are among the most abundant enzymes with an involvement in almost all cellular pathways.[119] The name ATPase is a generic term for enzymes that cleave ATP which is the "molecular unit of currency" of intracellular energy transfer[1] and does not describe one specific enzyme. The chaperone systems, all motor proteins responsible for cargo transfers, cell motilities and muscle contractions, as well as DNA helicases or enzymes in the DNA replication complex, some gene regulation enzymes or enzymes responsible for protein assembly are examples of various ATPases. Almost all ATPases contain well conserved amino acid sequences for nucleotide binding and hydrolysis.[119]

ATP, discovered in 1899 at Harvard Medical School[120], is composed by the base adenine, the sugar ribose, and three inorganic phosphate groups (**Figure 15a**). The bonding between the three inorganic phosphate anhydrides stores enough energy to make ATP the energy source of most metabolic reactions in cells. The cleavage of one inorganic phosphate (P_i) releases an energy of 32.2 kJ mol^{-1}. Hence, the hydrolysis of ATP releases energy which can be used by other enzymes to promote their reactions. Reactions which are driven forward by the hydrolysis of ATP are e.g., the transport of ions (Na/K-ATPase) or the contraction of muscle fibers (myosin ATPase). Due to the wide variety of ATPases,

the well characterized myosin is chosen to describe the mechanism of ATP cleavage in more detail.

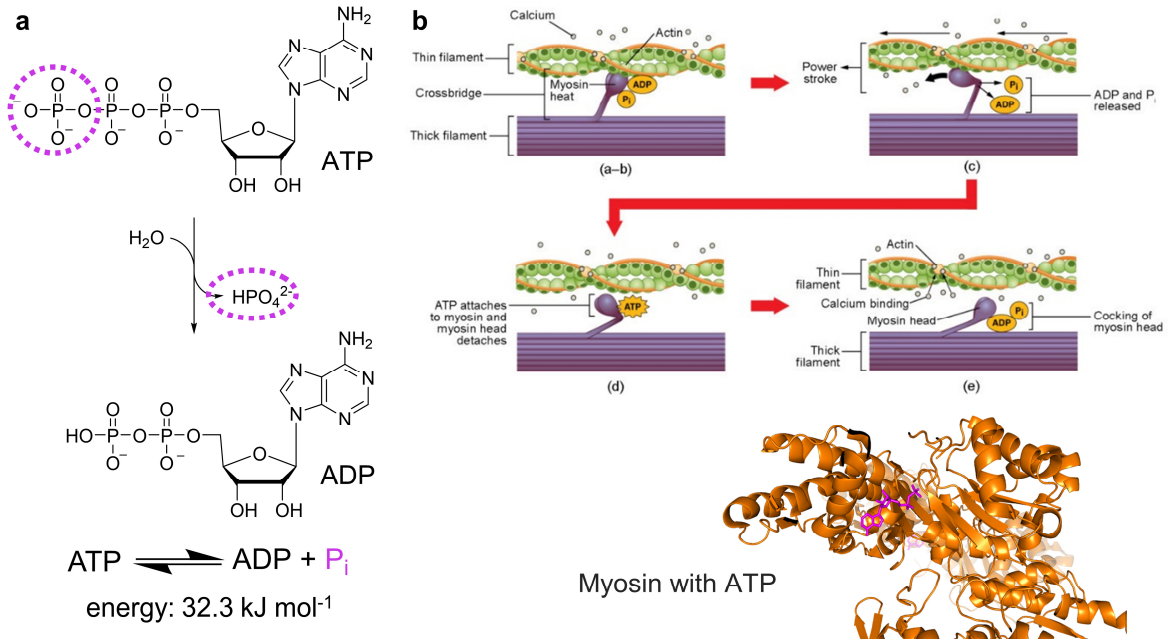

Figure 15: (a) Structure of ATP with the base adenine, the sugar ribose and three inorganic phosphate groups. The cleavage of one phosphate releases ADP and P_i and an energy of 32.3 kJ mol^{-1}. (b) Myosin protein as an example for a natural ATPase and its function in muscle contraction. Reprinted from the Northern Virginia Community College (*creative commons*)[121]

Myosin consists of a conserved head domain, located close to the N-terminus, which carries out the ATP hydrolysis and generates the movement (**Figure 15b**). The second part is a mostly variable tail domain which arranges the orientation of the biomolecule.[122] Myosin has several deep clefts and pockets. The nucleotide binding takes place in one of these areas. Another important cleft splits the myosin head into two domains which allow the binding to the actin filament, like a pair of pliers. ATPases belong to the group of hydrolases which use acid-base-mediated catalysis for the cleavage of the phosphate groups. For myosin, no amino acid is involved in the cleavage, instead the nucleotide acts as a base and the water transfers its proton directly to the γ-phosphate which is primarily cleaved off.[122] However, the binding and cleavage of ATP is not the primary cause for the movement of the myosin. At the beginning myosin-ADP is bound to the actin filament (**Figure 15b**). The release of this ADP and the binding of new ATP lead to dissociation of myosin from actin which is triggered by a conformational change in myosin through the binding of the γ-phosphate group. This change induces a movement of about 11 nm along the actin filament. Then, the ATP is hydrolyzed, and ADP and P_i remain first bound to myosin. Thus, a binding of myosin to actin is again possible and P_i diffuses from myosin

which induces another conformational change. After diffusion the interaction of myosin and actin increases again, and the myosin head moves back to its original position. Then the cycle starts from the beginning. This example demonstrates the mechanism and impact of natural ATPases in biological context.

Such a universal molecule as ATP, being so important to cellular processes, attracted researchers interest for long time. In 1966, *Miller et al.* described their first investigations of the hydrolysis of ATP.[123] In particular, the role of the adenosine group was previously not clearly defined, hence he investigated the hydrolysis of γ-phenylpropyl di- and triphosphates and compared it with the hydrolysis of ATP. Over the years the mechanism of ATP cleavage became clearer[124] by studying the role of involved ions[125] or with isotope-labeling experiments.[126] Since metal ions such as magnesium or calcium ions take part in the enzymatic hydrolysis, the role of metal-ion-promoted hydrolysis in artificial approaches was examined.[127-128] After using Cu^{2+}, Zn^{2+} or Mn^{2+} ions[129] with few success, the coordination of Cu^{3+} ions led to significant rate enhancements. *Suzuki et al.*[130] and later *Hediger et al.*[131] figured out that Co^{3+} complexes, trichlorodiethylene-triaminecobalt(III) [$CoCl_3$dien], accelerated effectively and specifically the ATP hydrolysis.

However, "natural" ATP hydrolysis by ATPases occurs by the interaction of peptides within the active sites of enzymes. Until 1983, very little was known about the ATP hydrolysis carried out by organic molecules. A strong electrostatic binding of the negatively charged nucleotides to various biological polyamines such as putrescine, spermidine or spermine (**Figure 16**), which are mostly positively charged, was observed but with no detectable catalytical properties.[132] Solely, the polyamines pentaethylene-hexamine and tetraethylenepentamine (**Figure 16**) enhanced the ATP hydrolysis rate by considerable factors.[133] The enhancing effect of hydrolysis increases with the number of nitrogen atoms in the polyamines, although spacing between the carbons plays also an important role. The hydrolysis reaction products were always adenosinediphosphate (ADP) and inorganic phosphate (P_i), no adenosinemonophosphate (AMP) or orthophosphate (PP_i) were observed which supports the specificity of hydrolysis.

Macrocyclic polyamines and dioxo polyamines demonstrated strong binding to AMP, ADP or ATP, with enzyme-substrate like affinities and a stronger binding as reported for linear polyamines (spermidine or spermine). [134-135] In 1983, *Hosseini, Lehn* and *Mertes* reported the first study of ATP hydrolysis carried out by macrocyclic polyamines (**Figure 16**) with various ring sizes and oxygen contents.[136] The highest catalytic rates for ATP hydrolysis

were observed for [24]N_6O_2 (**Figure 16**). The *O*-bisdien macrocycle was able to keep rate kinetics nearly at the same speed and constant over a wide pH range compared to hydrolysis without a catalyst which dramatically increases below pH 3. Over pH 8.5 the rate decreased rapidly to the same speed as the uncatalyzed reaction between pH 0 and 3. The protonation degree of the macrocycles plays consequently an important role.

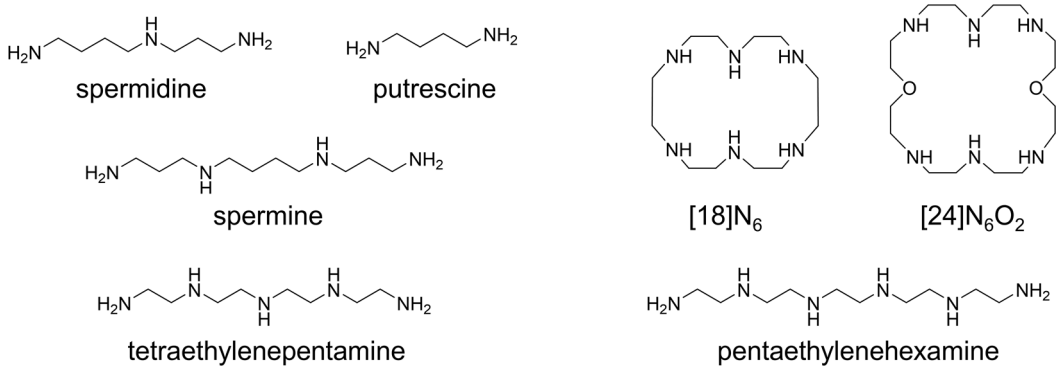

Figure 16: Linear and cyclic polyamine structures for binding and catalysis of nucleotides such as ATP.

The so-called "macrocyclic effect" was observed by comparing pentaethylenehexamine with its cyclic variant [18]N_6 which carried out the hydrolysis 3 times faster. In the following years, several papers on the outstanding performance of [24]N_6O_2 were published.[137-139] First, mechanistic studies were carried out to examine the exact reaction mechanism of ATP hydrolysis and figure out important structural parts of the catalysts.[137] For [24]N_6O_2, it was shown that catalytic efficiency is insensitive to ionic strength and that at neutral pH the reaction mechanism occurs via nucleophilic catalysis (**Figure 17**). Regarding the structural set-up of the catalyst, variants without oxygen [22]N_2C_4 or the oxygen replaced by amino groups [24]N_8 enhanced the reaction rate at pH 3 by a factor of 300. Furthermore, a phosphorylated reaction intermediate which transfers the phosphoryl group was detected. This fact was used in the subsequent paper to describe the pyrophosphate synthesis from acetyl phosphate mediated by macrocyclic polyamines which are not only able to catalyze bond-breaking but also bond-making reactions.[138] In this case, the first substrate, acetyl phosphate is first bound to the macrocycle, then a covalent intermediate is formed (the phosphorylated catalyst). The second substrate, a phosphoryl acceptor, binds also to the catalyst and finally, a second intramolecular phosphoryl transfer occurs. This example demonstrates that the simultaneous binding (ammonium) and transformation (amine) sites are located next to each other within the same macrocyclic scaffold.

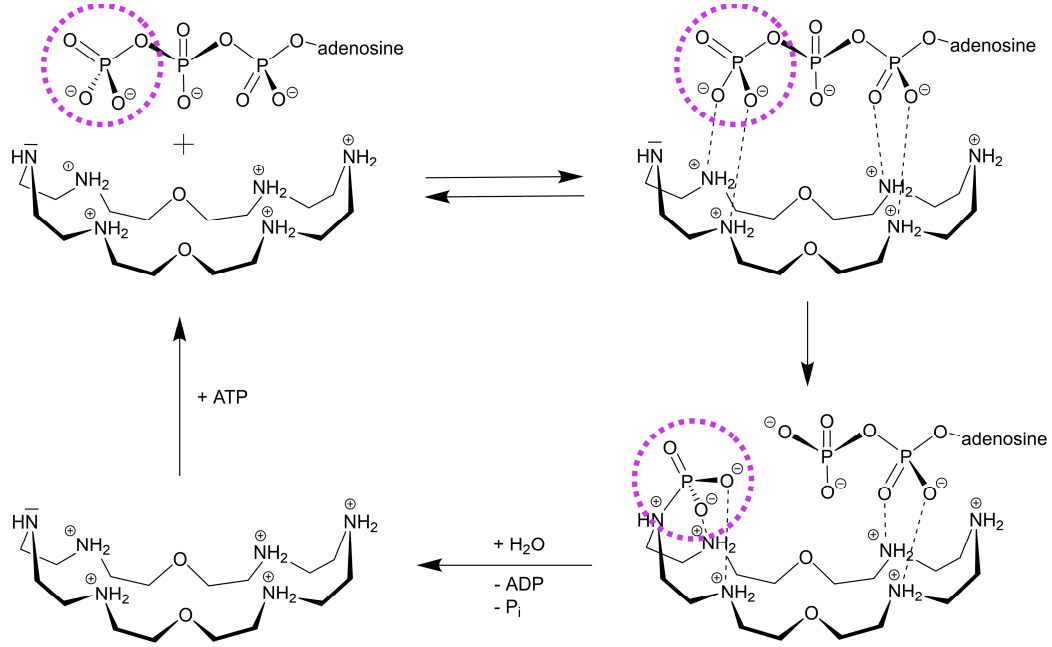

Figure 17: Proposed, catalytic cycle of ATP cleavage by [24]N_6O_2. ATP and the macrocyclic polyamine are in an equilibrium (upper part). As soon as ATP is in supramolecular interaction with the macrocycle, a nucleophilic attack of nitrogen takes place and cleaves the P_i from the remaining ADP. The cleaved molecules leave the host and a new guest ATP molecule gets into the equilibrium. Redrawn from *Hosseini et al.*[137]

In 1989 and 1990, the catalytic investigations of the macrocycles were intensified regarding a comparison between the ATPase-like enzyme mimic and the natural enzyme.[139-140] The results justified for several reasons a comparison to natural ATPases: The macrocyclic polyamines carry out hydrolysis reactions in aqueous medium and have affinity constants for binding between macrocycle and substrate that are similar to those found for natural enzymes. In addition, the reaction can be catalyzed by metals which are usually present during biological transformations. Competitive inhibition was observed by substrate analogs, and most importantly it was possible to measure Michaels-Menten kinetics for the macrocyclic polyamines. The same Michaelis-Menten constant of K_m of 10^{-4} M was determined for the natural ATPase and the macrocyclic polyamine [24]N6O2. The k_{cat} measured for the uncatalyzed reaction (no catalyst present = autohydrolysis) was $2.5 \cdot 10^{-4}$ min^{-1}, for the natural ATPase $3.2 \cdot 10^{4}$ min^{-1} and for [24]N_6O_2 a k_{cat} of $6.4 \cdot 10^{-2}$ min^{-1}.[140] By comparing the catalytic efficiency the still wide gap between both catalysts becomes evident because the value for the natural enzyme is $3.2 \cdot 10^{8}$ $min^{-1} \cdot M^{-1}$ and for the artificial ATPase, it is $6.4 \cdot 10^{2}$ $min^{-1} \cdot M^{-1}$. In order to improve these numbers, further investigations on macrocyclic ring sizes from a 21-membered [18]N_6 to 36-membered [36]N_{12} were carried out.[141] A 21-membered [21]N_7 showed best catalytic activities at the pH examined. In general, the group of *Bencini et al.* found that catalytic rates increase with

the degree of protonation (lower pH) but decrease with increasing macrocyclic size. In order to further investigate and to improve catalytic activity of the macrocycles and introduce additional functionalities, other, additional functional groups were attached to the macrocycles. The first approach was reported by *Hosseini et al.* in 1990 who designed a multifunctional macrocycle for molecular recognition as well as catalysis (**Figure 18a**).[142] They used an acridine side-chain for stacking interactions with the base adenine which supported the anion binding site of the macrocyclic polyammonium moiety and hence led to a double recognition within one molecule. The modified catalyst did not show higher catalytic rates than $[24]N_6O_2$ but a better hydrolytic selectivity between ATP and ADP and a tighter binding to the nucleotides, as also later confirmed for the modification with two acridine groups.[143]

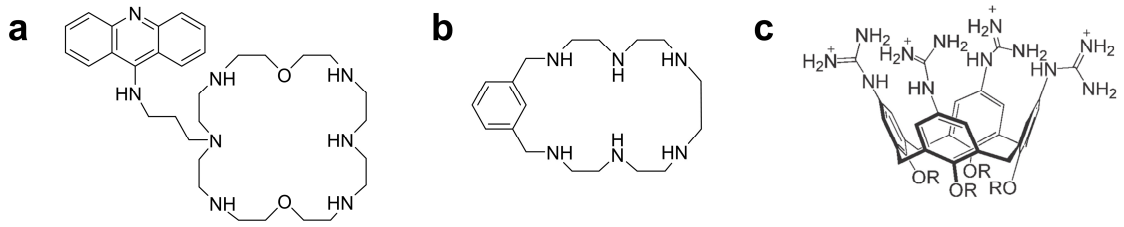

Figure 18: (a) Acridine side chain-modified $[24]N_6O_2$ for molecular recognition and catalysis.[142] (b) Macrocyclic polyamine containing a benzene spacer demonstrated very high rate enhancements for ATP hydrolysis.[144] (c) Cone-shaped calix[4]arene platform with four guanidine moieties at the upper rim for ATP hydrolysis in a wide pH range. Reprinted with permission from *Salvio et al.*[145]

One of the highest rate enhancements for ATP cleavage was observed by *Aguilar et al.*[144] They synthesized a macrocycle with an aromatic ring that demonstrates a multipoint binding scheme to ATP (**Figure 18b**). π-stacking between adenine and the benzene spacer, confirmed by NMR studies, leads to a guided orientation of polyphosphate chain and macrocycle, resulting in high catalytic efficiency. Also, a high degree of specificity for the conversion of ATP to ADP was detected.

More recently, the ATP cleavage by cone-tetraguanidinocalix[4]arene was reported.[145] *Salvio et al.* designed a cone-shaped calix[4]arene platform with four guanidine moieties at the upper rim (**Figure 18c**). The catalyst hydrolyzed ATP in a pH range from 8.8 to 10.4. Three protonated guanidines provide the electrostatic driving force for the substrate binding. The fourth guanidine stayed in a neutral state to be used in nucleophilic catalysis. The effective catalysis arises from combined action of two moieties. However, most of the reactions had to be carried out in DMSO/water mixtures and at high temperatures (80 °C).

So far, all potential ATPase mimics were investigated without a concrete application in biological systems. In 2003, *Frydman et al.* reported cyclopropane-containing polyamine analogs that demonstrated efficient growth inhibition of human prostate tumor xenografts in nude mice.[146] At that time, no correlation to the ATP balance was seen. However, the ATP pool in cells can be one target for ATPases and artificial ATPases. Derived from the budmunchamine alkaloid family[147], the same group showed that some macrocyclic polyamines have the ability to diminish the ATP level of cells by cleaving ATP and depleting so inner cellular ATP levels.[148] Most cancer cells produce their ATP in aerobic glycolysis compared to mitochondrial oxidative phosphorylation in healthy cells. This effect is called Warburg effect.[149] In solid tumors, when O_2 partial pressure goes down below 10 mm Hg, the ATP concentration diminishes due to the Warburg effect. Since tumor cells have lowered ATP levels compared to normal cells, macrocyclic polyamines were used to inhibit tumor cell proliferation. All of the synthesized budmunchamine-based macrocycles hydrolyzed ATP *in vitro* in a malachite green-based assay. *Frydman et al.* demonstrated their inhibition of cell proliferation in two different human prostate cell lines but more important was the shown decrease of ATP levels by two orders of magnitude after 72 hours. Both effects correlated and resulted in a high efficacy of cell toxicity.

Summing up, the current limitations and challenges for the production of artificial enzymes are the one-dimensional focus on either core-shell structures (dendrimers, star polymers with low or no catalytic activity) or on active site imitation of enzymes (e.g. by nanozymes or supramolecular cages). Combined approaches for enzyme-like reactions inside of cells by using biocompatible nanocarrier systems have not been carried out yet. Important factors for the combined approach are prolonged stability, cellular uptake and high activity of the catalytic site.

1.3 Enzymatic Cascade Reactions

The following chapters focus on multifunctionality of enzymes in clusters and networks. The scope is broadened from one enzyme considered individually as an operative unit to larger functional entities with multiple functional sites. In the first section, some examples of nature's highly specific and complex catalytic tools will be displayed, starting with small enzymes with two functionalities up to extraordinarily organized, functionalized molecular machines. All presented systems have in common that their assembly serves for the proceeding of cascade reactions. A closer look at cascade reactions and their definition will be presented in the second section. Different artificial approaches to mimic molecular machines are reviewed and provide a short overview of the latest and most important results.

1.3.1 Multifunctional Enzyme Clusters and Molecular Machines

As described in 1.1, enzymes can be classified according to the reaction they carry out. Almost all enzymes are specialized for single transformations. There are only a few examples of enzymes that can perform two different reactions at a time. The human enzyme paraoxonase-2 (PON2), an important enzyme in innate immunity, atherosclerosis, and cancer, shows lactonase activity (hydrolase) which hydrolyzes bacterial signaling and serves as protection against pathogenic offenses. In addition, it has peroxidase activity (oxidoreductase) for the reduction of reactive oxygen species.[150] Thus, it reduces cellular oxidative damage and has an influence on signaling occurring via reactive species. By introducing several point mutations into the enzyme, the exact mechanism of the relation between both functionalities was investigated. However, both activities showed that they act separately and have no obvious, reasonable interaction.

Another example is the microsomal cytochrome P-450 which can be found in adrenal, testis, ovary and placenta, and assists the biosynthesis of steroid hormones.[151] The main function of the enzyme is to work as an oxidoreductase for binding and reduction of oxygen in order to introduce a hydroxyl group in hormones. In addition, it also features a lyase function. However, exactly involved structural elements for catalysis are still unidentified.

In nature, fusion of single enzymes to greater, functional entities can be observed to meet the requirements of more complex and demanding transformations. Proteins often cluster

and work together in multifunctional molecular machines. These complexes range from small, few single proteins containing enzymes to highly sophisticated enzymatic assemblies which carry out multiple functions.

The tryptophan synthase is a simple, but still very effective model of a multienzyme complex. It carries out the final two steps in biosynthesis of L-tryptophan.[152] The enzyme consists of mainly two individual functional subunits, the monomeric α-subunit (2α, protein A with 29 kDa) with a TIM barrel conformation and the dimeric β-subunit (β_2, protein B with 90 kDa) (**Figure 19a**). Separated subunits catalyze a lyase reaction with the cleavage of indole-3-glycerolphosphate to indole and glyceraldehyde-3-phosphate at the monomeric α-subunit. The reaction is followed by a ligase reaction with the reaction of indole and L-serine to L-tryptophan at the dimeric β_2-subunit. In the presence of the reassembled $\alpha\beta_2\alpha$ complex, the rate of these partial reactions is 30-100 times higher than with individual subunits. Through assembly, a conformational change occurs which triggers this rate acceleration.[153] Both active centers have only a spacing of 3 nm and are connected with a tunnel.[154] The tunnel has a length of 2.5 nm and its diameter matches with the diameter of the hydrophobic indole.[155-156] It allows rapid flow of the respective products and substrates and prevents their escape by passive diffusion via the hydrophobic cell membrane.

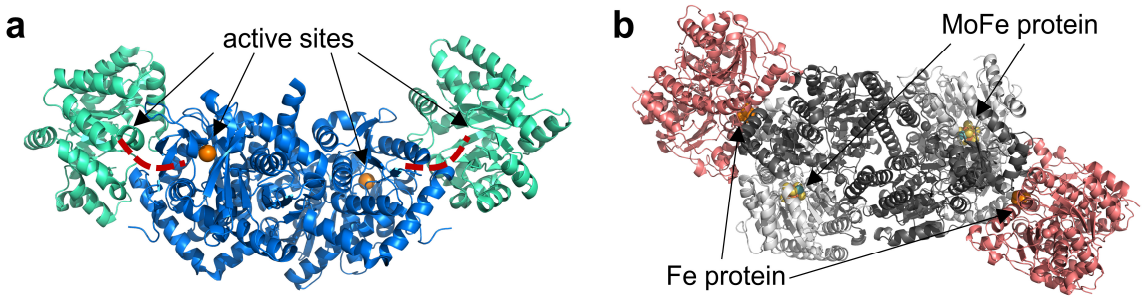

Figure 19: (a) Tryptophan synthase with two monomeric α-subunits (cyan) and the dimeric β-subunit (blue). Both subunits are linked with a 2.5 nm tunnel (red dotted line) allowing the rapid transfer of intermediates in the cascade reaction. (b) Nitrogenase with homodimeric Fe protein (rose) (dinitrogenase reductase) and heterotetrameric MoFe protein (dinitrogenase) which consists of two α-subunits (light grey) and two β-subunits (dark grey).

Another example is nitrogenase, a multienzyme complex consisting of two enzymes that reduces atmospheric nitrogen (N_2) to ammonia (NH_3).[157] Reduced nitrogen plays an important role in the biosynthesis of nucleic acids and proteins. However, only a few microorganisms such as cyanobacteria can use some of the 79% nitrogen (N_2) in the earth's atmosphere in their nitrogen fixation reaction. The process allows utilization of nitrogen

in biochemical reactions and biosynthesis. The multienzyme complex consists of two interacting enzymes: dinitrogenase and dinitrogenase reductase (**Figure 19b**). The latter is a homodimeric Fe protein (60-64 kDa) that transfers the required electrons for the reaction from reducing agents such as ferredoxin or flavodoxin.[158] The dinitrogenase is a heterotetrameric MoFe protein (240-250 kDa) which then performs the reduction of nitrogen to ammonia in its core $MoFe_8S_7$-cluster.

The clustering of several enzymes can be observed in the fatty-acyl-CoA synthase (**Figure 20**), a multienzyme with eight enzymatically active centers.[159-161] The complex, mainly found in brain, lung, and liver, catalyzes the biosynthesis of fatty acids, in particular, the synthesis of the most common fatty acid palmitoyl-CoA (16 carbons) by using one acetyl-CoA and seven malonyl-CoA. The reaction is the key step in lipogenesis and provides molecules that are primary components of cellular membranes or used for posttranslational protein modifications. These modifications are necessary for the complete functionality of proteins. Saturated fatty acids serve as "energy storage" molecules.

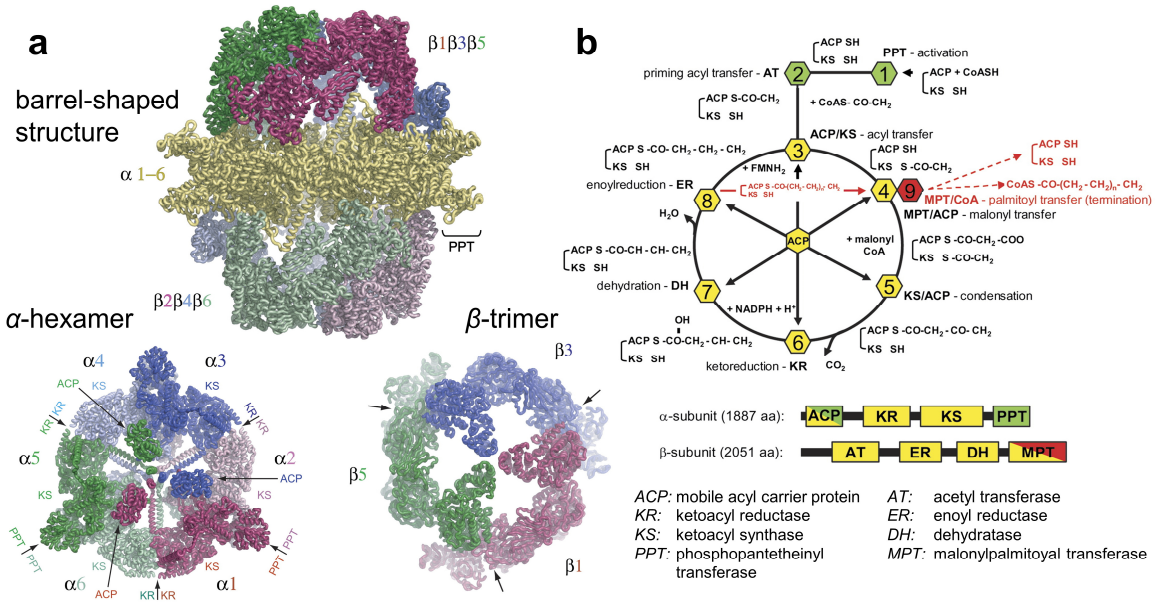

Figure 20: (a) Structure, architecture and organization of fatty-acyl CoA synthase (FAS) with α- and β-subunits. (b) Cyclic reaction scheme of fatty acid synthesis with initiation (green), elongation (yellow) and termination (red) of fatty acid synthesis and eight corresponding enzymatic functionalities. Reaction 3-8 are repeated seven times before releasing palmitoyl-CoA in step 9. Reprinted and adapted with permission from *Lomakin et al.*[162]

The complex consists of two multi-functional subunits: alpha and beta.[163] The subunits are arranged in an $\alpha_6\beta_6$ structure and form a barrel-shaped complex with a molecular weight of 2.6 MDa.[162] The six α-subunits assemble in an equatorial disk, which divides

the barrel into two separate cupolas, each consisting of three β-subunits. The α- and β-subunits represent three, sterically isolated reaction chambers per cupola and contain eight catalytic centers. The assignment of the subunits to their reactions and their contributions in fatty acid biosynthesis is shown in **Figure 20**. The complex biosynthesis of the fatty acids can only occur in a perfectly coordinated and intense interaction of the subunits.

Increasing the number of involved enzymatic functionalities and catalytically active domains leads to highly specific molecular machines. For example, ribosomes are big, functionally clustered entities that contain ribosomal RNA and approximately eighty proteins with enzymatic activity.[164] Ribosomes are granular particles with a diameter of 20-25 nm. They are composed of about one-third ribosomal proteins and have two different subunits which vary in size and functionality. The entire ribosome has a molecular weight of 4.2 MDa whereas the bigger subunit consists of about 49 proteins and has a molecular weight of 2.8 MDa. The smaller subunit contains 33 proteins and weighs 1.4 MDa. The cooperation of those various, different enzymes enables the readout of messenger-RNA during translation. The translation reaction plays an important role in complete gene expression and protein biosynthesis.[165]

A last example of a complex molecular machine which has been recently discovered and studied extensively is the CRISPR/CAS system.[166-167] The system is based on an adaptive antiviral defense mechanism of bacteria (CRISPR; Clustered Regularly Interspaced Short Palindromic Repeats).[168] It cuts precisely DNA at particular positions. allowing the specific cut-off and introduction of gene sequences. Hereby, the CAS9 protein complex plays a key role during cutting.[169] Briefly, the simplest method for artificial gene modification uses RNA injected in the cell which codes for the CAS9 and a random recognition sequence. The cell translates the RNA, synthesizes the protein which then finds the added recognition sequence. CAS9 cuts double-stranded DNA at exactly the position which is determined by associated recognition sequence. Afterwards, natural DNA reparation mechanisms occur, and the cut DNA is assembled again. If during that process unbound DNA with loose ends is present, this variable DNA sequence is incorporated into the gene leading to an irreversible change of the genome. This highly complex machinery represents the high specificity, accuracy, and efficacy of nature's molecular machines which can only perform these highly demanding reactions if all involved enzymes are subjected to extraordinary interaction.

1.3.2 Cascade Reactions Performed by Artificial Enzymatic Clusters

Looking more closely at general functions of the previously described molecular machines, it can be observed that their assembly is mainly favorable for the proceeding of enzymatic cascade reactions. Generally, these types of reactions combine several enzymatic transformations in concurrent one-pot processes without isolation of intermediates.[170] Cascade reactions can be divided into two groups: domino reactions and consecutive reactions.[171] A domino reaction, also called tandem or cascade reaction, is defined by a serial reaction of at least two (or more) reactions in which the formed product is directly used in the following reaction step. No intermediates can be detected and in a strict form of the definition, the reaction conditions (solvents or temperature) do not change during the domino reaction. In contrast, a consecutive reaction requires addition of an extra reagent, a catalyst or a mediator after the first reaction occurred. This group includes the reactions which take place at modified reaction conditions like enhanced temperatures.

Multi-enzymatic cascade reactions in solution have several advantages like decreased time exposure, reduced costs and chemicals for product recovery, and the use of toxic, harmful or chemically unstable compounds can be lowered to minimal amounts. These biocatalytic transformations allow the synthesis of enantiomerically enriched alcohols,[172] amines[173], and amino acids.[174] However, single enzymes are floating within the reaction mixtures and have no comparable properties with nature's molecular machines. In order to mimic natural, enzymatic cascade reactions with artificial methods, it is necessary to bring different enzymes in close proximity called metabolic channeling.[175] This ensures fast transfer of unstable compounds from one catalytic site to the other without diffusion as shown for example for the tryptophan-synthase[154] with its hydrophobic channel (**Figure 19a**). There are several approaches to achieve a small spatial distance between catalytically active reaction centers which will be presented in the following paragraphs.

Immobilization of Enzymes in Close Proximity

Enzymes can be immobilized by using various techniques[176] and different scaffolds.[177] Hereby, immobilization guarantees for spatial approximation but at the same time enables in some cases an enhanced enzyme activity, stability, and selectivity.[178] Immobilization can be distinguished by non-specific, random placement on the scaffold as well as specific, controlled arrangement within the biocatalytic assembly.

The first example of two non-specific, co-immobilized biocatalysts was reported in 1970.[179] Hexokinase and glucose-6-phosphate dehydrogenase were both covalently bound to Sepharose 4B and in addition to an acrylamide-acrylic acid polymer, respectively. A cascade reaction was carried out using glucose, ATP and $NADP^+$ monitoring the development of NADPH per time (**Figure 21**). Comparing the immobilized enzyme's activity with the activity of both enzymes in solution, an increased development of NADPH was observed for both matrices. Spatial proximity of both enzymes decreases the possibility of diffusion for the intermediate glucose-6-phosphate.

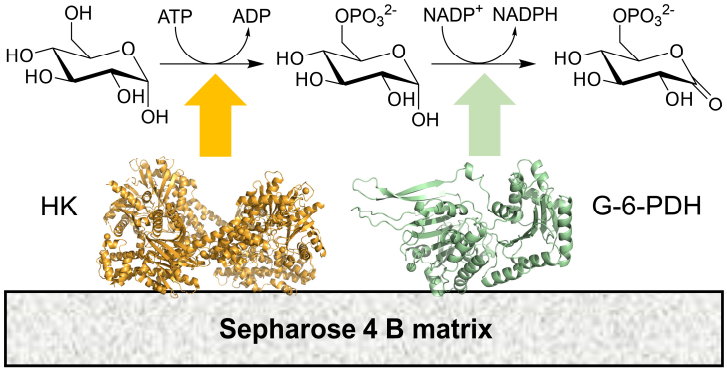

Figure 21: Cascade reaction carried out by immobilized hexokinase (HK) and glucose-6-phosphate dehydrogenase (G-6-PDH) leading to an increased formation of NADPH compared to the single enzymes in solution. Adapted from *Schoffelen et al.*[180]

Polymer-enzyme hybrid structures with a polymeric backbone and covalently attached enzymes carrying out a cascade reaction are one further example for co-immobilization of enzymes on a polymeric scaffold (**Figure 22**).[181] Hereby, a polymer chain of polymethacrylate was synthesized with 2000 repeating units. The polymer has an enormous number of amino groups which are protonated below pH 9, making the polymer backbone polycationic and water-soluble. For the attachment of the enzymes, a bis-aryl hydrazine (BAH) linkage was used. The linkage connects a polymer-bound aryl hydrazine with an introduced benzaldehyde group on the enzyme's surface.[182] The advantage of this conjugation method is the simple observation of the reaction with UV/Vis spectroscopy measuring the absorption band at 354 nm for the newly formed bond. It allows direct quantification of attached enzymes resulting in 60 attached superoxide dismutases (SOD) and 120 attached horseradish peroxidases (HRP). Several fluorescein molecules were linked in the same way for quantification of the polymer and for possible imaging. The attached enzymes remained fully active after conjugation. The individual activity of HRP was tested with H_2O_2 as oxidant and $ABTS^{2-}$ as oxidable substrate.[183] The enzymatic functionality of SOD was investigated with superoxide radical anions which are

transformed by SOD in a disproportionation reaction in dioxygen and hydrogen peroxide. In a cascade reaction, both reactions were combined, demonstrating an almost similar efficiency compared to free enzymes. By binding the two enzymes to the polymer backbone, local proximity for a cascade reaction was enabled.

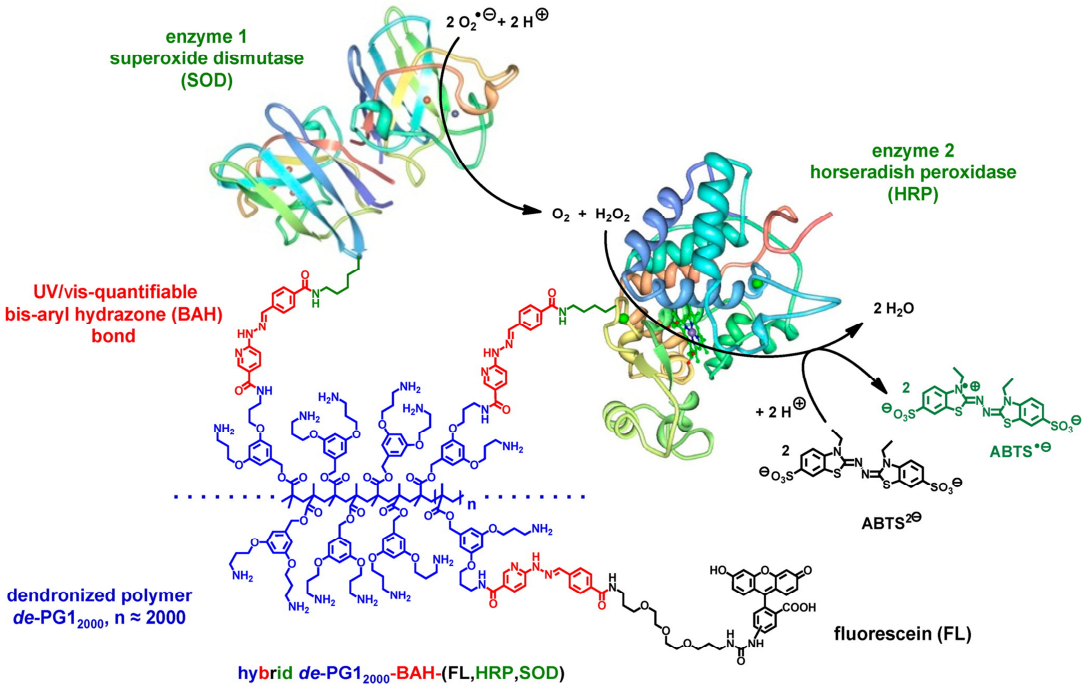

Figure 22: Polymer-enzyme hybrid structure with a polymethacrylate backbone and attached superoxide dismutases (SOD) and horseradish peroxidases (HRP). The cascade reaction occurs first at the SOD transforming superoxide radical anions generated by pulse radiolysis to hydrogen peroxide. In a peroxidase reaction at the HRP, the colorful ABTS dye is generated which confirms the successful proceeding of the cascade. Reprinted with permission from *Grotzky et al.*[181]

In further approaches, e.g. two different enzymes, acid phosphatase and fructose-1,1-diphosphate aldolase, were immobilized on methacrylate polymeric beads for the synthesis of complex chiral carbohydrates.[184] Also, glucoamylase and α-amylase were co-immobilized on magnetic chitosan beads. The beads were applied for consecutive starch liquefaction and saccharification.[185] As last example, immobilization of glycerol dehydrogenase and xylose reductase to nanoparticles made of methyl methacrylate, methyl acrylic acid, and ethylene dimethylacrylate will be mentioned.[186] Hereby, a parallel cascade system was created demonstrating the simultaneous generation of 1,3-dihydroxyacetone and xylitol from glycerol and xylose. The immobilized multi-enzyme system did not only demonstrate a significantly increased stability compared to enzymes in solution but rather increased their turnover numbers and catalytic efficiencies.

The above mentioned examples describe researcher's approaches to bring enzymes via immobilization in close proximity. However, there is limited control over distribution of enzymes on scaffolds. Even if the biocatalysts are on the same polymer or nanoparticle, there might still be a large distance between individual enzymes. Mimicking nature's models, it is necessary to regulate and dominate construction of the assemblies. On the one hand, a direction of the enzyme's position and its conjugation technique to the scaffold is desirable to prevent interference or hindrance with residues that are important for enzyme's activity. On the other hand, the orientation of multiple enzymes to each other is of great importance to ensure a smooth and direct transfer of substrate within the cascade reactions.

One possibility for specific immobilization is the use of affinity tags.[187] The common histidine tag can be introduced to enzyme's C- or N-terminus with genetic methods and allows for an interaction with Ni^{2+}. In one example, multiple enzymes for the synthesis of UDP-galactose were immobilized in controlled fashion via their hexahistidine tags onto nickel agarose beads.[188] The seven involved enzymes performed much better when immobilized compared to the single enzymes in solution. Recent literature reports even regulated orientation of a barrel protein on matrix and tunable binding strength when using histidine tags (**Figure 23**).[189]

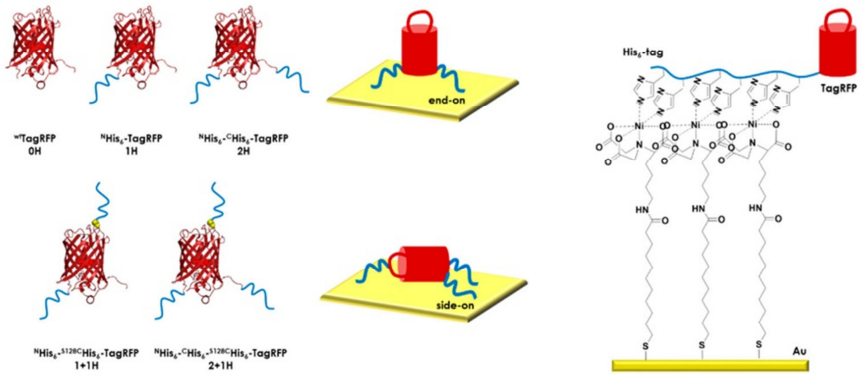

Figure 23: Controlled protein surface orientation by using hexahistidine tags.[189] Illustration of five possible variants and the corresponding end-on and side-on binding to the surface. Immobilization on the surface occurs via Ni^{2+} and NTA (nitrilotriacetic acid) complexation. Reprinted with permission from *Wasserberg et al.*[189]

A further tag is cellulose-binding domain (CBD). Pantothenate kinase (PanK), phosphopantetheine adenylyltransferase (PPAT), and dephosphocoenzyme A kinase (DPCK) were expressed in bacteria with CBD.[190] Their immobilization on cellulose enabled effective and straightforward synthesis of coenzyme A and coenzyme A analogs.

The attachment of enzymes to scaffolds either non-specific or directed leads often to an undesirable decrease in enzyme's activity. By using chemical conjugation methods, the structure often alters, leading to a modification of the active center and hence to reduced catalytical activity. One possibility to avoid chemical linkage is encapsulation or entrapment of enzymes into nanostructures.

Non-covalent Encapsulation or Entrapping of Enzymes

Multiple enzymes can be encapsulated in so-called nanoreactors.[191] For example, nitrobenzene nitroreductase (NBNR) and glucose-phosphate dehydrogenase (G-6-PDH) were co-encapsulated and co-localized in silica particles.[192] Encapsulation leads to a significantly increased stability of NBNR and was used for continuous reduction of nitroaromatic compounds (**Figure 24a**). In a recycling reaction, $NADP^+$ was reused by G-6-PDH *in situ*. Both enzymes did not show a reduction of activity after encapsulation.

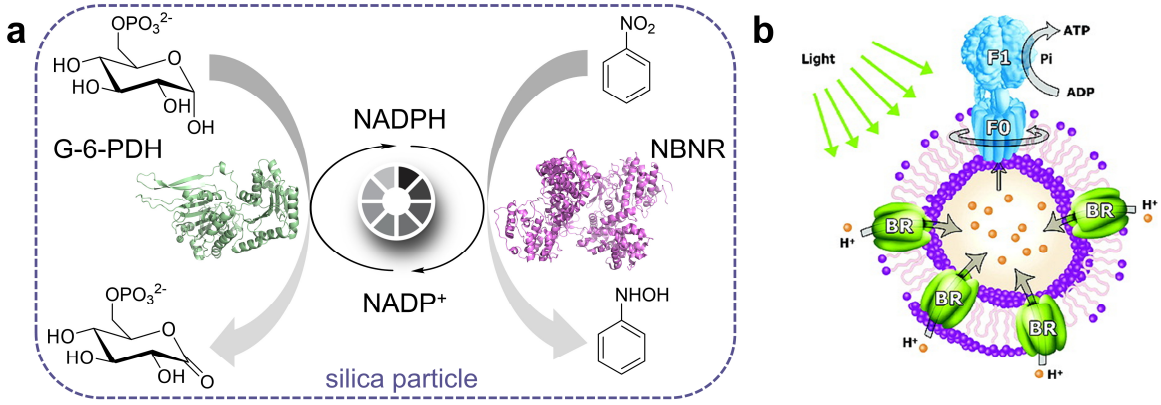

Figure 24: (a) Nitrobenzene nitroreductase (NBNR) and glucose-6-phosphate dehydrogenase (G-6-PDH) are co-encapsulated in silica particles. Nitrobenzene is continuously reduced to hydroxylaminobenzene whereas at the same time $NADP^+$ is recycled by G-6-PDH to NADPH in the oxidation reaction of glucose-6-phosphate. Adapted from *Schoffelen et al.*[180] (b) Proteopolymersome with encapsulated bacteriorhodopsin (BR) and F_0F_1-ATP synthase in their formed membrane. The light-induced proton gradient generated by BR enables ATP synthesis from ADP and inorganic phosphate. Reprinted with permission from *Choi et al.*[193]

Another approach is the use of proteopolymersomes.[193] Two enzymes, bacteriorhodopsin (BR) and F_0F_1-ATP synthase were encapsulated into the membrane formed by an amphiphilic triblock copolymer, PEtOz-PDMS-PEtOz [poly(2-ethyl-2-oxazo-line)-b-poly(dimethylsiloxane)-b-poly(2-ethyl-2-oxazo-line)] (**Figure 24b**). BR contains a photocycle which activates a proton pump. Consequently, a proton gradient is generated across the polymersome's membrane. The gradient is used by ATP-synthase to synthesize ATP from ADP and inorganic phosphate.

One last example is encapsulation of three enzymes performing a cascade reaction into a bacteriophage P22 virus-like particle.[194] The three enzymes are CelB, which is a tetrameric *β*-glucosidase enzyme carrying out hydrolysis of a wide range of disaccharides, ATP-dependent galactokinase (GALK) and dimeric ADP-dependent glucokinase (GLUK), which perform phosphorylation of galactose to galactose-1-phosphate and glucose to glucose-6-phosphate (G6P), respectively. The sequence performed by these three enzymes is the start of glycolysis and provides information for studies in sugar metabolism and biofuels generation. Here again, spatial proximity of encapsulated enzymes leads to an increased activity of enzymes compared to single enzymes in solutions.

However, the use of polymeric scaffolds or encapsulation materials is not always preferable. Often, immobilization or entrapment comes along with the presence of a large amount of non-catalytic material or with the use of expensive and complex carrier material. Therefore carrier-free methods were developed which are described in the following paragraphs.

Covalent Linkage of Enzymes with Each Other

In order to mimic the close proximity of catalytic centers in nature's molecular machines, direct covalent conjugation of enzymes suggests being a promising approach. The first section demonstrates a few examples of linking enzymes using various chemical concepts. The second paragraph deals with gene fusion. This method is using nature's biochemical methods for covalently conjugated multi-enzyme systems.

Cross-linked enzyme aggregates (CLEAs) have been developed as one model for covalently linked enzymes without using a solid carrier.[195-197] One advantage is that very high enzyme activities per volume can be obtained because no non-catalytical material is present. The method uses direct precipitation from aqueous solution and cross-linking with glutaraldehyde in millifluidic reactors as shown exemplarily in **Figure 25a** for one aggregate. An example is the widely studied combination of glucose oxidase (GOx) and horseradish peroxidase (HRP) to perform enzymatic cascade reactions in CLEAs.[198] Here, the reaction starts with the oxidation of glucose by GOx. The resulting H_2O_2 is then reduced to water by the heme group of HRP. The activated form of HRP can catalyze the formation of fluorescence dyes. This way, the initial concentration of sugar can be determined by measuring the amount of produced dye. Additionally, enzymes like *β*-glucosidase or *β*-galactosidase can be added to this system to achieve three-step cascades

by breaking down complex carbohydrates such as starch or glycogen into their monomers prior to the oxidation reaction.[199-200] In combi-CLEAs of HRP and GOx[198], the distance between the enzymes is supposed to be very small. When adding catalase (CAT), a peroxidase which quickly decomposes H_2O_2, to the CLEAs, the reaction rate of the cascade reaction decreased only by 19%. This is only possible if the distance between HRP and GOx is very small and the transfer of H_2O_2 occurs fast. The combi-CLEA particles with a size of 250 nm, were used as a colorimetric sensor for glucose.

A further CLEA system is the combination of (*S*)-selective oxynitrilase (HnL) and non-selective nitrilase (NLase) for the synthesis of enantiomerically pure (*S*)-mandelic acid.[201] Both enzymes were precipitated with 1,2-dimethoxyethane and cross-linked with dextran polyaldehyde which was then reduced with sodium borohydride ($NaBH_4$). Starting from benzaldehyde, the (*S*)-specific HnL introduces a cyano group sterically correct at the aldehyde group. The reaction cascade is followed by hydrolysis carried out by non-specific NLase resulting in enantiomerically pure (*S*)-mandelic acid. The conversion occurred very fast, but upscaling of the synthesis route remained challenging. Besides the use of dextran polymer introduces non-catalytic, high molecular weight, material to the system.

The two-described system both contained two enzymes within their CLEAs. A CLEA system which incorporates five enzymes was established for the synthesis of nucleotide analogs (**Figure 25a**).[202] It contains both a purine nucleotide analog pathway and an auxiliary ATP recycling system. The pathway is shown in **Figure 25b**. The enzymes ribokinase (RK), phosphoribosyl pyrophosphate synthetase (PPS), and hypoxanthine phosphoribosyl transferase 8B3PRT (8B3) represent the part of the cascade which catalyzes in a last step the addition of purine nucleobases to the activated sugar, providing a variety of nucleotide analogs. The synthesis requires ATP, releasing ADP and P_i. These components are recycled in an ATP recycling system consisting of adenylate kinase (AK) and pyruvate kinase (PK) using phosphoenolpyruvate (PEP) as a source of activated phosphate. This CLEA system carrying out five reactions, not all in a one-directional cascade, however, combining two different reaction cycles is a good example for a more complex and sophisticated, artificial molecular machine mimicking in first attempts nature's models of enzyme clusters.

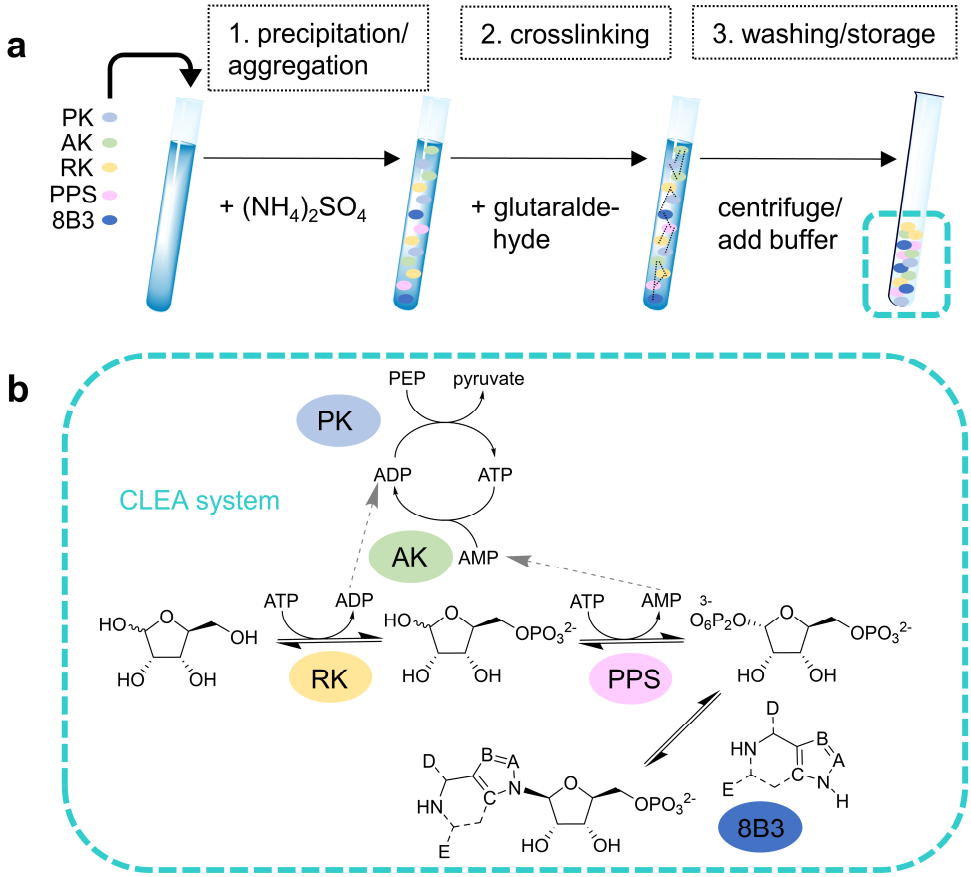

Figure 25: (a) General procedure for the formation of cross-linked enzyme aggregates (CLEA) using the example of *Scism et al.*[202] (b) Reaction cycle proceeding in mentioned CLEA system for the synthesis of nucleotide analogs. The three enzymes ribokinase (RK), phosphoribosyl pyrophosphate synthetase (PPS) and hypoxanthine phosphoribosyl transferase 8B3PRT (8B3) catalyze the synthesis of purine analogs whereas an ATP recycling system is linked to the three-step cascade reaction. The ATP regeneration cycle provides ATP for the first two reactions of the cascade using adenylate kinase (AK) and pyruvate kinase (PK). Adapted with permission from *Scism et al.*[202]

The formation of CLEAs is one concept of generating covalently linked enzymes. The method uses mainly abundant ε-lysine residues of the conjugated enzymes and might lead to uncontrolled cross-linking at multiple positions resulting in reduced catalytic activities. To meet this challenge a few approaches have been published such as the use of amino acid residues which are mainly present on the surface to a limited extent of the protein like cysteines, tyrosines, and tryptophans.[203] The cross-linking of bovine serum albumin (BSA) to a TLL lipase was carried out using click chemistry.[204] The lipase was selected because it has only one free accessible lysine on its surface which was then modified in an EDC coupling with an acetylene group. BSA on the other side only has one free accessible cysteine which was azide-modified. In a Cu^{+}-catalyzed [3+2] Huisgen cycloaddition reaction, both proteins were reacted in a controlled reaction procedure and used for the

preparation of protein dimers. The dimers demonstrated a higher catalytic activity than the lipase alone and a higher long term activity. Click chemistry is also used in the coupling of two immunoglobulin-binding protein G domains.[205] Azide and alkyne groups were introduced to the proteins by native chemical ligation reactions (NCL). The thioesters for NCL reactions at the N-termini were expressed in fusion proteins. The last example demonstrates the synthesis of streptavidin (SAv)-BSA polymer conjugates.[206] Biotin-maleimide telechelic polymers were synthesized which are able to bind site-specifically to the two different proteins. The dual functionality enables the conjugation of SAv and BSA to one polymer chain and in this manner a controlled cross-linking which might have a positive influence on the possible enzyme's activity.

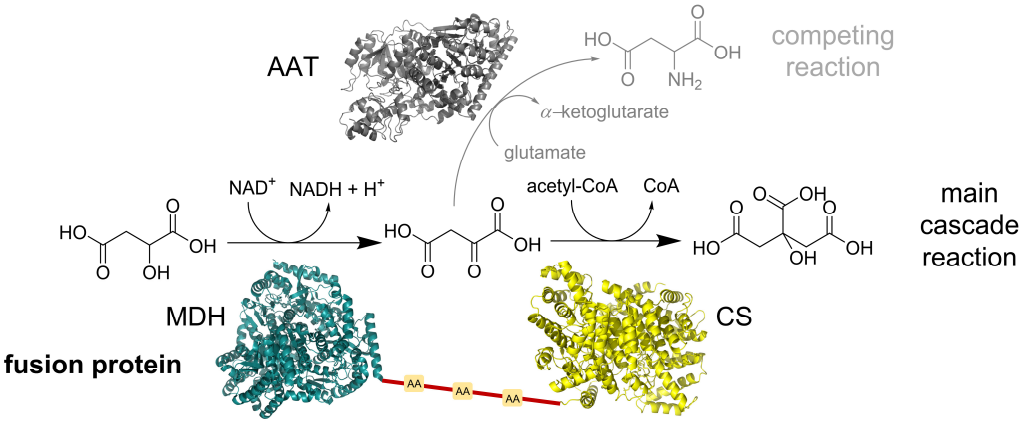

Figure 26: Reaction scheme of the reaction carried out by a fusion protein of malate dehydrogenase (MDH) and citrate synthase (CS). Both enzymes are expressed with a linker containing 3 amino acids (AA). The presence of the competing enzyme aspartate amino transferase (AAT) demonstrated the high efficacy of the protein fusion being a less potent competitor of the reaction intermediate. Adapted from *Schoffelen et al.*[180]

A completely different approach of linking enzymes without using chemicals is gene fusion. Genes, normally encoding for one specific enzyme, are joined with other enzyme genes resulting in a chimeric gene. The new gene codes for a polypeptide chain which has two active centers. The concept and first examples were described in 1991.[207] Generally, coalesced enzymes are prepared by removing the translational stop signal at the 3'-end and ligated into the start codon (ATG) of a second gene. The decision in which order enzymes are linked is chosen gratuitous. The linkage between both enzymes has a length of 3-10 amino acids because for longer spacers proteolytic degradation was observed. For example, two enzymes of the citric acid cycle were expressed as a fusion protein.[208] Mitochondrial citrate synthase (CS) and malate dehydrogenase (MDH) are expressed with a linker, containing three amino acids, in bacteria (**Figure 26**). The resulting dienzyme demonstrated in particular good activity once the cascade reaction was challenged by a

competing enzyme (aspartate amino transferase, AAT). AAT showed to be less effective when compared to free CS and MDH in reacting with the intermediate of the cascade.

Another example is the fusion of dihydroxyacetone kinase (DHAK) and fructose-1,6-bisphosphate aldolase (FBPA) to a bifunctional aldolase/kinase enzyme.[209] The linked enzyme system carried out a C-C bond formation starting from dihydroxyacetone (DHA). Both enzymes retained their structural integrity shown by circular dichroism (CD) spectroscopy and their activity. The proximity of the active centers promotes a 20-fold increased activity compared to the single enzymes which can be attributed to substrate channeling. This was confirmed by also using a competing enzyme, glycerol-3-phosphate dehydrogenase whose activity was almost twice as low when compared to GDH activity in the free enzyme system.

One recently published multi-enzyme is the combination of oxidase and peroxidase via gene fusion.[210] One bacterial peroxidase was fused to four different bacterial oxidases resulting in a biocatalyst that allows cascade reactions only requiring molecular oxygen. All enzymes remained active, able to bind their cofactors and performing a wide range of cascade reactions.

Despite the mentioned examples, gene fusion is mostly limited to the fusion of two, maybe three enzymes and not universally applicable. Microorganisms expressing the chimeric genes have often problems in folding the multidomain proteins properly and are not efficient in expression of large scales of fusion proteins.

In summary, nature's molecular machines are all distinguished by a high speed and efficiency in shuttling their substrates and products between spatially separated active sites. For a successful mimic, it is essential to minimize the distance between individual enzymes or functionalities as much as possible. The described artificial systems to mimic the cascade reactions are limited by either the bulky nature of enzymes or the use of a huge amount of inactive material (immobilization or encapsulation). Furthermore, available chemical means to organize and arrange two or several enzymes next to each other (CLEAs) and limited possibilities of natural biological systems (gene fusion) are major drawbacks in the state of the art of artificial cascade reactions.

2 Motivation and Objectives

Enzymes play an important and decisive role in nature's cellular processes as without the catalytic activity of enzymes, many reactions would not occur. Enzymes catalyze a wide range of biochemical reactions by reducing activation energy. Nature's biocatalysts possess outstanding properties which ensure their full functionality in complex and demanding biosystems. Their setup with a core-shell structure, often an active site-specific seclusion and their interactions with other enzymes in large clusters, raises the interest of researchers to mimic and study these special features with artificial methods.[38] The aim of this thesis is to mimic the architecture of natural enzymes, their individual catalytic activity as well as their interaction with other enzymes in so-called molecular machines. In the first project of this thesis, an enzyme will be regarded individually and recreated with its outstanding properties. It is planned to attach catalytically active moieties to a polymeric scaffold. The goal is to demonstrate catalytic activity of this biopolymeric conjugate in simple *in vitro* assays. In a second project, the aim is to mimic the cooperation of different enzymatic reactions in enzymatic clusters and their accomplished cascade reactions.

2.1 Artificial ATPase-like Enzyme

Inspired by the setup of nature's enzymes, it is the aim to design an ATPase-like enzyme mimic that is based on an innovative nanomaterial conjugate with active catalytic moieties (**Figure 27**). The conjugate allows a possible application in cells due to the utilization of highly biocompatible materials. So far, literature only reports efforts to mimic the setup of enzymes with their core-shell properties in dendrimers[75] or star polymers[76] with limited catalytic activity, or approaches to imitate only the active site of enzymes with inorganic nanozymes[40] or supramolecular structures[92-94, 97]. However, all these strategies have limitations, especially for a desirable utilization in cells, which could be mitigated by combining both approaches in one; a process that has not been carried out prior to this thesis.

As an artificial cleavage site, supramolecular catalysts such as macrocyclic polyamines (**Figure 27**) can be considered for an attachment to a polymeric scaffold using bioorthogonal linkage methods. The polyamines have outstanding ATP hydrolysis capabilities in cleaving adenosine triphosphate (ATP) to its diphosphate (ADP) and were

discovered and intensively investigated in the 1980s by *J. M. Lehn.*[136-137, 139] In addition, the ATP balance is an interesting target for artificial enzyme-like catalysis with ATPases following this design principle. The bonding between the three inorganic phosphate anhydrides of ATP stores sufficient energy to make ATP the energy source for most metabolic cell reactions. Hence, natural ATPases are a relevant and necessary part of cellular energy metabolism.[119] However, as previous literature shows, macrocyclic amines do not have the possibility for an attachment to a nanomaterial. To overcome this limitation, it is the aim to chemically synthesize and modify those supramolecular catalysts with a connectable functional group.

The carrier system of the artificial catalytic site has to ensure the generation of an enzyme-like local environment. It is planned to use the polysaccharide dextran as scaffold material.[211-212] Similar to the peptide backbone in natural enzymes, the polysaccharide represents a polymeric carrier scaffold with multiple attachment points and can be functionalized with macrocyclic polyamines. As a result, by attaching the macrocyclic polyamine-based catalyst to the dextran-based carrier an entire artificial enzyme can be created (**Figure 27**).

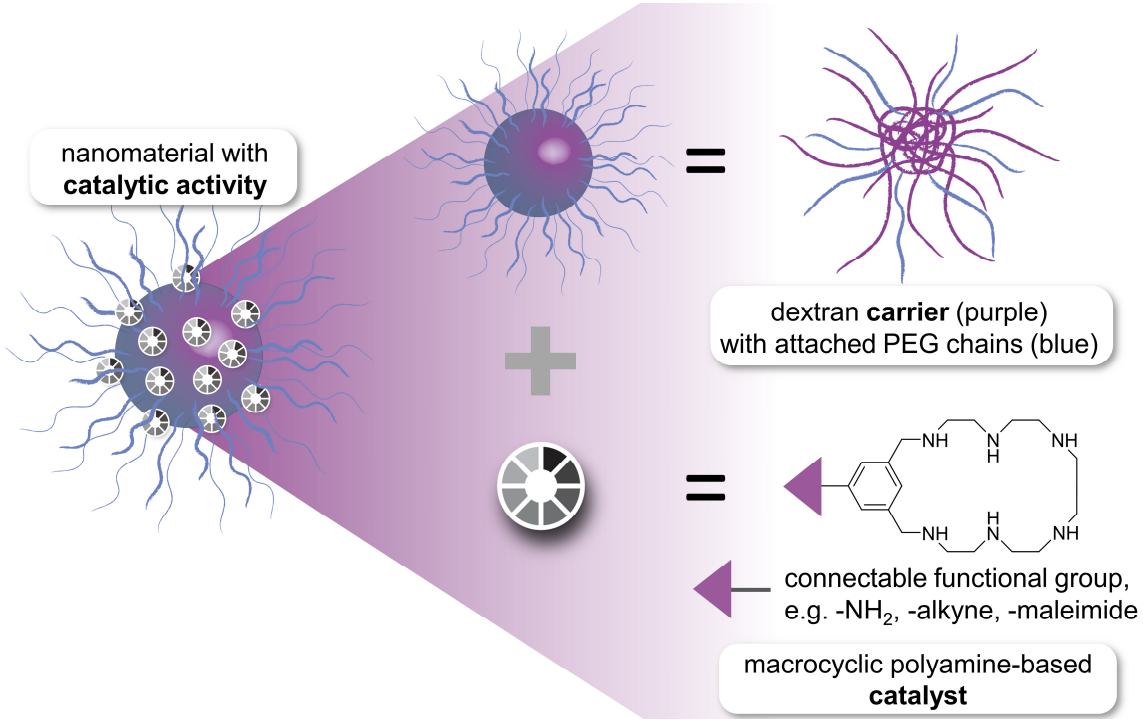

Figure 27: Design of an artificial ATPase-like enzyme which is planned to be based on a dextran carrier material and attachable supramolecular polyamine-based catalysts. The carrier material can be further modified with PEG chains to create an enzyme-like core-shell structure. It is the goal to demonstrate catalytic activity in ATP cleavage in relevant *in vitro* assays with the designed nanomaterial.

Inspired by nature's core-shell structures, it is planned to attach a poly(ethylene glycol) (PEG)[213] shell on top of the dextran carrier. It is the aim to investigate the biocompatibility of the system through toxicity screenings in HeLa cells. The catalytic activity, more precisely the ATP hydrolysis of the system shall be investigated in *in vitro* assays by using ^{31}P-NMR spectroscopy.

In conclusion, the first main aim of this thesis is the development, chemical synthesis and modification of synthetic polysaccharide-based biopolymers to obtain multifunctional carrier materials and if possible imitate the core-shell structure of natural enzymes. Functionalizing them with supramolecular, catalytically active moieties such as macrocyclic polyamines in order to mimic enzymatic activity will lead to entire artificial enzymatic structures. Through the study of such a system, significant advances can be made towards the creation and understanding of artificial enzymes.

2.2 Bioinspired Enzymatic Cascade Reactions

In nature, the association of single enzymes to greater, functional entities can be observed. Enzymes often assemble into multifunctional molecular machines, e.g. the tryptophan synthase[152] or in ribosomes[164], to meet the demands of more complex reactions. Looking more closely at the general function of such molecular machines, one can observe that their assembly is mainly favorable to the proceeding of enzymatic cascade reactions. Cascade reactions proceed optimally if close proximity between both active centers is given. This requirement can be fulfilled by various artificial techniques such as immobilization, encapsulation or gene fusion of different enzymes.[180] Nevertheless, there are currently no known ways to achieve small spatial distance without using catalytically non-active material or losing enzymatic activity.

In this thesis, a new innovative approach is planned. Catalytically active, short peptide sequences will be designed containing histidines, that are known for their esterase-like activity.[214-216] Using bioorthogonal conjugation techniques[217], these peptides shall then be attached to the surface of an enzyme, for example to cytochrome *c* (Cyt *c*), which has a distinct peroxidase activity (**Figure 28**). After conjugation, it is the plan to investigate the individual activity of both enzymatic reactions, the peptide-mediated esterase-like and the original, intrinsic peroxidase functionality, separately in respective assays. In subsequent

experiments, combination of both catalytic functionalities shall lead to the proceeding of an artificial cascade reaction.

In order to demonstrate the transferability of the developed system, enzymes other (or different) than Cyt *c* will be modified with the catalytically active peptide sequence and will be investigated towards their additional esterase-like functionality after the attachment of the peptide. A comparison regarding the extent of chemical modification with the peptide on the surface will be given.

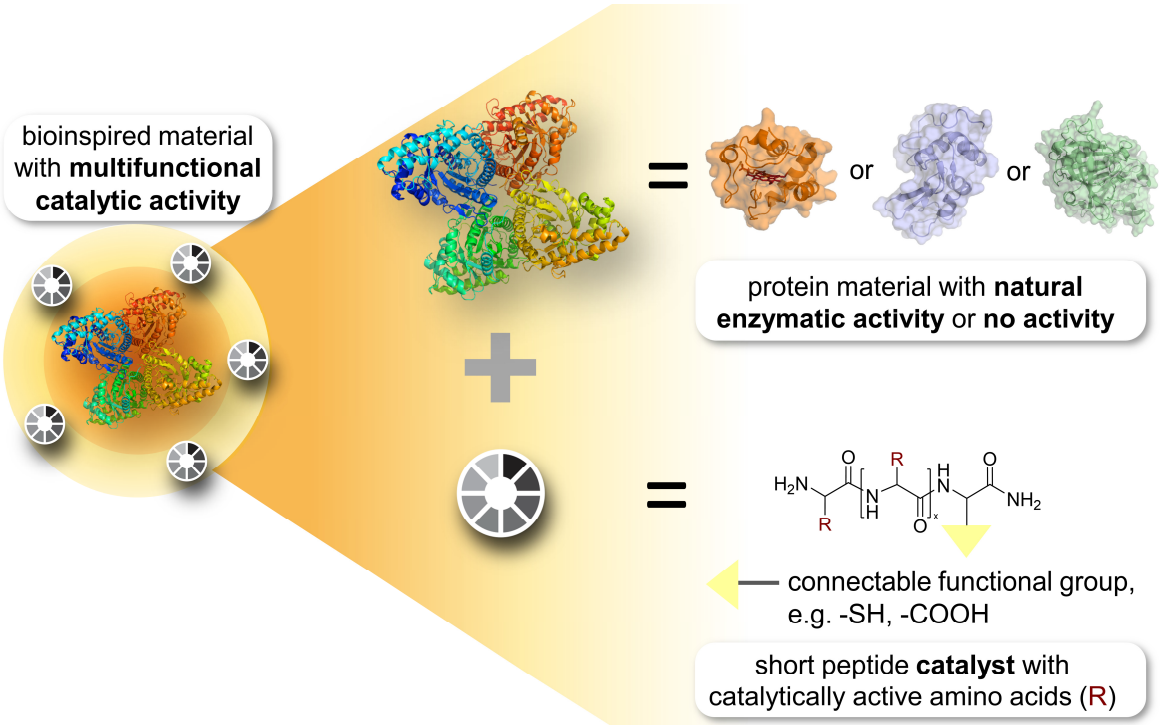

Figure 28: Design of a bioinspired material with multifunctional catalytic activity. The material itself consists of either an enzyme with a distinct activity or a protein with no catalytic activity. By attaching a short peptide sequence to the surface of the proteins using bioorthogonal linker chemistry, it is planned to introduce an additional catalytic activity to the material.

The second main aim of this thesis is the mild surface modification of enzymes with catalytically active peptide structures to obtain a biomaterial with additional functionality. If the selected enzyme has already intrinsic activity, it is planned to carry out cascade reactions between the catalytic surface layer and the active site of the enzyme. Such an artificial enzymatic cascade, performed within one biomaterial, can provide new opportunities for mimicking complex biochemical processes and to obtain understanding towards the development of novel, improved biocatalysts for industrial and therapeutic applications.

3 Results and Discussion

3.1 Artificial ATPase-like Enzyme

This first part of this chapter describes the design of an artificial enzyme-like system that mimics the function of ATPases. In a polymer-based approach, setup and features of a natural enzyme structure will be imitated. A new conjugate of a polysaccharide-based carrier material and a macrocyclic polyamine catalyst will be developed to obtain artificial ATPase-like enzymes. The synthesis, modification and evaluation will be established and described in the following chapters.

3.1.1 General Approach

The composition and architecture of natural enzyme structures are described in chapter **1.1**. As mentioned, previous approaches to mimic enzymes are limited to the use of either polymeric material with limited activity or supramolecular catalysts that imitate only the active sites of the enzymes. Inspired by nature's polypeptide chains, a polymeric scaffold will be used as a carrier material with multiple attachment points to conjugate supramolecular catalysts which have catalytic activity. Thus, a nanomaterial with catalytic properties is created. Furthermore, nature's core-shell organization with a catalytically active core and a protecting shield or corona around the active site is transferred to the artificial nanosystem. The core with the catalyst is based on the natural polysaccharide dextran[212] whose anhydrous glucose units (AGU) are functionalized with bioorthogonal reactive groups to allow the attachment of the catalyst and a shielding corona of hydrophilic poly(ethylene glycol), abbreviated PEG. The catalytic active sites inside of the enzyme mimic is built up by several supramolecular catalysts. Such supramolecular catalysts are macrocyclic polyamines which are known to be highly selective in cleaving ATP (adenosine triphosphate) to its diphosphate (ADP).[136]

Bioconjugation Chemistry and Bioorthogonal Reactions

First of all, the attachment of the active biocatalyst to the dextran-based carrier requires a conjugation method. The chemical strategy of linking two molecules of which at least one is a biomolecule is called bioconjugation chemistry. Biomolecules such as proteins or polysaccharides offer natural functional groups like amino- or hydroxyl groups which can

be used for conjugation of small molecules to the biomacromolecules[217] or for crosslinking of complex polysaccharide-protein conjugates.[218] Bioconjugation is often challenging because the used biomolecules offer only a limited number of functional groups and modifications have to be carried out under mild conditions. Room temperature or colder is often desired, and aqueous or buffered solutions have to be used. These demands are often not compatible with classical organic synthesis methods. A variety of reaction possibilities under mild conditions provide amino groups.[217] NHS-ester reactions[219] or classical amide formation[220] between acid and primary amine can be performed under physiological conditions such as low temperatures, aqueous solutions or pH range around 7. Amino groups are by far the most common functional groups present in crosslinking or modification reagents. Thus, an amino group-based approach was used for the modification of the macrocyclic polyamine and its application as catalytic active site.

However, the introduction of such a multifunctional and versatile group increases the possibilities for side reactions and undesired reaction products. Avoiding this issue, bioorthogonal chemistry can be used. A bioorthogonal reaction is defined as a selective and rapidly occurring reaction in the presence of various other functionalities like thiols, amines, carboxylates or sulfates.[221-222] One of the most popular examples is copper-mediated click-chemistry between azides and alkynes. The 1,4-cycloaddition which was developed 20 years ago has been constantly improved. To date copper-free variants[223] using strained cyclooctynes (**Figure 29**) are well known. This bioorthogonal conjugation methods allows the application even in living organisms.[224-225]

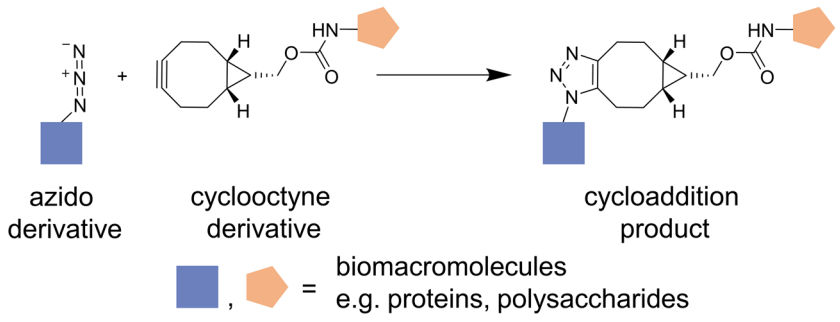

Figure 29: General cycloaddition reaction of an azide group with a strained cyclooctyne group resulting in a triazole.

A second bioorthogonal reaction is using sulfur chemistry. Right after amino-reactive groups, sulfhydryl-containing molecules are the second most common functional group used in crosslinking or modification reagents. The reactions occur quite fast and in high

yields resulting in stable thioether or disulfide bonds. A common used reaction is the nucleophilic attack of thiols with soft electrophilic alkenes such as maleimides (**Figure 30**) or iodoacetamides. Maleimides or more specifically maleic acid imides are formed by the reaction of maleic anhydrides with ammonia or primary amine-containing compounds.

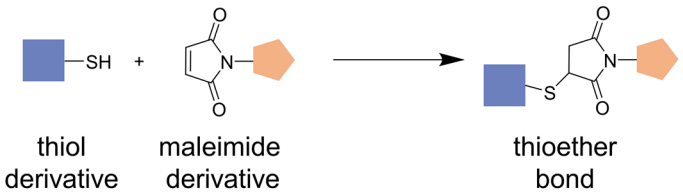

Figure 30: Bioconjugation reaction using sulfur chemistry. A thiol reacts with a maleimide resulting in a stable thioether bond.

The pH value matters for the reactivity of the thiol with the maleimides, because only in a pH range of 6.5 to 7.5 the reaction is specific for thiols.[226] At pH 7 the reaction is approximately 1000-fold enhanced compared to the reaction with amines. If the pH increases, side reactions with amino groups can occur.[227] A further disadvantage of the reaction is, that at long reaction times maleimide groups can hydrolyze to their open, unreactive form. These issues must be considered once applying this bioconjugation strategy.

A third, very selective reaction is the reaction of aldehydes with aminooxy (alkoxyamine) groups or hydrazines (**Figure 31**). In contrast to the reaction of primary amine with aldehydes or ketones (*Schiff* bases) which results in a relatively labile, reversible bonding the oxime linkage is a very stable bond. The bond does not require further stabilization through reduction as used for the *Schiff* base formation and has been used in many bioconjugation reactions.[228-229] The reaction is not completely considered as bio-orthogonal because in biochemical process a lot of aldehyde and ketone metabolites are present.

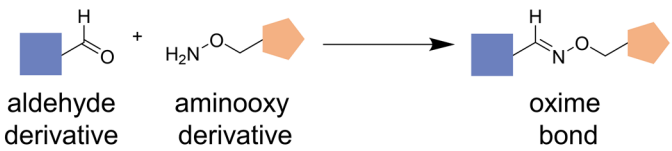

Figure 31: Formation of an aldoxime using a type of irreversible *Schiff* base formation.

The reaction speeds up if using aniline as catalyst.[230] The aniline reacts first with the aldehyde resulting in an imine, which represents an intermediate *Schiff* base and activates the aldehyde. The formed imine is then subsequently replaced by the aminooxy group yielding the oxime linkage in high yields.[231-232]

The three presented bioorthogonal conjugation methods will be used in the design of the artificial enzyme mimic and applied as strategies to connect the supramolecular catalyst to the dextran-based carrier as well as the attachment of a shielding corona.

3.1.2 Modified Macrocyclic Polyamines as Active Sites

This chapter deals with the synthesis and modification of catalytically active, supramolecular structures which can introduce artificial cleavage sites to the enzyme mimic.

As early as the 1980s, J. M. Lehn and co-workers reported the synthesis and properties of polyammonium macrocycles as anion receptor molecules[134] and later on their catalysis abilities[136] regarding the ATP hydrolysis. The supramolecular investigations of the macrocyclic polyamine 1,13-dioxa-4,7,10,16,19,22-hexaazacyclotetracosane called *O*-bis-dien or [24]N_6O_2 **1** (**Figure 32**) with various phosphates[138, 142, 233] were their focus and led among other findings to the Nobel Prize in chemistry in 1987. He is said to be one of the earliest innovators in the field of supramolecular chemistry and his work is the basis for the development of the herein described modifications of macrocyclic polyamines as catalytic active sites for artificial enzyme mimics. In the beginning of this PhD project, macrocyclic polyamines derived from the budmunchamine family of alkaloids[147] were modified for an attachment to a carrier system. Those compounds were already used in biological contexts to deplete cellular ATP levels.[148] The results of these syntheses and their ATP hydrolysis evaluation are mainly reported elsewhere.[234] In fact, the hereby synthesized structures did not lead to desired ATP cleavage, hence other macrocyclic polyamines with an aromatic unit were used as basis for the development of an attachable macrocyclic polyamine.[144] The cyclophane receptor 2,5,8,11,14,17-hexaaza[18]meta-cyclophane **2** (**Figure 32**) has one of the largest rate enhancements for the hydrolysis of ATP[144] compared to published macrocyclic polyamines, published by that time.

The increased rates can be explained by the introduced benzylic unit which forces the electrostatic interactions and the π-stacking of host and guest in supramolecular cooperation. Before, it has been shown that up to two acridine units attached to *O*-bisdien enhance the ATP binding and hydrolysis.[143] Additionally, the published synthesis route of 2,5,8,11,14,17-hexaaza[18]metacyclophane **2** seemed straightforward and alterable.

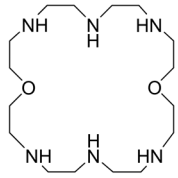

1

1,13-dioxa-4,7,10,16,19,22-hexa-azacyclotetracosane

O-bisdien

[24] N_6O_2

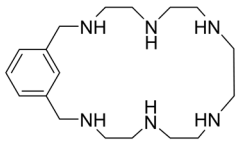

2

2,5,8,11,14,17-hexaaza[18] metacyclophane

Figure 32: Structures and names of published macrocyclic polyamines with high ATP hydrolysis rates.

Synthesis of the Reference Compound 2,5,8,11,14,17-Hexaaza[18]metacyclophane

In order to have a comparable, reference compound for further studies regarding especially the ATP cleavage measurements, the literature known macrocyclic amine (MCA), 2,5,8,11,14,17-hexaaza[18]metacyclophane **2** was synthesized (**Figure 33**). Another reason was, that the synthesis route for the amino-modified polyamine should be based on the one for MCA **2**. Additionally, getting used to the handling of the polyamines and their purification was a positive side effect. For the synthesis, the published route by *Aguilar et al.*[144] was overall optimized. In particular the first step, the protection of the polyamine and the last step, the remove of the protecting groups were transferred from other molecules. First, the protection of the 3,6,9,12-tetraazatetradecan-1,14-diamine **3** with *p*-toluene sulfonic acid **4** was evaluated and optimized based on different literature procedures. The tosyl protecting group is used here because it is a relatively bulky protecting group that shields the secondary amines and allows reactions mainly at terminal amino groups.

Published synthesis routes for the protection of analogous, shorter polyamine sequences in tetrahydrofuran (THF) with an aqueous solution of the base sodium hydroxide (NaOH)[235] as well as a synthesis in diethyl ether (Et_2O) at 0 °C[236] afforded either no desired product or product in yields below 5%. However, the protection carried out in pyridine at 50-60 °C and a slow addition of 3,6,9,12-tetraaza-tetradecane-1,14-amine **3** [237] led to the protected polyamine **5** as a beige solid in 40% yield. The structure was confirmed by standard techniques like nuclear magnetic resonance (NMR) analysis, in particular ^1H, ^{13}C, DEPT-135 (distortionless enhancement by polarization transfer), COSY (homonuclear correlation spectroscopy), HSQC (heteronuclear single quantum coherence) and HMBC (heteronuclear multiple bond correlation) spectra.[238-240] Mass spectrometry (LC-MS) and

if applicable infrared spectroscopy (IR) were utilized as standard analytical methods for structure determination of organic compounds and will not further be highlighted if used.

The macrocyclic amine MCA **2** was prepared by K_2CO_3 templated cyclisation of the linear tosylamide precursor **5** with 1,3-bis(bromomethyl)benzene **6**.[144, 235] In a nucleophilic substitution reaction the free electron pair of the protected terminal amino groups attacks the positively polarized methyl carbon in the 1 and 3 position of the aromatic unit. The reaction occurs in the nonpolar solvent acetonitrile with high excesses of the base K_2CO_3. 1,3-bis(bromomethyl)benzene **6** was highly diluted and added during 18 h considering the *Ruggli-Ziegler* dilution principle which implies that the intramolecular reaction is favored compared to the intermolecular reaction if the reaction is carried out in high dilutions. The principal bases on the fact that the probability of the end to end reaction of the corresponding molecules (intramolecular reaction) is independent of the concentration of the molecules. However, the probability that two different molecules meet (intermolecular reaction) decreases with dilution. With the help of the principle, the already low yields of cyclisation reactions can be optimized and afforded 2,5,8,11,14,17-hexakis(*p*-tolylsulfonyl)-2,5,8,11,14,17-hexaaza[18]metacyclophane (MCA(Ts)$_6$) **7** as a white solid in 65% yield.

The release of the free, secondary amino groups after deprotection can be performed in various synthesis routes.[241] A *Birch*-similar reduction in condensed ammonia at −70 °C with lithium is one possibility[144] as well as the detosylation with phenol and 48% HBr[236]. 2,5,8,11,14,17-Hexaaza[18]metacyclophane **2** was received after the latter procedure. After refluxing **7** in 48% HBr at 130 °C for 50 h and washing of the aqueous phase with chloroform ($CHCl_3$), the strongly acidic, aqueous solution of the bromide salt of the deprotected polyamine was cooled to 0 °C. The pH was gradually increased up to 12 while a significant color change from purple to yellow occurred, demonstrating the change of the electron density and distribution in the aromatic system. The product 2,5,8,11,14,17-hexaaza[18]metacyclophane (MCA) **2** was again extracted with $CHCl_3$ and obtained as a yellow oil in 37% yield. The ATP hydrolysis of MCA **2** was successfully evaluated with ^{31}P-NMR resulting literature comparable kinetic rates (see for details **3.1.6**).[144] The described synthesis of 2,5,8,11,14,17-hexaaza[18]metacyclophane **2** was used as the basis for development and synthesis of a macrocyclic polyamine that can be linked to the dextran-carrier.

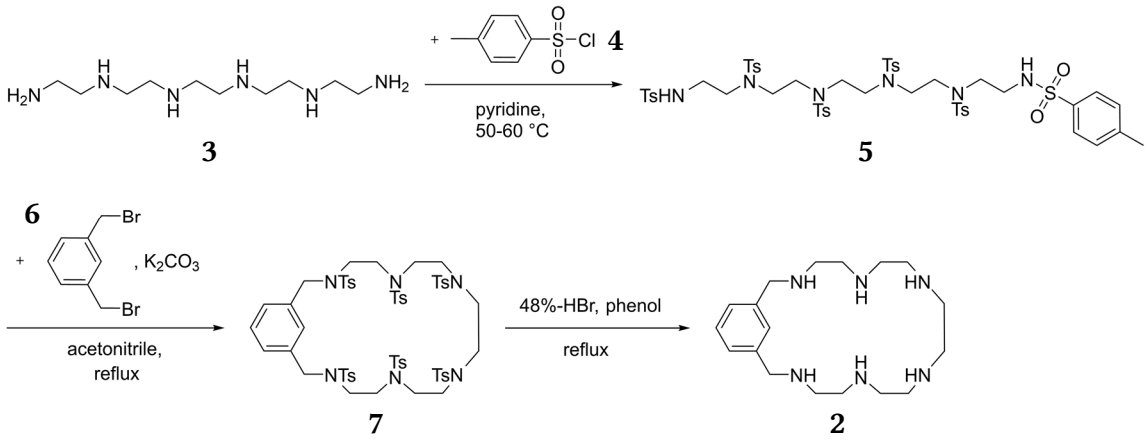

Figure 33: Synthesis of published macrocyclic amine **2** in a slightly modified procedure of *Aguilar et al.*[144] Especially the first and the last step of the synthesis was optimized.

Synthesis of Functionalized Macrocyclic Amines

As described in the paragraph on Bioconjugation Chemistry, introduction of an amino group to the aromatic ring unit of 2,5,8,11,14,17-hexaaza[18]metacyclophane **2** (**Figure 34**) provides a powerful tool for further conjugation possibilities. As an ideal position for the amino group the meta position referring to the -(CH_2)-Br groups was considered. In first experiments, various nitration strategies of 1,3-bis(bromomethyl)benzene **6** were evaluated. The nitro group serves as a precursor for amino groups at aromatic compounds because the nucleophilic aromatic substitution proceeds very slowly compared to the electrophilic aromatic substitution with a nitrosyl cation. The introduced nitro group can be easily reduced to an amine afterwards. The reaction in pure 65% HNO_3 at −5°°C[242] yielded no separable product, only mixtures of miscellaneous mono-substituted 1,3-bis(bromomethyl)-nitrobenzenes were obtained. Such mixtures were obtained with reaction mixtures of Ac_2O and 65% HNO_3 at −20 °C[243] and as well the classical nitrating solution[244] consisting of a mixture of concentrated sulfuric acid and nitric acid at 0 °C. Since introduction of an amino group via direct nitration of 1,3-bis(bromomethyl)benzene **6** failed, the synthesis of the desired molecule was approached in a different way. Already 1,3,5-substituted aromatic amino compounds were used as starting point for modifications. As one example, 3,5-dimethylaniline was brominated with *N*-brom-succinimide (NBS) **9** and azobisisobutyronitrile (AIBN)[245] in dichloromethane (DCM) in a radical substitution process. This reaction resulted in multiple bromine-substituted product mixtures even substituted at the aromatic protons probably due to the +M (mesomeric) effect which is here significantly higher than the –I (inductive) effect. The reaction did obviously not occur in a radical mechanism rather in a typical electrophilic substitution. The reaction

was also carried out in carbon tetrachloride (CCl_4), a nonpolar solvent in which the developed succinimide precipitates and can be easily removed. However, those reactions conditions led also to a substitution at the aromatic core. In order to have a different aromatic environment, in particular, a different distribution of the electron density at the aromatic ring, a further approach was the protection of the amino group of 3,5-dimethylaniline with a protecting group hoping that this leads to the desired substitution pattern. The protection of the amino group was successfully carried out with benzyl phenyl carbonate (Cbz) as well as *tert*-butyloxycarbonyl (Boc) intolerably yields. However, the subsequent radical substitution reactions with NBS and AIBN led to a substitution at the aromatic core and not to the desired substitution with bromine at the 1,3-methyl groups. The combination of both evaluated strategies – using a nitro group and bromination with NBS and AIBN – led finally to the successful synthesis of 1,3-bis(bromomethyl)-5-nitrobenzene **10** (**Figure 34**).

5-nitro-1,3-xylene **8** was used as starting material in a modified radical substitution with NBS **9** and benzoyl peroxide (BPO) in CCl_4 after a published procedure.[246] The product was obtained in 27% yield after column chromatography. The low yield can be explained by the various developed side products. All of them were isolated in different fractions and analyzed after the purification process demonstrating the appearance of multiple substituted brominated methyl groups in not negligible yields. Various attempts were carried out to increase the yield of 1,3-bis(bromomethyl)-5-nitrobenzene **10** but either different amounts of NBS **9** nor altered reaction times or temperatures led to yields over 30%.

The second building block, the 1,4,7,10,13,16-hexakis(*p*-tolylsulfonyl)-1,4,7,10,13,16-hexaaza-hexadecane **5** was synthesized as described for 2,5,8,11,14,17-hexaaza[18]meta-cyclophane **2**.[237] (**Figure 34**).

The cyclisation of 1,3-bis(bromomethyl)-5-nitrobenzene **6** with 1,4,7,10,13,16-hexa-kis(*p*-tolylsulfonyl)-1,4,7,10,13,16-hexaaza-hexadecane **5** was carried out in a similar manner as described for the precursor described above.[144] In this case, the reaction is supported by the strong –M and –I effect of the nitro group which additionally withdraws electron density from the aromatic ring.

After 2 days of refluxing the reaction mixture was purified by column chromatography and 2,5,8,11,14,17-hexakis(*p*-tolylsulfonyl)-21-nitro-2,5,8,11,14,17-hexaaza[18]metacyclo-phane (NO_2-MCA$(Ts)_6$) **11** was obtained as a colorless solid in 35% yield. The formation of

the side products, like the polyamine chain with two aromatic units at each end was observed as well as bigger macrocyclic products.

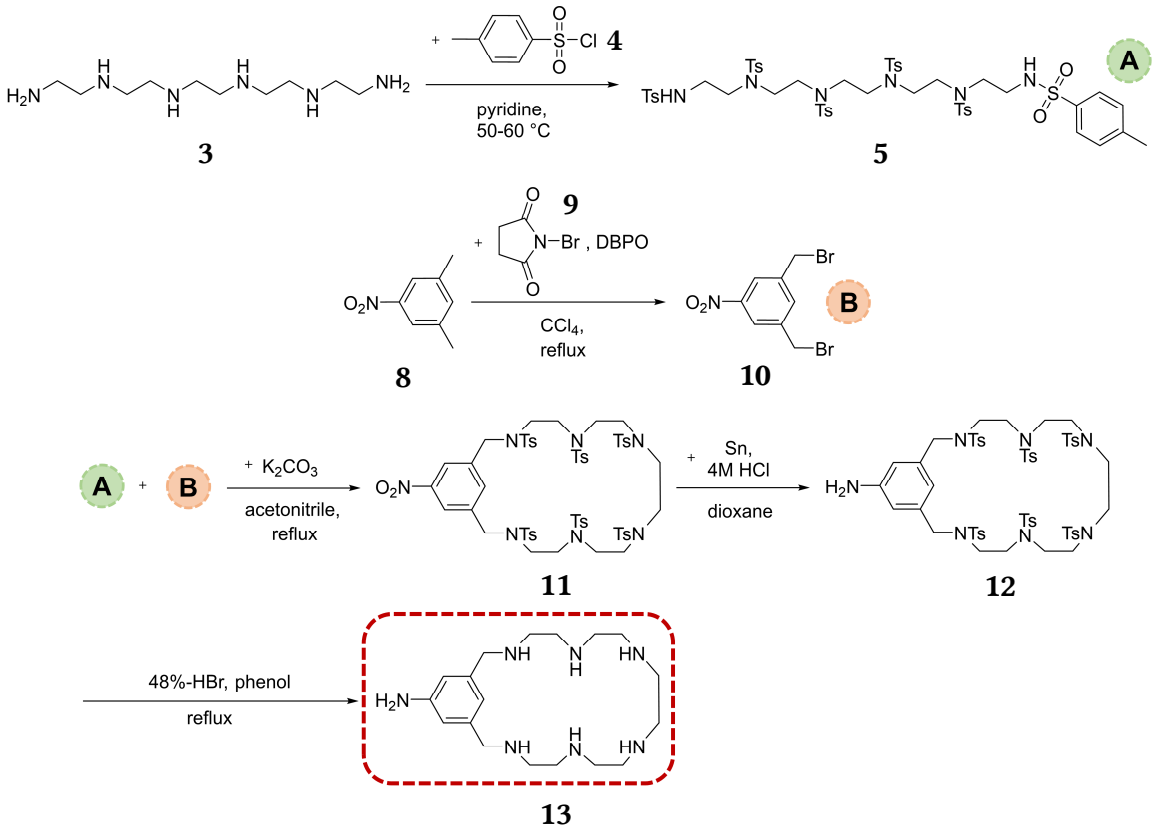

Figure 34: Synthesis of the amino-modified macrocyclic amine **13** (NH_2-MCA).

The next step was the reduction of the nitro group to an aromatic amine group. Therefore, various reduction methods were evaluated. In order to keep as much as possible of the in multistep synthesized compound NO_2-MCA(Ts)$_6$ **11**, 5-nitro-1,3-xylene **8** was used as a model molecule. First, the typical reduction conditions with tin powder in hydrogen chloride (HCl 36%)[244] under reflux for 1 h was carried out. However, this failed for the reduction of 2,5,8,11,14,17-hexakis(*p*-tolylsulfonyl)-21-nitro-2,5,8,11,14,17-hexaaza[18]-metacyclophane **11** because of the bad solubility of the starting material in aqueous solutions. As an alternative, the reduction was tried with hydrogen (H_2) and palladium (Pd) on carbon in methanol (MeOH).[247] Palladium on carbon (Pd/C) is a form of palladium distributed on activated carbon to maximize its surface area and its activity. The successful reduction in a hydrogenation pressure vessel was shown by the ninhydrin reagent which colors primary amines in a significant purple color. The reaction process can be observed by comparing the starting material's color with the product's dye. However, this reduction method failed for **11**, since the compound is not soluble in MeOH. One possible solvents is ethyl acetate (EtOAc) which was tested with H_2 and Pd/C in the hydrogenation vessel but

leading mainly to the development of acetic acid and dioxane which did not show any conversion of the starting material. Nevertheless, the use of dioxane as possible solvent for **11** led finally to a successful reduction. With the application of 4 M HCl solution in 1,4-dioxane and tin granulate the complete reduction was achieved after 5 h under reflux and a slightly yellow product of NH_2-MCA(Ts)$_6$ **12** was obtained in 98% yield.

The almost quantitative yield was obtained after optimization of the work-up procedure in which instead of column chromatography the organic phase was washed with an aqueous sodium hydroxide as well as aqueous sodium chloride solution.

The final synthesis step, the deprotection of the tosylated macrocyclic amines NH_2-MCA(Ts)$_6$ **12** was first carried out in a same manner as successfully accomplished for the unfunctionalized MCA **2**. NH_2-MCA(Ts)$_6$ **12** was refluxed for 48 h in 48% HBr with phenol and extracted with chloroform ($CHCl_3$) to remove the water-insoluble, cleaved tosyl residues. After a pH change from acidic to basic, the product was attempted to be extracted with $CHCl_3$. For MCA **2** this worked well, however, the yields were not very good. With the introduction of an additional, seventh amine to the compound the solubility in $CHCl_3$ decreased so much, or rather the solubility in the basic aqueous phase increased so much that this extraction strategy did not work as well as before. The product 21-amino-2,5,8,11,14,17-hexaaza[18]metacyclophane (NH_2-MCA) **13** remained in the aqueous phase with a lot of different salt ions from the HBr deprotection and the pH increase with 1 M NaOH. Lyophilization of the aqueous phase resulted in a significant mass increase but it was not possible to separate the organic compound **13** from the salts in any extraction method due to the high solubility of **13** in aqueous environment.

Alternative purification methods were evaluated however the common isolation as a chloride or bromide salt was no option because of the later application in ATP hydrolysis. *Compagnone et al.* reported the use of an anionic exchange resin after detosylation.[248] The resin contains uniform particle size beads consisting of a poly(styrene-co-divinylbenzene) gel with the functional group of a quaternary amine (-NH_4^+) on its surface. Hydroxide ions are bound as counterions in the shipped form and can easily be exchanged through other stronger binding ions in the described case here through the bromine ions. **Figure 35** displays the exchange of counterions which takes place on the surface of DOWEX™ MARATHON™ A resin. The exchange of the ions can be pursued by checking the pH value of the resulting product. As a bromine salt, the aqueous solution reacts strongly

acidic. As soon as the bromide ions are then exchanged against hydroxide ions, an aqueous solution of **13** reacts basic as expected for such amine rich compounds.

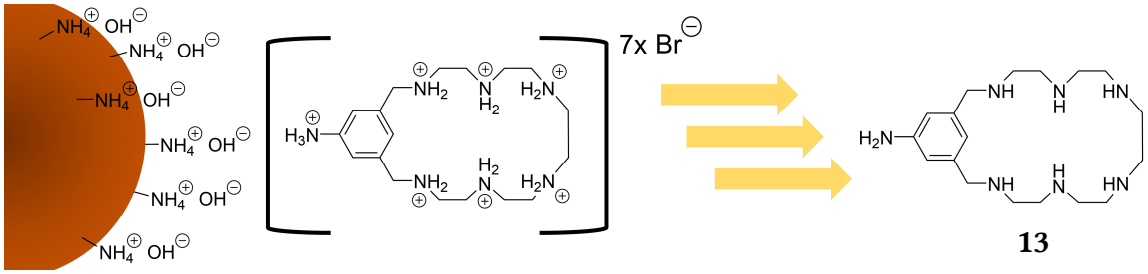

Figure 35: Purification of bromide salt of NH_2-MCA **13** with DOWEX™ MARATHON™ A resin. The anion exchange gel beads (brown sphere) carrier quaternary amine groups on their surface with hydroxide ions as counter ions. By incubating the bromide salt of NH_2-MCA with the beads, the hydroxide ions are exchanged to the bromide ions, releasing H_2O and the purified, uncharged NH_2-MCA **13**.

Since the application of the resin in a column format did not result in a complete exchange of all ions and did not result in a basic solution, respectively, the DOWEX beads were incubated with the aqueous phase of NH_2-MCA **13** which was obtained after the detosylation reaction with 48% HBr and phenol. After regeneration of the anion exchange resin with 5% NaOH, the incubation and washing had to be repeated several times. 21-amino-2,5,8,11,14,17-hexaaza[18]metacyclophane **13** was obtained as a brown oil in 86% yield. Structural clarification with NMR analytics confirmed the successful synthesis of NH_2-MCA **13**. The NMR of the bromide salt and the uncharged polyamine demonstrate a significant difference in shift due to the disparate electron density within the aromatic and the whole macrocyclic amine (**Figure 36**). The charged molecule was measured by LC-MS mass spectrometry with a mass to charge relation of 350.5 m/z which comes along with the calculated molecular weight of 349.53 g mol^{-1}. The successful synthesis of 21-amino-2,5,8,11,14,17-hexaaza[18]metacyclophane (NH_2-MCA) **13** provides an amino group-modified version of 2,5,8,11,14,17-hexaaza[18]metacyclophane (MCA) **2**. The functional group enables either the direct attachment to a carrier system using amine-based conjugation techniques or establishes new possibilities for further conjugation strategies like click-chemistry or thiol-maleimide reactions via bifunctional linker systems. Both last-mentioned approaches are used in **3.1.4** to connect the supramolecular catalysts as a catalytically active moiety to their dextran-based carrier systems.

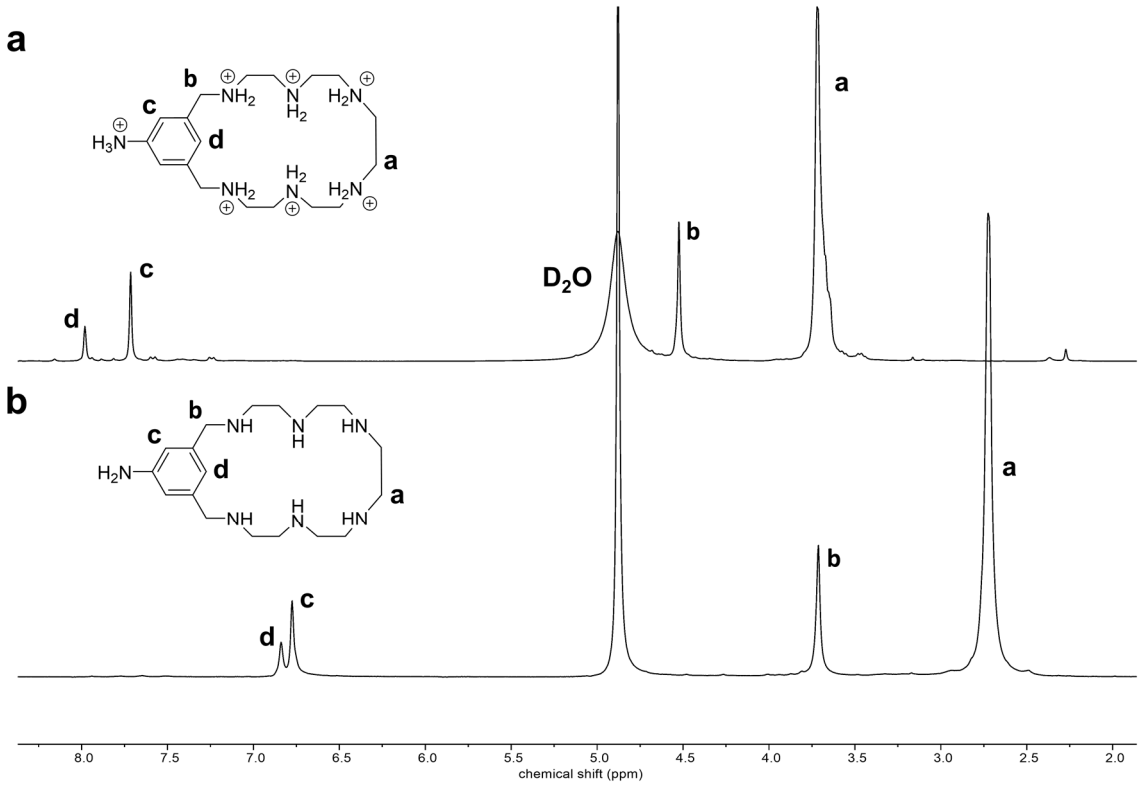

Figure 36: The ^{1}H-NMR displays significant shifts of the signals of protonated form of NH_2-MCA **13** (a) and uncharged structure (b).

Interaction of Amino-modified Macrocyclic Polyamine with ATP

The binding of nucleotides to macrocyclic polyamines has been shown over 35 years ago.[134] The interaction of ATP with the amino-modified MCA **13** is studied in ^{1}H-NMR (**Figure 37**). By comparing the spectra of ATP, NH_2-MCA **13** and the mixture of both compounds, significant signal shifts are observed. The signal of the anomeric proton of the ribose of ATP is shifted 0.11 ppm downfield as soon as NH_2-MCA **13** interacts with ATP. The adenine protons are also shifted downfield by 0.1 ppm. The benzene protons demonstrated even a signal splitting with a shift of 0.47 ppm and 0.21 ppm downfield, respectively. The shift of the single aromatic proton (**Figure 36**, Signal d) is remarkable. The demonstrated three shifts prove the involvement of π-stacking in the stabilization of the supramolecular complex. The signals of the ethylene bridges are also significantly shifted by 0.93 ppm which displays their interaction with the three phosphate groups of ATP.

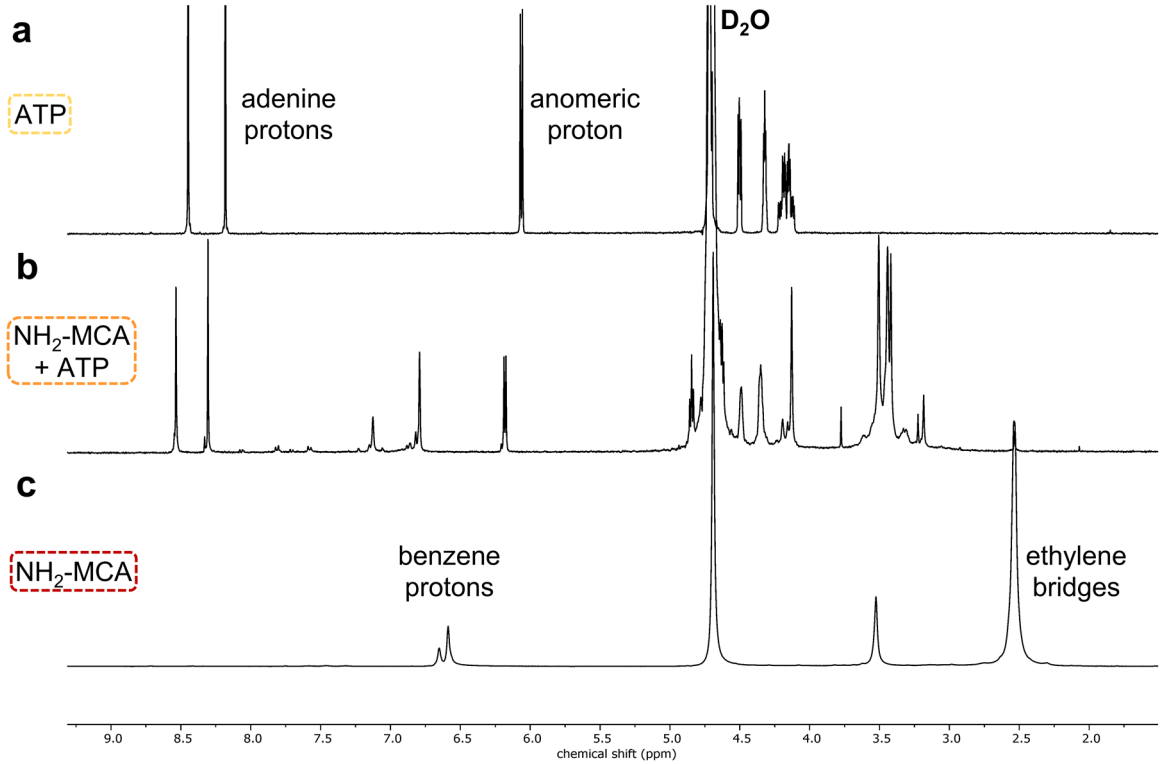

Figure 37: ^{1}H-NMR spectra of ATP (a), an equivalent mixture of NH_2-MCA **13** and ATP (b) and pure NH_2-MCA **13** (c) in same concentrations measured in D_2O. The shifts of the indicated signals of the adenine, the benzene and the anomeric proton prove π-stacking between the aromatic ring of NH_2-MCA **13** and adenine of ATP. The shift of the ethylene bridges occurs after interaction with the phosphate groups.

Cyclooctyne-modified Variant of Macrocyclic Amine

In order to have a macrocyclic amine that allows bioorthogonal conjugation, NH_2-MCA **13** was further reacted with (1*R*, 8*S*, 9*s*)-bicyclo[6.1.0]non-4-yn-9-ylmethyl *N*-succinimidyl carbonate **14**, short BCN-NHS (**Figure 38**). The hetero-bifunctional linker has an amine-reactive NHS-ester on one side and an azide-reactive cyclooctyne structure on the other end. The cyclooctyne part enables the utilization of copper-free click chemistry which is supposed to be important while working with macrocyclic polyamines (**Figure 29**). The six-membered nitrogen rings are capable of complexing copper and eliminate the transition metal, which is absolutely necessary for the azide-alkyne-cycloaddition reaction. Besides free electron pairs of macrocyclic amines are not able to interact in supramolecular catalysis with the ATP if they complex copper. Hence, a possible cleavage of ATP is excluded.

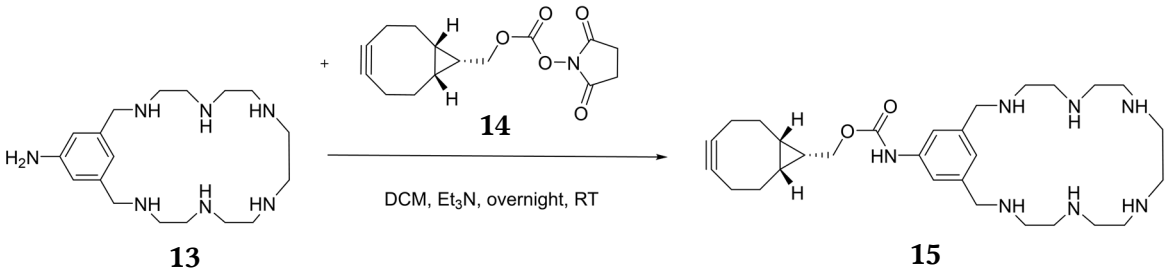

Figure 38: Reaction of NH_2-MCA **13** with BCN-NHS **14**. A cyclooctyne-modified macrocyclic amine **15** was obtained after the conjugation.

BCN-NHS **14** was reacted with NH_2-MCA **13** in a 1.1:1 (BCN-NHS: **13**) molar ratio at 0 °C overnight. This ratio allows, on one hand, full modification of the aromatic amine and prevents, on the other hand, modification of secondary amines within the macrocyclic ring which has been observed in former experiments of that kind of reaction. The purification of the reaction product turned out to be very challenging due to the amphiphilic behavior of NH_2-MCA **13** and its reaction product, the BCN-modified macrocyclic polyamine **15**. Before, the purification was possible with extraction methods shown in literature,[225] but in a reaction mixture of the BCN-modified **15** and the unmodified version **13**, this is not applicable. Standard column chromatography on silica, which was used for BCN-derived molecules,[249] was also challenging because of the smearing behavior of the amines. All amines can take on different protonation stadia which make a separation of the different species almost impossible. The use of concentrated ammonia in the solvent mixture of the column can overcome this issue by trying to keep a constant protonation environment. However, high amounts of ammonia can destabilize the product molecules which are on the column to be purified. For **15**, purification was tried several times with different solvent mixtures and furthermore with various purification methods like preparative HPLC (high-performance liquid chromatography). The product BCN-MCA **15** was always confirmed by NMR and LC-MS, but isolated in very low yields (<10%) which could not be improved. However, unpurified reaction mixtures were used for the click chemistry approach of the conjugation of catalyst and carrier (see chapter **3.1.4**).

Maleimide-modified Variant of Macrocyclic Amine

An alternative bioorthogonal conjugation method is the thiol-maleimide Michael addition reaction (**Figure 30**). For this, the amino-modified macrocyclic amine NH_2-MCA **13** was modified with a heterobifunctional linker **16** (**Figure 39**). The SM(PEG)$_4$-linker (NHS-PEG(4)-Mal) **16** has an amine-reactive NHS-ester on one end and a thiol-reactive

maleimide on the other end. Both functional groups are connected via four amphiphilic PEG units.

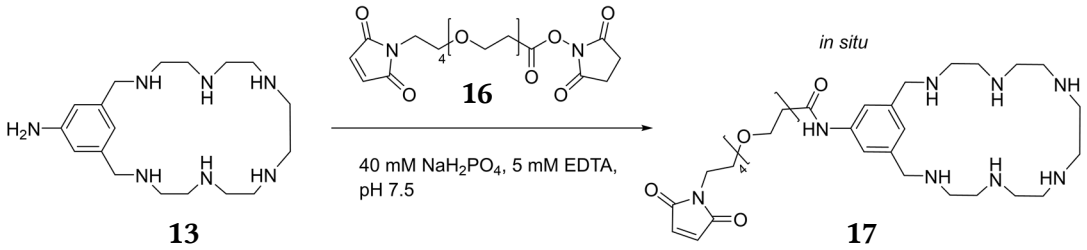

Figure 39: Reaction of NH_2-MCA **13** with $SM(PEG)_4$ (NHS-PEG(4)-Mal) linker **16**. A maleimide-modified macrocyclic amine **17** was obtained after the conjugation. The reaction product was not isolated but rather used for the attachment to a thiol-modified material.

It was not possible to purify and isolate the reaction product, because of the challenging handling with the free secondary amines of the macrocyclic polyamine as described in the previous paragraph. However, LC-MS measurements confirmed the successful synthesis of the maleimide-modified macrocyclic amine Mal-MCA **17 (6.2.2)**. The maleimide-modified variant was used for a thiol-maleimide conjugation approach in the development of the enzyme mimic.

3.1.3 Modified Dextrans as Carrier Materials

This chapter describes the design and synthesis of carrier and an additional corona for the shielding of the artificial cleavage sites of the enzyme mimic. The polysaccharide dextran **18** is functionalized with chemical groups that facilitate bioorthogonal chemistry. In detail, two different approaches will be demonstrated for the attachment of the synthesized supramolecular catalysts, as well as the possibility for further conjugation of a shielding layer to the polymeric scaffold.

The Polysaccharide Dextran

Dextran **18** is a water- and organic soluble polysaccharide. It is one of the most important polysaccharides used for biomedical applications[250] and in drug delivery (**Figure 40**).[211] Dextran belongs to the group of neutral polysaccharides and consists of an α-(1,6)-D-glucose main chain with varying proportions of linkages and branches which can be at all three remaining hydroxyl groups at position 2, 3 or 4 (**Figure 40**). Different bacterial strains, mostly gram-positive, can synthesize dextran from different varieties of sucrose. These bacteria were discovered in 1861 by Pasteur[251] and in 1878 van Tieghem termed them Leuconostoc mesenteroides.[252] The bacteria strains are found in fermented foods of plant origin. The name "dextran" was given by Scheibler.[253] Nowadays, dextran is established especially in the medical field due to its excellent solubility in water as well as in other solvents like DMSO or DMF. Dextran is a physiologically harmless biopolymer due to its biocompatible, biodegradable, non-immunogenic and non-antigenic properties. Dextran is already used in aqueous solution as blood plasma expander where it replaces blood proteins like albumin in preventing colloid osmotic pressure collapses. [254]

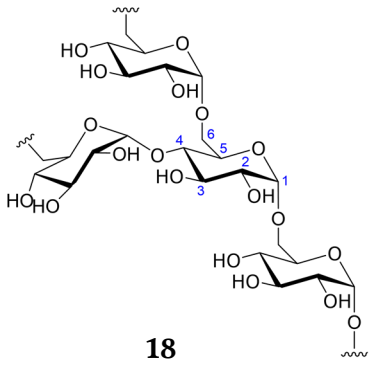

18

Figure 40: Detail structure of dextran **18** with α-(1,6)-glucose main chain and branching point in 4-position.

Dextran can be obtained with different molecular weights. Native dextran is generally of high average molecular weight ranging from $9 \cdot 10^6$ to $5 \cdot 10^8$ g·mol^{-1}. Hereby, polydispersity

increases with molecular weight which is due to increasing branching density. In the following project, dextran **18** with a molecular weight of 10000 g·mol^{-1} is used. It has 61.68 anhydrous glucose units (AGU) and one glucose unit has ideally three hydroxyl groups which are available for chemical modifications. To determine the number of chemical modifications the degree of substitution (DS) was introduced. The degree of substitution is the average number of introduced functional groups per dextran chain.

Oxidized Azide-modified Dextrans

The widely used polysaccharide dextran **18** (**Figure 40**) serves as starting material for the construction of a polymeric scaffold for the artificial catalytic site. It offers with its hydroxyl groups many derivatization possibilities[255] however modification of polysaccharides in general is challenging. Quantification and structural analysis of the modified chain by ^{1}H-NMR is difficult because of the wide distribution and high intensity of all sugar proton signals, often overlaying the signal of attached small molecules. Mass spectrometry is limited because of high molecular weights and IR spectroscopy can only provide partly information once significant groups are present. Besides, dextran is only soluble in limited organic solvents, most suitable is DMSO or water.

The experiments which led to the introduction of an azidobenzoic acid (AZBA) **19** group to dextran are extensively described elsewhere.[234] Briefly, functionalization was carried out after a published DCC/DMAP coupling procedure[256] and the resulting material Dex-$(N_3)_9$ **20** was fully characterized by NMR, IR and UV-Vis spectroscopy (**Figure 41**).

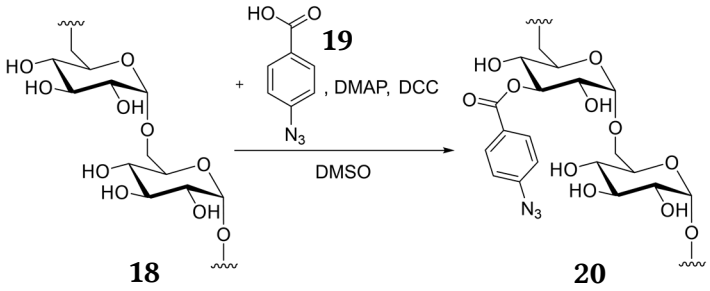

Figure 41: Reaction of dextran (Dex) **18** with azidobenzoic acid (AZBA) **19** in a DCC/DMAP coupling procedure.[256]

The azidated dextran Dex-$(N_3)_9$ **20** was obtained as a white, fluffy powder. With NMR spectroscopy the degree of substitution (DS) was determined to be 9.35 (**Figure 42**). Since the ^{1}H signals of the aromatic ring structure are located between 7.1 and 8.1 ppm and thus beyond the intense sugar proton signals. The integrals of those signals can be set in relation to the anomeric proton signal, resulting in a DS of 9.35. According to that result, every

sixth to seventh AGU is esterified. This result was confirmed by UV-Vis spectroscopy using the absorbance of the aromatic azide at 276 nm (**6.2.3**).

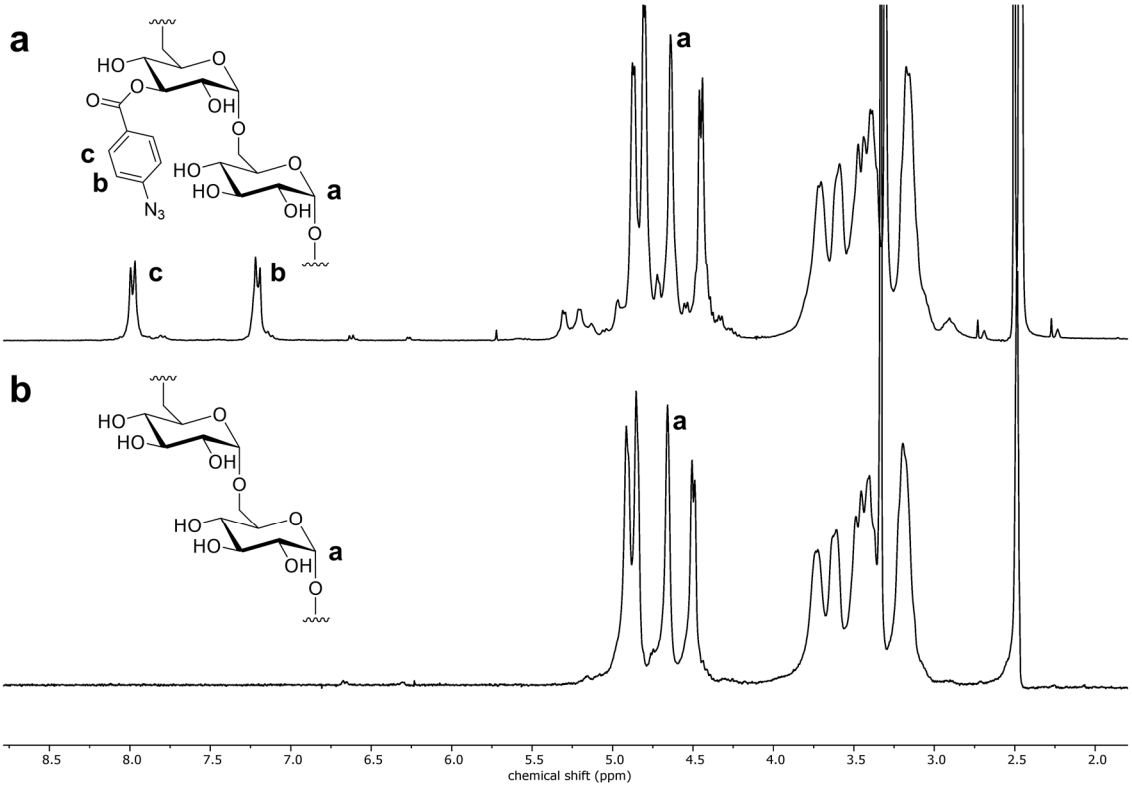

Figure 42: ^{1}H-NMR of Dex-$(N_3)_9$ **20** (a) and unmodified Dex **18** (b). By comparing the integrals of the two aromatic signals **c** and **b** and the anomeric proton **a,** the degree of substitution (DS) was determined to 9.35.

Furthermore, introduction of an azide group was confirmed by IR spectroscopy (**Figure 47**) due to the appearance of a characteristic azide bond at 2124 cm^{-1}.[244] The IR spectra shows an additional bond at 1270 cm^{-1} which can be assigned to the C-O-C valence of esters which is an extra confirmation for the successful reaction with the acid.

As part of this PhD thesis, experiments for improvement of the DS with azidobenzoic acid **19** were carried out but no enhancement was achieved. The Dex-$(N_3)_9$ **20** backbone was further oxidized with sodium periodate (**Figure 43**). This modification of polysaccharides is known since the 1950's[257-258] and often used for the introduction of a secondary, different target structure to the sugar scaffold.[259] Aldehyde groups represent important reactive sites because they offer a variety of reactions such as hydrazine linkage, *Schiff* base formation, reductive amination, *Mannich* condensation or oxime linkage.[217] However, analytics of the oxidized material is difficult because there are barely characterization methods. Since the NMR and IR spectra did not show a significant change concerning the functional azide group, the successful periodate oxidation was assumed for OxDex-$(N_3)_9$ **21**.

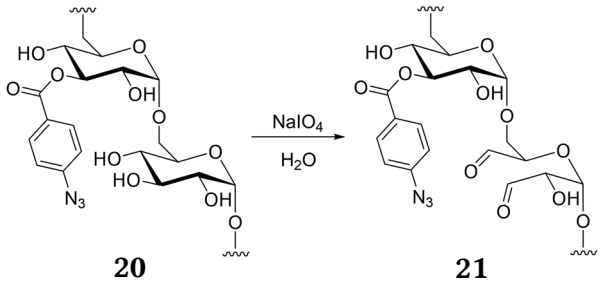

Figure 43: Periodate mediated oxidation of Dex-$(N_3)_9$ **20** resulting in accessible aldehyde groups on dextran backbone.

Dextran-PEG Polymer Brush as Full Shielding Corona System

The esterification of hydroxyl groups with azidobenzoic acid **19** and the subsequent oxidation of the polysaccharide backbone led to a biomaterial with two disparate target structures for bioconjugation (OxDex-$(N_3)_9$ **21**). The azide group is reserved for the attachment of the artificial cleavage site and the aldehyde group can be used for the conjugation of a further shielding corona to the dextran backbone. Similar to nature's core-shell approach, linear arms of poly(ethylene glycol)(PEG), can be attached to the linear dextran chain resulting in a comb-like nanosystem (**Figure 44**). With formation of such a polymer brush the architecture of natural enzymes with their core-shell properties can be mimicked more precisely.

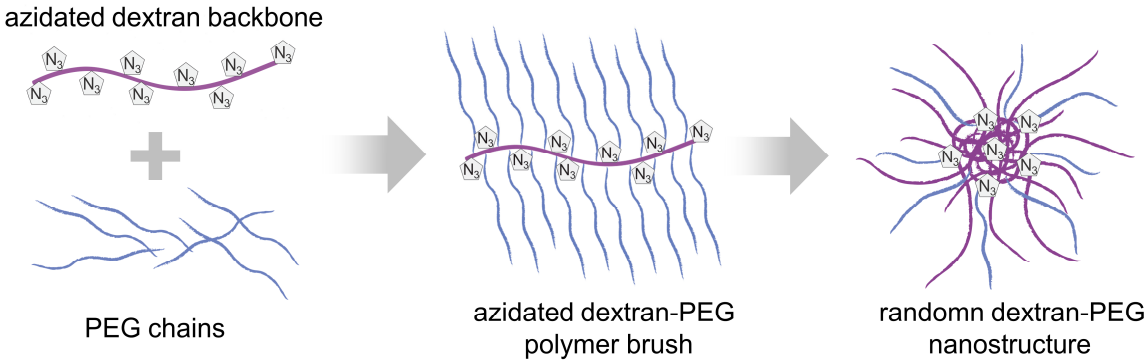

Figure 44: Formation of a full shielding corona system by combining the OxDex-$(N_3)_9$ **21** backbone with end group functionalized PEG chains **26** resulting a comb-like nanosystem which then forms a random core-shell structure.

Similar dextran-PEG conjugates were already published in 2004 for the application as long-circulating pharmaceutical carrier.[260] PEG **22** is a polyether compound with many applications in pharmaceutical research and industry.[261] It is described as a hydrophilic compound with stealth properties and often used as shell or corona material.[213, 262-263] Due to the extensive description of its properties and the diverse applications found in

literature, PEG will not be further discussed in the present thesis. The published dextran-PEG conjugate was synthesized by activating the hydroxyl groups with carbonyldiimidazole (CDI) followed by the subsequent reaction with ethylenediamine. The introduced amino groups are then able to react with NHS-ester end group-functionalized PEGs. This approach was tested elsewhere[234] but did not lead to a successful synthesis of a biomaterial with two disparate, addressable target functionalities. For the bioorthogonal modification of the dextran-based backbone, described in this new approach here, a different modification strategy was applied.

First, PEG mono methylether 2000 (2 kDa) **22** was functionalized at its hydroxyl group-end with an aminooxy group similarly to a published literature protocol.[264] The modification allows the use of the oxime ligation strategy (**Figure 31**). In a Mitsunobu reaction[265], the end group was first activated with *N*-hydroxyphthalimide (NHP) **23** using the Mitsunobu reagents diisopropyl azodicarboxylate (DIAD) and triphenylphosphine $(PPh)_3$ (**Figure 45**). After reaction overnight, the product PEG-NHP **24** was purified and obtained as a rose solid in 77% yield. The NMR displayed complete activation of all PEG chains with NHP. In a second reaction step, the phthalimide moiety was cleaved using hydrazine monohydrate **25**.

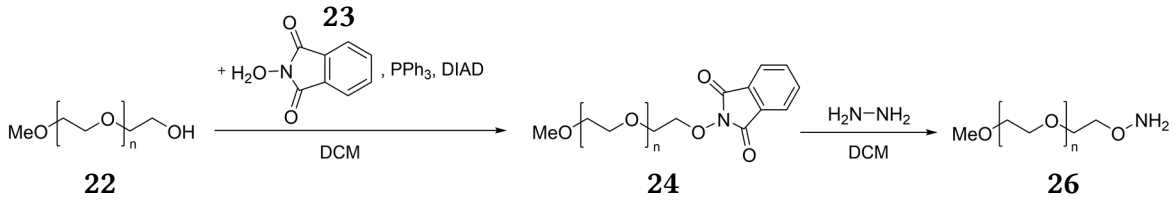

Figure 45: End-group functionalization of mPEG 2000 **22** (n=45.5). In a Mitsunobu reaction the end group is first activated with *N*-hydroxyphthalimide (NHP) **23** and then replaced by hydrazine monohydrate **25**.

After addition of the diamine, the mixture was stirred for further 30 min. A white precipitate of phthalylhydrazine occurred during the reaction. The precipitate was filtered off over glass wool and removal of solvent under reduced pressure resulted in a white solid of aminooxy-modified PEG **26** with 82% yield. NMR analytics demonstrated full conversion of the activated chain end group. Additionally, aminooxy-modified PEG **26** was stained with ninhydrin on a TLC plate resulting in a purple color compared to the starting material mPEG **22** and the intermediate PEG-NHP **24** which had no significant coloration. Synthesis was likewise successfully carried out with mPEG 5 kDa but not yet applied for the design of a core-shell material.

The polymer brush based on the dextran backbone was then completed by the oxime ligation reaction of OxDex-$(N_3)_9$ **21** and aminooxy-modified PEG **26** (**Figure 46**). The

reaction was carried out in pH 6.5 buffered solution using aniline as a catalyst[230] in equivalent amounts to the aminooxy-modified PEG **26** . After a first reaction of aniline with the aldehydes of the dextran backbone for 45 min, the end-group functionalized PEG **26** was added to the stirring solution and stirred for further 7 h. After purification by extensive dialysis first in a dialysis tube with molecular weight cut-off (MWCO) of 12–14 kDa followed by using a dialysis tube with MWCO 50 kDa, the product OxDex-$(N_3)_9$ $(PEG)_{16}$ **27** was obtained after lyophilization as a colorless powder with a 2.5-fold mass increase.

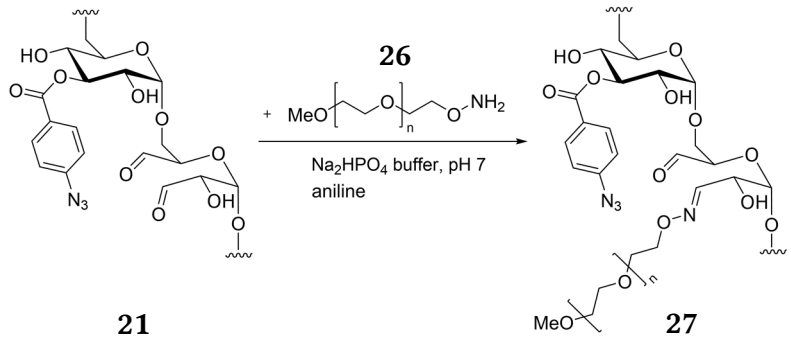

Figure 46: Reaction of OxDex-$(N_3)_9$ **21** with aminooxy-modified PEG **26** resulting in comb-like polymer brush of OxDex-$(N_3)_9$ $(PEG)_{16}$ **27**.

NMR spectroscopy confirmed attachment of the PEG chains **26** to the dextran-based backbone **21**. By comparing the integrals of the anomeric proton of the dextran AGUs and the methyl end group of PEG, DS can be determined to 16.5. Molecular weight of the resulting polymer brush amounts thus to 43000 g mol^{-1}. This molecular weight was confirmed by size exclusion chromatography (SEC, same as gel permeation chromatography, GPC).[266] The technique separates analytes on the basis of their sizes and is often used for the analysis of polymers.[267] SEC measures rather the molecular volume than the retention time on the column. Using comparable standards, the relative molecular volume values are used to determine the molecular weights within ±5% accuracy. Often, polystyrene is used as standard. Due to difficult comparability of dextran and polystyrene measured and calculated molecular weight can only be used as an encouraging information not as an absolute indicated value.

In addition, IR spectroscopy was carried out to compare the spectra of the linear OxDex-$(N_3)_9$ **21** with the polymer brush **27** (**Figure 47**). The azide signal at 2124 cm^{-1} was preserved after reaction with PEG-O-NH_2 **26**. Besides the polymer brush **27** has a significant increase in signal at 2880 cm^{-1} which can be clearly assigned[244] to the valence of methyl ethers. Dextran samples show already a weak signal due to the glycosidic bond

between the AGUs which is similar to such an ether bond. However, intensity of signal is clearly intensified which confirms the introduction of PEG arms to the dextran backbone.

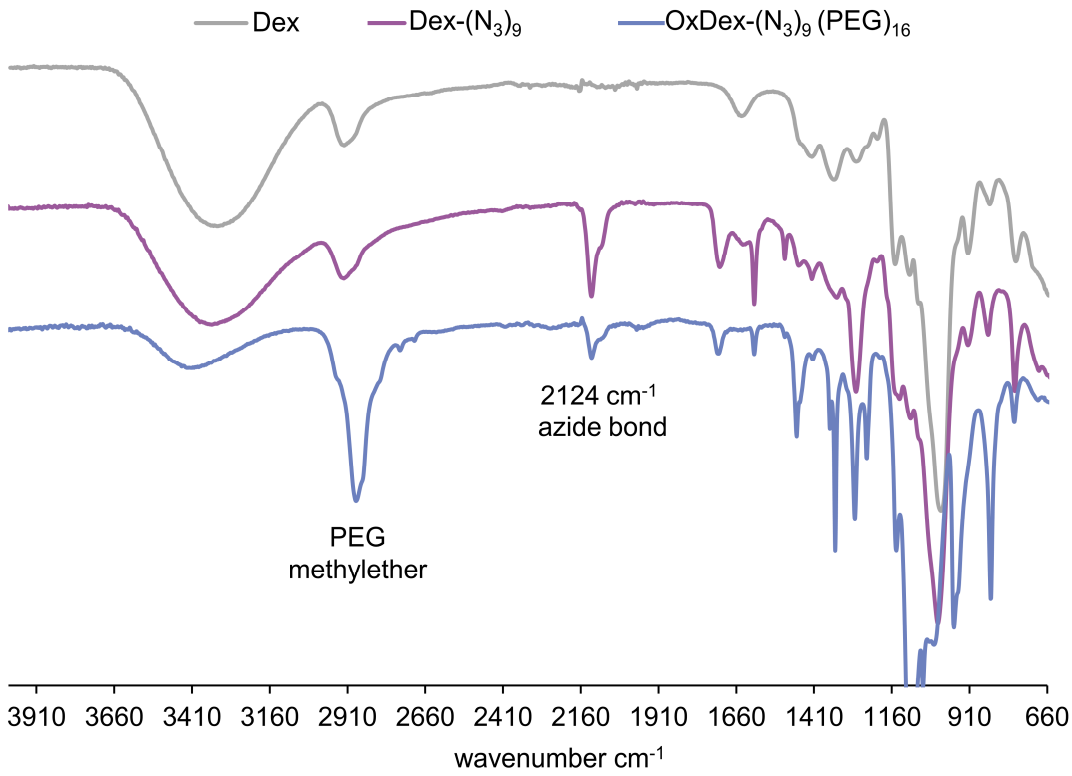

Figure 47: IR spectra of dextran **18**, azide-modified dextran **20** and polymer brush OxDex-$(N_3)_9(PEG)_{16}$ **27**. The azide group has a significant signal at 2124 cm^{-1} and after the conjugation with the PEG, a methylether signal appears at 2880 cm^{-1}.

Furthermore, the core-shell nanosystem was visualized by transmission electron microscopy (TEM). This microscopy technique uses an electron beam that transmits an ultrathin sample (<100 nm) or a suspension on a grid. The images of the samples are formed by the different densities and compositions of the samples and allow high resolutions of the specimen up to 0.045 nm.[268] **Figure 48** displays the TEM images of the dextran-based polymer brush **27**. The structures are between 0.5-1 μm in size and have similarity to published $[(PEG_{16}\text{-alt-}PCL_{21})_4\text{-S-S-}(PEG_{16}\text{-alt-}PCL_{21})_4$ polymer brushes.[269] The PEG arms are visible as linear structure elements. The magnification illustrates their linkage to one central point which is most likely the supercoiled dextran backbone. It looks like that the whole polymer brush is relatively coiled and in a bulky arrangement on the copper carbon grid.

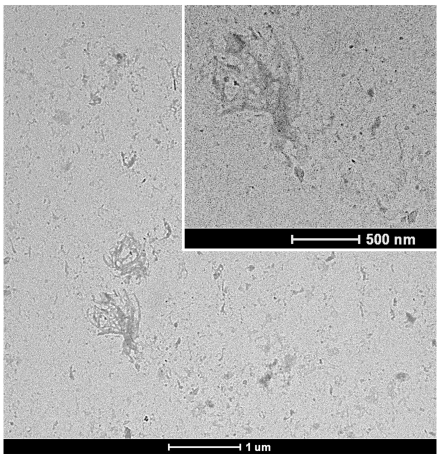

Figure 48: TEM image of dextran-based polymer brush **27** with attached linear PEG chains. The shown structures have a size of approximately 500 nm.

Thiol-modified Dextrans

As alternative to the previously described click-chemistry approach and further introduction of linear PEG arms to the dextran backbone, another bioorthogonal conjugation was used. Aiming to use thiol-maleimide Michael addition reaction (**Figure 30**), the polysaccharide was functionalized with sulfuric groups. First attempts were carried out using reductive amination on the aldehyde enriched dextran backbone. Cysteamine (2-aminoethanethiol) **28** was reacted with oxidized dextran forming the unstable imine structure. The addition was followed by the reduction of the *Schiff* base with either sodium borohydride ($NaBH_4$) or sodium cyanoborohydride ($NaBH_3CN$). However, multiple experiments with different reaction conditions were carried out, no successful introduction of thiol groups to the polysaccharide was observed. Besides, structure determination and analytics of the synthesized compound turned out to be challenging since neither NMR due to the wide distribution and high intensity of sugar proton signals overlaying the signal of the attached cysteamine nor mass spectrometry due to the high molecular weight could be applied. Thus, the synthesis route was changed to a published procedure.[270] In a first step, hydroxyl groups of dextran **18** are activated with 4-nitrophenyl chloroformate **29** using pyridine as basic catalyst (**Figure 49**).[271] The reaction is carried out in dimethylformamide (DMF) with the addition of lithium chloride (LiCl). As illustrated before the solvents are limited when working with dextran. The solubility in DMF is only possible as soon as LiCl is added in a concentration of at least 2% of solvent amount. Besides, the solution has to be heated up to 90 °C. LiCl has an extraordinary solubility in organic solvents in contrast to other ionic salts due to the small

size of the Li^+ cation. Using LiCl while dissolving dextran, the salt enhances solubility of the polysaccharide with its properties.[272] Since an activated carbonate structure in the reaction with 4-nitrophenyl chloroformate **29** is formed which can be easily hydrolyzed, the reaction has to be carried out in very dry solvents and water-free chemicals have to be used. The modification was carried out at 0 °C for 2 h and the product purified with precipitation yielding a colorless, fluffy powder after drying under reduced pressure. The introduction of aromatic nitro groups is relatively easy to track with NMR spectroscopy (**Figure 53**). The aromatic protons can be used to determine the DS of the polymer as described earlier for the modification with azidobenzoic acid yielding a DS of 7.5 per dextran chain. IR spectrum of Dex-(4-NC)$_{7.5}$ **30** showed typical appearance of acyclic carbonates at 1765 cm^{-1} and no cyclic carbonates within one glucose unit at 1805 cm^{-1} as described in literature (**Figure 54**).[271] The amount of activated carbonates group within dextran was increased with the use of large excess 4-nitrophenyl chloroformate **29** up to a DS of 27. However, such a high activation of hydroxyl groups led in the following substitution step with cysteamine to a water-insoluble product which was useless for the application as carrier material in the enzyme mimic system.

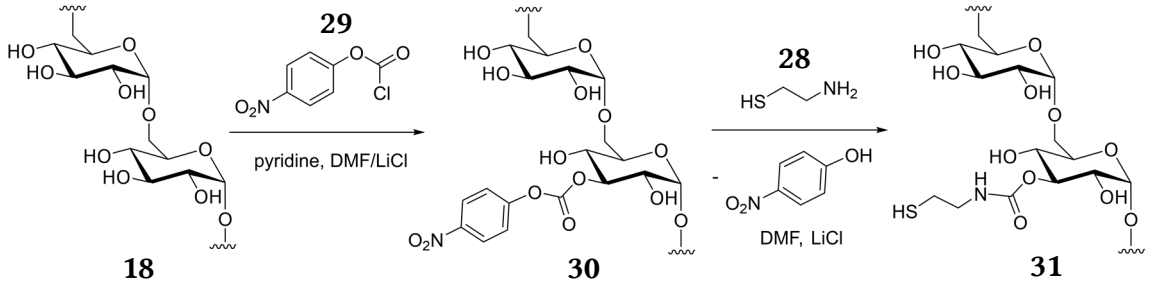

Figure 49: Synthesis of thiol-modified dextran Dex-(SH)$_7$ **31**. Dextran is first activated with 4-nitrophenyl chloroformate **29** and then subsequently reacted with cysteamine **28** resulting in Dex-(SH)$_7$.

In a second step activated hydroxyl groups of Dex-(4-NC)$_{7.5}$ **30** were subsequently reacted with cysteamine. The reaction was again carried out in extra dry DMF/LiCl solvent mixture. With the addition of cysteamine **28** the solution turned immediately yellow demonstrating the release of *p*-nitrophenol. The reaction was stirred for 16 h and reduced with tris(2-carboxyethyl)-phosphine (TCEP) before lyophilization to ensure the reduction of all possible formed disulfide bonds. The thiol-modified dextran Dex-(SH)$_7$ **31** was obtained as a colorless powder.

The DS was determined by ^{1}H-NMR to 7 cysteamine groups per dextran chain (**Figure 53**). However, this analysis method can only be considered as an approximated value due to the overlaying proton signals of sugar backbone and introduced cysteamine (as described

previously). Additionally, amount of addressable thiol groups in the dextran sample was determined by an Ellman's assay.[273] The assay uses water-soluble 5,5'-dithiobis-(2-nitrobenzoic acid) (DTNB), called Ellman's reagent, for the reaction with free sulfhydryl groups at neutral pH (**Figure 50**).

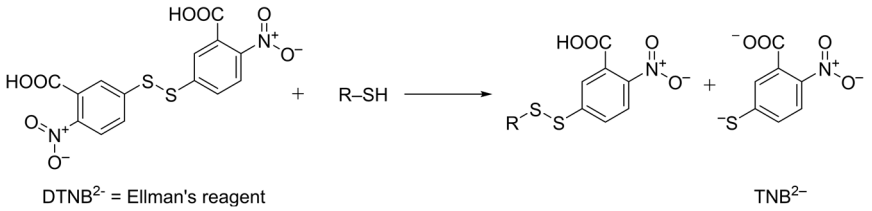

Figure 50: Reaction of Ellman's reagent ($DTNB^{2-}$) with a thiol-containing compound resulting in the yellow product TNB^{2-}.

The reaction releases the water-soluble yellow product TNB^{2-} (2-nitro-5-thiobenzoic acid) whose absorbance can be measured at 412 nm. Using *N*-acetylcysteine as a standard the quantification of thiol groups in Dex-$(SH)_7$ **31** sample resulted in a DS of six which roughly confirms the DS measured with NMR spectroscopy.

This chapter described the successful chemical modification of the polysaccharide dextran with two different functional groups (azide and thiol) that allow in the following step bioorthogonal conjugations of the synthesized catalysts (**3.1.4)**. Comparing both modified materials, it was possible to introduce more azide functional groups to Dex-$(N_3)_9$ **20** than thiol functional groups to Dex-$(SH)_7$. The main reasons for this are the different synthetic strategies for the modifications.

3.1.4 Conjugation of Catalyst and Polymeric Carrier Material

In this chapter the two components, the dextran-based carrier and the macrocyclic polyamine-based catalyst are linked to each other. Using both, the click-chemistry as well as the thiol-maleimide strategy, a full artificial enzyme-like nanosystem will be established.

Click Chemistry Approach

This conjugation strategy used BCN-modified macrocyclic amine BCN-MCA **15** as an artificial cleavage site and the OxDex-$(N_3)_9$ **21** as a carrier (see similar to **Figure 29**). For the click reaction the linear dextran backbone was chosen solely without the linear PEG arms in order to simplify the system (**Figure 51**). Besides PEG arms were expected to work in their original purpose as a real shielding corona which complicates the access of the small BCN-MCA **15** to the azides inside of the nanosystem. As described in chapter **3.1.2**, it was not possible to isolate the BCN-MCA **15** in high yields. In order to use the appropriate excesses compared to present azido groups, large amounts of **15** were needed. This was not compatible with the found synthetic route, why in first click experiments, non-purified reaction mixtures of the BCN-MCA **15** were used. The click reaction was carried out under various conditions following published reaction procedures for similar cyclooctyne-based click reactions.[225, 249, 274-276] However, in none of the experiments a water-soluble product was obtained. Mostly, the purification procedure with dialysis against water started with clear solution and after several hours slightly yellow precipitate occurred. Dialysis against DMSO first, followed by dialysis against water was no helpful alternative in purification. Resulting colorless, fluffy powder after lyophilization was not water-soluble which excludes its application as artificial enzyme mimic since the solubility in water is an unconditional, necessary criterion for the designed ATPase like system. It is most likely that the reaction between the aromatic azide group of the dextran backbone and the BCN, yielding a triazole, results in the formation of a very hydrophobic structure element. This water-repellent part of the nanosystem leads probably to the precipitation of the whole system in water and cannot be compensated by the hydrophilic hydroxyl groups of dextran nor by the introduced macrocyclic amines. The phenomenon of a water-insoluble dextran-backbone due to only small modifications and the attachment of few small molecules is also described in the previous chapter for the synthesis of Dex-$(SH)_7$ **31**.

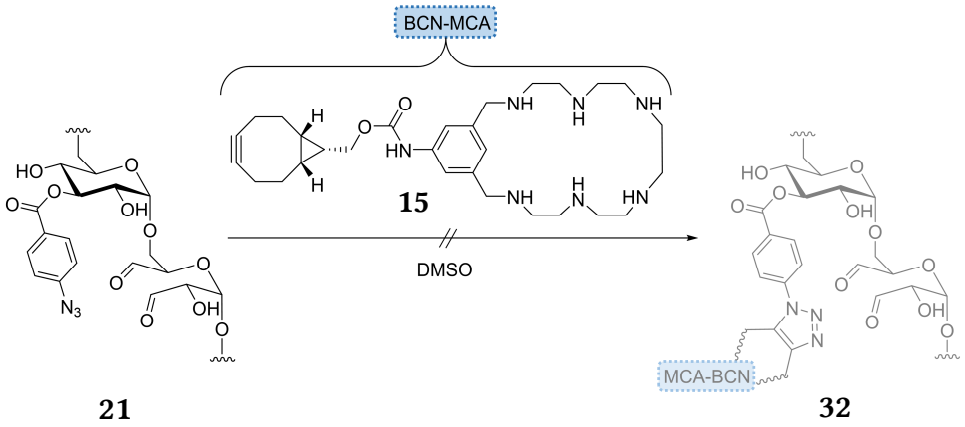

Figure 51: Cu-free click reaction of OxDex-$(N_3)_9$ **21** and BCN-MCA **15**. The product BCN-Dex **32** was not obtained as a water-soluble compound.

Due to this failed synthesis with a water-insoluble product, this approach was no longer pursued, and no evaluation of the conjugated nanomaterial has been carried out. The project based on the click chemistry strategy was ceased on this stage of development.

Thiol Maleimide Approach

This conjugation strategy used maleimide-modified macrocyclic amine Mal-MCA **17** as an artificial cleavage site and thiol-modified dextran Dex-$(SH)_7$ **31** as carrier material. For reaction the Mal-MCA **17** was generated *in situ* right before the reaction and used in a 5-fold excess to the present thiol groups (**Figure 52**).

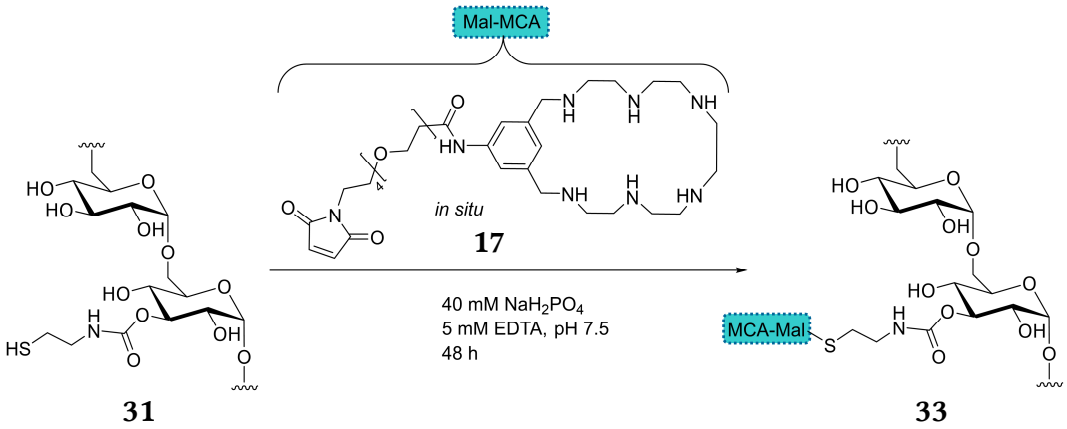

Figure 52: Reaction of Dex-$(SH)_7$ **31** with Mal-MCA **17**.

The Michael addition reaction was carried out for 48 h and the Dex-(S-Mal-MCA)$_6$ **33** product was obtained as a slightly brown, fluffy powder. ^{1}H-NMR was used to determine the number of six macrocyclic amines attached to the dextran backbone (**Figure 53**). Ninhydrin coloration was used a qualitative evidence resulting in a deep purple coloration of **33** compared to Dex-$(SH)_7$ **31**. An Ellman's assay comparing the number of thiols before

and after the reaction illustrates the disappearance of all thiol groups present on the dextran backbone.

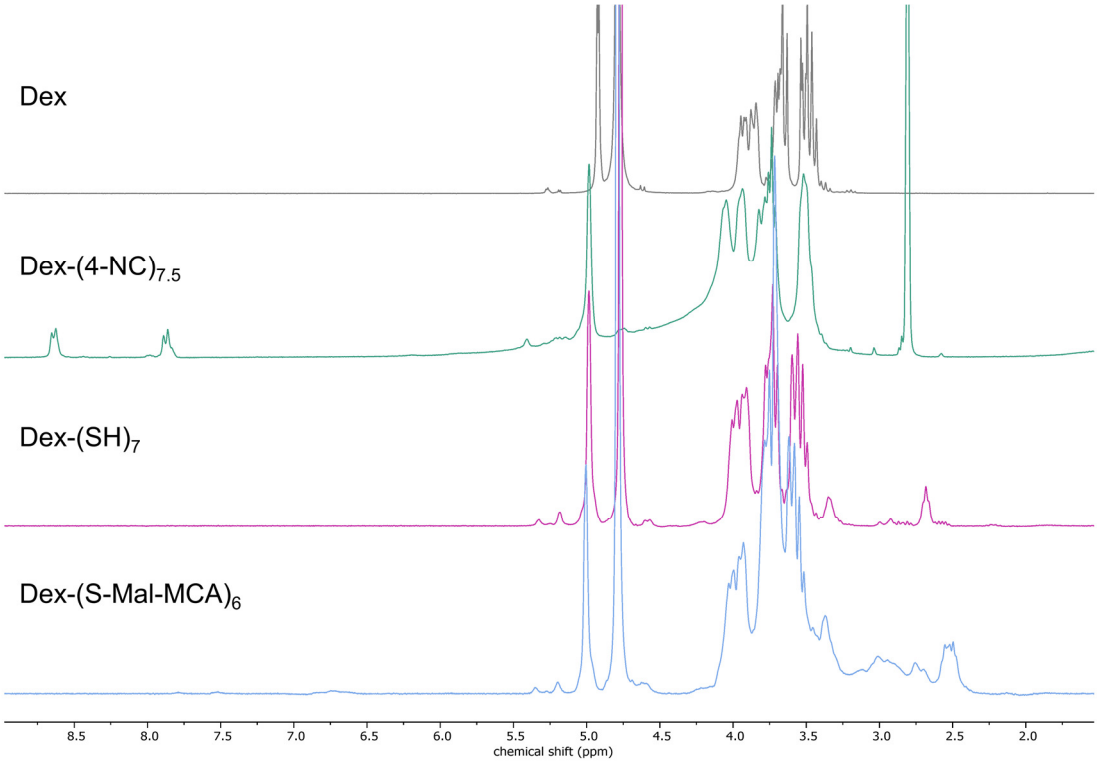

Figure 53: Stacked NMR spectra of dextran **18**, Dex-(4-NC)$_{7.5}$ **30**, Dex-(SH)$_7$ **31** and Dex-(S-Mal-MCA)$_6$ **33** showing the appearance and disappearance of significant signals like the aromatic protons of Dex-(4-NC)$_{7.5}$ **30** at 8.65 and 7.85 ppm or the thiol protons of Dex-(SH)$_7$ **31** at 2.7 ppm. Also, the polyamine protons of the conjugate Dex-(S-Mal-MCA)$_6$ **33** are visible between 2.7 and 3.13 ppm.

In addition, comparing the IR spectra of all dextran-modified compounds it can be demonstrated that the appearance of a carbamate bond at 1699 cm^{-1}, primary and secondary amine bonds at 1633 cm^{-1}, and secondary acid amides at 1546 cm^{-1} as shown in **Figure 54** support the attachment of Mal-MCA **17** to Dex-(SH)$_7$ **31**.

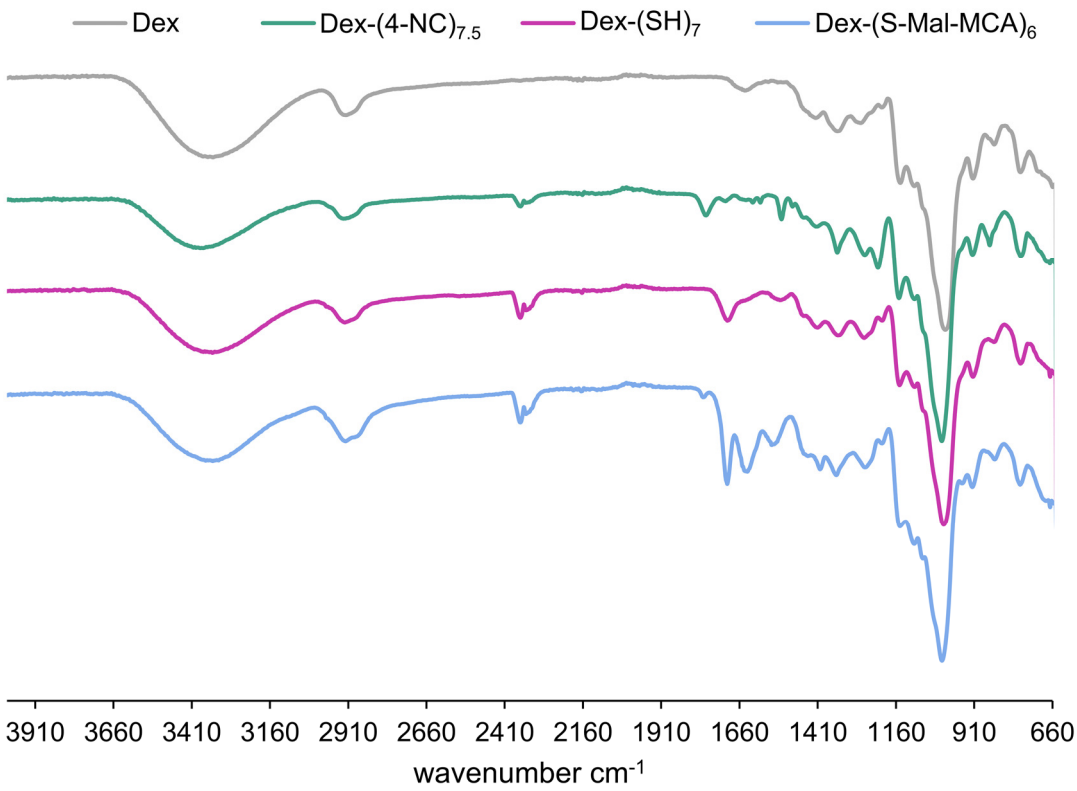

Figure 54: IR spectra of dextran **18**, Dex-(4-NC)$_{7.5}$ **30**, Dex-(SH)$_7$ **31** and Dex-(S-Mal-MCA)$_6$ **33** displaying the appearance and disappearance of significant carbamate and primary and secondary amine bonds.

With the successful linkage of catalyst and carrier, a nanomaterial was established which has multiple artificial cleavage sites attached to a polymeric scaffold. The material was fully characterized and evaluated concerning its application *in vitro* and its functionality.

3.1.5 Biocompatibility of Enzyme Mimics

In order to investigate how realistic an application of the designed artificial enzyme-like structures in cellular environment is, a first step is to prove their biocompatibility and their toxicity, respectively. Thus, modified dextran samples were incubated with HeLa cells, a cervical carcinoma cell line, and the cell viability was investigated with MTT assay.[277] The assay uses MTT (3-(4,5-dimethylthiazol-2-yl)-2,5-diphenyltetrazolium bromide) which is a water-soluble, bright yellow salt that is reduced by cellular oxidoreductase enzymes. The product of reduction, the water-insoluble purple formazan which is dissolved in organic solvents after reaction, can be measured at 595 nm (**Figure 55**). The amount of released formazan is an indicator for the functioning metabolism of the HeLa cells and corresponds to the number of living cells. If the modified dextran materials are toxic, the metabolism of the cells will slow down or even worse lead to cell death. The HeLa cells were incubated for 48 h with dextran samples in ranging concentrations from 62.5 μg up to 1 mg mL^{-1} before the MTT assay was carried out.

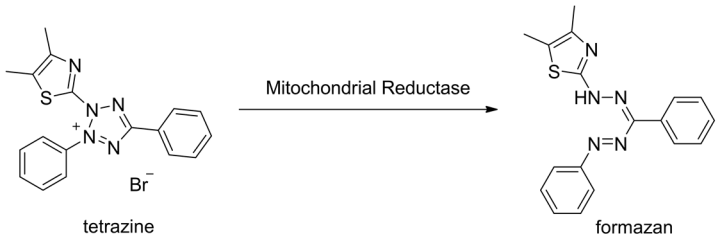

Figure 55: Conversion of tetrazine salt to formazan by mitochondrial reductase. The formed formazan is an insoluble purple compound which after dissolving in organic solvents has a specific absorption at 595 nm.

Click Chemistry Approach

Although the conjugation of Dex-$(N_3)_9$ **20** and BCN-modified macrocyclic amine **15** led to a water-insoluble product as shown in chapter **3.1.4**, starting materials for conjugation as well as the full dextran-PEG polymer brush **27** were tested towards their cytotoxicity (**Figure 56**). These experiments were carried out long way before conjugation of carrier and biocatalyst and for reasons of thoroughness the results are presented in here.

Figure 56 shows the cell viability of Dex-$(N_3)_9$ **20** and the dextran-PEG polymer brush **27** at commonly used dilutions from 31.25 μg mL^{-1} up to 1 mg mL^{-1}. For both materials no cytotoxicity can be observed at applied concentrations. The cell viability over 100% can be explained by the fact, that HeLa cells can use dextran and the modified versions of it as an additional food and energy source which leads to an increased growth. Due to

water-insolubility of the click conjugated dextran **32**, it was not possible to test the new bioconjugate towards its cytotoxicity. However, the results shown in **Figure 56** show that the Dex-$(N_3)_9$ **20** and the dextran-PEG polymer brush system **27** represent fully biocompatible systems for possible further applications.

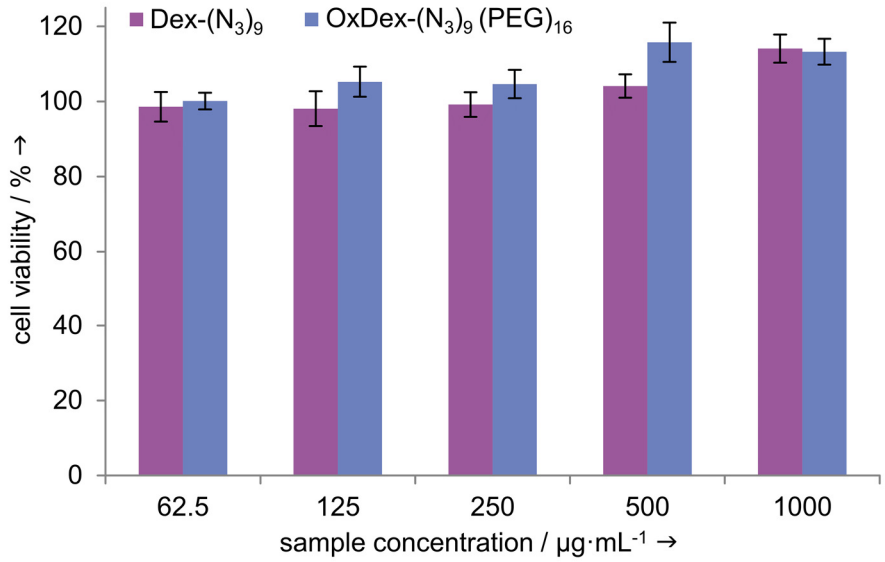

Figure 56: MTT assay of Dex-$(N_3)_9$ **20** and OxDex-$(N_3)_9$ $(PEG)_{16}$ **21** demonstrating the very good biocompatibility of the designed polymeric nanosystem.

Thiol-Maleimide Approach

This work was mainly carried out in cooperation with Matthias Konhäuser (JGU Mainz). **Figure 57** shows the cell viability of Dex-$(SH)_7$ **31**, Dex-(S-Mal-MCA) **33** and solely the amino-modified macrocyclic amine NH_2-MCA **13** at concentrations from 62.5 μg mL^{-1} up to 1 mg mL^{-1}. The concentration of NH_2-MCA **13** was adjusted to the corresponding number of macrocyclic polyamine attached to the dextran backbone of **33** After 48 h, all samples show at all concentrations no cytotoxicity in HeLa cells. The possible cell viability over 100% was explained in the previous paragraph.

The illustrated cell viability experiments show that these established dextran-based nanomaterials are uncritical regarding their further application *in vitro* as artificial enzyme-like systems.

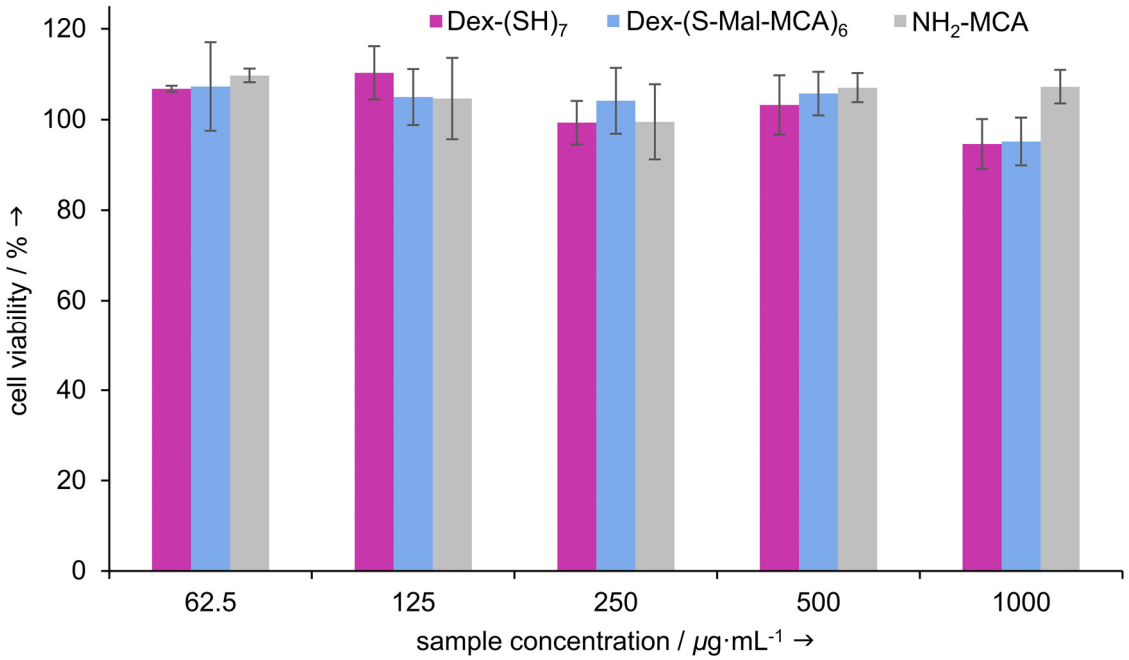

Figure 57: Cell viability of HeLa cells after incubation with Dex-$(SH)_7$ **31**, the bioconjugate Dex-(S-Mal-MCA)$_6$ **33** and adjusted concentrations of NH_2-MCA **13** similar to the number of macrocyclic polyamines attached to the dextran scaffold. No toxicity can be observed for all applied concentrations and the artificial ATPase demonstrated its high biocompatibility.

3.1.6 Evaluation of ATPase-like Functionality

ATP Hydrolysis Determination by ^{31}P-NMR Spectroscopy

The artificial enzyme-like functionality was investigated by using ^{31}P-NMR spectroscopy.[278] The ^{31}P phosphorous is a common NMR nucleus because it has an isotopic abundance of 100% and a relatively high gyromagnetic ratio. The spin of ½ makes the nuclei highly sensitive. ATP contains three different phosphorus species with characteristic splitting (**Figure 58a**). The α- and the γ-phosphorous have two duplet signals whereas the β signal has a triplet signal since it couples with both other phosphorous nuclei. As soon as the α-phosphorous is cleaved from the ATP, three new signals develop. The leftover ADP has two duplet signals which couple with each other (**Figure 58b**). The inorganic phosphate (P_i) has a characteristic singlet signal downfield of the ATP and ADP signals at around 0 ppm.

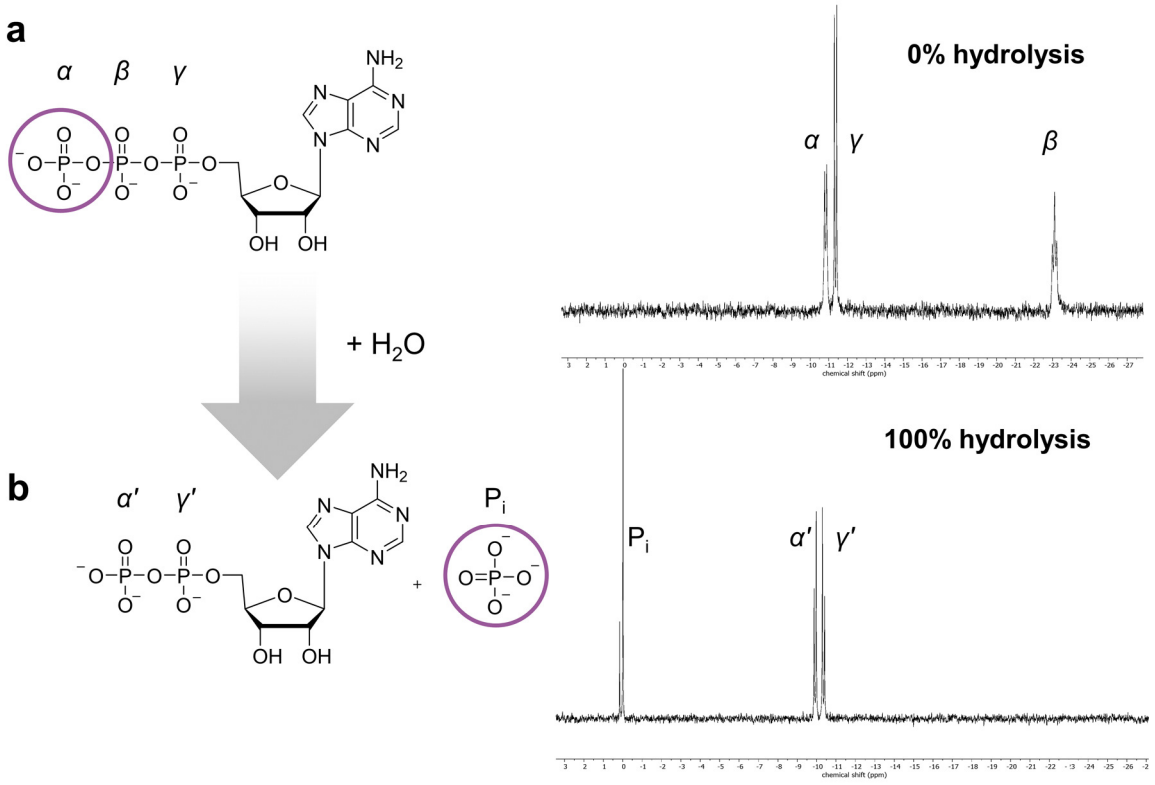

Figure 58: ^{31}P-NMR of ATP with respective assignment (a). After hydrolysis, a new peak of P_i develops which can be used to calculate catalytic rates (b).

The comparison of the integral ratio of the P_i and the β signal allows the determination of the amount of hydrolyzed product. Since, hydrolyzed ATP releases exactly one P_i, the total concentration of [P_i]+[ATP] stays constant during the reaction. The remained amount of ATP can be determined by integrating the characteristic β triplet peak of ATP at -23 ppm

(ADP has no triplet signal); the amount of P_i can be determined by integrating the P_i singlet peak. The equations of the calculations are:

$$[ATP] = \frac{\int P_\beta}{\int P_\beta + \int P_i} \quad \text{and} \quad [P_i] = \frac{\int P_i}{\int P_i + \int P_\beta} \qquad (1.1 \text{ and } 1.2)$$

The kinetic of the hydrolysis of ATP can be best described by first-order kinetics. Herein, the reaction rate depends on ATP, water and a fixed number of catalyst like MCAs or in the case of autohydrolysis just H^+. Water is disregarded in the kinetic equation because it is used as solvent and present in great excess. The reaction depends on the pH value because H^+ catalyzes the reaction and thus the pH has to be set in advance of the cleavage experiments. The first order kinetics are described by

$$[ATP]_t = [ATP]_0 \cdot e^{-k \cdot t} \qquad 1.3$$

in which $[ATP]_t$ describes the ATP concentration at the time point t and $[ATP]_0$ the ATP concentration at the start of the reaction (t=0).

Thus, the reaction rate can be mathematically expressed by

$$reaction\ rate = -\frac{d[ATP]}{dt} = k[ATP] \qquad 1.4$$

and integration at a certain time point t of 1.4 leads to

$$-\ln \frac{[ATP]_t}{[ATP]_0} = kt \qquad 1.5$$

By rearrangement, the calculation yields the reaction rate k

$$k = \frac{-ln\frac{[ATP]_t}{[ATP]_0}}{t} \qquad 1.6$$

in which $[ATP]_t$ can be calculated by using equation 1.1.

The displayed mathematic equations are used in the following sections to calculate the catalytic activity of the artificial ATPase measured in time-course NMR experiments.

Catalytic Activity of Modified Macrocyclic Polyamines and Artificial ATPases

Kinetic measurements of ATP hydrolysis were carried out by investigating the time-dependent change of the significant P_i and the β-signal. **Table 2** displays the measured rate constants for a first-order kinetics of ATP hydrolysis at pH 5.2 and 40 °C. This temperature was chosen because it is close to body temperature where much enzymes perform and at

the exact body temperature of 37 °C no literature was published so far. The pH of 5.2 was chosen because the hydrolytic activity of the macrocycles is raising with a decreasing pH. The presence of more H^+ protons facilitates the electrostatic interactions of the then charged nitrogens with the polyphosphate chain. A pH value of 5.2 was considered as a reasonable middle between optimal ATP hydrolysis at low pH and realistic pH values which can occur in the body, e.g. in lysosomes with 4.5–5.5.[1] Although, comparisons with the literature have to be made carefully because the hydrolysis with the supramolecular structures is a sensitive system that depends much on concentration of catalysts, ionic strengths and adjusted pD for NMR measurements.[140, 144] Considering these issues, the published rate constant for MCA **2** is k=0.023 min^{-1} at pH 5.2 and 40 °C and thus slightly higher than k=0.016 min^{-1} which was measured in this thesis (**Figure 59**, **Table 2**). For the original [24]N_6O_2 **1** much slower rate constants were published, such as k=0.0037 min^{-1} at pH 3.6 and 50 °C.[137] Only at 60 °C and 70 °C the catalyst [24]N_6O_2 **1** reaches similar values as the rates measured here with k=0.011 min^{-1} and k=0.029 min^{-1}, respectively.

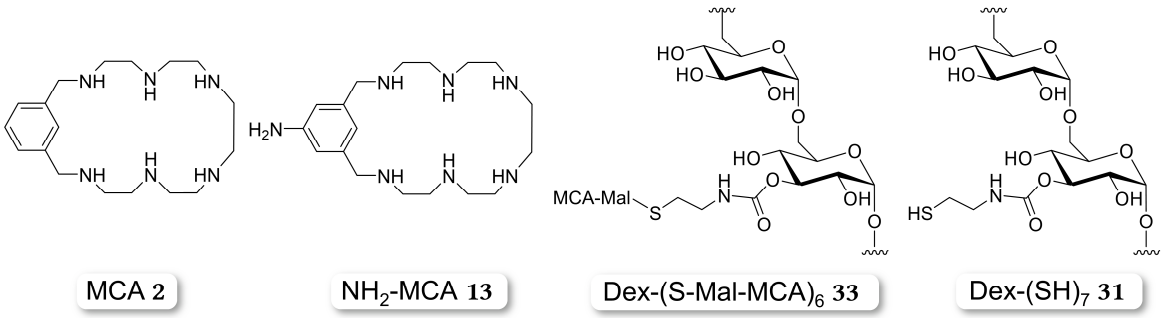

Figure 59: Chemical structures of all investigated compounds in ^{31}P-NMR spectroscopy.

Table 2: Rate constants k of ATP hydrolysis in equimolar concentrations at pH 5.2 and 40 °C by macrocyclic polyamines and the entire artificial ATPase system.

	rate constant k (min^{-1})
MCA 2	0.016
NH_2-MCA 13	0.015
Dex-(S-Mal-MCA)$_6$ 33	0.012
Dex-(SH)$_7$ 31	-

The modification of MCA **2** with the amino group to NH_2-MCA **13** led to a slight, negligible rate decrease to k=0.015 min^{-1} which is within the inaccuracy of the measurement (**Table 2**, **6.2.1**). In a first conclusion, a new supramolecular catalyst with a functional group that allows an attachment to a carrier system with similar catalytic activity was created with this thesis.

The conjugation of NH_2-MCA **13** to Dex-$(SH)_7$ **31**, using a linker, led to the entire artificial ATPase system Dex-(S-Mal-MCA)$_6$ **33** (**Figure 59**). The conjugate demonstrates catalytic activity with a rate constant of k=0.012 min^{-1} which is in the range of the unbound catalyst NH_2-MCA **13** with k=0.015 min^{-1} (**Table 2**). **Figure 60** displays the time-course ^{31}P-NMR experiment of Dex-(S-Mal-MCA)$_6$ **33** and visualizes the ATP cleavage carried out by the nanomaterial.

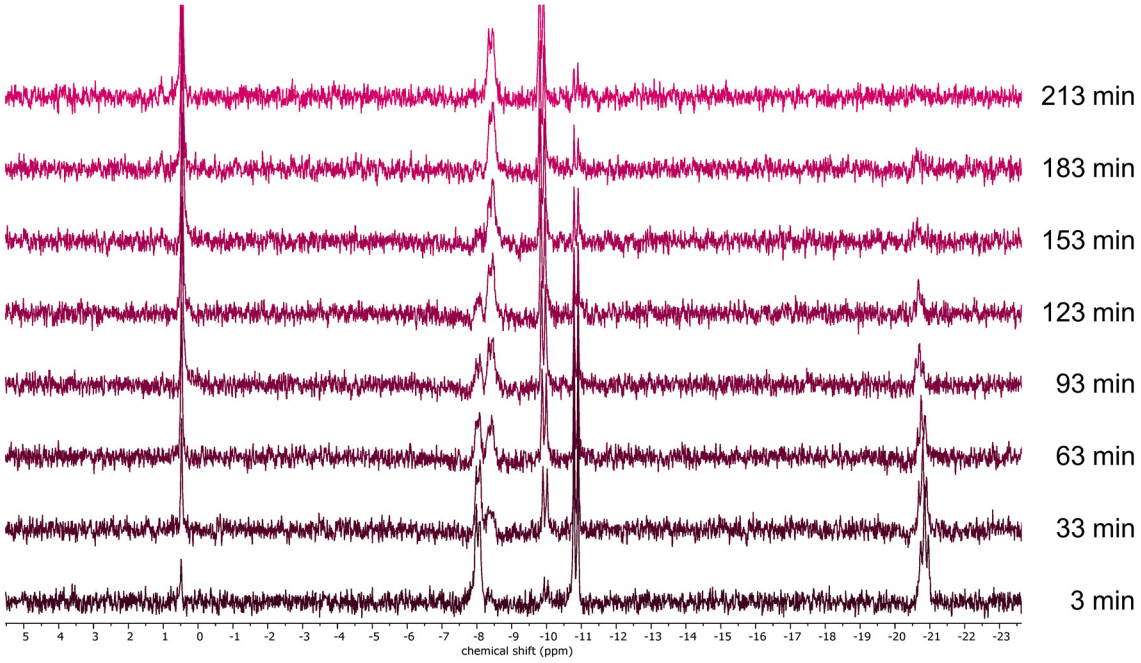

Figure 60: Time-course ^{31}P-NMR experiment of ATP cleavage of ATPase-like system Dex-(S-Mal-MCA)$_6$ **33**. The sample contains 30 mM ATP and the respective amount of catalytically active compounds. The developing of the P_i signal at 0.45 ppm and the decrease of the β-signal of ATP (as described in **Figure 58**) at -20.82 ppm can be observed. In the middle the change of the α- and γ-signals to α' and γ' is noticeable.

For the kinetic measurement the concentration of Dex-(S-Mal-MCA)$_6$ **33** was adjusted to the same amount of catalyst as in the samples of MCA **2** and NH_2-MCA **13**. Compared to the kinetic rate of MCA **2** and NH_2-MCA **13** a slight decrease of 0.004 min^{-1} and 0.003 min^{-1} is observed, respectively. This can be attributed to the bulky nature of the conjugate. Compared to the unbound catalysts MCA **2** and NH_2-MCA **13** diffusion decreases, and the reachability of the macrocyclic polyamines is aggravated.

To ensure that the pure carrier material Dex-$(SH)_7$ **31** (**Figure 59**) has no ATPase-like functionality, the polymer was also investigated in ^{31}P-NMR spectroscopy. As expected, it did not demonstrate any catalytic activity (**Table 2**, **6.2.1)**.

By comparing the here shown artificial ATPase systems with other macromolecular structures such as a dendrimer, which showed similar ATPase behavior[279] or cone tetra-guanidinocalix[4]arenes[145], the outstanding properties of Dex-(S-Mal-MCA)$_6$ **33** become clear. Literature known systems only perform well at high temperatures (70 °C or 80 °C) or with high amounts of organic solvents (80% DMSO), whereas Dex-(S-Mal-MCA)$_6$ **33** catalyzes the hydrolysis of ATP at moderate temperatures and in pure aqueous solution. Thus, the new designed bioconjugate provides a new promising approach for artificial enzymes. Not only its excellent performance under physiological conditions and its literature comparable catalytic activities make the artificial ATPase Dex-(S-Mal-MCA)$_6$ **33** an outstanding catalytic nanomaterial. The material allows even further chemical modification of its carrier to optimize the catalytic activity to achieve a possible *in vitro* application in the future.

3.2 Peptide-Enzyme Conjugates for Cascade Reactions

The previous chapter demonstrated an artificial approach to mimic the setup, architecture and functional activity of one single enzyme. The following section will describe an artificial approach to nature's molecular machines and enzymatic clusters. A dual enzymatic activity of cytochrome *c* (Cyt *c*) was achieved by attaching a hexapeptide to the surface of the enzyme. By combining the esterase-like peptide with the peroxidase functionality of the protein, a unique artificial enzymatic material has been created which allows the efficient performance of an enzymatic cascade reaction.

Most of the following data is submitted for publication. Herein, the results are described and discussed in greater detail. Besides, first results of the transfer of the developed system to other proteins are displayed demonstrating the wide application potential of this approach.

3.2.1 Mild Surface Modification of Cytochrome *c*

Design and Synthesis of an Esterase-like Peptide

The design of the peptide was inspired by the esterase-like performance of imidazole[280-281] as part of histidine units.[282-284] Enzymatic activity of imidazoles has been first reported by *Hartley et al.* when he observed the ester cleavage of *p*-nitrophenyl acetate by *N*-benzoyl-L-histidine.[285] Similarly, *β*-cyclodextrinyl-bisimidazole has been described as a model for ribonucleases for the cleavage of cyclic phosphate substrates.[103, 286] In all cases, the imidazole residue provides hydrogen bridges with donor and acceptor characteristics and shows activity both in nucleophilic or base mediated catalysis.[287] In nature, histidine is the only natural amino acid containing an imidazole unit in its side group and often occurs in the catalytic center of enzymes as an acid-base catalyst. Examples are serine proteases like chymotrypsin or thrombin which contain the catalytic triad aspartic acid, histidine and serine.[1] The catalytic features of histidines were utilized over the years in several artificial systems by the introduction of histidines in short peptide sequences to obtain esterase-like functionality.[282, 284] In 2007 for example, a self-assembled nanofiber system with esterase-like activity has been reported.[215] Peptide amphiphiles, based on a long palmitoyl tail were functionalized with peptides containing 6-8 amino acids. The conclusive amino acids within the peptides were histidines. These peptide amphiphiles aggregated in nanofibers with 15-20 nm diameter and were able to catalyze the hydrolysis

of a *p*-nitrophenyl ester. *Zaramella et al.* have shown that self-assembled layers of small peptides containing mainly histidines on the surface of gold nanoparticles have the capability to cleave esters.[214] Recently, a peptide-nanoparticle conjugate has been published which is catalytically active on its surface.[288] Gold nanoparticles were modified with a peptide designed after the heterodimeric α-helical coiled-coil principle. Histidines on the surface of the particles showed catalytic activity in ester hydrolysis.

For this reason, the designed peptide for this thesis was supposed to contain exactly three histidines, the first being capped at the amino-terminus with an acetyl group. In a first approach, the hexapeptide sequence was completed by three glycines on the side of the carboxy terminus. The peptide was synthesized using an Fmoc-Gly-HMPA-resin, which releases the carboxy terminus of the peptide from the resin. The conjugation strategy was to use common carbodiimide crosslinker chemistry with EDC (1-Ethyl-3-(3-dimethyl-aminopropyl)-carbodiimide) and sulfo-NHS (*N*-hydroxysulfosuccinimide) to conjugate the carboxy terminus with the amino groups presented on the surface of the Cyt *c* enzyme.[217] Cyt *c* has 19 nucleophilic ε-amino groups of lysines on its surface (PDB ID: 1HRC) which can easily be functionalized, as is known in literature.[289] This approach seemed reasonable after successful conjugation of PEG-COOH (poly(ethylene glycol) end group functionalized with a carboxy group) as a dummy molecule to the surface of Cyt *c*. However, it was not possible to attach the synthesized peptide to the protein.

In a second approach, a different bioorthogonal conjugation was chosen. The catalytically active peptide still contains three histidines followed by two glycines as spacer molecules. The peptide sequence ends with a cysteine to provide a thiol group to allow for biorthogonal conjugation to the protein surface (**Figure 61**).[290] The six amino acids containing peptide Ac-His-His-His-Gly-Gly-Cys-NH_2 (HHHGGC) was synthesized using standard Fmoc-based solid phase peptide synthesis (SPPS). For this purpose, an automated batch peptide synthesizer with a Rink-amide-aminomethyl-polystyrene resin was used releasing the peptide amide. Cleavage from the resin was followed by manual acetylation of the amino-terminus affording the pure hexapeptide HHHGGC in 95% yield.

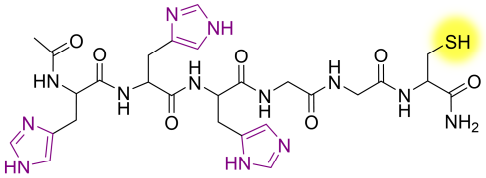

Figure 61: Structure and label of designed, synthesized hexapeptide with catalytically active imidazole residues (purple) in the histidines and a thiol group for bioorthogonal conjugation (yellow).

Conjugation of Peptides to Cytochrome *c*

The designed and synthesized short peptide HHHGGC was attached to the surface of Cyt *c* using thiol-maleimide chemistry. The chosen enzyme is obtained from horse heart and plays an important role in the transfer of electrons in the respiratory chain in eukaryotes.[291] It has one single peptide chain with 104 amino acids. Thus, it has a low molecular weight of 12.4 kDa which allows for easy monitoring of the extent of chemical modification.[292-293] Cyt *c* contains a heme group as a prosthetic group which is covalently bound via two thioether bridges to the polypeptide chain. The central iron ion is coordinated octahedrally by the 4 nitrogen atoms of the porphyrin ring in the equatorial plane and additionally by one histidine and one methionine residue in the vertical axis. Furthermore, as previously described 19 nucleophilic *ε*-amino groups of lysines are available for conjugation on the surface of Cyt *c*. For the attachment of synthesized peptide HHHGGC a heterobifunctional crosslinker was introduced (**Figure 62**). The linker contains an NHS (*N*-hydroxysuccinimide) ester for conjugation with the amines on the enzyme surface and a maleimide function required for Michael addition with the free thiol of the synthesized peptide.[294] In this case, a PEG-containing linker (NHS-PEG(4)-Mal) was chosen, since the commonly used hydrophobic sulfo-SMCC linker (sulfosuccinimidyl 4-(*N*-maleimidomethyl) cyclohexane-1-carboxylate) led to the precipitation of the protein as a red solid in a colorless solution. The reaction of the linker with the protein was followed by several centrifugation steps in which excess linker was removed. During purification of the maleimide-functionalized Cyt *c*, named Cyt(Mal), the peptide was prepared for conjugation by reducing the cysteine thiol with tris(2-carboxy-ethyl)phosphine (TCEP).[295] Excess of TCEP was neutralized with azidobenzoic acid (AZBA) because it was shown that TCEP can react with maleimides as well.[296] Conjugation of the peptide to the surface modified enzyme was performed in phosphate buffer over 16 h.

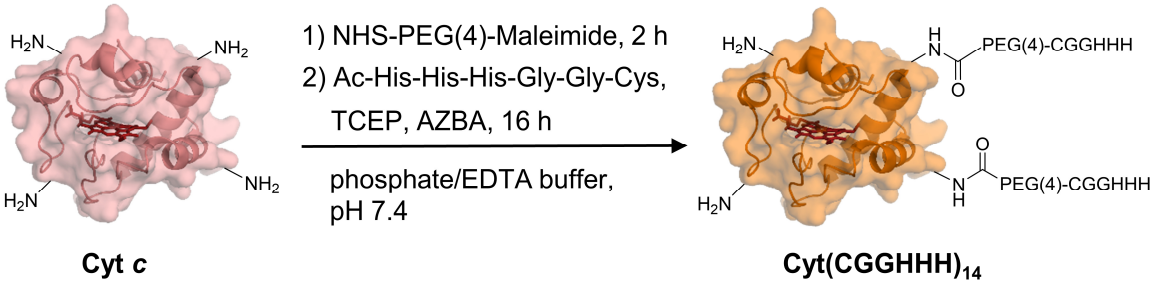

Figure 62: Modification of Cyt *c* with hexapeptide using an NHS-PEG(4)-Maleimide linker. The thiol of the peptide is reduced with TCEP which is neutralized by AZBA.

To ensure the complete oxidation of the iron core of Cyt *c*, 1 mM H_2O_2 solution was added before purification. The provided Cyt *c* contains ca. 10% Fe^{2+} which is unfavorable for later application (chapter **3.2.3**). After lyophilization of the purified peptide-protein conjugate, red crystals of Cyt(CGGHHH)$_{14}$ were obtained. The material will be in detail characterized in the following chapter, specifically regarding the amount of introduced peptide on the surface of the enzyme.

3.2.2 Properties of Modified Cytochrome *c*

The peptide-modified protein Cyt(CGGHHH)$_{14}$ and its maleimide-modified precursor Cyt(Mal) were analyzed in terms of their increased masses by SDS-PAGE and MALDI-ToF MS measurements. Furthermore, the number of modified amines on the surface was determined by a TNBS assay. Dynamic light scattering (DLS) was used to determine the physical size of the protein after modification. Finally, Cyt(CGGHHH)$_{14}$ was investigated regarding its structural integrity using CD spectroscopy.

Molecular Weight Analysis by SDS Gel Electrophoresis

A commonly used technique for the determination of molecular masses is SDS-PAGE (sodium dodecyl sulfate-polyacrylamide gel electrophoresis).[297] With this technique, mixtures of charged molecules are separated in an electric field due to their different electrophoretic mobility. The latter is a function of length, conformation and charge of the molecule. All protein samples are denaturized by heat and addition of mercaptoethanol. The anionic surfactant, SDS (sodium dodecyl sulfate) covers the intrinsic charges of the proteins. The porous polyacrylamide gel used leads to longer proteins moving more slowly than the shorter ones causing separation by chain length proportional to the protein's mass. **Figure 63** displays the SDS-PAGE of unmodified Cyt *c*, maleimide-functionalized

Cyt *c* and peptide-modified protein Cyt(CGGHHH)$_{14}$. A protein ladder with proteins in different sizes ranging from 15-170 kDa is used as a reference. The native, unmodified Cyt *c* shows a sharp protein band at approximately 13 kDa and a light dimer formation at 25 kDa. Cyt(Mal) displays a first increase in molecular mass with a broadened band slightly below the 15 kDa marker band. The dimer of this sample can be clearly seen below 35 kDa. The significant mass increase occurs once Cyt(Mal) is modified with the hexapeptides. Cyt(CGGHHH)$_{14}$ shows a broad band around 25 kDa and a dimer formation at around 50-55 kDa, which refers to the introduction of about 14 peptides to the surface of Cyt *c*. This calculation is based on the molecular weight of the peptide attached to the linker: MW (peptide) + [MW(NHS-PEG-Maleimide)-MW(NHS-OH)] = 687.27 g/mol + (513.50-112.62) g mol^{-1} =1088.15 g mol^{-1}. In both lanes of the modified proteins, no remains of native Cyt *c* can be observed.

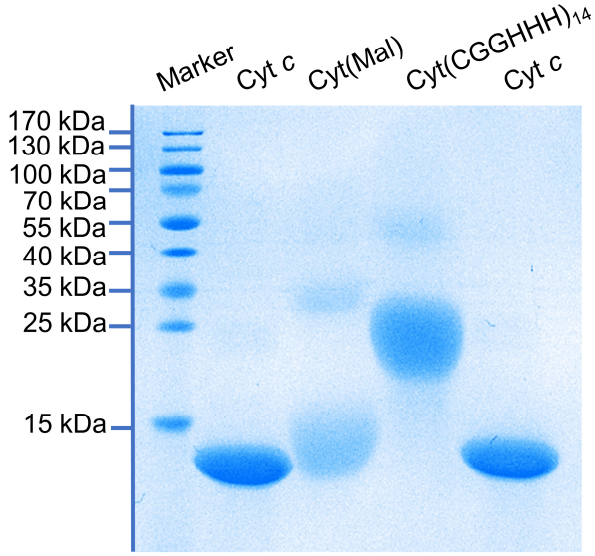

Figure 63: SDS-PAGE of native Cyt *c*, Cyt(Mal) and Cyt(CGGHHH)$_{14}$ demonstrating the mass increase of the modified enzymes.

Molecular Weight Analysis by MALDI-ToF MS Measurements

The exact molecular weight of Cyt(CGGHHH)$_{14}$ was determined by using matrix-assisted laser desorption/ionization time of flight mass spectrometry (MALDI-ToF MS). Herein, a matrix containing the co-precipitated sample absorbs laser energy leading to the generation of ions with minimal fragmentation.[298] The applied ionization technique is very mild and has been used for the analysis of biopolymers such as peptides or proteins which are likely fragile or tend to fragment if harsher ionization techniques are applied.[1] The MALDI-ToF MS spectra of native Cyt *c* and Cyt(CGGHHH)$_{14}$ are shown in **Figure 64**.

The native sample displays a typical mass spectrum of an unmodified protein with a sharp peak at 12.37 m/z. The spectrum of Cyt(CGGHHH)$_{14}$ shows two distinct peaks at 26.37 m/z and 52.3 m/z. As the protein is singly charged in this case, Cyt(CGGHHH)$_{14}$ has a molecular weight of 26.37 kDa. The peak around 52-53 kDa can be assigned to the dimer of the modified protein. The results obtained and shown in **Figure 64** allow to determine the exact number of peptides on the surface of Cyt *c* as 14 individual attached peptide chains.

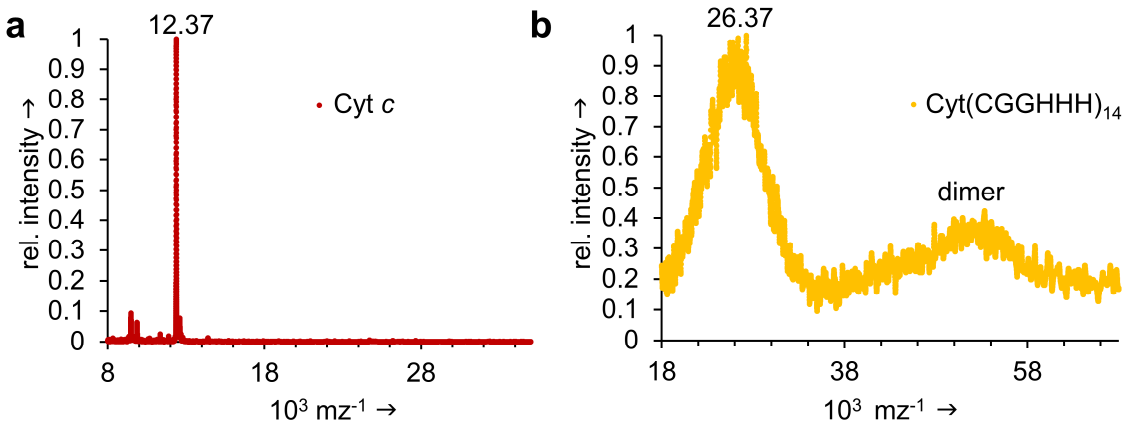

Figure 64: MALDI-ToF MS of native Cyt *c* (a) and Cyt(CGGHHH)$_{14}$ (b).

Modified Amino Groups on the Surface of Cyt *c*

The number of attached peptides described in the previous paragraph was confirmed by performing a TNBS (2,4,6-trinitrobenzene sulfonic acid) assay to determine the number of remaining free amino groups on the surface of Cyt *c*. Primary amines can react with TNBS to form a highly chromogenic orange-colored derivative that can be measured at an absorbance of 335 nm.[299-300] The assay was able to detect 5 free amino groups based on originally 19 available lysine groups on the surface of Cyt *c*. This result concurs with the molecular weight measurements and confirms the attachment of 14 peptides.

Hydrodynamic Diameter of Cyt(CGGHHH)$_{14}$

Dynamic light scattering (DLS) was applied to determine the physical size of the protein after modification with the hexapeptide.[301] A hydrodynamic diameter of 3.25 ± 0.76 nm for Cyt(CGGHHH)$_{14}$ compared to 2.09 ± 0.54 nm for the unmodified Cyt *c* was measured for the native protein in PBS buffer pH 7.4 (**Figure 65**). Literature describes native Cyt *c* with a diameter of 3.4 nm[302-303], but a precise description of DLS measurement conditions e.g. applied buffers or salt concentrations is missing. However, size comparison of the

native protein and Cyt(CGGHHH)$_{14}$ shows a slight increase after the modification which was confirmed by measurements using various different sample concentrations.

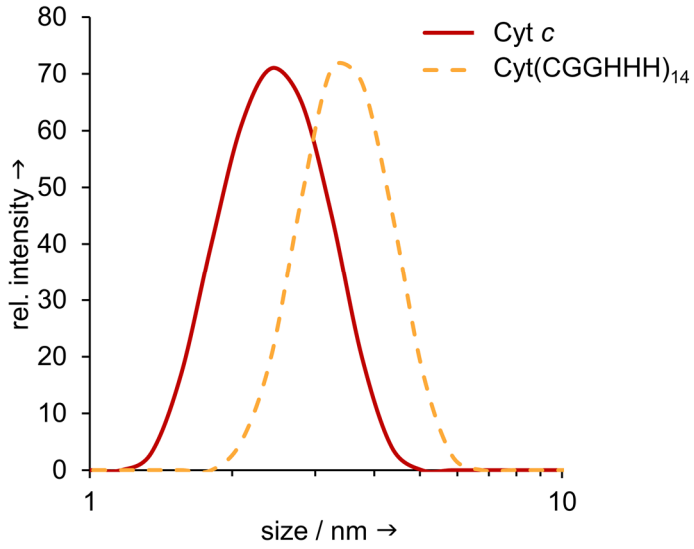

Figure 65: Dynamic Light Scattering (DLS) studies to determine size distribution of the hydrodynamic diameter of native Cyt c (red line) and Cyt(CGGHHH)$_{14}$ (orange dashed line).

Analysis of Structural Changes by Circular Dichroism Spectroscopy (CD)

Structural integrity of the modified proteins Cyt(Mal) and Cyt(CGGHHH)$_{14}$ was analyzed by circular dichroism spectroscopy. CD spectroscopy is an absorption measurement of left-handed and right-handed circularly polarized light. Asymmetric molecules like proteins interact differently with light depending on the direction of circular polarization. Especially if the chromophores of the amides of the amino acid backbone are adjusted in a specific arrangement, their optical transitions are drifted or broken into numerous changeovers resulting from different exciton interactions.[304] This phenomenon leads to different CD spectra of α-helix, β-sheet or random coil formations of a protein. Therefore, CD spectra can be used to predict and estimate secondary structural elements. More precisely, the far UV area (170 nm-250 nm) was used to investigate the structural integrity of the modified enzymes. Proteins with dominant α-helical structural elements like Cyt *c* have negative bands at 222 nm and 208 nm and a positive band at 193 nm.[305] Each protein has its own individual CD spectrum and a loss in secondary structural elements such as α-helix or β-sheet leads in general to an increase in the number of unordered segments. **Figure 66** shows the CD spectra of Cyt *c* (red line), Cyt(Mal) (purple dotted line) and Cyt(CGGHHH)$_{14}$ (orange dotted line). No significant change of the structure of Cyt *c* after linker attachment to the amino groups of the protein was detected. Introduction of the

hexapeptides, led to a slight decrease of α-helices and an increase of unordered structure elements.

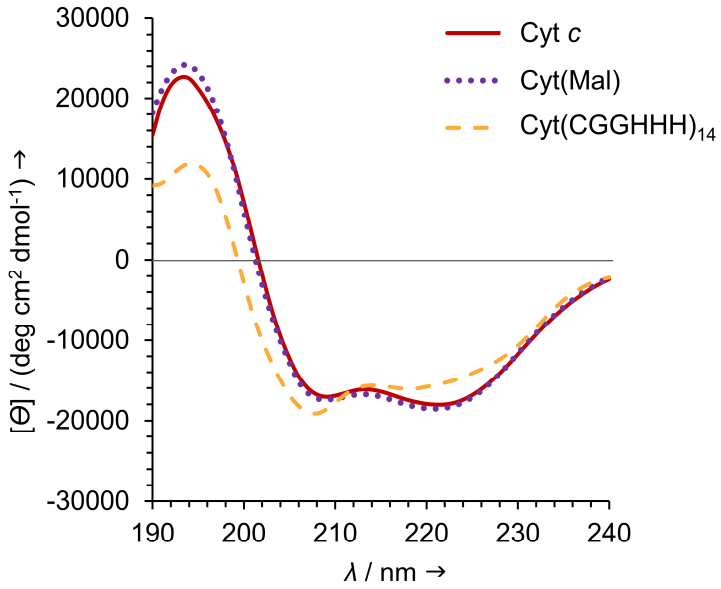

Figure 66: Far-UV spectra of Cyt c (red line), Cyt(Mal) (purple dotted line) and Cyt(CGGHHH)$_{14}$ (orange dashed line). The reaction with NHS-PEG(4)-Maleimide has no effect on secondary structure at all. However, the second modification step with the peptide leads to a slight alteration of secondary structure elements.

These qualitative considerations can be confirmed by calculations of the secondary structure elements using DICHROWEB[306-307] and the CONTIN-LL method with reference set 7 for the appropriate far-UV area (**Table 3**).[308]

Table 3: Calculated percentages of secondary structure elements for Cyt *c*, Cyt(Mal) and Cyt(CGGHHH)$_{14}$; Results calculated with DICROWEB using the CONTIN-LL method (reference Set 7).

	Cyt *c*	**Cyt(Mal)**	**Cyt(CGGHHH)$_{14}$**
α-helix	61.8	57.0	52.8
β-sheet	2.4	3.4	3.4
turns	15.3	14.5	12.2
unordered	20.6	25.3	31.5

Linker attachment leads to a slight decrease of α-helices and an increase of unordered structure elements. This change continues with the conjugation of the hexapeptides to the linker modified surface of Cyt *c*. Compared to native Cyt *c* the α-helices decreased about 10% whereas the unordered structures increased from 20.6% to 31.5%. The β-sheet and turn elements changed only marginally. Overall it can be concluded that the structure was mostly unharmed when compared to the native enzyme[309] and all essential secondary structure elements are preserved after surface modification.

3.2.3 Evaluation of Catalytic Activity

Peroxidase Functionality

Cyt *c* is known for its peroxidase activity due to the iron core containing heme group in the catalytic center of the protein.[310] The heme group is covalently bound by two thioether groups provided by Cys14 and Cys17. The iron in the center of the heme group is coordinated in an octahedral arrangement surrounded by four equatorial nitrogens of the pyrroles in the porphyrin ring and optimally present in the oxidized Fe^{3+} form. The amino acids Met80 and His18 are coordinating with their residues in axial positions. As the mechanism is extensively described in literature it is not discussed in detail herein. Briefly, peroxidase uses four steps to eliminate the harmful peroxide.[310] The sequence of reaction steps allows the use of a chromogen to measure the enzyme's activity. The catalytic parameters such as Michaelis-Menten constant K_M, turnover rate k_{cat} and catalytic efficiency (k_{cat}/K_M) (described in **1.1**) can be determined by using 2,2'-azinobis-(2-ethyl-benzothiazoline-6-sulfonate) (ABTS) as a chromogen and H_2O_2 as substrates (**Figure 67**).[311]

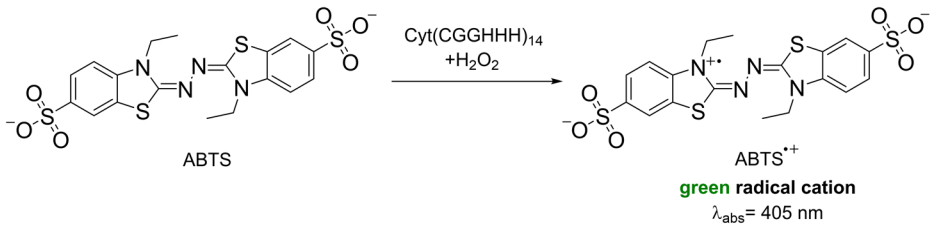

Figure 67: Formation of green ABTS radical cation with Cyt(CGGHHH)$_{14}$ and H_2O_2.

The assay was performed in order to test if the peroxidase activity of the modified cytochrome *c* is preserved after the peptide conjugation. For this, a sample of cytochrome *c* called Cyt *c** was treated in a parallel fashion like during modification of Cyt(CGGHHH)$_{14}$. This allows a more direct comparison of activity, disregarding possible effects on enzymatic activity[312] due to synthetic procedures like centrifugation, stirring overnight and lyophilization. Concentrations of Cyt *c*, Cyt *c** and Cyt(CGGHHH)$_{14}$ were adjusted with the absorbance value at 409 nm to ensure that all solutions contain the same amount of Cyt *c* enzyme. In all cases, the peroxidase activity showed typical Michaelis-Menten kinetics for H_2O_2 (Table 4 and 5.3.3). A K_M value of 0.297 mm was determined for untreated, native Cyt *c*, compared to an increased value of K_M = 5.50 mm for Cyt *c** and K_M = 7.24 mm for Cyt(CGGHHH)$_{14}$. The Michaelis constant K_M is an inverse measurement of the substrate's affinity for the enzyme and thus a higher K_M value indicates a reduced substrate

binding. In this case here, it can be concluded that the lower affinity of Cyt(CGGHHH)$_{14}$ for H_2O_2 results mainly due to the modification conditions, since Cyt *c** shows similar kinetic parameters. The slightly lower affinity of Cyt(CGGHHH)$_{14}$ compared to Cyt *c** can be explained by the 14 peptide molecules on the surface of Cyt *c*, most likely due to steric shielding around the catalytic center. However, despite the lower affinity for the substrate, increasing turnover rates (v_{max}/enzyme concentration) for Cyt *c** and Cyt(CGGHHH)$_{14}$ compared to Cyt *c* can be observed. That means, that at high substrate concentrations and when v_{max} is reached, the conversion of substrates with Cyt *c** and Cyt(CGGHHH)$_{14}$ is more rapid than in native Cyt *c*. The overall catalytic efficiency (k_{cat}/K_M) describes how efficiently an enzyme works and combines the speed of product formation with the affinity for the substrate. Herein, values of 0.14 s^{-1} mM^{-1} and 0.13 s^{-1} mM^{-1} for Cyt *c** and Cyt(CGGHHH)$_{14}$ were determined, respectively. Hence, it can be concluded that the attached peptides have no significant effect on the catalytic efficiency of the underlying Cyt *c*. Only the conditions during the modification slightly change the efficiency.

Table 4: Michaelis-Menten parameters of Cyt *c*, Cyt *c**, and Cyt(CGGHHH)$_{14}$. All measurements were carried out in triplicate.

	Michaelis constant K_M (mM)	**turnover rate k_{cat} (s^{-1})**	**catalytic efficiency k_{cat}/K_M (s^{-1} mM^{-1})**
Cyt *c*	0.30 ± 0.05	0.23	0.77
Cyt *c**	5.50 ± 0.93	0.77	0.14
Cyt(CGGHHH)$_{14}$	7.24 ± 1.01	0.93	0.13

Introduced Esterase-like Functionality

The conjugation of the hexapeptides to the surface of Cyt *c* added an additional function to the peroxidase active enzyme. This additional feature was investigated independently from the original enzyme activity using 4-methylumbelliferyl butyrate (MUF) as cleavable substrate.[313] The coumarin-derived ester is a non-fluorescent compound which is hydrolyzed by lipases into the highly fluorescent 4-methylumbelliferone (4-MU) (**Figure 68**).

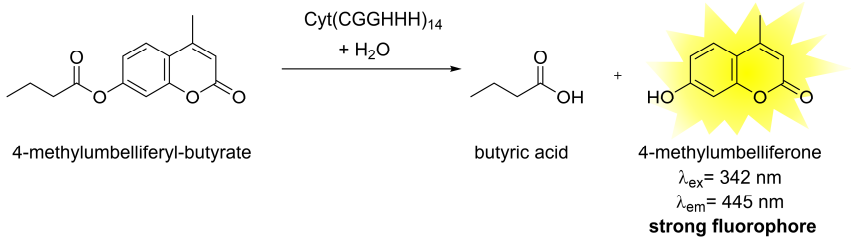

Figure 68: Ester cleavage reaction of 4-methylumbelliferyl-butyrate by Cyt(CGGHHH)$_{14}$ resulting in the highly fluorescent 4-methylumbelliferone.

The MUF assay has so far been used mostly for the identification[314] and determination[315] of lipases and was not yet associated with esterases or even artificial esterase-like activity. Since lipases cleave mainly ester structures and 4-methylumbelliferyl-butyrate is a simple ester molecule, the application for the investigation of the induced esterase-like activity herein was possible.

Table 5: Michaelis-Menten parameters for esterase-like functionality of Cyt(CGGHHH)$_{14}$. For unmodified Cyt *c* no esterase activity was observed. All measurements were performed in triplicate.

	Michaelis constant K_M (mM)	**turnover rate k_{cat} (s^{-1})**	**catalytic efficiency k_{cat}/K_M (s^{-1} mM^{-1})**
Cyt *c*	-	-	-
Cyt(CGGHHH)$_{14}$	6.48 ± 0.93	81.92	12.64

No esterase-like activity of native Cyt *c* was observed whereas Cyt(CGGHHH)$_{14}$ showed esterase-typical Michaelis-Menten kinetics for the substrate (**Table 5**, **5.3.3**). The K_M value was determined to a concentration of 6.482 mM and the turnover rate k_{cat} to about 82 s^{-1}. Compared to literature known examples of similar artificial esterase-like systems, a significantly higher catalytic activity was observed. Examples include gold nanoparticles with immobilized peptides[288] or self-assembled peptide nanostructures[316] that show turnover rates of k_{cat}=0.00072 s^{-1} and k_{cat}=0.00441 s^{-1}, respectively. The pure peptide HHHGGC alone was also investigated towards its esterase-like activity (**6.2.4**). The pure peptide in similar concentrations as attached on Cyt(CGGHHH)$_{14}$ displayed also an esterase-like activity which was even higher than for the conjugated peptide. This can be explained by a higher diffusion of the small molecules compared to more bulky nature of Cyt(CGGHHH)$_{14}$.

In summary, these results confirm the ability of the peptide to cleave ester structures both as individual peptide and also when attached to the surface of Cyt *c*. This confirms that it was possible to introduce an additional, completely new catalytic function to an enzyme.

Coupled Stepwise Catalysis of Peptide and Enzyme

The individual activity of the peroxidase and the esterase-like functionality has been described in the previous two chapters. The combination of both functionalities in a coupled stepwise catalysis is a new approach for mimicking nature's enzymatic cascade reactions. The hexapeptide-modified enzyme material Cyt(CGGHHH)$_{14}$ provides with its close, spatial proximity of both active sites a good environment for transformations. The immediate proximity of both catalytic centers simplifies the quick transfer of respective products to the following reaction site. The cascade reaction which combines the esterase-like and the peroxidase functionality also stands out because it combines two fundamentally different types of enzymatic reactions from the enzymatic reaction classes[1] in one reaction sequence. As test reaction, a modified version of the oxidative coupling of homovanillic acid (HVA) was selected. HVA has been widely utilized in the literature for the determination of H_2O_2 levels[317] or enzyme concentrations of various oxidases. [318] HVA is a non-fluorescent molecule which forms a highly fluorescent dimer (2,2'-dihydroxy-3,3'-dimethoxybiphenyl-5,5'-diacetic acid) under oxidative conditions, e.g. in the presence of free hydroxyl radicals. [319] In detail, the literature-known mechanism for the dimerization of HVA occurs via 4 steps. In a first reaction, the hydroxyl radicals are formed from hydrogen peroxide by the cytochrome *c* peroxidase activity. These radicals attack in a free radical mechanism the HVA molecule which forms under the release of H_2O a dimer molecule (**Figure 69**). The fluorescent product 2,2'-dihydroxy-3,3'-dimethoxybiphenyl-5,5'-diacetic acid, called HVA dimer, has been in detail characterized in the literature.

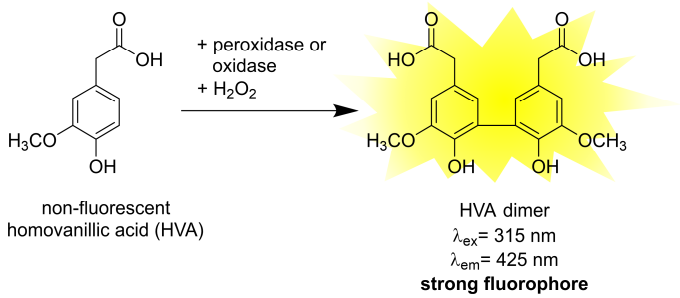

Figure 69: Literature-known dimerization of non-fluorescent HVA monomer by peroxidases or oxidases in the presence of H_2O_2 to the highly fluorescent HVA dimer.

For the study here, the HVA ethyl ester (**Figure 70**) was used in order to analyze the ability of the dual functionalized system to perform coupled stepwise reactions. However, the exact sequence of the single steps in the cascade reaction is so far undiscovered, it is most likely that the reaction starts with the cleavage of the ethyl esters by the peptides on the

surface of Cyt(CGGHHH)$_{14}$ (**Figure 70**). The resulting HVA is then subjected to an oxidative coupling using the peroxidase activity of the Cyt *c* core, resulting in the highly fluorescent HVA dimer (**Figure 70**). This presumption is based on the relation of catalytically active peptides on the surface of Cyt *c*. The amount of 14 "catalytic centers" compared to only one heme group in the center of the enzyme suggests that the esterase-like activity occurs before the oxidative coupling takes place.

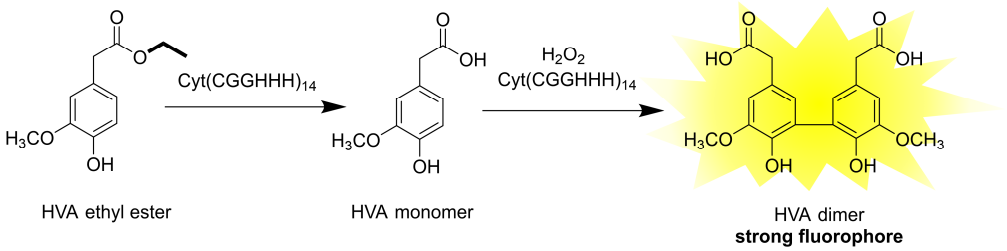

Figure 70: Cascade reaction of Cyt(CGGHHH)$_{14}$ using the HVA ethyl ester. The presumption is, that first, the hexapeptide on the surface of Cyt(CGGHHH)$_{14}$ cleaves the ester, then the peroxidase functionality forms the highly fluorescent HVA dimer.

The development of a strong fluorescence signal is observed within one hour for the reaction of Cyt(CGGHHH)$_{14}$ with the ethyl ester of HVA (**Figure 71**). In the beginning, the reaction is slightly delayed, but the fluorescence increases steadily over time reaching a maximum after 40 min.

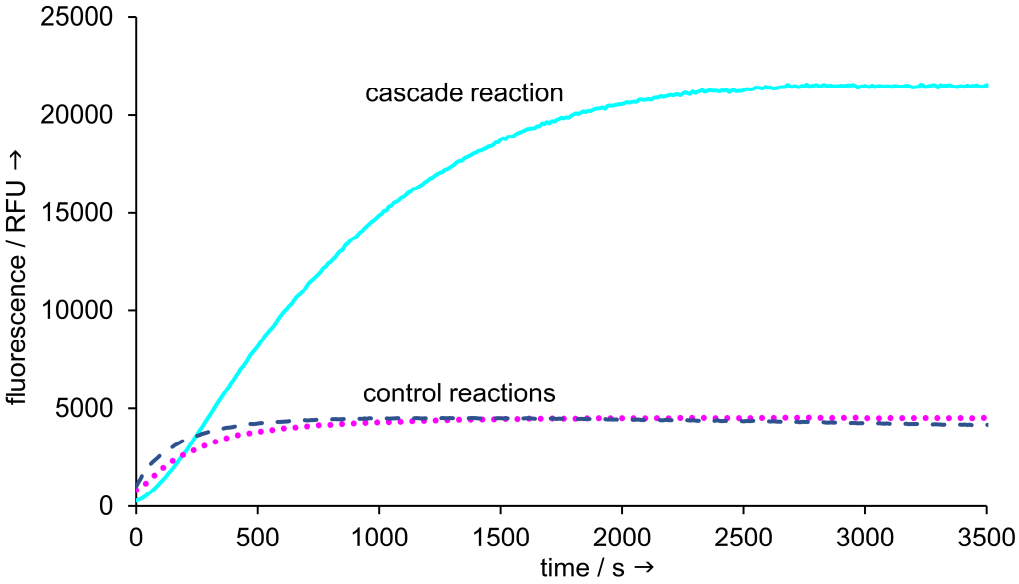

Figure 71: Development of fluorescence in the cascade reaction of Cyt(CGGHHH)$_{14}$ (cyan line). It is presumed, that the reaction is first carried out on the surface with the esterase-like reaction of the attached hexapeptides then and proceeds to the peroxidase functionality in the core of Cyt(CGGHHH)$_{14}$. The three control reactions (purple dotted, blue dashed line and one not visible) will be discussed in **Figure 72**.

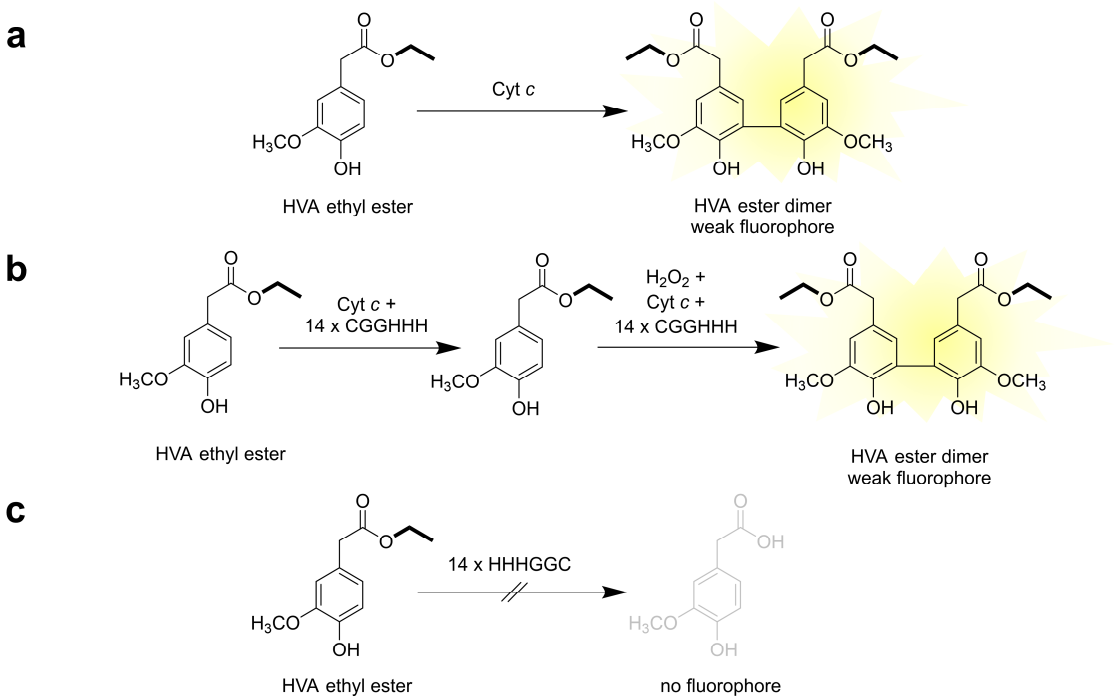

Figure 72: Control reactions of the cascade. (a) The reaction of native Cyt *c* resulted in the dimer of the HVA ester which is only a weak fluorophore. (b) A mixture of Cyt *c* and non-conjugated peptide resulted in the same ester with weak fluorescence. (c) The reaction of the HVA ethyl ester with the pure peptide resulted in no fluorescent product.

The control reactions are in detail described in **Figure 72**. Surprisingly, the first control reaction, the reaction of native Cyt *c* with the HVA ethyl ester resulted in a fluorescence signal, however with much less intensity. Mass spectrometry of the reaction products confirmed the formation of the HVA ester dimer, which is a weak fluorophore (**Figure 72a**). However, when analyzing the mass products of the cascade reaction carried out by Cyt(CGGHHH)$_{14}$, the dimer of the ester cannot be detected. Only the mass of the highly fluorescent HVA dimer is found.

The mixture of Cyt *c* and non-conjugated peptide also resulted in the same weak fluorophore (**Figure 72b**). This second control reaction confirms that for an effective stepwise cascade reaction close proximity between both catalytic centers is essential. Only if the peptides are attached to the surface of the enzyme, the cascade reaction can be performed successfully with the cleavage of all ester groups.

In the third control reaction, the reaction of the pure peptide CGGHHH with the HVA ethyl ester (**Figure 72c**), no fluorescence was observed over one hour which is not surprising since no peroxidase functionality is present which could couple the HVA molecules. Additionally, blank measurements of the assay were carried out with samples

containing no Cyt *c*/Cyt(CGGHHH)$_{14}$ or in another blank measurement no H_2O_2 or lastly no HVA ethyl ester. All of these controls did not show a significant fluorescence signal.

In summary, monitoring the developing fluorescence over one hour, a significantly higher fluorescence for the cascade reaction compared to the control reactions is observed. This fluorescence difference can only occur in an effective combination of the esterase-like and the peroxidase functionality of Cyt(CGGHHH)$_{14}$ and confirms a successful cascade reaction. The comparison between Cyt(CGGHHH)$_{14}$ and Cyt *c* mixed with unbound peptide demonstrates the necessity of proximity between both functionalities. Cyt(CGGHHH)$_{14}$ represents an enzymatic material with two functionalities in close proximity that can carry out a successful stepwise catalysis.

3.2.4 Transfer of the Cascade System to Other Proteins

In the following paragraphs, first results of a carryover and extension of the evaluated and described system from the previous chapters are presented. As part of his internship, Max Scherger evaluated, the modifications of two other proteins with the described hexapeptide Ac-HHHGGC-NH_2 and carried out first experiments regarding the additional esterase-like functionality.

Modification of Lysozyme with the Hexapeptide Ac-HHHGGC-NH_2

Lysozyme (Lyz) is an antibacterial enzyme which is found in almost all human secretion body fluids, e.g. tears, gastric juice, saliva or breast milk. It breaks down the β-1,4-glycosidic bond between *N*-acetylmuramic acid and *N*-acetyl-D-glucosamine residues in the peptidoglycan of gram-positive bacteria and contributes to the destruction of the bacteria's cell walls.[320] It has a well-defined size of 14.3 kDa and seven nucleophilic amino groups on its surface which are available for modification. The modification of Lyz was carried out in the same manner as described for cytochrome *c* and is shown in **Figure 73**. During the modification with the NHS-PEG(4)-Maleimide linker, the hexapeptide was treated with TCEP to ensure the reduction of the cysteine-thiol.

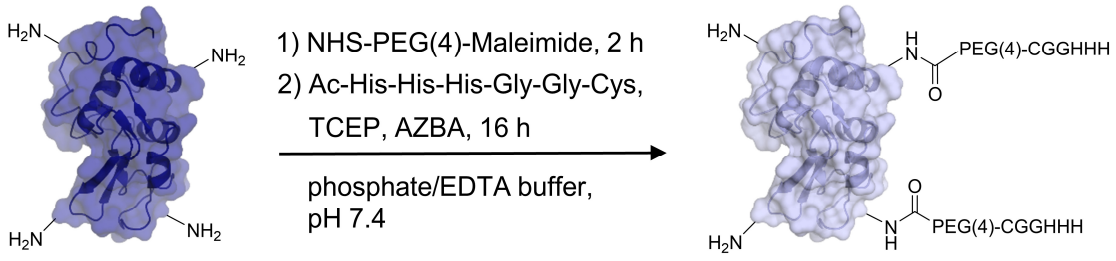

Figure 73: Modification of Lyz with hexapeptide using an NHS-PEG(4)-Maleimide linker. The thiol of the peptide is reduced with TCEP which is neutralized by AZBA.

The Michael addition resulted in the modified lysozyme Lyz(CGGHHH)$_5$ with a weight increase of 31% (3 mg to 3.94 mg). **Figure 74** shows the SDS-PAGE of native Lyz, Lyz(Mal) and Lyz(CGGHHH)$_5$. A protein marker with proteins ranging from 15-170 kDa is used as a reference. The native Lyz forms a sharp band below the 15 kDa marker band which confirms its size of 14.3 kDa. Lyz(Mal) displays a slight increase in size with a broadened band at around 15 kDa. The conjugation with the peptide leads to an even more significant shift with a band between 15-18 kDa. The band broadens compared to the native Lyz which is explained by the size distribution and the modification with different quantities of the

hexapeptide. No remains of unmodified, native Lyz are found in the lanes of Lyz(Mal) and Lyz(CGGHHH)$_5$. In all three sample lanes no dimer formation is observed.

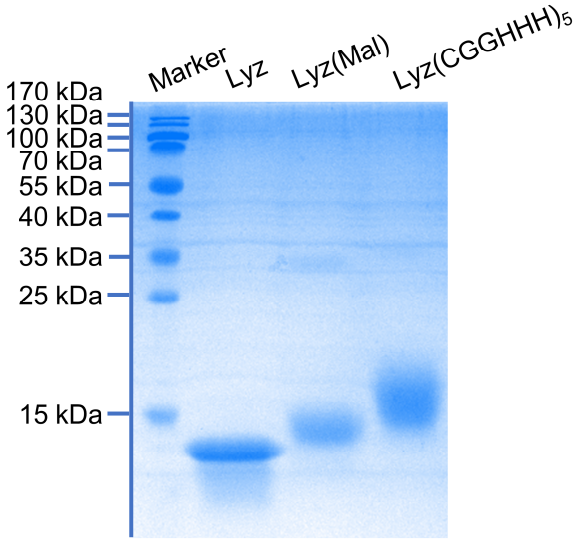

Figure 74. SDS-PAGE of native Lyz, Lyz(Mal) and Lyz(CGGHHH)$_5$. An increase in size can be observed for the two modifications of native Lyz.

For the exact determination of the molecular mass, MALDI-ToF MS was carried out. The spectra of native Lyz and Lyz(CGGHHH)$_5$ are shown in **Figure 75**. The unmodified protein has a sharp peak at expected 14.3 m/z which refers to the single charged enzyme and corresponds to the mass of 14.3 kDa. The spectrum displays also the dimer at 28.7 m/z.

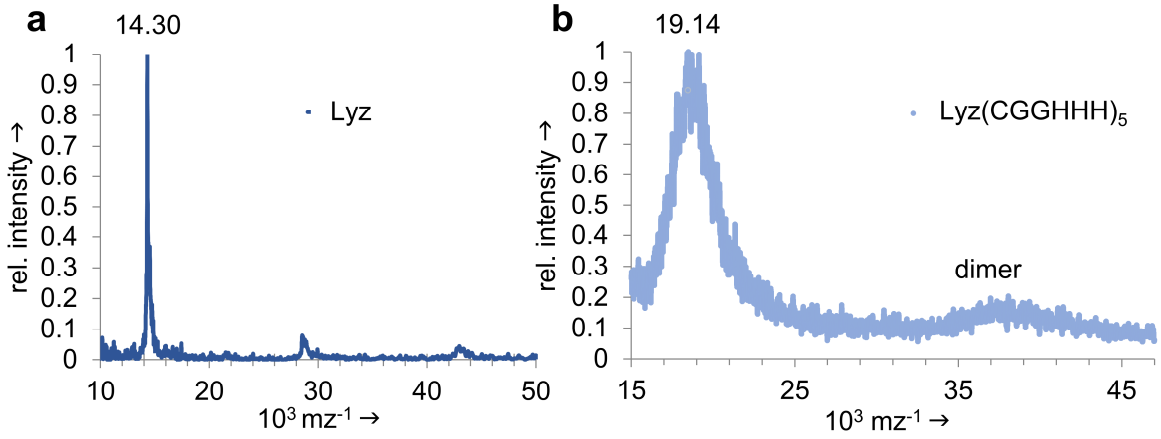

Figure 75. MALDI-ToF MS of native Lyz (dark blue) and Lyz(CGGHHH)$_5$ (light blue).

The spectrum of Lyz(CGGHHH)$_5$ shows one significant peak with a maximum at 19.1 m/z which refers to the single charged molecule with a molecular mass of 19.1 kDa. Between 35 and 40 m/z, a slight second peak is observed which belongs to the dimer of the peptide-modified lysozyme. The mass increases from 14.3 kDa to 19.1 kDa by 4.8 kDa which comes along with the result from the SDS-PAGE and corresponds to about five attached peptides on the surface of Lyz.

Evaluation of Esterase-Like Functionality of Lyz(CGGHHH)$_5$

The introduced hexapeptides result in an additional functionality of lysozyme which was investigated by the MUF assay. In this case here, a simplified version of the assay was used and no Michaelis-Menten parameters were determined for Lyz(CGGHHH)$_5$. The esterase-like activity was only compared between native Lyz and peptide-modified Lyz at one substrate concentration (1.5 mM). **Figure 76** shows the autohydrolysis of MUF as a reference over the measured time, as well as the esterase-like activity of unmodified, native Lyz and Lyz(CGGHHH)$_5$. The sample of native Lyz displays a slight esterase-like activity which can be explained by remaining esterases in the native lysozyme sample after isolation and purification of the enzyme during manufacturing processes. In summary, Lyz(CGGHHH)$_5$ shows a significant 11-fold increased reaction rate towards MUF and therefore the additional esterase-like activity of Lyz(CGGHHH)$_5$ was successfully demonstrated.

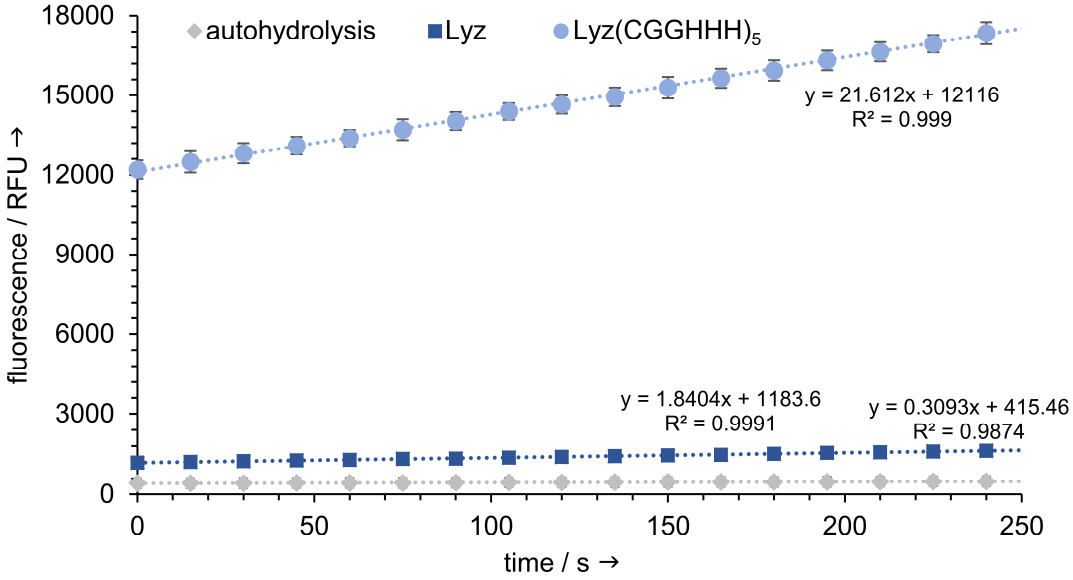

Figure 76. Simplified MUF assay of Lyz and peptide-modified Lyz at a substrate concentration of 1.5 mM MUF.

Modification of *β*-Lactoglobulin with the Hexapeptide Ac-HHHGGC-NH$_2$

A further protein which was modified with the peptide was *β*-Lactoglobulin (BLG). BLG is the major whey protein of cow and sheep's milk with a concentration of ca. 3 g/L and is also present in other mammalian secrets except for human beings. At neutral pH, BLG forms a hydrogen bridge stabilized dimer.[321] It has a molecular weight of 18.3 kDa and 12 potential nucleophilic amino groups on its surface. The protein has no known catalytic

functionality and is therefore no classical enzyme like cytochrome *c* or lysozyme. However, it belongs to the lipocalin proteins, a family of proteins which transport small hydrophobic molecules such as steroids, bilins, retinoids like vitamin A or small lipids.[322-323] The transport is possible through the unique tertiary structure of the lipocalins with its eight-stranded antiparallel beta barrel. The modification of BLG with the hexapeptide was carried out using a different linker than before (**Figure 77**). In contrast to cytochrome *c* and lysozyme, where an NHS-PEG(4)-maleimide linker was necessary to prevent the precipitation of the protein, it was now possible to use the common hydrophobic sulfo-SMCC linker (sulfosuccinimidyl 4-(*N*-maleimidomethyl) cyclohexane-1-carboxylate) for the linkage of the protein amines with the thiols of the peptides.

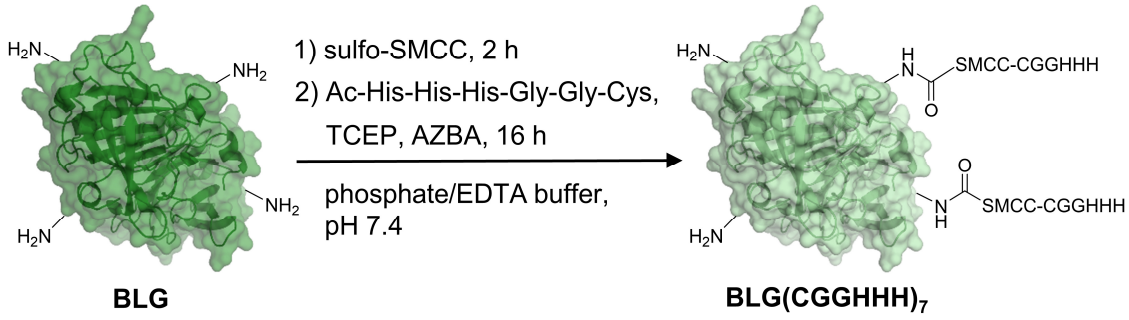

Figure 77: Modification of BLG with the hexapeptide using a sulfo-SMCC linker. The thiol of the peptide is reduced with TCEP which is neutralized by AZBA.

For BLG the modification with this linker worked successfully as shown in **Figure 78**. The SDS-PAGE shows the comparison of native BLG, BLG(SMCC-Mal) and BLG(CGGHHH)$_7$. The native protein forms a sharp band slightly above 15 kDa which is a little bit smaller than the literature known molecular weight of 18.3 kDa. However, a dimer formation is observed between 35 and 40 kDa which confirms the established weight. BLG(SMCC-Mal) displays an increase in molecular weight with a broadened band between 16 and 20 kDa. The dimer formation between 37 and 40 kDa is clearly visible. The sample contains additionally a huge amount of proteins with high molecular weights between 55 and 170 kDa. Probably some sample remained in the stacking gel. These large aggregates can be explained by crosslinking of BLG proteins. In contrast to Cyt *c* and Lyz, BLG contains five cysteines in its peptide backbone per monomer. Four of these cysteines form two disulfide bridges but one is still accessible for chemical modification. The reaction of BLG with the s-SMCC linker does not only lead to a modification of the amines on the surface of the protein but also to a covalent linkage between two or more full proteins. The concentration, storage and multiple dissolving steps of the sample foster this crosslinking. Nevertheless, BLG(CGGHHH)$_7$ does not display higher aggregates. The peptide-modified

protein has a broadened band between 20 and 30 kDa and a dimer which confirms this weight with a mass between 40 and 55 kDa. Both modified BLG samples contain no residues of unmodified, native protein sample.

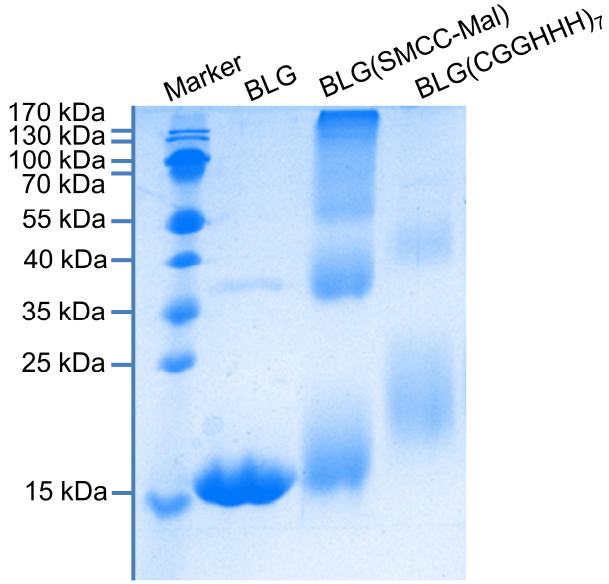

Figure 78. SDS-PAGE of native BLG, BLG with SMCC-Mal linker modified and the peptide modified BLG(CGGHHH)$_7$.

The exact molecular weight was determined by MALDI-ToF MS measurements (**Figure 79**). Native BLG has a sharp peak at 18.3 m/z which corresponds to the single charged molecule with a molecular mass of 18.3 kDa. The spectrum displays also the doubled charged (M^{2+}) protein at 9.2 m/z.

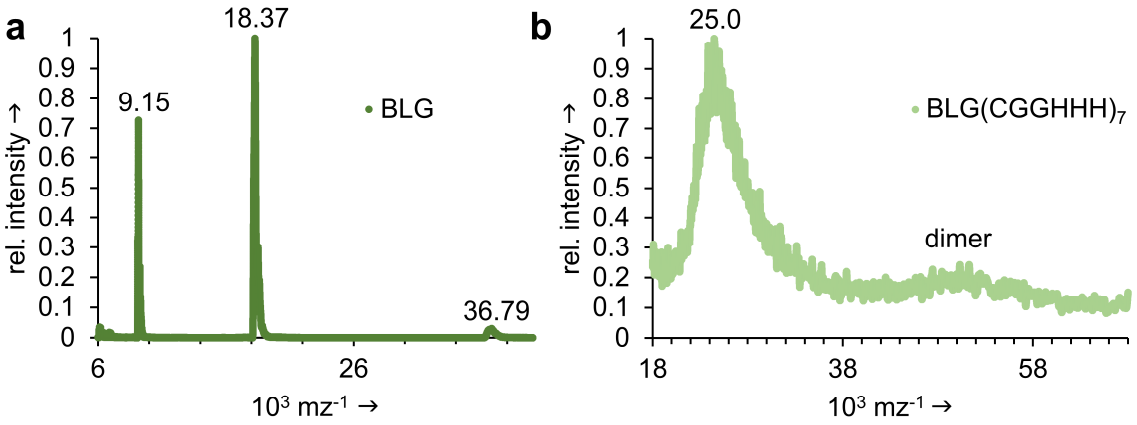

Figure 79. MALDI-ToF MS of native BLG (dark green) and BLG(CGGHHH)$_7$ (light green).

The peptide-modified BLG (**Figure 79b**) has a more broadened peak between 21 and 31 m/z with a maximum at 25 m/z. The increase of the mass by around 7 kDa equals seven attached peptides on the surface of the protein and confirms the results shown by SDS-PAGE.

Evaluation of Esterase-Like Functionality of BLG(CGGHHH)$_7$

The peptide-modified protein material was also investigated towards its esterase-like activity with a MUF assay. For BLG(CGGHHH)$_7$ the simplified version of the assay was used without a determination of Michaelis-Menten parameters. **Figure 80** compares the ester cleavage capability of native, unmodified BLG with BLG(CGGHHH)$_7$. The autohydrolysis of MUF under the chosen conditions was also evaluated but no fluorescence development is observed. Native BLG shows a slight esterase-like activity, which can be again explained by esterases that remain in the isolated protein sample after the manufacturing process. However, BLG(CGGHHH)$_7$ shows a five-fold increased rate of esterase-like activity compared to the native protein. The assay successfully demonstrates that an additional functionality is introduced to the originally non-active BLG protein.

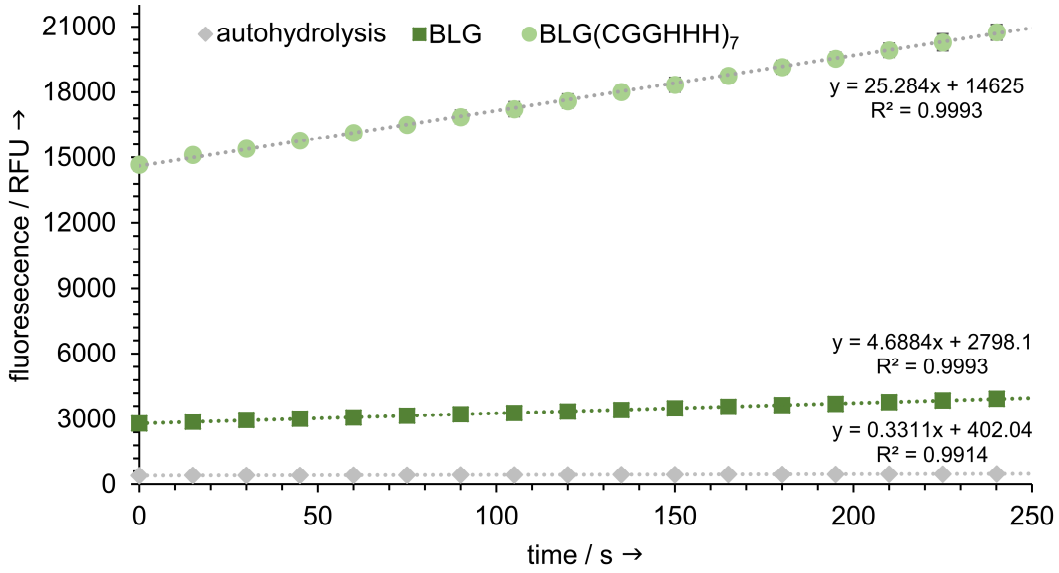

Figure 80. Simplified MUF assay of BLG and peptide-modified BLG at a substrate concentration of 1.5 mM MUF.

In summary, it was possible to successfully transfer the hexapeptide modification as described for cytochrome *c* in chapters 3.2.1 to 3.2.3 to the enzymes lysozyme and *β*-lactoglobulin, resulting in esterase-like protein materials. The comparison of the number of peptides on the surface of the respective protein demonstrates significant differences between the proteins. Cyt *c* has 19 amino groups on its surface of which 14 are modified with the hexapeptide which corresponds to a modification rate of 74%. For Lyz this number reaches almost the same value with 5 modified amino groups out of 7 possible, which equals 71%. BLG has a lower peptide modification with 7 modified amines out of 12 possible ones, which corresponds to 58%. Overall, the modification has to be considered individually

for every protein but first steps of a general transfer of the fundamental research approach were successfully carried out. The transfer demonstrates the wide application field of the approach, even non-active transport or structural proteins can obtain catalytical functions with the small peptide sequences. It is also imaginable to introduce other catalytically active peptide sequences or other catalytic small molecules to the surface of the proteins to mimic nature's complex molecular machines with their multiple functionality.

4 Conclusion and Outlook

The main focus of this work was the synthesis and evaluation of bioinspired catalytic active materials and artificial enzymatic cascade reactions. Both projects contribute significantly to the proceeding of the development of artificial enzyme mimics and the imitation of nature's molecular machines. The demonstrated, innovative approaches provide lots of possibilities for the ultimate goal to manipulate the complex and fundamental interactions happening in cellular environments. This thesis provides first approaches for novel biomimetic approaches to study cellular processes. Future studies in this scope have the potential to produce next-generation delivery and manipulation platforms for innovative applications in biomedical and pharmaceutical research.

In detail, an artificial ATPase was designed by conjugating supramolecular structures such as macrocyclic polyamines to a polysaccharide-based scaffold with bioorthogonal chemistry. New synthetic routes were developed for modified polyamines, containing functional groups that enable an attachment to the biopolymer dextran. The new biopolymer conjugate showed catalytic activity in cleaving ATP and high biocompatibility. In parallel, nature's complex molecular machines were mimicked by attaching short hexapeptide sequences to the surface of cytochrome *c*. An artificial cascade reaction was successfully performed on the surface of the enzyme and then in its inner core.

The following summary will conclude the most important results and discoveries from the two projects. An individual future perspective for each part will be given.

4.1 Artificial ATPase-like Enzyme

Successful Modification of Macrocyclic Polyamines with Functional Groups

The potential ATPase-like activity of polyammonium macrocycles is known for many years.[140] Thus, these supramolecular structures, in particular, the extraordinary catalytically active 2,5,8,11,14,17hexaaza[18]metacyclophanes, were chosen as artificial cleavage sites for the enzyme mimic and were modified with functional groups allowing an attachment to a carrier material. As amino groups provide many possibilities for functionalization, a published synthesis route for macrocyclic polyamines (MCA)[144] was modified in order to obtain amino-modified macrocyclic polyamines. Since a directly introduced amino group at the aromatic ring decomposed during the harsh 5-step

synthesis route, the indirect way via a nitro group was successfully accomplished. After optimization, an amino-modified macrocyclic polyamine with 30% overall yield was obtained. In order to allow bioorthogonal chemistry, the amino group was then further functionalized with heterobifunctional linkers, that introduced successfully cyclooctyne as well as maleimide groups to the MCAs (**Figure 81**). The successful synthesis of functionalized, conjugatable supramolecular structures provides the basis for the development of artificial ATPases.

Effective Synthesis of a Polysaccharide-based Carrier for Active Sites

Dextran was chosen as ideal carrier material for the artificial enzyme. In combination with a further hydrophilic polymer (PEG), a similar setup to nature's core-shell structures was successfully established. Two different approaches were carried out to modify the hydroxyl groups of dextran facilitating the attachment of functionalized MCAs with bioorthogonal chemistry. In a first approach, azide groups, the counterpart for the cyclooctynes, were successfully introduced to the backbone by using DCC/DMAP chemistry. After modification, each dextran chain contains seven potentially connectable groups. In parallel, the backbone of dextran was oxidized leading to an enhanced number of aldehydes which allowed in a bioorthogonal way the attachment of an aminooxy-modified PEG shielding corona. Polymer brushes, visualized in TEM images, with a molecular weight of about 40,000 g mol^{-1} and high biocompatibility, shown in toxicity tests, were obtained. In a second approach, dextran was functionalized with thiol groups, the counterparts for the maleimides. Based on literature[270], a synthesis of water-soluble, sulfur-containing dextran was successfully developed (**Figure 81**). The modified dextran contains also seven potentially connectable groups. Both approaches provide functionalized polymer scaffolds that serve as powerful carriers for the MCAs.

Evaluation of ATPase-like Activity

To complete the enzyme mimic, the supramolecular structures were conjugated to the carrier material (**Figure 81**). In the case of the click chemistry approach, the triazole formation led to water-insoluble products. Although, dextran itself and the MCAs should ensure water-solubility with their hydrophilic groups, surprisingly the big hydrophobic part with the aromatic azidobenzoic acid and the triazole conjugated to the cyclooctyne introduce much hydrophobicity to the entire system leading to an insoluble enzyme mimic.

The project was successfully accomplished until this point and was ceased here because water solubility is an inevitable criterion for an artificial ATPase. In contrast, the thiol-maleimide approach was completed successfully and led to a water-soluble enzyme mimic system with six attached catalytic cleavage sites. Likewise, the artificial enzyme was highly biocompatible and showed no cytotoxicity. The catalytic activity was shown in simple *in vitro* studies by the hydrolysis of ATP in ^{31}P-NMR experiments choosing conditions that are similar to the natural environment of enzymes in the body. For the amino-modified MCA a similar rate constant was determined as for the unmodified, already published MCA. The new ATPase-like bioconjugate demonstrates also catalytic activity, albeit with slightly lower reaction rates. However, this decrease can be attributed to the slower diffusion and the hindered reachability of the supramolecular catalysts within the polymeric scaffold. In contrast to published artificial system, the ATPase here performs in aqueous media and at mild temperatures. Thus, the described synthetic nanomaterial, based on a thiol-modified dextran that carries multiple macrocyclic polyamines as supramolecular catalysts, represents an innovation in the field of artificial enzymes.

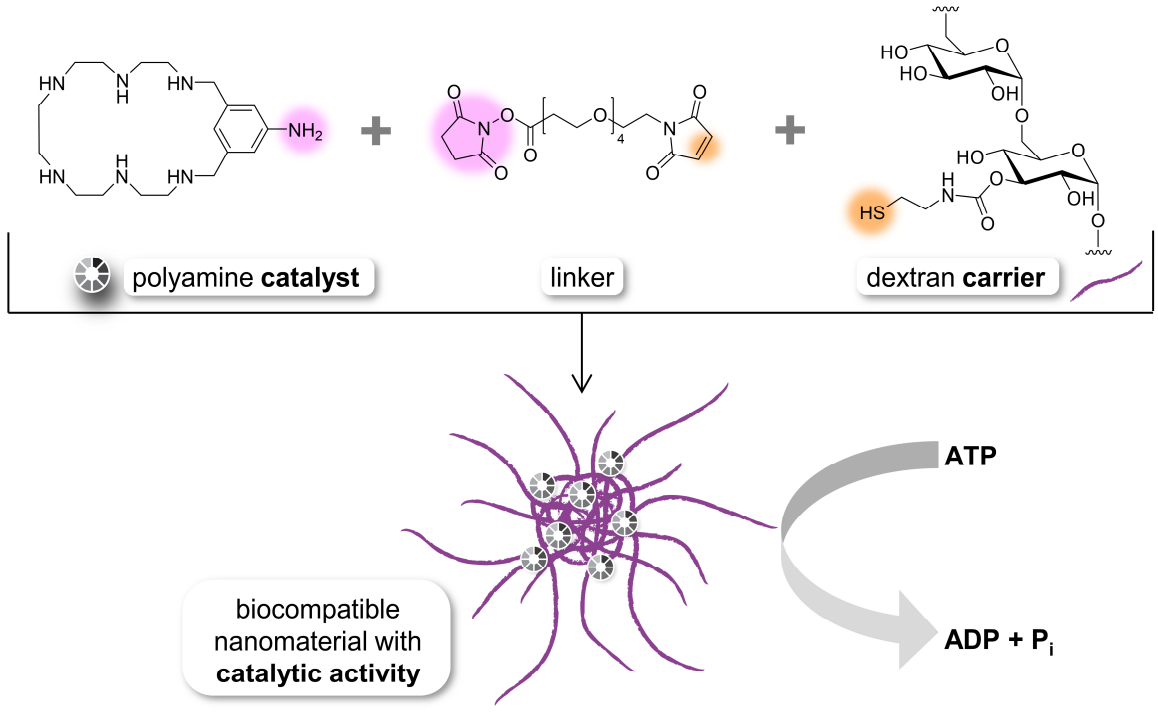

Figure 81: Chemical synthesis of artificial ATPase with an amino-modified supramolecular macrocyclic polyamine catalyst and a dextran-based carrier. Both building blocks are connected with a bifunctional linker resulting in a biocompatible nanomaterial that demonstrates catalytic activity in cleaving ATP to ADP and inorganic phosphate.

Outlook

The designed artificial ATPase provides new opportunities for the construction of enzyme mimics, based on synthetic biopolymers and chemically synthesized active sites, with a potential *in vitro* applicability. Of course, the catalytic activity of the system can be enhanced by attaching more catalysts to the dextran backbone, however the application of these enzyme mimics in cellular environment should be the main goal of this project in the future. Since the regulation of the ATP-ADP levels is of great importance for almost all cellular processes, an artificial "enzyme-like" control is desirable. Such ATPase-like enzymes could e.g. if targeted selectively for cancer cells, exhaust their ATP levels and thus inhibit uncontrolled cell growth.[148] With their small size below 100 nm, the further modification possibilities of the hydroxyl groups of dextran and no cytotoxicity, the artificial ATPase designed in this thesis is a distinguished material for such an *in cell* catalysis. The activity of the ATPase can be investigated by a luciferase/luciferin detection system in cells which allows a direct quantification of ATP.[324] This detection is dependent on the efficacy of the MCAs in catalyzing ATP hydrolysis and correlates the cytotoxicity directly to the endogenous ATP levels of tumor cells. Furthermore, the prolonged effects of these enzyme-like biopolymers can be evaluated, if the reduced levels of ATP finally lead to slower cancer cell growth and death. Hence, a possible new class of cancer treatment drugs can be created.

4.2 Peptide-Enzyme Conjugates for Cascade Reactions

Dual Functionality of Cytochrome *c*

In order to generate a dual enzymatic system, Cyt *c* was surface-modified with catalytically active, short histidine-containing peptide sequences HHHGGC using bioorthogonal chemistry (**Figure 82**). The sequence of the peptide was inspired by the known, esterase-like performance of imidazoles and histidines, respectively. Introducing the thiol-containing cysteine, the possibility for a bioorthogonal thiol-maleimide conjugation was enabled. Cyt *c* was used as a model compound because of its peroxidase activity and its common nucleophilic groups for surface modification. After modification, Cyt *c* carries fourteen peptides on the surface while still preserving its structural integrity and peroxidase activity. The introduced esterase-like activity of Cyt$(CGGHHH)_{14}$ was independently shown. Both functionalities were combined in a cascade reaction. The

reaction was confirmed by a highly developing fluorescence which can only occur in a successful course of the cascade. Remarkable is that the fluorescent product is only generated in case that the peptide is conjugated to the surface of the enzyme, supporting the importance of a small spatial distance between both functionalities. The peptide-modified Cyt *c* represents a catalytic active artificial biomaterial that combines two different enzymatic functionalities within one biomacromolecule.

Transfer of the Approach to Various Proteins

The fully evaluated system of Cyt(CGGHHH)$_{14}$ was then successfully transferred to the enzyme lysozyme (Lyz) and the catalytically inactive protein *β*-lactoglobulin (BLG). The two biomacromolecules differ in structure and enzymatic activity. Both proteins were successfully modified with the hexapeptide on their surfaces. For both synthesized biomaterials an additional esterase-like activity was observed (**Figure 82**). The proteins must be further investigated regarding their structural integrity as well as the conservation of their original enzymatic activity (in the case of lysozyme). Nevertheless, these first results demonstrate the broad applicability of the approach and can serve as a basis for the further advancement in mimicking nature's cascade reactions.

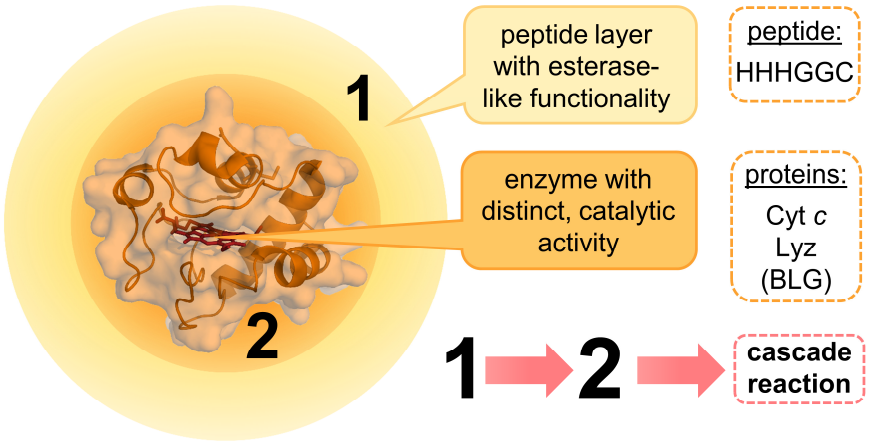

Figure 82: Successful surface modification of two different enzymes (Cyt *c*, Lyz) and one protein (BLG) with hexapeptide (1, yellow) that demonstrates esterase-like activity. In the case of Cyt *c* it was possible to perform a cascade reaction at the surface and then in the inner core (2, orange) of the enzyme. Both other proteins showed an additional esterase-like activity.

Outlook

The successful surface modification of proteins and enzymes with catalytically active small hexapeptides to introduce additional functionality to biomaterials offers the opportunity for an innovative approach to multifunctional enzymatic structures. As alternative to expensive and effortful protein expression with biotechnology, chemical synthesis and conjugation methods can be used to create enzymes with multiple functionality. Furthermore, catalytic activity can be introduced to proteins with no activity that are rather transport proteins such as albumins or the modified *β*-lactoglobulin. These modified proteins can then transport important molecules such as bilirubin, fatty acids, hormones or drugs while at the same time catalyzing reactions related to their cargos. In the future, more than one additional functionality such as e.g. catalytically active guanidine moieties[43, 145] can be introduced to the surface of the enzymes or proteins by using bioorthogonal chemistry. These guanidine structures can be attached using e.g. click chemistry or aldoxime linkers to introduce a group which has RNAase-like activity. Furthermore, the supramolecular catalysts synthesized in the first project of this thesis can be attached to the surface to obtain an additional ATPase-like functionality. An enzymatic material with two or more different, catalytically active functionalities in close proximity opens the opportunity for the development of novel, improved biocatalysts that can carry out complex cascade reactions using for example the energy generated from ATP cleavage. Consequently, using Cyt *c* with its peroxidase activity introducing the hexapeptide with the esterase-like and the RNAase- or ATPase-like functionality would create an enzymatic material with three different functionalities that has similarity to nature's complex molecular machines. New potential, artificial molecular machines can be generated with miscellaneous industrial and therapeutic applications.

5 Experimental Part

5.1 Materials

5.1.1 Reagents and Solvents

Chemicals, reagents and commercial buffers were obtained from German suppliers unless otherwise mentioned.

Chemical	Supplier	CAS
2,2'-Azinobis-(2-ethylbenzthiazoline-6-sulfonate) (ABTS)	Alfa Aesar	30931-67-0
Acetic acid	Sigma-Aldrich	64-19-7
Acetic anhydride	Sigma-Aldrich	108-24-7
Acetonitrile	VWR	75-05-8
N-Acetyl-*L*-cysteine	Sigma-Aldrich	616-91-1
Ammonium acetate	Sigma-Aldrich	631-61-8
Ammonium hydroxide	Sigma-Aldrich	1336-21-6
Aniline	Sigma-Aldrich	62-53-3
Adenosine triphosphate disodium salt hydrate (ATP)	Sigma-Aldrich	34369-07-8
Azidobenzoic-acid (AZBA)	TCI Chemicals	6427-66-3
Benzoyl peroxide (DBPO)	Alfa Aesar	94-36-0
1,3-Bis(bromomethylene)benzene	Alfa Aesar	626-15-3
(1*R*, 8*S*, 9*s*)-Bicyclo[6.1.0]non-4-yn-9-ylmethyl *N*-succinimidyl carbonate (BCN-NHS)	Sigma-Aldrich	n.a.
Boric Acid	Sigma-Aldrich	10043-35-3
tert-Butanol	Carl Roth	75-65-0
n-Butanol	Carl Roth	71-36-3
Chloroform-*d*	Deutero	865-49-6
Coomassie Brilliant Blue	Carl Roth	6104-59-2
Cysteamine	Carl Roth	156-57-0
Cytochrome *c* from horse heart	Serva	n.a.

Chemical	Supplier	CAS
Deuterium chloride 38% in deuterium oxide	Carl Roth	7698-05-7
Deuterium oxide	Deutero	7789-20-0
Dextran, from Leuconostoc mesenteroides, 10 kDa	Sigma-Aldrich,	9004-54-0
Dicyclohexylcarbodiimide (DCC)	Sigma-Aldrich	538-75-0
Diisopropyl azodicarboxlate (DIAD)	Sigma-Aldrich	2446-83-5
N,N-Diisopropylethylamine (DIPEA)	Sigma-Aldrich	7087-68-5
Dichloromethane anhydrous, ≥99.8%, contains 40-150 ppm amylene as stabilizer	Sigma-Aldrich	75-09-2
Dimethylaminopyridine (DMAP)	Sigma-Aldrich	1122-58-3
Dimethyl formamide (DMF)	Sigma-Aldrich	68-12-2
Dimethyl sulfoxide anhydrous, ≥99.9%	Sigma-Aldrich	67-68-5
3-(4,5-dimethylthiazol-2-yl)-2,5-diphenyltetrazolium bromide (MTT)	Sigma-Aldrich	298-93-1
5,5'-Dithiobis(2-nitrobenzoic acid) (DTNB, Ellman's reagent)	Sigma-Aldrich	69-78-3
DMEM GlutaMAX™ (Dulbecco's Modified Eagle's Medium high glucose)	Sigma-Aldrich	n.a.
Ethanol	VWR	64-17-5
Ethyl acetate	VWR	141-78-6
Ethylenediaminetetraacetic acid (EDTA)	Sigma-Aldrich	60-00-4
Ethyl Homovanillate (HVA ester)	Sigma-Aldrich	60563-13-5
Fmoc-rink-amide-aminomethyl-polystyrene resin	Novabiochem Merck Millipore	n.a.
Fmoc-Cys(Trt)-OH	Iris Biotech	103213-32-7
Fmoc-Gly-OH	Iris Biotech	29022-11-5
Fmoc-His(Trt)-OH	Sigma-Aldrich	1428125-83-0
Fetal Calf Serum (FCS)	Life Technologies	n.a.
Glycine	Sigma-Aldrich	56-40-6

Chemical	Supplier	CAS
HBTU (2-(1-Benzotriazol-1-yl)-1,1,3,3-tetramethyluronium hexafluorophosphate)	Sigma-Aldrich	94-790-37-1
Homo vanillic acid (HVA)	Sigma-Aldrich	306-08-1
Hydrazine monohydrate	Sigma-Aldrich	7803-57-8
Hydrobromic acid 48%	Sigma-Aldrich	10035-10-6
Hydrochloric acid 37%	Carl Roth	7647-01-0
Hydrochloric acid 1 M	Carl Roth	7647-01-0
Hydrogen peroxide (H_2O_2)	Sigma-Aldrich	7722-84-1
β-Lactoglobulin	Sigma Aldrich	9045-23-2
Lysozyme	Sigma-Aldrich	12650-88-3
Methanol	Sigma-Aldrich	67-56-1
4-Methylumbelliferyl butyrate (MUF)	Sigma-Aldrich	17695-46-4
N-Bromsuccinimide (NBS)	Alfa Aesar	128-08-5
N-Hydroxyphtalimide (NHP)	Sigma-Aldrich	524-38-9
N-Hydroxysuccinimide (NHS)	Sigma-Aldrich	6066-82-6
Ninhydrin	VWR	485-47-2
5-Nitro-*m*-xylene	Alfa Aesar	99-12-7
4-Nitrophenylchloroformate	TCI Chemicals	7693-46-1
PEG2000	Sigma-Aldrich	9004-74-4
Phosphate buffered saline (10x concentrate, BioPerformance Certified) (PBS)	Sigma-Aldrich	n.a.
Penicillin-streptomycin (5,000 U/mL) Gibco™ (P/S)	Thermo Scientific	n.a.
Phenol	Sigma-Aldrich	108-95-2
Potassium carbonate (K_2CO_3)	Carl Roth	584-08-7
Pyridine	Carl Roth	110-86-1
Rotiphorese Gel Mix 30%	Carl Roth	n.a.
RotiLoad	Carl Roth	n.a.
$SM(PEG)_4$ (NHS-PEG(4)-Mal)	Thermo-Fisher	n.a.
Sodium acetate	Sigma-Aldrich	127-09-3

Chemical	Supplier	CAS
Sodium borohydride	Sigma-Aldrich	16940-66-2
Sodium chloride	Carl Roth	7647-14-5
Sodium deuteroxide 40% in D_2O	Deutero	14014-06-3
Sodium hydroxide	Carl Roth	1310-73-2
Sodium hydroxide solution 1 M	Carl Roth	n.a.
Sodium (*meta*)periodate	Sigma-Aldrich	7790-28-5
Sodium phosphate monobasic monohydrate	Amresco, USA	7558-80-7
Sodium pyruvate (100 mM) Gibco™	Thermo Scientific	n.a.
Sodium sulfate (Na_2SO_4)	Carl Roth	7757-82-6
3-Sulfo-*N*-succinimidyl 4-(*N*-Maleimidomethyl) cyclohexane-1-carboxylate Sodium Salt (sulfo-SMCC)	TCI, Belgium	92921-24-9
TCEP (Tris(2-carboxyethyl)phosphine)	Carl Roth	51805-45-9
Tetraazatetradecane or pentaethylenehexamine	Sigma-Aldrich	4067-16-7
Tetracarbonchloride	Sigma-Aldrich	56-23-5
Tin	Carl Roth	7440-31-5
Toluene	VWR	108-88-3
p-Tolylsulfonyl-chloride	Sigma-Aldrich	98-59-9
Triethylamine > 99,5%	Carl Roth	121-44-8
Trifluoroacetic acid (TFA)	Sigma-Aldrich	76-05-1
Triphenylphosphine (PPh_3)	Sigma-Aldrich	603-35-0
2,4,6-Trinitrobenzene sulfonic acid (TNBS)	Alfa Aesar	2508-19-2
Water, sterile-filtered, BioReagent, suitable for cell culture	Sigma-Aldrich	7732-18-5

5.1.2 Buffers and Media

All buffers were prepared in a volume of 0.1 liter and filtered through a sterile syringe filter with a pore size of 0.22 μm (CME membrane, Rotilabo®). Aqueous buffers were usually stored at room temperature.

Borate buffer (0.1 M, pH 9)

6.18 g boric acid (M_W 61.83 g mol^{-1}) were dissolved in water and adjusted with NaOH to pH 9.

DMEM for HeLa cells

DMEM GlutaMAX^{TM} (high glucose) with phenol red was mixed with 10% FCS, 1% pyruvate and 1% penicillin-streptomycin.

Ninhydrin staining solution (acidic)

0.2 g ninhydrin were dissolved 0.5 mL acetic acid, 100 mL *n*-butanol and 4.5 mL *d*-H_2O. The solution was stored in the fume hood protected from light.

PBS buffer (pH 7.4)

PBS 10x concentrate (Sigma-Aldrich, 100 mL) was diluted with *dd*-H_2O (900 mL); containing 154 mM NaCl, 8 mM $NaHPO_4$ and 2 mM KH_2PO_4 with a final pH of 7.4.

Phosphate buffer (10 mM, pH 7.4)

120 mg sodium dihydrogen phosphate (Amresco, M_W 119.98 g mol^{-1}) were dissolved in *dd*-H_2O and adjusted to pH 7.4 with NaOH.

Phosphate buffer (20 mM, pH 6)

240 mg sodium dihydrogen phosphate (Amresco, M_W 119.98 g mol^{-1}) were dissolved in *dd*-H_2O and adjusted to pH 6 with phosphoric acid.

Phosphate buffer (40 mM, 5 mM EDTA, pH 7.4)

479.92 mg sodium dihydrogen phosphate (Amresco, M_W 119.98 g mol^{-1}) and 186.12 mg ethylenediaminetetraacetic acid dihydrochloride (Alfa, M_W 133.02 g mol^{-1}) were dissolved in *dd*-H_2O and the pH was adjusted to pH 7.4 with NaOH.

Phosphate buffer (0.1 M, pH 8)

1.2 g sodium dihydrogen phosphate (Amresco, M_W 119.98 g mol^{-1}) were dissolved in *dd*-H_2O and adjusted to pH 8 with NaOH.

Potassium phosphate (10 mM)/Sodium sulfate (50 mM) buffer (pH 7)

This buffer was mainly used for measurements of circular dichroism spectra. 212 mg potassium phosphate (M_W 212.28 g mol^{-1}) and 710.2 mg sodium sulfate (M_W 142.04 g mol^{-1}) were dissolved in *dd*-H_2O and adjusted to pH 7 with H_2SO_4.

5.1.3 Disposables

Consumables	Manufacturer
CELLSTAR® cell culture flasks 25 cm^2, 75 cm^2	Greiner Bio-One
Disposable hypodermic needles (size: 21 G)	B.Braun
Disposable pipettes 2 mL, 5 mL, 10 mL, 20 mL	Sarstedt
Disposable syringes 1 mL, 2 mL, 5 mL, 10 mL, 20 mL	B.Braun
Eppendorf Tubes 1.5 mL, 2 mL, 5 mL	Eppendorf
Eppendorf Tubes 1.5 mL (black)	Eppendorf
Filtropur S 0.2 (sterile, non-pyrogenic)	Sarstedt
Glass pipettes	Carl Roth GmbH
Locking clips for dialysis	Carl Roth GmbH
Microplate 12-well, flat bottom, clear, sterile	Greiner Bio-One
Microplate 24-well, flat bottom, clear, sterile	Greiner Bio-One
Microplate 96-well, flat bottom, clear	Sarstedt
Microplate 96-well, flat bottom, clear, sterile	Greiner Bio-One
Microplate 96-well, flat bottom, black	Greiner Bio-One
Microplate 96-well, flat bottom, white	Corning-Costar, USA
NMR tubes	Sigma-Aldrich
Parafilm	Pechiney Plastic Packing
Pipette tips 2 µL, 250 µL, 1000 µL	Sarstedt
Tubes 13 mL, 100x16 mm, PP	Sarstedt
Tubes 15 mL, 120x17 mm, PP	Sarstedt
Tubes 50 mL, 114x28 mm, PP	Sarstedt

5.1.4 Cell Lines

HeLa Cells

An epitheloid cervix carcinoma cell line, established from a cervical cancer tissue sample of Henrietta Lacks in 1951. Cells were a kind gift from the group of [redacted] (Institute of Pharmacy and Biochemistry, Johannes Gutenberg-University, Mainz).

5.1.5 Equipment

Absorption and Fluorescence Measurements

Equipment: Infinite® M200 Pro Plate Reader, Tecan Group Ltd., Switzerland. Analysis was carried out using i-control 1.7 software and Microsoft Excel

Absorption measurements were performed with clear 96-well microplates (flat bottom). Fluorescence measurements were performed with black 96-well microplates (flat bottom).

Bath-Sonicator

Equipment: Sonorex Super RK 102 H, Bandelin electronic

Samples were sonicated until complete dissolving could be observed. Nanoparticles were suspended until no aggregates were detectable.

Centrifuges

Equipment: Heraeus™ Multifuge™ X3R, Thermo Scientific
Heraeus™ Megafuge™ 8 R, Thermo Scientific

Centrifugation was performed at the indicated times in each experiment.

Centrifugal Filter Units

Equipment: Amicon Ultra-4, regenerated cellulose, 3500-10000 g mol^{-1} MWCO, Merck Millipore Ireland

The separation of low molecular and biopolymers was carried out using centrifugal filter units with 4 mL loading capacity. They were centrifuged at 7500 g for 15 min unless otherwise stated.

Circular Dichroism (CD) Spectroscopy

Equipment: J-815 Circular Dichroism Spectrometer, JASCO International co., LTD., Hachioji, Tokyo, Japan

The exact settings and procedure are described in chapter 5.3.2.

Column Chromatography (CC)

Equipment: Kieselgel 60, 0.063-0.2 mm, Firma Merck, Darmstadt
Polygoprep® 60-50 C_{18}, Macherey-Nagel GmbH & Co. KG, Düren

Column chromatography was performed on either normal phase silica gel (NP-SiO_2) or reversed phase (RP-C_{18} SiO_2) with the indicated solvent mixtures on columns of different diameter and length. Solvent mixtures used for column chromatography are shown in volume percent. SiO_2 was first suspended then columns were charged wetly. The mentioned yields refer to chromatographically purified and spectroscopically pure compounds unless otherwise stated.

Dialysis

Equipment: Spectra/Por® 6, regenerated cellulose, MWCO 1,000 g mol^{-1}, Carl Roth GmbH
ZelluTrans Roth, regenerated cellulose, various MWCO, Carl Roth GmbH
Slide-A-Lyzer® Dialysis cassettes, 0.5-3 mL capacity, various MWCO, Thermo Scientific

Dialysis membranes were pre-swelled in *d*-H_2O for 30 minutes and rinsed with water before using. Dialysis was performed against *d*-H_2O unless otherwise stated under constant stirring against 1 L water. Water was changed at least every 2 h for 48 h.

Dynamic Light Scattering Measurements (DLS)

Equipment: Malvern Zetasizer Nano ZS

The exact settings and procedure are described in chapter 5.3.2.

FT-IR

Equipment: Nicolet Avatar 330-IR ATR-Einheit, Thermo Electron Corporation

The compounds were measured directly on the diamant crystal of the device. The maxima are classified into five intensities: vs (very strong), s (strong), m (middle), w (weak), vw

(very weak). The signals are reported in [cm^{-1}] and assignments were carried out according to the literature.[244]

High-Performance-Liquid-Chromatography-Mass-Spectrometry (HPLC-MS)

Equipment: HP Agilent 1100 Series HPLC system

All HPLC-MS measurements were carried out on an HP Agilent 1100 Series HPLC system with a binary pump, a diode array detector, and an automatic sampler. binary pump, a diode array detector, and an automatic sampler. The integrated column was an Agilent Poroshell 120 EC-C_{18} (150 · 2.1 mm) 4 μM which was used with MeCN/H_2O (+0.1% formic acid) solvent mixtures. The attached LC/MSD Ion Trap was from Agilent Technologies and the applied column oven temperature was kept at 40 °C.

Incubator

Equipment: Heraeus® BB15 FUNCTION Line, Thermo Scientific

Cell incubations were performed in a humidified incubator at 37 °C with 5% CO_2 atmosphere.

Inert Gas

Equipment: Argon gas bomb in 99.998% purity N46, Air Liquide Deutschland GmbH

Argon was used as inert gas to flood flasks and reaction containers. Balloons with attached with needles were attached to the reaction flasks to prevent the contact with air.

Lyophilizer

Equipment: ALPHA 1-4 LSC, Martin Christ Gefriertrocknungsanlagen GmbH

Samples were dissolved or suspended in water, frozen in liquid nitrogen and then stored in the lyophilizer for freeze-drying for at least one day.

Mass Spectrometry (ESI-MS)

Equipment: Agilent 6545 Q-TOF-MS, Institute of Organic Chemistry, Johannes Gutenberg-University Mainz

MALDI-ToF (Matrix-assisted Laser Desorption/Ionization Time of Flight)

Equipment: Shimadzu Axima CFR MALDI-ToF mass spectrometer, nitrogen laser Microscopy

The exact settings and procedure are described in chapter 5.3.2.

Nuclear Magnetic Resonance (NMR)

Equipment: Bruker Topspin Fourier 300 MHz

For standard analytical purpose, ^{1}H-NMR spectra were recorded at 300 MHz and ^{13}C-NMR spectra at 90 MHz. The experiments were performed at room temperature using the indicated solvents, mostly $CDCl_3$ and D_2O. The chemical shifts were reported in ppm against the solvent signal of TMS. For the description of the signals, the following abbreviations were used: s = singlet, d = doublet, t = triplet, q = quartet, m = multiplet, br = broad signal. Integrals were calculated by using MestReNova Software. Assignments were carried out according to literature. Peaks resulting from solvent residues were determined by literature.[325]

pH Measurement

Equipment: SevenCompact™ pH/Ion S220 with an InLab® Micro special electrode, Mettler Toledo, Mettler-Toledo Ltd., Beaumont Leys, Leicester, United Kingdom

The pH-meter was calibrated with commercially available buffer standards (pH 4.00, pH 7.00, and pH 11.00).

Rotary Evaporation

Equipment: IKA RV06-ML Janke-Kunkel rotavapor; IKA HB4 basic water bath; Vacuubrand CVC24 vacuum controller; Vacuubrand 1715550193 Membrane pump

Sample concentration under reduced pressure was performed by rotary evaporation in a water bath at 40–50 °C and the adjusted pressure for the used solvent.

Safety Cabinet

Equipment: HERA Safe®, Kendro Laboratory Products, Langenselbold, Germany

All cell culture experiments were performed in a sterile environment using a safety cabinet.

Scales

Equipment: Mettler Toledo Excellence Plus
Sartorius™ M-Prove™ Scales AY303, Sartorius, Göttingen, Germany

Samples below 500 mg were weighed on the fine balance from Mettler. For samples above 500 mg, the standard laboratory balance from Sartorius was used.

SDS Gel Electrophoresis

Equipment: Mini Vertical Electrophoresis Unit Hoefer SE260, Hoefer Inc., Holliston, Massachusetts, USA

GelDoc XR+ with Image LabTM Software, Bio-Rad Laboratories Inc., Hercules, California, USA.

The exact procedure is described in chapter 5.3.2.

Solvents

All solvents were either bought dry or dried before use. Methanol (Sigma-Aldrich) was purified before use by distillation with a rotary evaporator.

Thin Layer Chromatography (TLC)

Equipment: Universal UV-Lampe CAMAG TL-900, West-Berlin

Pre-coated TLC sheets Alugram Xtra SIC G/UV254, Layer 0.2 mm with fluorescent indicator UV254, Macherey-Nagel GmbH & Co. KG, Düren

Pre-coated TLC sheets Alugram RP-18W/UV254, Layer 0.15 mm with fluorescent indicator UV254, Macherey-Nagel GmbH & Co. KG, Düren

Reaction control was carried out with by TLC on silica gel precoated plates either on normal phase or reversed phase. Visualization of the spots was carried out by fluorescence detection at 254 nm UV light or by staining TLC plates.

Transmission Electron Microscopy (TEM)

Equipment: Tecnai T12 (FEI, acceleration voltage: 120 kV, electron source: LaB6 BIO-TWIN cathode, TVIPS-F416 camera), Hillsboro, Oregon, USA

300-mesh copper carbon grids (Plano GmbH) were used for sample preparation.

Water

Equipment: Direct-Q® 5 UV Remote Water Purification System, Merck Millipore, Germany

Water (*dd*-H_2O) for buffers and washing steps was purified by a Direct-Q® 5 UV Remote Water Purification System.

5.2 Synthesis of an Artificial ATPase

5.2.1 Synthesis of Macrocyclic Amine (MCA)

Synthesis of Protected Polyamine

(1,4,7,10,13,16-Hexakis(*p*-tolylsulfonyl)-1,4,7,10,13,16-hexaaza-hexadecane **5**)

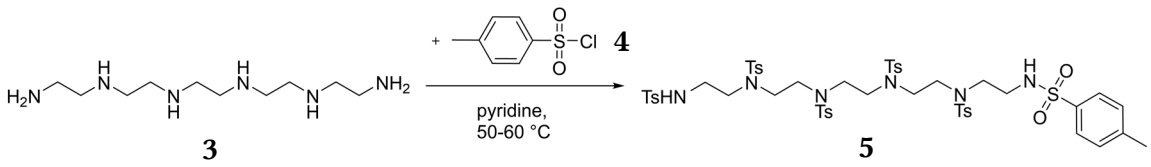

The protected polyamine was synthesized after slightly modified published procedures.[236-237] Briefly, *p*-tolylsulfonyl-chloride **4** (74.41 g, 391.89 mmol, 6 equiv) was dissolved in 200 mL pyridine in a 500 mL round-bottom flask and warmed to 50–60 °C. 3,6,9,12-tetraaza-tetradecane-1,14-amine **3** (15.20 g, 65.41 mmol, 1 equiv) was added during 75 min while the temperature was kept between 50–60 °C. After complete addition of the amine the reaction was stirred for another 30 min at 50–60 °C and then 105 mL of distilled water were added. The mixture was stirred for further 2 h and then cooled down with a mixture of ice and sodium chloride. The precipitate was filtered off and washed two times with 150 mL hot ethanol. The product **5** was obtained as a beige solid (30.61 g, 40%).

^{1}H-NMR (300 MHz, DMSO): δ = 7.73-7.59 (m, 12H, 2,6-TsAr*H*), 7.45-7.32 (m, 12H, 3,5-TsAr*H*), 3.23-3.05 (m, 16H, 2,3,5,6,11,12,13,14-CH_2), 2.84 (q, 4H, 8,9-CH_2), 2.43 2.32 (m, 18H, TsAr-CH_3)

^{13}C-NMR (75 MHz, DMSO): δ =144.18, 144.01, 143.22 (6x -*C*SO_2), 137.72, 135.66, 135.43 (6x -*C*CH_3), 130.45, 130.38, 130.12 (6x arom. 3,5-*C*H), 127.54, 127.38, 127.01 (6x arom. 2,6-*C*H), 49.10, 48.54, 48.29 (5x -TsN-(*C*H_2)$_2$-NTs-), 42.03 (2x TsAr*C*H_2), 21.45 (6x -*C*H_3)

LC-MS (m/z): calculated for [M+H$^+$]: 1158.47, found: 1158.6
calculated for [M+Na$^+$]: 1180.46, found: 1180.5

Synthesis of Tosylated Macrocyclic Amine MCA(Ts)$_6$

(2,5,8,11,14,17-Hexakis(*p*-tolylsulfonyl)-2,5,8,11,14,17-hexaaza[18]metacyclophane **7**)

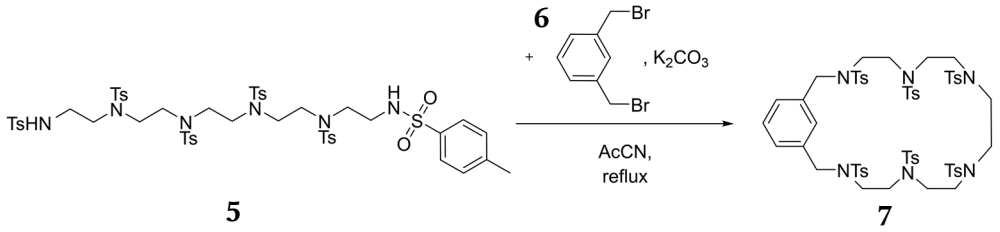

5 **7**

The cyclisation of **5** with 1,3-bis(bromomethyl)-benzene **6** was carried out in the same manner as published.[144, 236] Briefly, **5** (2 g, 1.73 mmol) and K_2CO_3 (4.78 g, 34.59 mmol, 20 equiv) were suspended in refluxing 100 mL acetonitrile. The suspension was refluxed for 30 min. 1,3-bis(bromomethyl)-benzene **6** (0.68 g, 3.39 mmol, 1.5 equiv) was dissolved in 80 mL acetonitrile and added dropwise to the refluxing solution. The suspension was refluxed for further 36 h. The white precipitated was filtered off and the solvent was removed under reduced pressure. The dark brown, oily residue was purified by column chromatography on silica (toluene:ethyl acetate, 9:1). The product **7** was obtained as a white solid (1.41 g, 1.12 mmol, 65%).

^{1}H-NMR (300 MHz, $CDCl_3$): δ =7.66-7.55 (m, 12H, TsAr*H*), 7.27-7.16 (m, 12H, TsAr*H*), 6.98-6.91 (m, 3H, Ar*H*), 4.19 (s, 4H, ArCH_2), 3.22-3.04 (m, 20H, 5x -TsN-(CH_2)$_2$-NTs-), 2.37-2.36 (m, 6H, -CH_3), 2.30 (s, 6H, -CH_3), 2.25 (s, 6H, -CH_3)

^{13}C-NMR (75 MHz, $CDCl_3$): δ = 144.02, 143.81, 143.74 (-*C*SO$_2$), 137.22 (arom. 19,23-*C*-CH$_2$), 135.99, 134.93, 134.74 (12x arom. 2,6-*C*H), 130.03 (arom. 24-*C*H), 129.15, 128.90, 128.34 (12x arom. 3,5-*C*H), 127.50, 127.09 (12x arom. 2,6-*C*H), 125.41 (arom. 20,22-*C*H), 53.25 (2x Ar*C*H$_2$), 50.50, 50.36, 49.90, 48.78, 48.39 (5x -TsN-(*C*H$_2$)$_2$-NTs), 21.68-21.58 (6x -*C*H$_3$)

LC-MS (m/z): calculated for [M+H$^+$]: 1298.57, found: 1298.6
calculated for [M+Na$^+$]: 1282.59, found: 1282.6

Synthesis of MCA

(2,5,8,11,14,17-Hexaaza[18]metacyclophane **2**)

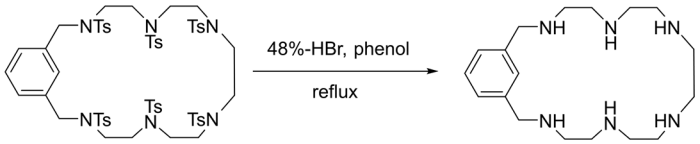

7 **2**

The deprotection of **7** was carried out after a published procedure.[236] Briefly, 2,5,8,11,14,17-hexakis(*p*-tolylsulfonyl)-2,5,8,11,14,17-hexaaza[18]metacyclophane **7** (1.07 g, 0.85 mmol) was mixed with phenol (2 g, 21.25 mmol, 25 equiv) and dissolved in 30 mL 48% HBr. The mixture was refluxed at 130 °C for 50 h. The mixture was washed with chloroform (3x) and the aqueous phase was cooled to 0°C. The strong acidic pH was adjusted to 12 with NaOH pellets. The product **2** was extracted with chloroform (3x) and received after removing of the solvent under reduced pressure as a yellow oil (0.11 g, 3.14 mmol, 37%).

^{1}H-NMR (300 MHz, $CDCl_3$): δ = 7.46 (s, 1H, Ar*H*), 7.14-7.12 (m, 2H, Ar*H*), 3.79 (s, 4H, ArCH_2), 2.76-2.71 (m, 20H, 5x -NH-(CH_2)$_2$-NH-), 1.88 (m, N*H*)

^{1}H-NMR (300 MHz, D_2O): δ = 7.45-7.31 (m, 3H, Ar*H*), 3.81 (s, 4H, ArCH_2), 2.75 (m, 20H, 5x -NH-(CH_2)$_2$-NH-)

^{13}C-NMR (75 MHz, D_2O): δ = 138.54, 129.09, 128.93, 128.16 (Ar*C*), 52.19 (2x ArCH_2), 47.31, 47.00, 46.88, 46.78, 46.02 (10x -NH-(CH_2)$_2$-NH-)

LC-MS (m/z): calculated for [M+H$^+$]: 335.52, found: 335.6
calculated for [M+Na$^+$]: 357.49, found: 357.5

5.2.2 Synthesis of Modified Macrocyclic Amines

Synthesis of 1,3-Bis(bromomethyl)-5-nitrobenzene

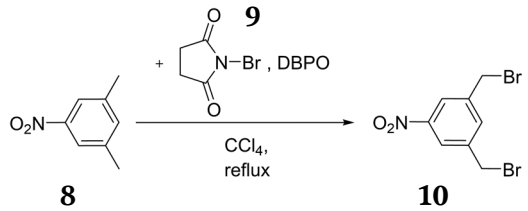

The compound was synthesized in a slightly modified procedure as published.[246] 5-nitro-*m*-xylene **8** (11.21 g, 74.16 mmol, 1 equiv) and *N*-bromosuccinimide **9** (29.09 g, 163.42 mmol, 2.2 equiv) were dissolved in 200 mL CCl_4 in a 500 mL round-bottom flask. 5 spatulas of the radical initiator benzoyl peroxide were added to start the radical aromatic substitution reaction. The mixture was refluxed for 5 h. After cooling to room temperature, the precipitated succinimide was filtered off and the solvent was removed. The solid, slightly yellow product **10** (6.20 g, 27%) was purified by column chromatography (CC) on silica using petrol ether and ethyl acetate in a solvent gradient (50:1→5:1).

^{1}H-NMR (300 MHz, $CDCl_3$): δ = 8.19 (s, 2H, Ar*H*), 7.75 (s, 1H, Ar*H*), 4.52 (s, 4H, -CH_2)

^{13}C-NMR (75 MHz, $CDCl_3$): δ = 148.69 (-*C*NO_2), 140.53 (2x -*C*CH_2), 135.42 (-*C*H), 123.85 (2x -*C*H), 30.78 (2x -*C*H_2Br)

LC-MS (m/z): calculated for [M+Na^+]: 331.94, found: 331.9
calculated for [M+2ACN+H^+]: 392.02, found: 392.4

Synthesis of NO_2-MCA(Ts)$_6$

(2,5,8,11,14,17-Hexakis(*p*-tolylsulfonyl)-21-nitro-2,5,8,11,14,17-hexaaza[18]metacyclophane **11**)

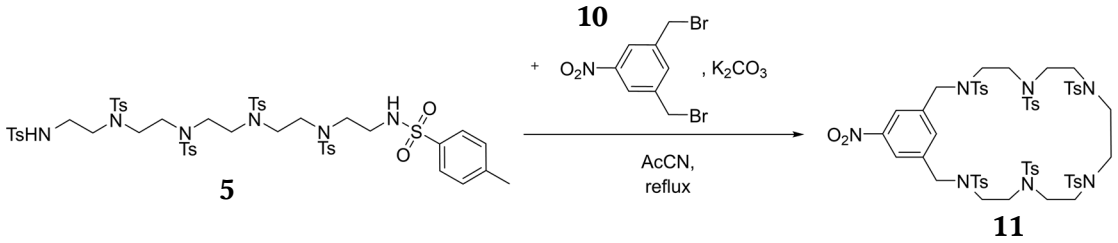

For the cyclisation a modified procedure of Aguilar et al. has been used.[144] 1,4,7,10,13,16-hexakis(*p*-tolylsulfonyl)-1,4,7,10,13,16-hexaaza-hexadecane (11.82 g, 10.21 mmol, 0.8 equiv) **5** and an excess of K_2CO_3 (9.21 g, 66.69 mmol, 5.2 equiv) were suspended in refluxing acetonitrile (200 mL). 1,3-bis(bromomethyl)-5-nitrobenzol **10** (3.94 g, 12.75 mmol, 1 equiv) was dissolved in 200 mL acetonitrile and transferred to a dropping

funnel and added to the suspension during 6 h. The suspension was refluxed for further 48 h. The precipitate was filtered off and the solution was evaporated to dryness. The solid product **11** was chromatographed on silica using dichloromethane. 4.71 g (35.4%) of a colorless solid were obtained.

^{1}H-NMR (300 MHz, CD_2Cl_2): δ = 7.93-7.20 (m, 27H, Ar*H*), 4.43-4.31 (m, 4H, ArCH_2), 3.37-3.05 (m, 20H, 5x -TsN-(CH_2)$_2$-NTs-), 2.49-2.33 (m, 18H, -CH_3)

^{13}C-NMR (75 MHz, CD_2Cl_2): δ= 149.37 (-*C*NO_2), 144.85, 144.77, 144.58 (-*C*SO_2), 140.38 (arom. 19,23-*C*-CH_2), 136.20, 135.65, 135.35 (12x arom. 2,6-*C*H), 133.14 (arom. 24-*C*H), 130.59, 130.50, 130.40 (12x arom. 3,5-*C*H), 127.87, 127.74 (12x arom. 2,6-*C*H), 122.02 (arom. 20,22-*C*H), 53.28 (2x Ar*C*H_2), 50.43, 50.33, 49.94, 49.50 (5x -TsN-(*C*H_2)$_2$-NTs), 21.95-21.69 (6x -*C*H_3)

LC-MS (m/z): calculated for [M+CH_3OH+H^+]: 1337.64, found: 1337.6
calculated for [M+K^+]: 1343.57, found: 1343.6
calculated for [M+Isoprop+H^+]: 1365.68, found: 1365.7
calculated for [M+ACN+Na^+]: 1368.63, found: 1368.6
calculated for [M+2K^++H^+]: 1381.53, found: 1381.6

Synthesis of NH_2-MCA(Ts)$_6$

(2,5,8,11,14,17-Hexakis(*p*-tolylsulfonyl)-21-amino-2,5,8,11,14,17-hexaaza[18]metacyclophane **12**)

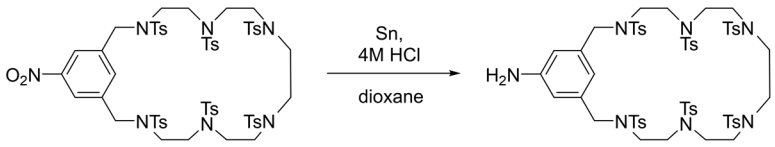

11 **12**

2,5,8,11,14,17-Hexakis(*p*-tolylsulfonyl)-21-nitro-2,5,8,11,14,17-hexaaza[18]metacyclophane **11** (2.13 g, 1.64 mmol, 1 equiv) was dissolved in dioxane with HCl (4 M) and tin (2.14 g, 18.04 mmol, 11 equiv) and refluxed for 5 h. The precipitate was filtered off and the organic solution was washed 3x with 5 M NaOH solution. The organic phase was dried with Na_2SO_4 and evaporated to dryness. A slightly yellow solid **12** (2.05 g, 98%) was obtained.

^{1}H-NMR (300 MHz, CD_2Cl_2): δ = 7.72-7.59 (m, 12H, Ar*H*), 7.38-7.29 (m, 12H, Ar*H*), 6.38 (s, 2H, 20,22-Ar*H*), 6.26 (s, 1H, 24-Ar*H*), 4.12 (m, 4H, Ar-CH_2), 3.27-3.08 (m, 20H, 5x -TsN-(CH_2)$_2$-NTs), 2.44-2.39 (m, 18H, -CH_3)

^{13}C-NMR (75 MHz, CD_2Cl_2): δ= 147.50 (-*C*NH_2), 144.12, 143.91, 143.78 (6x –*C*SO_2), 138.13 (arom. 19,23-*C*-CH_2), 135.93, 135.01, 134.77 (-*C*CH_3), 129.89, 129.82 (12x arom. 3,5-*C*H), 127.50, 127.38, 127.29 (12x arom. 2,6-*C*H) 116.86 (arom. 24-*C*H), 113.28 (arom. 20,22-*C*H), 54.56-53.83 (2x Ar*C*H_2), 51.50, 50.22, 49.75, 49.60, 48.14 (5x -TsN-(*C*H_2)$_2$-NTs-), 21.24 (6x -*C*H_3)

LC-MS (m/z): calculated for [M+H^+]: 1275.64, found: 1275.6
calculated for [M+Na^+]: 1297.62, found: 1297.6
calculated for [M+K^+]: 1313.59, found: 1313.5

Synthesis of NH_2-MCA

(21-Amino-2,5,8,11,14,17-hexaaza[18]metacyclophane **13**)

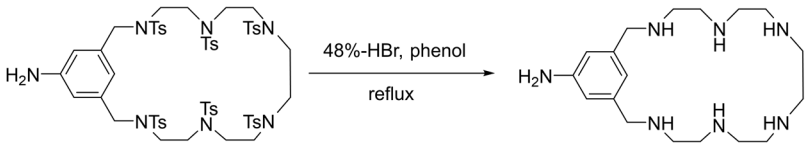

12 **13**

The deprotection of **12** (2.00 g, 1.57 mmol, 1 equiv) was carried out with phenol (3.92 g, 41.60 mmol, 26.5 equiv) and 45 mL HBr (48%). The mixture was refluxed for 15 h at 130 °C. The solution was 3x washed with 50 mL chloroform and purified by ion exchange chromatography on Dowex Marathon (hydroxide form). The solvent was removed under pressure and by lyophilization. The product **13** was obtained as a brown oil (0.47 g, 86%).

^{1}H-NMR (300 MHz, D_2O): δ = 6.75 (s, 1H, Ar*H*), 6.69 (s, 2H, Ar*H*), 3.62 (s, 4H, Ar-CH_2), 2.64 (m, 20H, 5x -NH-(CH_2)$_2$-NH-)

^{13}C-NMR (75 MHz, D_2O): δ = 146.66 (1x -*C*NO_2), 140.60 (2x 19,23-*C*CH_2), 119.69 (1x arom. 24-*C*H), 115.35 (2x arom. 20,22-*C*H), 52.36 (2x Ar-*C*H_2), 47.73, 47.49, 47.39, 47.26, 46.63 (10x -NH-(*C*H_2)$_2$-NH-)

LC-MS (m/z): calculated for [M+H^+]: 350.3, found: 350.5
calculated for [M+Na^+]: 372.49, found: 372.4

Synthesis of BCN-MCA

((1*R*, 8*S*, 9*s*)-Bicyclo[6.1.0]non-4-yn-9-ylmethyl-21-amino-2,5,8,11,14,17-hexaaza[18]metacyclophane **15**)

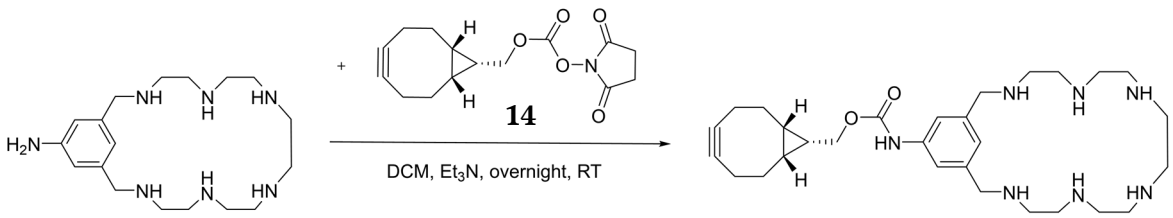

13 **15**

21-Amino-2,5,8,11,14,17-hexaaza[18]metacyclophane **13** (30 mg, 0.0858 mmol, 1 equiv) was dissolved in 10 mL dry DCM. The solution was cooled to 0 °C and 33 μL (26.04 mg, 0.26 mmol, 3 equiv) of triethylamine (Et_3N) were added. The mixture was stirred for 10 min. (1*R*, 8*S*, 9*s*)-Bicyclo[6.1.0]non-4-yn-9-ylmethyl *N*-succinimidyl carbonate, short BCN-NHS **14** (27.5 mg, 0.0944 mmol, 1.1 equiv) was dissolved in DCM and added to the mixture. The reaction was stirred overnight and slowly warmed up to room temperature. The solvent was evaporated under reduced pressure and the reaction mixture was tried to purify under several conditions with column chromatography and the solvents DCM, EtOH and NH_4OH (15:4:1) used as the best conditions. The product **15** was obtained as a brown oil (4.23 mg, 9%).

^{1}H-NMR (300 MHz, D_2O): δ = 6.83 (s, 3H, Ar*H*), 4.35-4.32 (d, 2H, -CH-CH_2-O-CO-), 4.17 (s, 4H, Ar-CH_2-), 3.15-2.92 (m, 20H, 5x -NH-(CH_2)$_2$-NH-), 2.23 (s, 6H, 2x alkyne-CH_2-, 2x alkyne-CH_2-CH_2- only one of them), 1.70 (m, 2H, 2x alkyne-CH_2-CH_2- only one of them), cyclopropyl protons: 1.48 (t, 1H, -CH-C*H*-CH_2-O-), 1.00 (m, 1H, -CH_2-C*H*-CH-CH_2-), 0.88 (m, 1H, -CH_2-C*H*-CH-CH_2-)

^{13}C-NMR (75 MHz, D_2O): not enough substance

LC-MS (m/z): calculated for [M+H$^+$]: 526.38, found: 526.7
calculated for [M+Na$^+$]: 549.37, found: 549.5
calculated for [M+ACN+Na$^+$]: 567.41, found: 567.8

Synthesis of Mal-MCA

(Maleimide-poly(ethylene glycol)-21-amino-2,5,8,11,14,17-hexaaza[18]meta-cyclophane **17**)

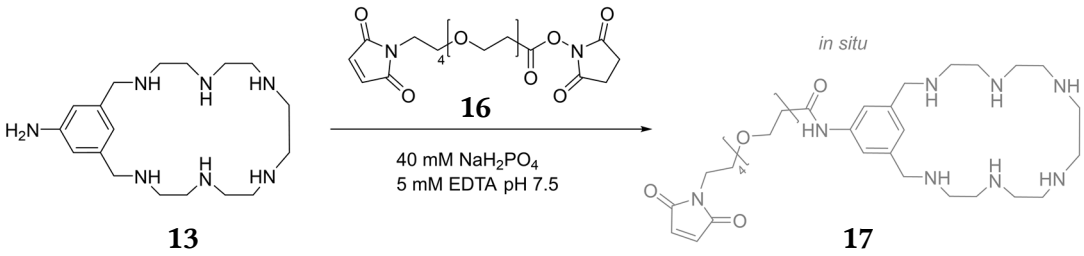

13 **17**

21-amino-2,5,8,11,14,17-hexaaza[18]metacyclophane **13** (28.8 mg, 0.0824 mmol, 1 equiv) was dissolved in 1 mL phosphate buffer (40 mM, 5 mM EDTA, pH 7.4). $SM(PEG)_4$ (NHS-PEG(4)-Mal) **16** (63.5 mg, 0.124 mmol, 1.5 equiv) was also dissolved in 1 mL buffer. The mixture was stirred for 30 min and further used without purification. LC-MS measurements of the reaction product mixture demonstrated the clear formation of the desired product.

^{1}H-NMR (300 MHz, D_2O): not available

^{13}C-NMR (75 MHz, D_2O): not available

LC-MS (m/z): calculated for $[M+H^+]$: 748.46, found: 748.47
calculated for $[M+Na^+]$: 770.46, found: 770.45
calculated for $[M+CH_3OH+H^+]$: 780.49, found: 780.49

5.2.3 Synthesis of Dextran-based Carrier

Synthesis of Dex-$(N_3)_9$

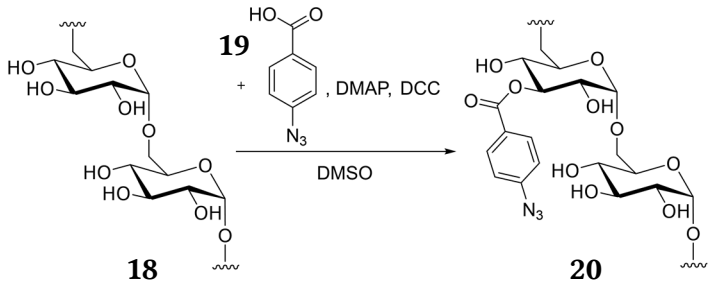

The synthesis was done analogously to a published procedure.[256] Dextran **18** (100 mg) was dissolved in 5 mL dry DMSO in a 10 mL round-bottomed flask protected from light. 4-azidobenzoic acid (AZBA) **19** (50 mg, 0.306 mmol) and DMAP (3.75 mg, 0.0306 mmol) were added to the solution while stirring. The solution was cooled to 0 °C. DCC (62.5 mg, 0.303 mmol) was added and stirring was continued for 5 h. After filtering off the precipitated dicyclohexyl urea, the azidated dextran **20** was precipitated into an excess methanol. The precipitate was centrifuged, washed several times with methanol, centrifuged again in order to remove any free 4-azidobenzoic acid and finally lyophilized. The white, fluffy powder (0.085 g) of Dex-$(N_3)_9$ **20** was stored protected from light in the freezer.

DS (^{1}H-NMR): 9 per chain (61.68 AGU)

^{1}H-NMR (300 MHz, d_6-DMSO): δ = 8.02 (d, *m*-C_6H_5), 7.24 (d, *o*-C_6H_5), 4.85-4.91 (m, OH_3 + OH_4), 4.67 (s, anomeric H), 4.49 (s, OH_2), 3.19-3.76 (m, AGU-H)

^{13}C-NMR (90 MHz, d_6-DMSO): δ = 98.73 (anomeric *C*), 73.79 (*C*H-OH-3), 72.29 (*C*H-OH-2), 70.87 (C*H*-CH_2-5), 70.59 (*C*H-OH-4), 66.59 (*C*H_2-6), C atoms of AZBA not determinable

FT-IR [cm^{-1}]: 3330 (vs, br, OH), 2921 (m, CH_2), 2124 (m, N_3), 1707 (w, ester C=O), 1597 (w), 1503 (vw), 1421 (w), 1339 (w), 1278 (m), 1147 (m), 1098 (m), 1005 (vs, sec. OHs), 947 (m), 910 (m), 845 (w), 763 (w)

Synthesis of OxDex-$(N_3)_9$

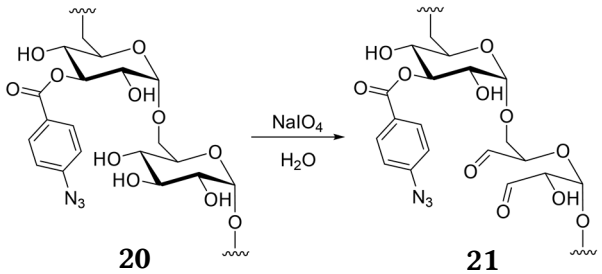

20 **21**

The oxidation was carried out similarly to a published procedure for the oxidation of dextran.[259] Briefly, Dex-$(N_3)_9$ **20** (200 mg) were dissolved in 4 mL water. Sodium periodate ($NaIO_4$) (44 mg, 0.206 mmol) were added in one portion and the solution was stirred for 5 h. Afterward, the reaction mixture was dialyzed (MWCO 3.5 kDa) against distilled water for 2 d and lyophilized. The OxDex-$(N_3)_9$ **21** was obtained as a fluffy, white powder (143 mg) which was not further characterized.

Synthesis of Aminooxy-PEG (PEG-O-NH_2)

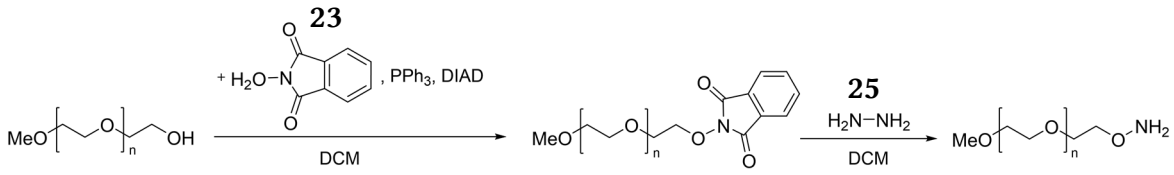

22 **24** **26**

The end group modification of PEG 2000 **22** was carried out after a published procedure.[264] Briefly, PEG monomethyl ether **22** (5 g, 2.5 mmol), triphenylphosphine (PPh_3) (1.92 g, 7.313 mmol, 3 equiv) and *N*-hydroxyphthalimide (NHP) **23** (1.2 g, 7.313 mmol, 3 equiv) were dissolved in 20 mL dry dichloromethane under an argon atmosphere. Diisopropyl azodicarboxylate (DIAD) (1.380 mL, 1.378 g, 6.813 mmol, 2.7 equiv) was added dropwise during 15 min. After complete addition, the reaction was stirred for further 18 h. The mixture was precipitated in 400 mL diethyl ether and stirred vigorously for 20 min. The precipitate was filtered off, washed with ether and dried under reduced pressure. A rose solid of PEG-NHP **24** was obtained (3.849 g, 77% based on unsubstituted PEG).

DS (^{1}H-NMR): complete conversion

^{1}H-NMR (300 MHz, $CDCl_3$): δ = 7.84-7.80 (m, 2H, Ar*H*), 7.77-7.72 (m, 2H, Ar*H*), 4.36 (t, 2H, CH_2-O-N), 3.63-3.52 (m, PEG backbone), 3.38 (s, 3H, -CH_3)

The phthalimide moiety was cleaved using hydrazine hydrate. 3 g (1.5 mmol) of PEG-NHP **24** were dissolved in 10 mL dichloromethane and hydrazine monohydrate **25** (187.7 mg, 182 μL, 3.75 mmol, 2.5 equiv) was added in one portion. The mixture was stirred for 30 min and a white precipitate was observed. The mixture was filtered over glass wool and concentrated carefully under reduced pressure. The product PEG-O-NH_2 **26** was obtained as a white powder (2.62 g, 87%).

DS (^{1}H-NMR): complete conversion

^{1}H-NMR (300 MHz, $CDCl_3$): δ = 4.30 (t, 2H, CH_2-O-NH_2), 3.88-3.52 (m, PEG backbone), 3.37 (s, 3H, -CH_3)

Synthesis of Dextran-PEG Polymer Brush (OxDex-$(N_3)_9$ $(PEG)_{16}$)

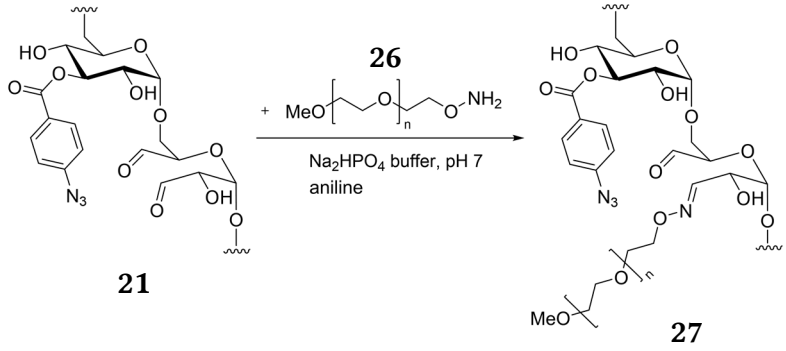

OxDex-$(N_3)_9$ **21** (100 mg, 1.616 mmol) were dissolved in 2 mL phosphate buffer (40 mM, pH 6.5) until complete dissolution was achieved. Aniline (12.2 mg, 16.86 μL, 0.185 mmol, 2 equiv) was added in one portion and the mixture was stirred for 45 min. Aminooxy-modified PEG **26** 2 kDa (370 mg, 0.185 mmol, 2 equiv) was dissolved in 1 mL buffer and added to the stirring solution. The mixture was stirred for 7 h, before transferring the solution first to a dialysis bag (MWCO 12-14 kDa), then to a dialysis bag with larger cut-off (50 kDa). The polymer brush **27** was obtained as a colorless powder (364 mg).

DS (^{1}H-NMR): 16.5 per chain (61.68 AGU), calculated MW 43000 g mol^{-1}

^{1}H-NMR (300 MHz, D_2O): δ = 8.10 (d, m-C_6H_5), 7.25 (d, o-C_6H_5), 4.96 (s, anomeric H), 4.25-3.43 (m, dextran glucosidic protons and PEG signal), 3.37 (s, 3H, -CH_3)

GPC (DMF, PEG-Standard): distribution from 40000 to 50000 g mol^{-1}

Transmission Electron Microscopy (TEM)

The dextran suspension (1 mg mL^{-1}) was applied in 5 μL drops on a 300-mesh copper carbon grid from Plano GmbH for TEM measurements. The pictures were taken with a transmission electron microscope as described in **5.1.5**.

Synthesis of Dex-$(SH)_7$ via Dex-$(4\text{-NC})_{7.5}$

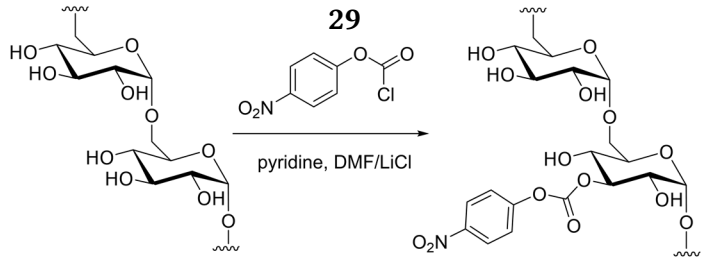

Dextran **18** was modified after a published procedure.[270-271] Briefly, the hydroxyl groups of dextran were first activated with 4-nitrophenyl-chloroformate (4-NC) **29** and then reacted with cysteamine. Dextran **18** (250 mg, 1.54 mmol AGU) was dissolved in 4 mL, hot dry DMF containing 80 mg (2% of solvent) LiCl. After cooling to 0 °C 42.7 μL (41.41 mg, 0.52 mmol, 0.34 equiv referred to AGU) pyridine and 105.53 mg (0.52 mmol, 0.34 equiv) 4-nitrophenyl chloroformate **29** were added and stirred for 2 h at 0 °C. The mixture was precipitated in ice-cold ethanol, washed with diethyl ether and filtered off. The colorless powder **30** (265 mg) was dried *in vacuo*.

DS (^{1}H-NMR): 7.5 per chain (61.68 AGU)

^{1}H-NMR (300 MHz, DMSO): δ = 8.35-8.32 (dd, aromatic protons), 7.58-7.55 (dd, aromatic protons), 5.11 (s, dextran glucosidic protons at positions which have nitrophenyl substituents), 4.68 (s, anomeric protons), 3.21-4.18 (m, dextran glucosidic protons)

FT-IR [cm^{-1}]: 3330 (vs, br, OH), 2914 (m, CH_2), 1765 (w, acyclic carbonate), 1525 (w), 1348 (w), 1261 (m), 1217 (m), 1149 (m), 1012 (vs, sec. OHs), 916 (m), 860 (w), 760 (w)

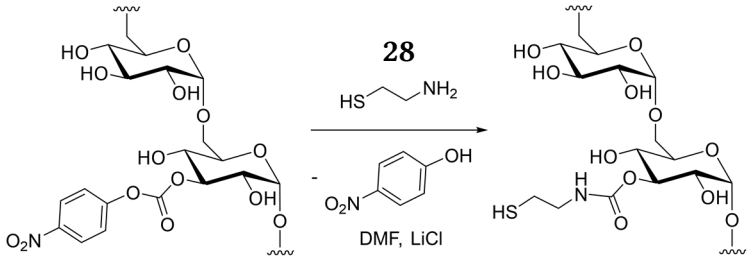

30 **31**

In a second reaction, the carbonates were replaced by cysteamine. Dextran-4-NC **30** (100 mg, 0.62 mmol) was dissolved in 3 mL hot DMF containing 30 mg (1% of solvent) LiCl. After cooling to room temperature cysteamine **28** (45.6 mg, 0.59 mmol, 8 equiv referred to activated OH groups) was added in DMF. The solution turned instantly yellow demonstrating the cleavage of the *p*-nitrophenolate. After stirring overnight, the mixture was precipitated in ice-cold ethanol, washed several times and finally dissolved in water. A spatula of tris(2-carboxyethyl)-phosphine (TCEP) was added to reduce any disulfide bonds. The solution was again precipitated in ice-cold ethanol, washed and rapidly dissolved in water and lyophilized. 87.12 mg of a colorless powder of Dex-$(SH)_7$ **31** was obtained.

DS (^{1}H-NMR): 7

DS (Ellman's assay): 6-7

^{1}H-NMR (300 MHz, D_2O): δ = 5.36, 5.20 (s, dextran glucosidic protons at positions which have cysteamine substituents), 5.01 (s, anomeric protons), 4.03-3.96 (m, dextran glucosidic protons), 3.80-3.72 (m, dextran glucosidic protons), 3.62-3.52 (m, dextran glucosidic protons), 3.37 (m, cysteamine protons), 2.70 (m, cysteamine protons)

FT-IR [cm^{-1}]: 3330 (vs, br, OH), 2914 (m, CH_2), 1695 (w, carbamate), 1408 (w), 1338 (w), 1147 (m), 1149 (m), 1005 (vs, sec. OHs), 912 (m), 843 (w), 762 (w)

Ellman's Assay for the Quantification of Thiol Groups

For the Ellman's assay[273], thiol-modified dextran **31** (3 mg mL^{-1}) was dissolved in sodium phosphate buffer (0.1 M, pH 8) containing 1 mM EDTA. Ellman's reagent was dissolved in the reaction buffer (4 mg mL^{-1}) and 8 μL of this solution were added to 400 μL reaction buffer in black 1.5 mL Eppendorf tubes. 40 μL of sample or *N*-acetylcysteine were added. The mixtures were vortexed and incubated for 20 min at RT in the dark. 100 μL of each sample were pipetted in triplicate in a clear, flat bottom 96-well microplate (Sarstedt). The

absorbance was measured with an Infinite® M200 Pro Plate Reader Tecan microplate reader at 412 nm. *N*-acetylcysteine at concentrations of 9.77 µM to 2.5 mM was used to prepare the standard curve. As control, unmodified dextran was measured.

Synthesis of Dex-(S-Mal-MCA)$_6$

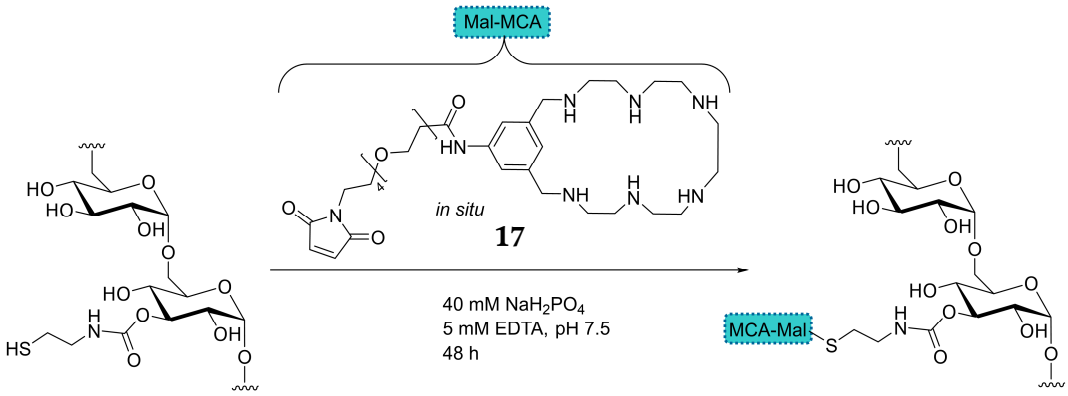

The conjugation was carried out by a thiol-maleimide reaction of Dex-(SH)$_7$ **31** and Mal-MCA **17**. The Mal-MCA **17** was generated *in situ* right before the reaction by mixing SM(PEG)$_4$ (NHS-PEG(4)-Mal) **16** (63.5 mg, 0.124 mmol, 7.5 equiv) with NH$_2$-MCA **13** (28.8 mg, 0.0824 mmol, 5 equiv) for 30 min in 1 mL phosphate buffer (40 mM, 5 mM EDTA, pH 7.4). Dex-(SH)$_7$ **31** (30 mg, 0.185 mmol, 0.0165 mmol thiol groups, 1 equiv) was reduced with TCEP (1 spatula tip) for 30 min and precipitated in ethanol. The reduced Dex-(SH)$_7$ **31** was dissolved in buffer and mixed with the Mal-MCA **17** and stirred for 48 h at room temperature. The solution was purified with centrifugal filters (MWCO 3.5 kDa), washed 7 times and lyophilized. The product **33** was obtained as a slightly brown, fluffy powder 41.69 mg.

^{1}H-NMR (300 MHz, D$_2$O): δ = 7.77 (s, 1H, aromatic protons), 7.52 (s, 4H, aromatic protons), 6.71 (m, 22 H, aromatic protons), 5.35, 5.20 (s, dextran glucosidic protons at positions which have cysteamine substituents), 5.01 (s, anomeric protons), 4.03-3.37 (m, dextran glucosidic protons), 3.37 (m, cysteamine protons), 2.72-2.49 (m, cysteamine protons and polyamine protons)

^{13}C-NMR (75 MHz, D$_2$O): not available

Ninhydrin coloration: deep purple

FT-IR [cm^{-1}]: 3330 (vs, br, OH), 2914 (m, CH_2), 1699 (w, carbamate), 1633 (w, prim. and sec. amines), 1548 (w, sec. acid amides), 1402 (w), 1349 (w), 1257 (m), 1149 (m), 1010 (vs, sec. OHs), 914 (m), 843 (w), 762 (w)

Ellman's Assay: 0 thiols detectable

5.2.4 Cell Culture

HeLa cells were grown in Dulbecco's Modified Eagle Medium (DMEM GlutaMAX™) supplemented with 10% (V/V) fetal calf serum (FCS), 1% pyruvate, and 1% penicillin-streptomycin. Cell incubations were performed in a humidified incubator at 37 °C with 5% CO_2 atmosphere. All used buffers were either autoclaved, sterile filtered or already sterile when supplied and were preheated to 37 °C before usage. Cells were grown in 25 cm^2, 75 cm^2 or 225 cm^2 standard cell culture flasks.

Determination of Cell Viability by MTT Assay

The cytotoxic effects of dextrans and dextran-modified samples were evaluated by MTT assay[277] using human HeLa cells. Cells were precultured in DMEM containing 10% FCS and 1% P/S and then seeded in sterile clear, flat bottom 96-well cell culture microplates at a concentration of 15,000 cells per well and a volume of 100 μL. Cells were allowed to attach and grow overnight. Dextran samples and corresponding samples of small molecules were prepared by dissolving the sample solutions in DMEM in a concentration range from 62.5 μg to 1 mg mL^{-1}. The next day, DMEM was removed from HeLa cells and replaced by 100 μL of the sample solutions as well as DMEM as blank solutions. All measurements were carried out in triplicate. The cells were incubated for 48 h at 37 °C in 5% CO_2. After 48 h, 40 μL MTT solution (3 mg mL^{-1} in DMEM) was added to each well and incubated at 37 °C for 30 min. After total removal of the medium, a mixture of 200 μL DMSO and 25 μL glycine buffer (0.1 M glycine, 0.1 M NaCl, pH 10.5) was added to each well and softly shaken for 15 min to dissolve the purple formazan salt. 50 μL of this concentrated, purple DMSO solution was added to a second clear, flat bottom 96-well microplate containing a mixture of 17 μL glycine buffer and 133 μL DMSO per well. Finally, the absorbance of the formazan was read using an Infinite 200 PRO (Tecan) plate reader at 595 nm. Furthermore, the background was measured at 670 nm and subtracted from the data obtained from the first read out.[326] Cell viability was calculated with Microsoft Excel. Cell viability was normalized to the absorbance of the blank samples.

5.2.5 Evaluation of ATPase-like Functionality

^{31}P-NMR measurements

The ATP cleavage was investigated with ^{31}P-NMR measurements. All measurements were carried out at 313 K (40 °C) in D_2O solutions. Small amounts of NaOD (40% in D_2O) and DCl (38% in D_2O) were used to adjust the solutions pD. The pH was calculated from the measured pD value by using pH = pD-0.4.[327] The reaction progress was monitored by following the time dependent changes of the integrals of ATP, ADP and inorganic phosphate in the ^{31}P-NMR spectrum. The NMR acquisition time was set to d1=5 s and 8 scans were carried out per measured time point. The quantity of cleaved ATP was calculated by

$$[\text{ATP}] = \frac{\int P_\beta}{\int P_\beta + \int P_i} \qquad \text{and} \qquad [P_i] = \frac{\int P_i}{\int P_i + \int P_\beta}$$

Time-course kinetics were obtained for the cleavage of 30 mM ATP in the presence of the respective catalytically active compounds. The MCAs were used in a 10 mM concentration if administered alone. The amount of dextran conjugate was adjusted that the same number of catalytic moieties is present in the measurements. All experiments were repeated twice. The catalytic rates were calculated by using Mestrenova Reaction Monitoring®.

5.3 Modification of Proteins for Artificial Enzymatic Cascade Reactions

5.3.1 Protein Surface Modification

Synthesis of Hexapeptide Ac-His-His-His-Gly-Gly-Cys-NH_2 (short HHHGGC)

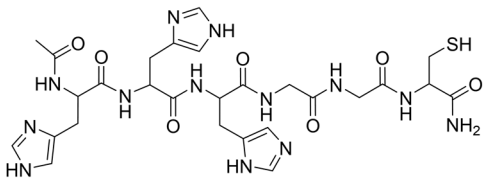

Ac-His-His-His-Gly-Gly-Cys-NH_2
short: HHHGGC

For the solid phase peptide synthesis, Fmoc-Rink-amide-aminomethyl-polystyrene resin was used. The step-wise chain elongation of the peptide was performed using the CS Bio CS136XT peptide synthesizer which is an automated batch peptide synthesizer. The detailed procedure is described elsewhere.[328] Briefly, the dried resin beads were swollen in DCM for 10 min in a shaking reaction vessel. Afterward, the solution was removed, and the vessel was shaken for 20 min with a mixture of piperidine (20% in DMF). The resin beads were washed four times with DMF, then twice with DCM and the corresponding protected amino acid (6.0 mmol, 4 equiv), the coupling reagent HBTU (4 equiv) and the base DIPEA (6 equiv) were added in DMF. This mixture was shaken with the resin for 1 h. Then the resin was washed five times with DMF. This protocol was repeated for every corresponding amino acid in the coupling process. The first step was always the Fmoc deprotection on the resin. After the last amino acid was coupled, the resin was washed with DCM.

Then the resin was treated manually and was washed three times with DCM, three times with MeOH and three times with DCM. A mixture of 10 mL Ac_2O and 10 mL DMF was shaken with the resin for 1 h to ensure the complete acyl capping of the terminal amino group. The cleavage of the protected peptide from the resin was carried out with a mixture of 1 mL TIPS (5%) in 19 mL TFA (95%) incubated for 1.5 h. During that time a color change of the resin from yellow to deep red occurred. The solution was removed from the resin and the resin was washed with pure TFA and pure DCM. All filtrates were collected, and the solvents were removed under pressure. The resulting white residue was dissolved in little DCM and precipitated in ice-cold diethyl ether. The precipitate was centrifuged down,

redissolved and reprecipitated for four times. Afterward, the sample was dissolved in H_2O, a few drops HCl were added to ensure the exchange of anions and the sample was lyophilized (95%).

^{1}H NMR (300 MHz, DMSO, Me_4Si, 298 K): δ(ppm) = 9.01 (s, 3H, ε-CH^{His}), 8.54-8.33 (m, 5H, α-NH), 8.14 (m, 1H, α-NH), 7.46-7.09 (m, 6H, δ-CH^{His}, NH^{His}), 4.60 (m, 3H, α-CH^{His}), 4.29 (m, 1H, α-CH^{Cys}), 3.80 (s, 4H, α-CH^{Gly}), 3.14-2.74 (m, 8H, β-CH_2^{His}, β-CH_2^{Cys}), 1.84 (s, 3H, -CH_3)

LC-MS (m/z): calculated for $[M+H]^+$: 688.74, found: 688.8

Synthesis of Cyt(Mal)

Cyt *c* (3.00 mg, 0.242 μmol) was dissolved in 1.5 mL phosphate buffer (40 mM, 5 mM EDTA, pH 7.4). NHS-PEG(4)-Maleimide linker (7.08 mg, 0.014 mmol) was also dissolved in 0.75 mL phosphate buffer. Both solutions were combined and shaken at room temperature for 2 h. The solution was purified with a centrifugal filter unit (3 kDa, 7500 rpm, 12 min, 6 °C) and washed twice with phosphate buffer. For the reaction with the peptide, the modified protein was used directly. In case of the isolation of maleimide-functionalized cytochrome Cyt(Mal), the solution was purified 3 more times with the centrifugal filter unit using distilled water. Red crystals were obtained after lyophilization (4.6 mg).

Synthesis of Cyt(CGGHHH)$_{14}$

The peptide (13.47 mg, 19.6 μmol) was dissolved in 250 μL phosphate buffer (40 mM, 5 mM EDTA, pH 7.4) and pretreated with TCEP (49.01 mg, 196 μmol, in 250 μL phosphate buffer). Both solutions were combined, and the pH value was adjusted to 2 with 1 M NaOH. The mixture was shaken for 2 h. Excess of TCEP was removed by adding AZBA (63.95 mg, 392 μmol, in 2 mL buffer). 120 μL 1 M NaOH were added to ensure the complete dissolution of AZBA (pH >5.5). The AZBA solution was added to the peptide TCEP solution and shaken for 1 h. The pH value of the peptide mixture was adjusted to the buffered protein solution (7.4) of Cyt(Mal) and the mixtures were combined and stirred overnight. The next day the solution was mixed with 1 mM H_2O_2 solution to ensure the complete oxidation of Fe^{2+} to Fe^{3+} (checked with absorption spectra). The Cyt(CGGHHH)$_{14}$ conjugate was purified with a centrifugal filter unit (3 kDa, 7500 rpm, 10 min, 6 °C) and five times washed with distilled water. After lyophilization red crystals were obtained (7.93 mg).

Synthesis of Lyz(Mal) and Lyz(CGGHHH)$_5$

Lysozyme (Lyz) (3.00 mg, 0.210 μmol) was modified in an analog procedure as described for Cyt *c*. The NHS-PEG(4)-Maleimide linker (2.26 mg, 0.0044 mmol) and the peptide (5.05 mg, 0.0073 mmol) were adjusted to the amount of seven amines present on the surface of lysozyme. White crystals of Lyz(CGGHHH)$_5$ were obtained after lyophilization (3.94 mg).

Synthesis of BLG(SMCC-Mal) and BLG(CGGHHH)$_7$

β-Lactoglobulin (BLG) (3.00 mg, 0.164 μmol) was modified in an analog procedure as described for Cyt *c*. Here the sulfo-SMCC (sulfosuccinimidyl 4-(*N*-maleimidomethyl) cyclohexane-1-carboxylate) linker was used for the surface modification of the amines. s-SMCC (2.58 mg, 0.0059 mmol) and the peptide (13.47 mg, 0.0196 mmol) were adjusted to the amount of twelve amines present on the surface of BLG. Light brown crystals of BLG(CGGHHH)$_7$ were obtained after lyophilization (6.21 mg).

5.3.2 Protein Characterization Techniques

SDS-Gel

The SDS-PAGE was performed as described elsewhere[297] using a polyacrylamide gel (Rotiphorese® 30 gel mix) with a thickness of 0.75 mm (C.B.S. Scientific) and stained with Coomassie Brilliant Blue G. 5 μL of PageRuler pre-stained protein ladder (10-170 kDa) were used as marker. Samples of the proteins were dissolved of a concentration of 4 mg mL^{-1} in water. The proteins were denaturized by adding 5 μL of Roti®-Load 1 (Carl Roth) to 15 μL protein solution and heating in a boiling water bath for 10 min. 20 μL were loaded on each bag. Images of SDS-PAGE gels were taken with the GelDocTM XR$^+$ (Bio-Rad Laboratories Inc.) and processed with the Image LabTM Software (camera filter 1).

MALDI-ToF (Matrix-assisted Laser Desorption/Ionization Time of Flight)

The measurements were carried out on a Shimadzu Axima CFR MALDI-ToF mass spectrometer, equipped with a nitrogen laser delivering 3 ns laser pulses at 337 nm. Samples were prepared by dissolving the sample in CH_3CN/TFA 0.1% at a concentration of ~1 mg mL^{-1}. 1 μL of this mixture was applied to a multistage target to evaporate and create a thin analyte film. Sinapic acid was used as matrix and applied to the target before adding the sample. The samples were measured in positive ion and in a linear mode of the spectrometer.

TNBS Assay for the Quantification of Amino Groups

The number of modified amino groups of the respective protein was determined by a TNBS (2,4,6-trinitrobenzene sulfonic acid) assay (**Figure 83**).[299-300] The detailed protocol is described elsewhere.[329] Briefly, to 500 μL of protein solution with various concentrations (ranging from 2.5 to 20 μM in 0.1 M borate buffer, pH 9) were added 3 μL 2.5% TNBS solution in an opaque container. The mixtures were incubated at 37 °C for 2 h. Afterward, 100 μL of each solution were pipetted in a clear 96-well plate and the absorbance was measured in triplets at 335 nm at a Tecan plate reader (as described above) (**Figure 84**). For all protein concentrations, blank measurements (without TNBS) were carried out at 335 nm and subtracted from the original values.

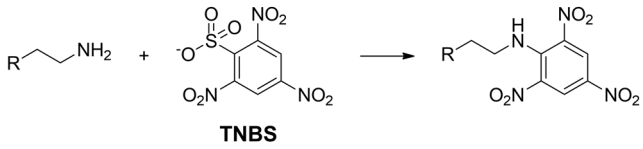

Figure 83: Reaction scheme of primary amines on the surface of Cyt *c* with 2,4,6-trinitrobenzene sulfonic acid resulting in a colored reaction product.

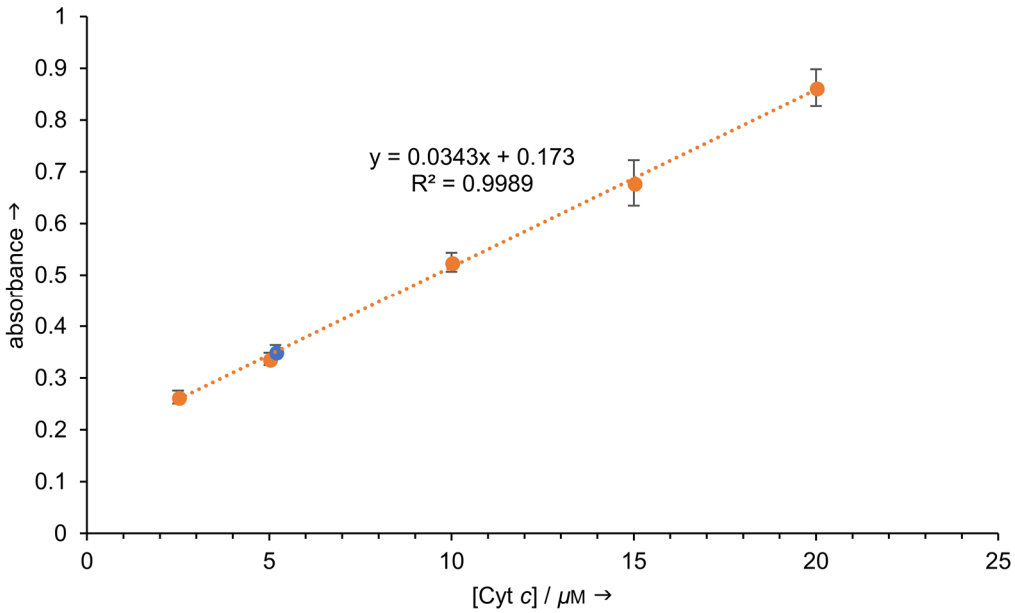

Figure 84: TNBS assay of modified amino groups with Cyt *c* (orange) as a standard curve and a 20 μM concentration of Cyt(CGGHHH)$_{14}$ (blue). The assay shows that Cyt(CGGHHH)$_{14}$ has 4.92 ± 0.31 amino groups left corresponding to 14 introduced peptides on the surface of the enzyme.

Dynamic Light Scattering (DLS) Measurements

Dynamic light scattering experiments were performed on a Malvern Zetasizer Nano ZS in disposable polystyrene micro cuvettes (VWR) using 120 μL of freshly prepared protein and modified protein solutions in PBS (pH 7.4). Generally, after equilibration to 25 °C, three measurements were performed, with the instrument optimizing the number of runs for each measurement. The refractive index (RI) of the dispersant (preset: water) was set to 1.330 and the viscosity to 0.8872 cP, respectively. The RI of the particle was set to 1.45. The absorption of the protein was set to 0.00, both attenuator and measurement position were controlled by the instrument and all measurements were performed at a scattering angle of 173°. The measurements are normalized to each other.

Circular Dichroism (CD) Spectroscopy

CD spectra were recorded on a J 815 (JASCO) using the software Spectra Manager 2.12.00. All spectra for the Cyt(CGGHHH)$_{14}$ were recorded at 20 °C with a total concentration of 0.1 mg mL^{-1} protein in 10 mM K_3PO_4/50 mM Na_2SO_4 buffer pH 7 using quartz cells with a path length of 1 mm. All spectra were corrected by subtraction from the background

(buffer). Data points were collected at a resolution of 1 nm. Secondary structure contents were predicted with DICHROWEB using the CONTIN-LL method (reference set 7).

5.3.3 Evaluation of Enzymatic Activity

Peroxidase Functionality (ABTS Assay)

A published protocol of the assay has been slightly modified.[311] Briefly, ABTS was dissolved at a concentration of 2 mM in 10 mM phosphate buffer pH 7.4. The protein samples were dissolved at a concentration of 40 μM and their concentration was adjusted to the same values by absorption measurements at 409 nm. The H_2O_2 concentration ranged between 0.4 mM and 30 mM. In a 96-clear well plate, 50 μL ABTS solution were pipetted and 25 μL protein sample were added. 25 μL of the respective H_2O_2 concentrations were added to the ABTS/protein sample mixture and the absorption was measured at 410 nm for 3 min every 10 s in a kinetic cycle. As a blank, measurement buffer was added to the samples instead of H_2O_2. All measurements were carried out in triplicate and were corrected by subtraction of the blank sample. The data analysis (determination of Michaelis-Menten values) was carried out with GraFit 7.0.3 (**Figure 85**).

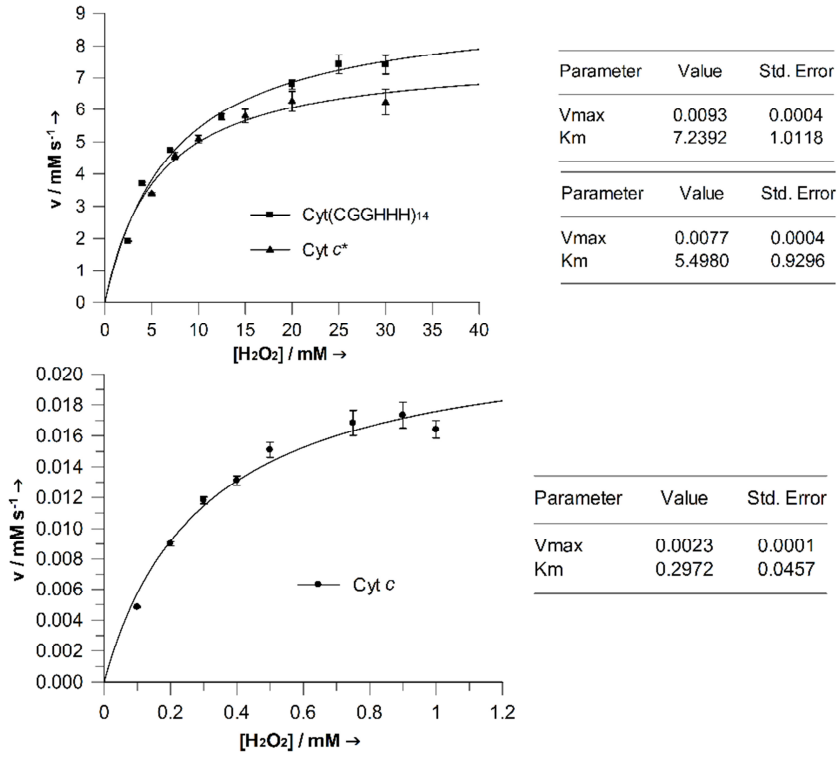

Parameter	Value	Std. Error
Vmax	0.0093	0.0004
Km	7.2392	1.0118

Parameter	Value	Std. Error
Vmax	0.0077	0.0004
Km	5.4980	0.9296

Parameter	Value	Std. Error
Vmax	0.0023	0.0001
Km	0.2972	0.0457

Figure 85: Michaelis-Menten kinetics of peroxidase activity of peptide-modified Cyt(CGGHHH)$_{14}$, Cyt *c** (in parallel to the synthesis treated cytochrome) and native Cyt *c*. Data represent averages with error bars from three independent experiments performed in triplicate.

Esterase-like Activity (MUF Assay)

The induced esterase activity was determined using 4-methylumbelliferyl butyrate (MUF).[313] The ester is a non-fluorescent compound, which is hydrolyzed by esterases and lipases into the highly fluorescent 4-methylumbelliferone (4-MU).

Two different procedures for the MUF assay were carried out. In the case of Cyt *c*, the Michaelis-Menten parameters of the esterase-like functionality were determined. For lysozyme and *β*-lactoglobulin a simpler form was used which is only comparing the esterase-like activities of the modified proteins with the native ones.

Determination of Michaelis-Menten Kinetics

All cytochrome *c* samples were dissolved at a concentration of 3.5 mg mL^{-1} in 20 mM phosphate buffer (pH 6.0). MUF was dissolved in acetonitrile at a concentration of 40 mM. In a black 96-well plate, 25 μL phosphate buffer (for blank/autohydrolysis) or protein solution were pipetted. 25 μL of the MUF solution in concentration ranges from 1.875 mM to 40 mM were added right before the measurement started. The fluorescence (Ex: 342 nm, Em: 445 nm) was measured for 3 min every 10 s in a kinetic cycle. All measurements were carried out in triplicate and were corrected by subtraction of the blank sample. The data analysis was carried out with GraFit 7.0.3 (**Figure 86**).

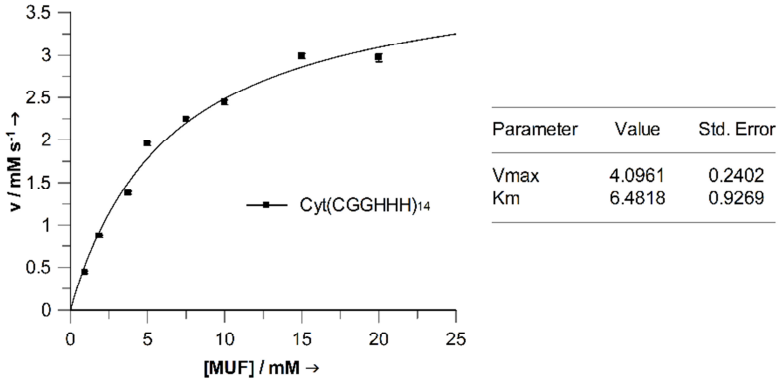

Figure 86: Michaelis-Menten kinetics of esterase-like activity of peptide-modified $Cyt(CGGHHH)_{14}$. Native Cyt *c* did not show any activity concerning the cleavage of MUF. Data represent averages with error bars from three independent experiments performed in triplicate.

Simple Form of Assay

The protein samples were dissolved at a concentration of 0.5 μmol mL^{-1} in 20 mM phosphate buffer (pH 6.0). MUF was dissolved in an acetonitrile/water mixture (50:50) at a concentration of 0.738 mg mL^{-1}. In a black 96-well plate, 25 μL phosphate buffer (for

blank/autohydrolysis) or protein solution were pipetted. 25 μL of the MUF solution were added right before the measurement started. The fluorescence (Ex: 342 nm, Em: 445 nm) was measured for 3 min every 15 s in a kinetic cycle. All measurements were carried out in triplets. The autohydrolysis of MUF was observed with buffer instead of protein sample.

Coupled Esterase and Peroxidase Activity (HVA Assay)

The coupled catalytic activity of Cyt(CGGHHH)$_{14}$ was assayed with the ethyl ester of homovanillic acid (HVA). The HVA ester was dissolved at a concentration of 13.7 mM in 100 mM phosphate buffer (pH 8). 30% H_2O_2 solution was diluted to 1% for the experiments. The protein samples were dissolved at a concentration of 16 μM in phosphate buffer. The concentration of Cyt(CGGHHH)$_{14}$ was adjusted by absorption measurements at 409 nm. In a black 96-well plate 100 μL buffer were pipetted and in each case 9 μL protein sample, 9 μL HVA ester and 9 μL H_2O_2 were added. The developing fluorescence was observed (Ex: 315 nm, Em: 425 nm) in triplicate over 60 min in kinetic cycles of 10 s. After the reaction, the triplicates were collected and purified with a centrifugal filter unit (3 kDa, 7500 rpm, 10 min, 6 °C). The filtrates were analyzed by HPLC-MS.

6 Appendix

6.1 List of Abbreviations

Abbreviation	Meaning
Ø	diameter
abs.	absorbance
ADP	adenosinediphosphate
AGU	anhydrous glucose unit
AMP	adenosinemonophosphate
anhyd.	anhydrous
approx.	approximately
aq.	aqueous
ATP	adenosinetriphosphate
Boc	*tert*-butoxycarbonyl
Br	bromine
br	broad
BSA	Bovine Serum Albumine
Bz	benzoyl
c	centi-
C	carbon
°C	degrees Celsius
CD	Circular dichroism, Cyclodextrin
$CDCl_3$	deuterated chloroform
conc.	concentration
COOH	carboxyl group
COSY	homonuclear correlation spectroscopy
cP	centipoise
CPP	cell penetrating peptide
CTF	cell titer fluor
δ	chemical shift (ppm), downfiled from TMS
dd-	double distilled
D_2O	deuterium oxide
d_6	deuterated (6-times)
Da	Dalton
DBU	1,8-diazabicyclo[5.4.0]undec-7-ene

Abbreviation	Meaning
DCC	*N,N'*-dicyclohexylcarbodiimide
DC	dendritic cell
DCl	deuterium chloride
DCM	dichloromethane
DEAD	diethyl azodicarboxylate
DEPT	distortionless enhancement by polarization transfer
Dex	dextran
DIAD	diisopropyl azodicarboxylate
DIPEA	*N,N*-diisopropylethylamine
DLS	Dynamic Light Scattering
DMAP	4-(*N,N*-dimethylamino)pyridine
DMEM	Dulbecco's modified Eagle's medium
DMF	dimethylformamide
DMSO	dimethyl sulfoxide
DS	Degree of Substitution
DTNB	5,5'-dithio-bis-(2-nitrobenzoic acid)
EDC	*N*-(3-dimethylaminopropyl)-*N'*-ethylcarbodiimide
EDTA	ethylenediaminetetraacetic acid
e.g.	*exempli gratia*, means: for example
em.	emission
equiv	equivalent
et al.	*et alii*, means: and others
etc.	and so forth
Et_2O	diethyl ether
EtOH	ethanol
ex.	excitation
FCS	fetal calf serum
Fmoc	fluorenylmethyloxycarbonyl
FTIR	Fourier transform infrared spectroscopy
g	gram
g	gravity of Earth
GPC	Gel Permeation Chromatography
h	hour
H	hydrogen
H_2O	water

Abbreviation	Meaning
HeLa	tumor cells from the patient Henrietta Lacks
HEPES	4-(2-hydroxyethyl)-1-piperazineethanesulfonic acid
HMBC	heteronuclear multiple bond correlation
HPLC	high performance liquid chromatography
HSQC	heteronuclear single quantum coherence
IR	infrared spectroscopy
k	kilo-
KBr	potassium bromide
λ	wavelength
L	liter
LC-MS	liquid chromatography-mass spectrometry
Lys	lysine
μ	micro-
m	mass
m	meter
m	milli-
M	molar
max.	maximum
MeOH	methanol
MHz	megahertz
min	minute
mL	milliliter
mm	millimeter
mol	mole(s)
MS	mass spectrometry
MTT	3,(4,5-dimethylthiazol-2-yl)-2,5-diphenyl-tetrazoliumbromide
MW	molecular weight
MWCO	molecular weight cut-off
m/z	mass to charge ratio (in MS)
N	nitrogen
N_3	azide
n.a.	not available
$NaBH_4$	sodium borohydride
NBS	*N*-bromosuccinimide
NHS	*N*-hydroxysuccinimide

Abbreviation	Meaning
NMR	nuclear magnetic resonance
OVA	ovalbumin
ox	oxidized
p	pico-
P	phosphorous
PBS	phosphate buffered saline
PEG	poly(ethylene glycol)
pH	proton log units
ppm	part per million
P/S	penicillin-streptomycin
RI	refractive index
RT	room temperature
SD	standard deviation
SDS-PAGE	sodium dodecyl sulfate polyacrylamide gel electrophoresis
SMCC	succinimidyl 4-(*N*-maleimidomethyl)cyclohexane-1-carboxylate
Sp	spermine
TEA	triethylamine
TLC	thin layer chromatography
TMS	tetramethylsilane
ToF	Time of Flight (in MS)
tosyl	*p*-toluenesulfonyl
UV	ultraviolet
V	Volt
V	volume
vs.	versus

6.2 Supplemental Data

6.2.1 ^{1}H-NMR and ^{31}P-NMR Spectra

Amino-modified Macrocyclic Polyamine NH_2-MCA

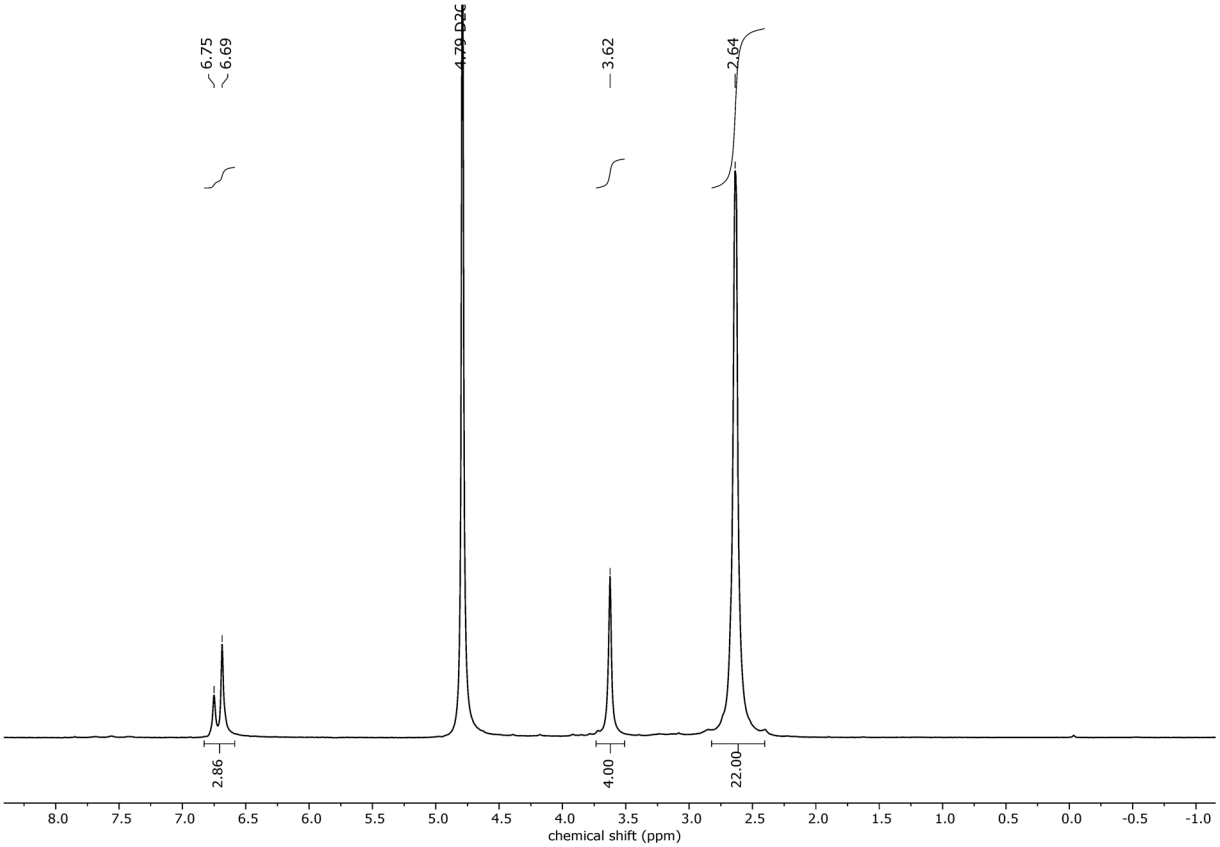

Figure 87: ^{1}H-NMR spectra of NH_2-MCA **13.**

BCN-modified Macrocyclic Polyamine BCN-MCA

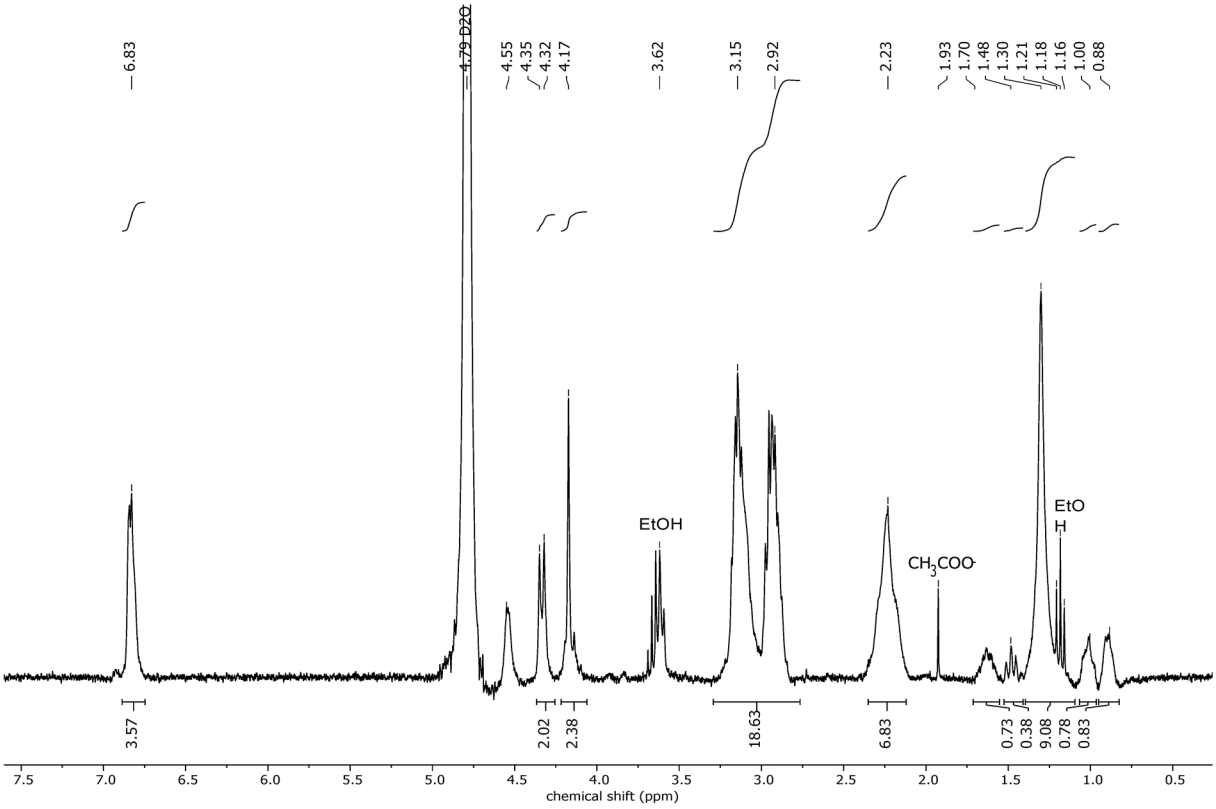

Figure 88: ^{1}H-NMR of BCN-MCA **15**.

Azidated Dextran Dex-$(N_3)_9$

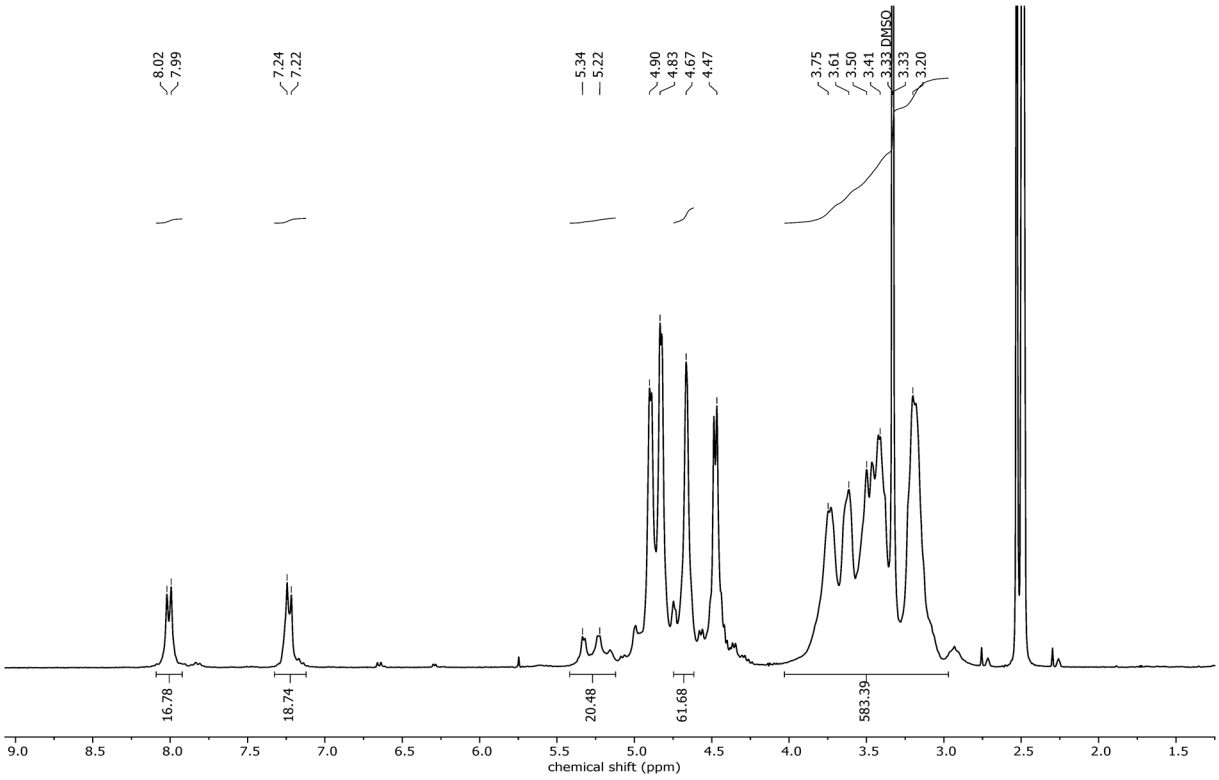

Figure 89: ^{1}H-NMR of Dex-$(N_3)_9$ **20**.

End group functionalized PEG

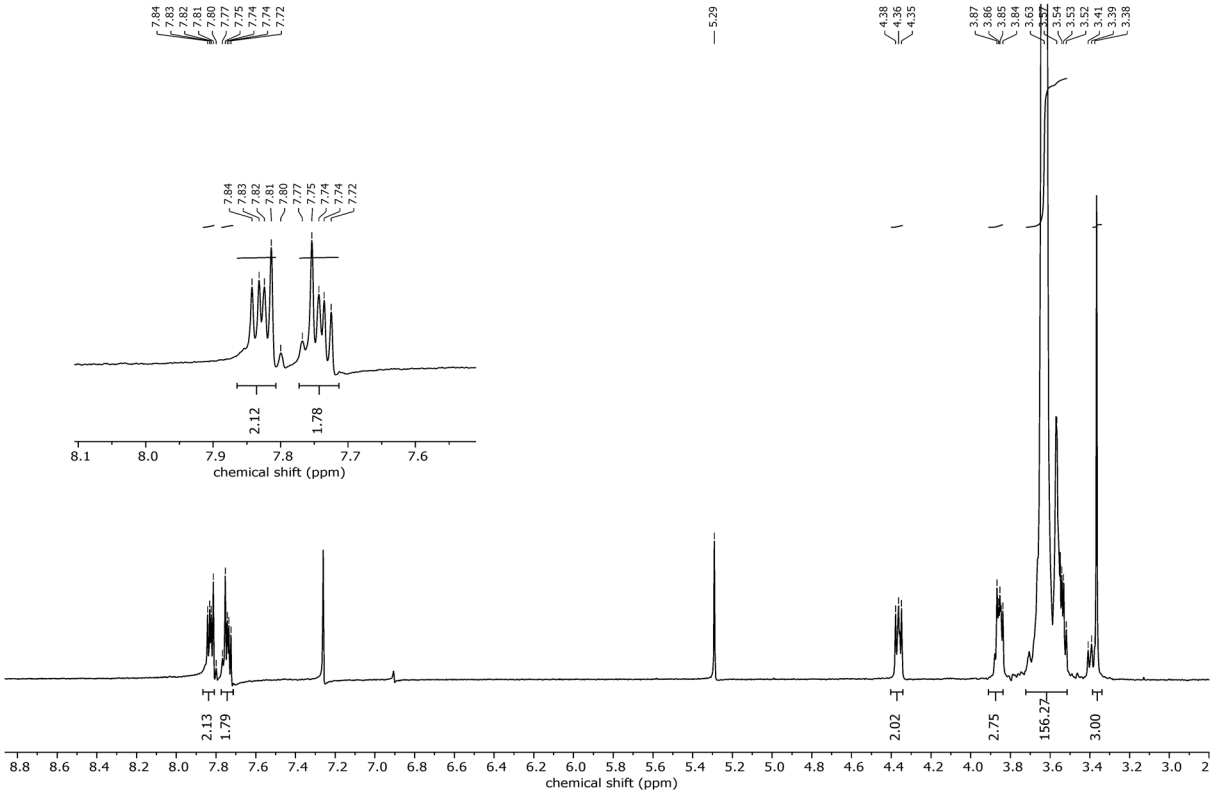

Figure 90: ^{1}H-NMR of PEG-NHP **24**.

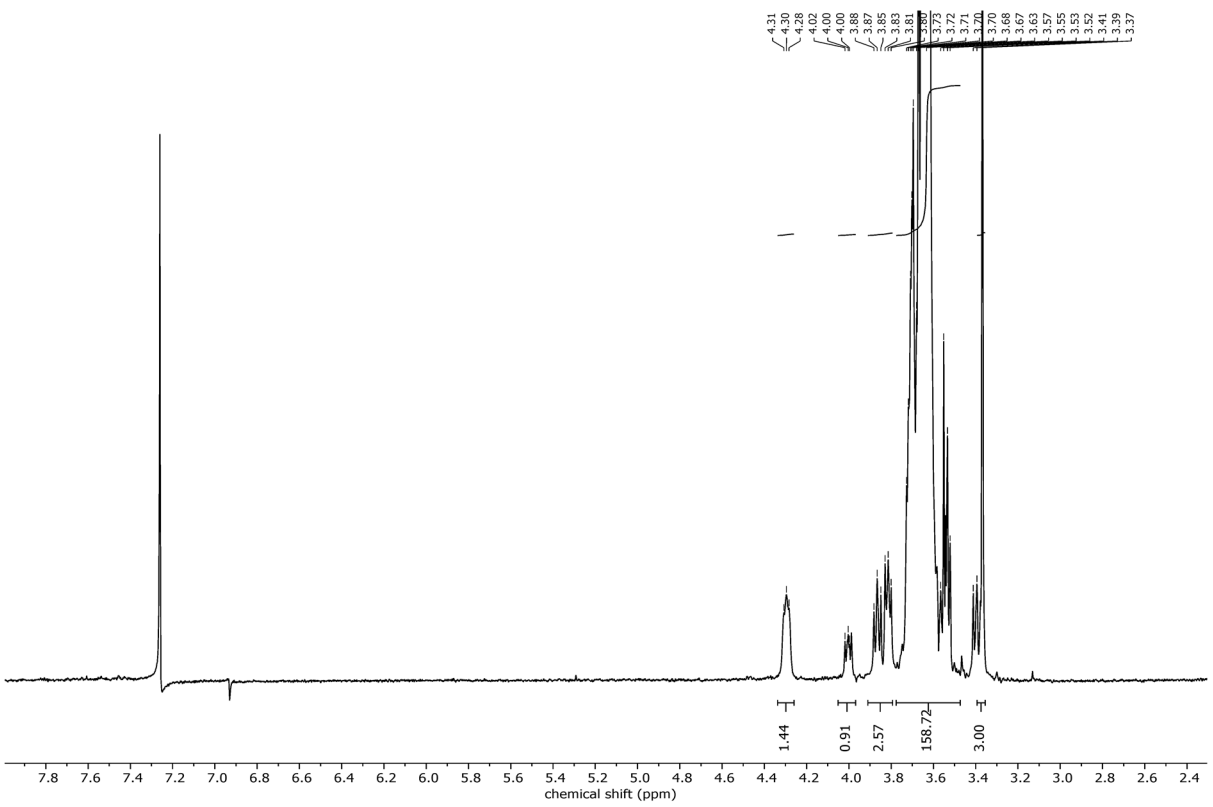

Figure 91: ^{1}H-NMR of PEG-O-NH_2 **26**. All aromatic protons have disappeared.

Dextran-PEG polymer brush

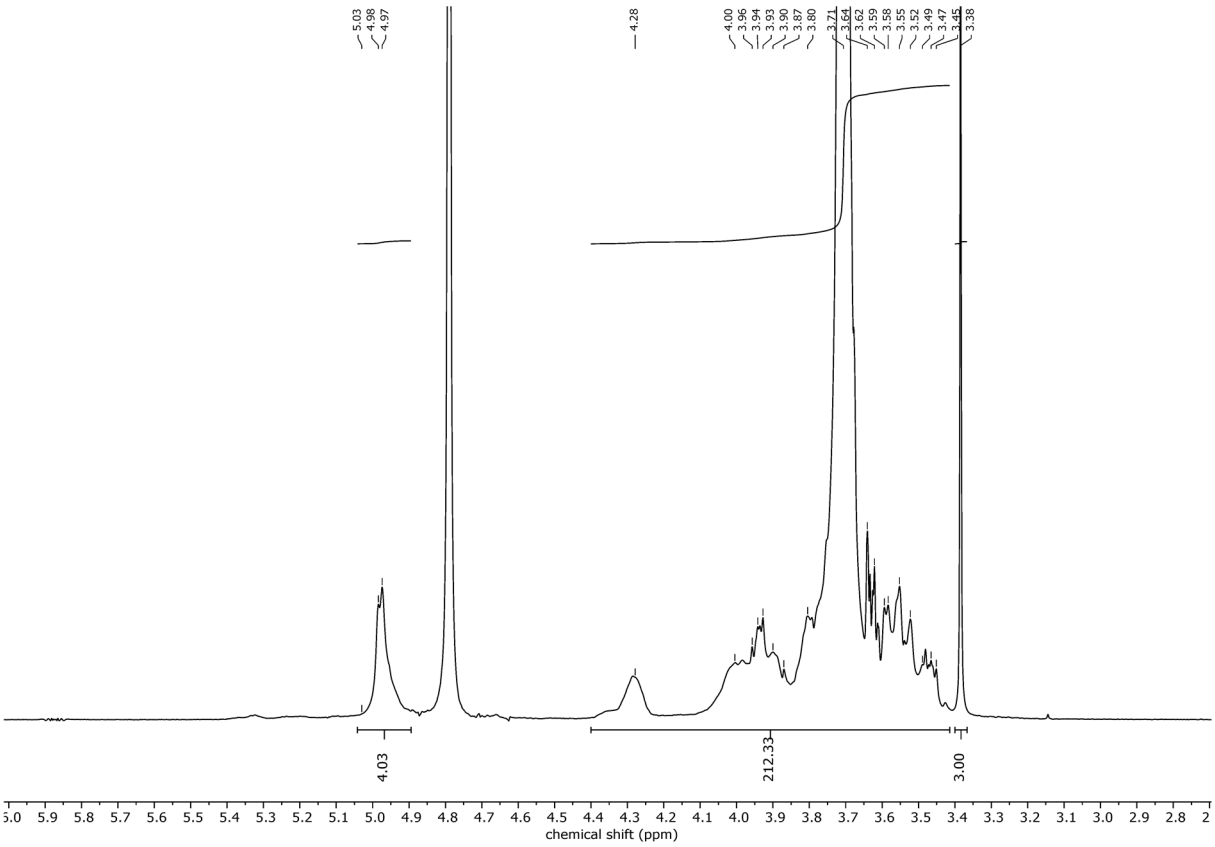

Figure 92: ^{1}H-NMR of Dextran-PEG polymer brush **27.**

Activated Dextran Dex-(4-NC)$_{7.5}$

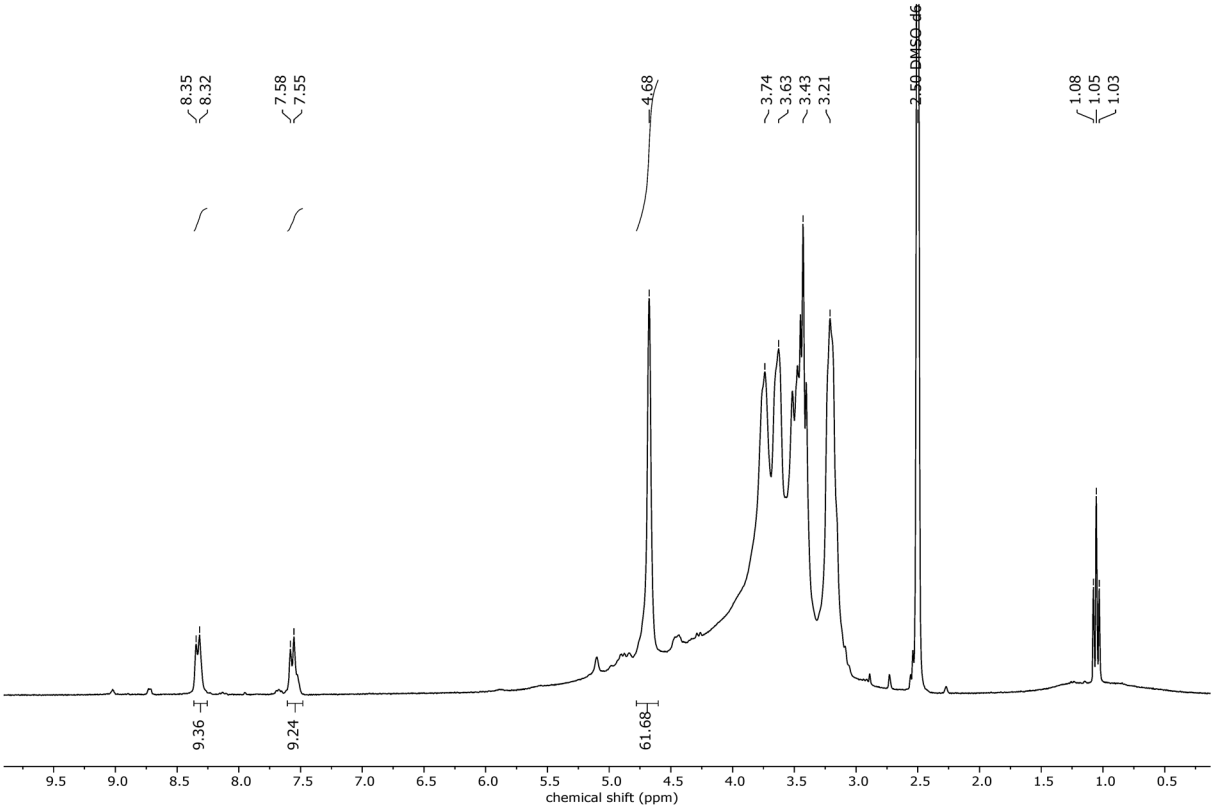

Figure 93: ^{1}H-NMR of Dex-(4-NC)$_{7.5}$ **30**.

Thiol-modified Dextran Dex-(SH)$_7$

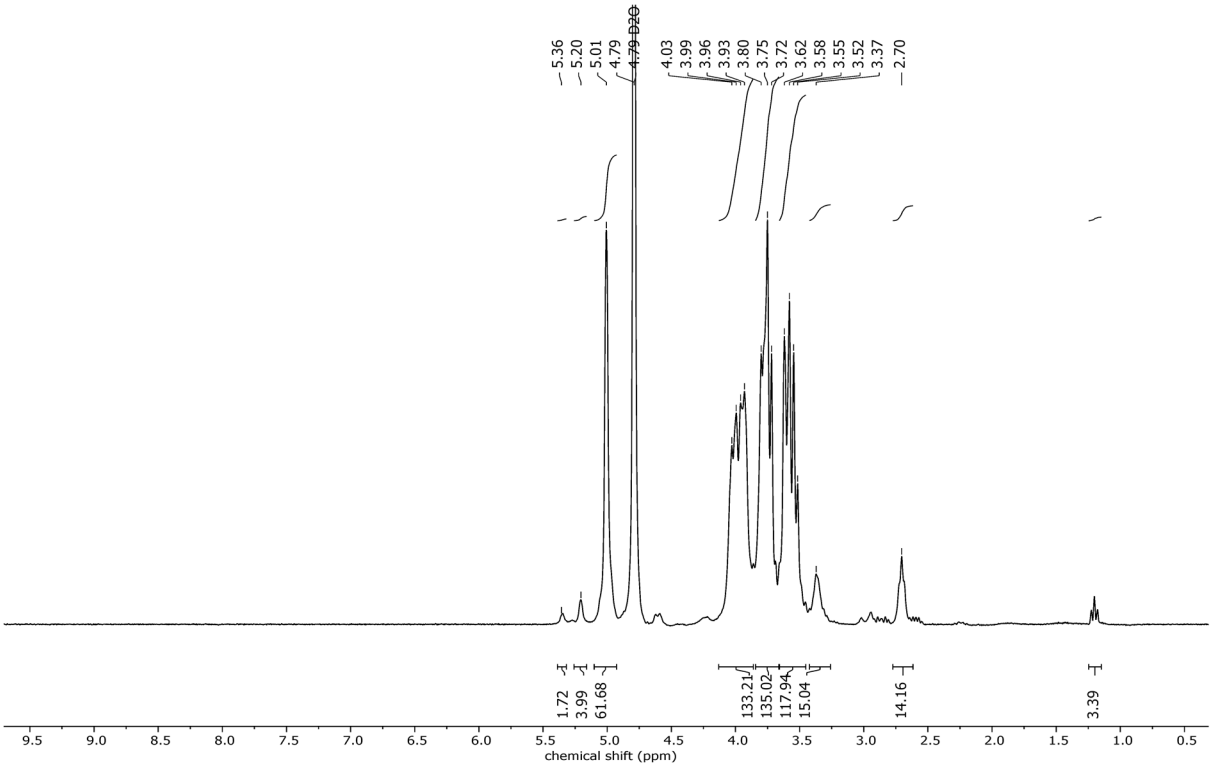

Figure 94: ^{1}H-NMR of Dex-(SH)$_7$ **31**.

Carrier-Catalyst Conjugate Dex-(S-Mal-MCA)$_6$

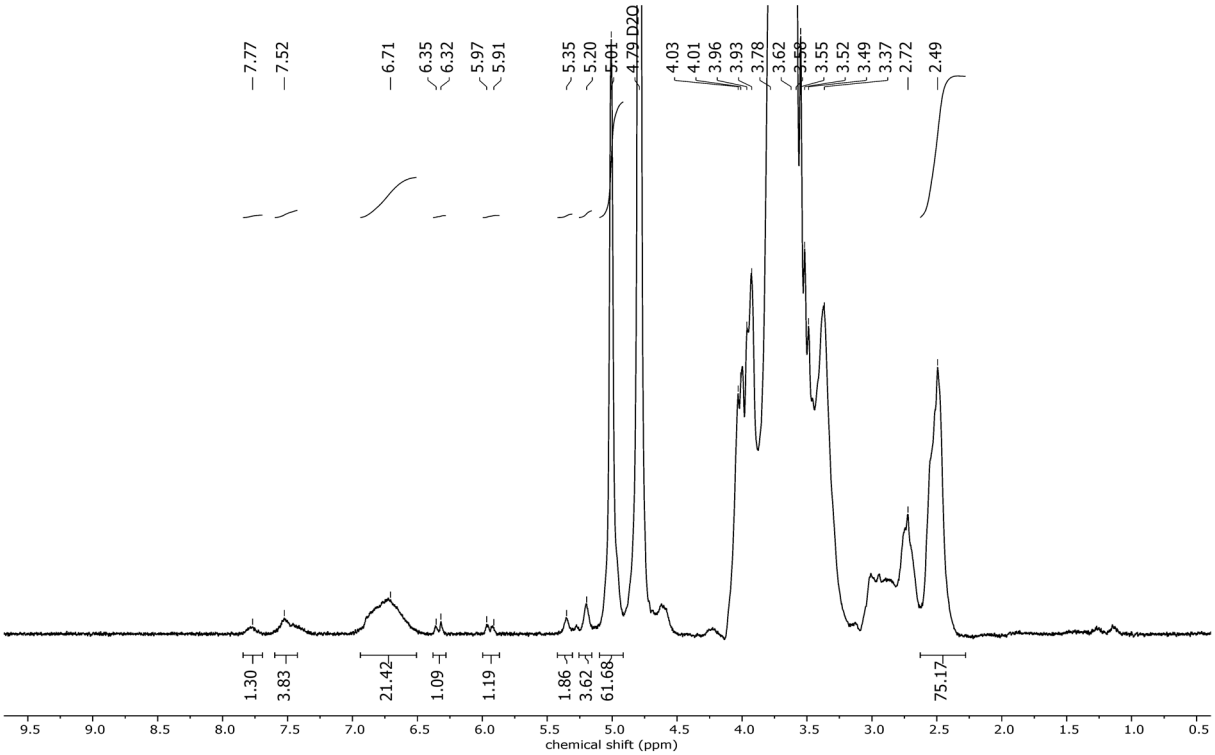

Figure 95: ^{1}H-NMR of Dex-(S-Mal-MCA)$_6$ **33**.

Hexapeptide Ac-HHHGGC-NH$_2$

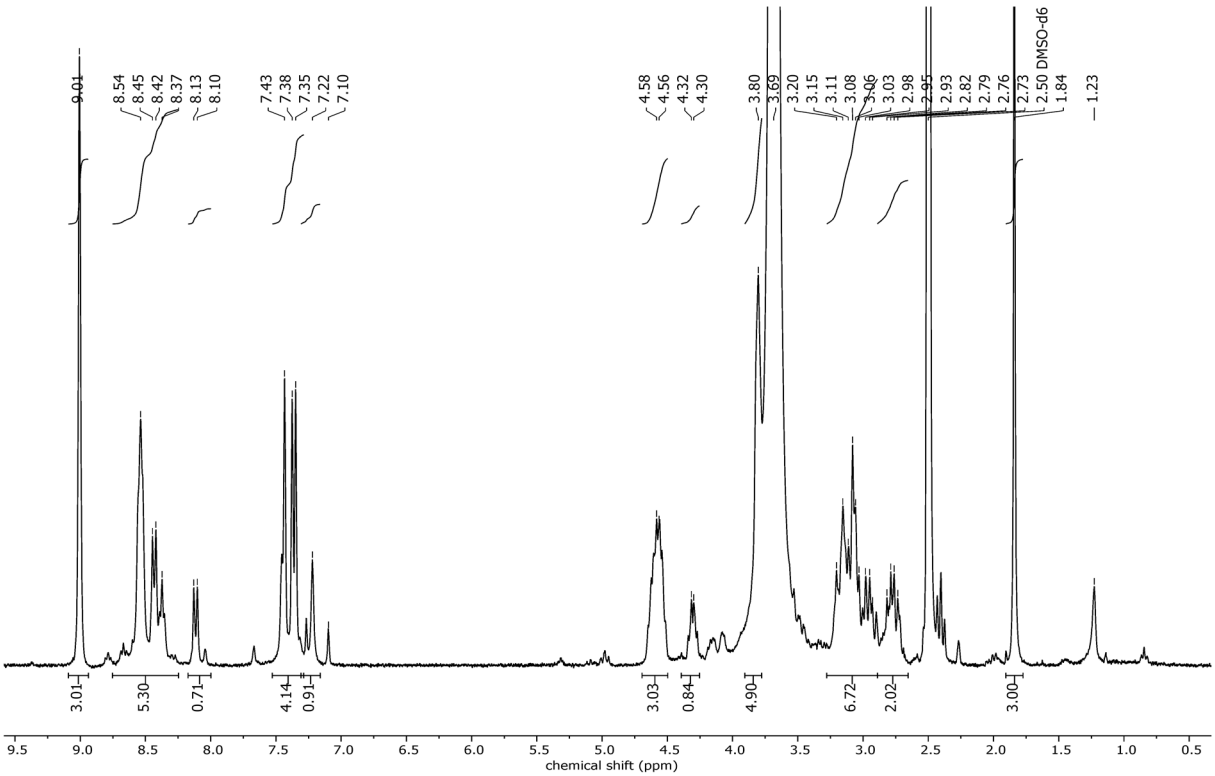

Figure 96: ^{1}H-NMR of hexapeptide Ac-HHHGGC-NH$_2$.

^{31}P-NMR Kinetics

Time-Course Kinetics of NH_2-MCA

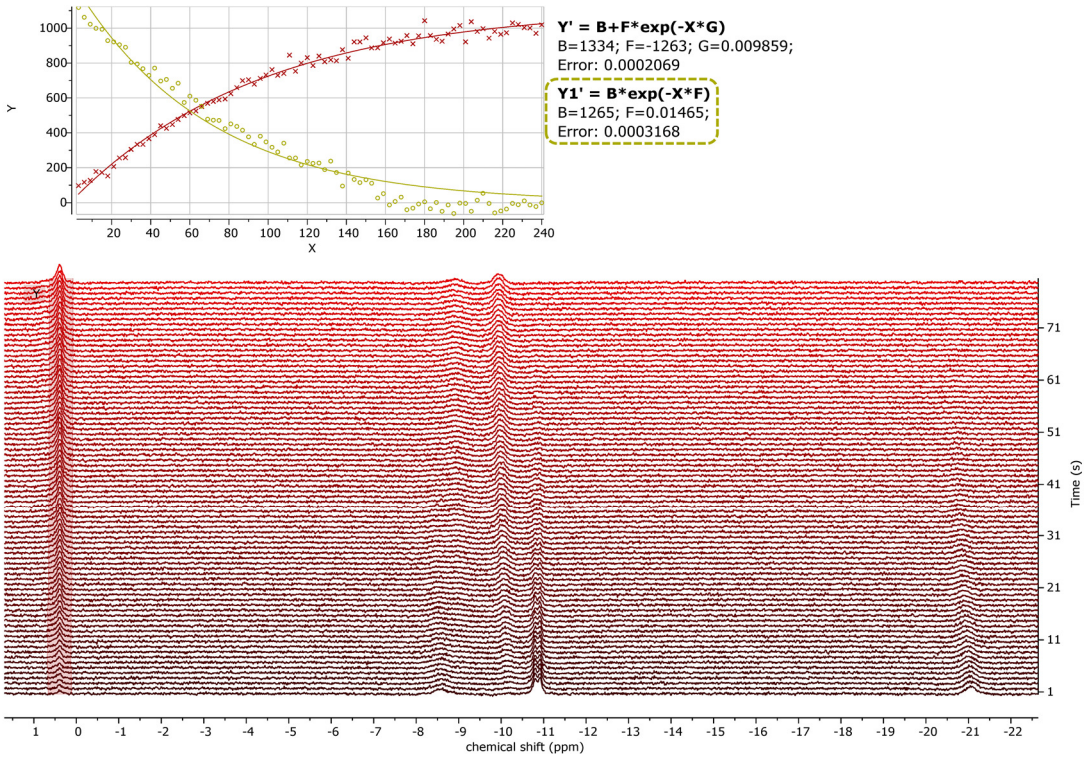

Figure 97: ^{31}P-NMR time-course kinetics of NH_2-MCA **13**. Plotted and fitted to first order kinetics (green line) and Y' equation with Mestrenova.

Time-Course Kinetics of Dex-(S-Mal-MCA)$_6$

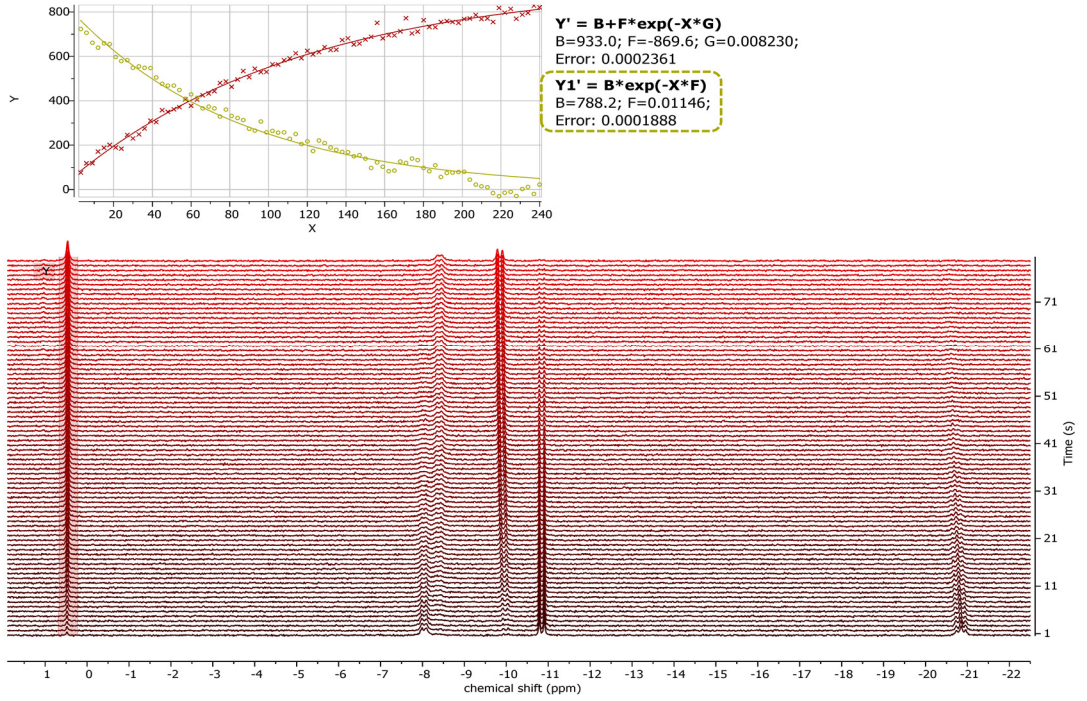

Figure 98: ^{31}P-NMR time-course kinetics of Dex-(S-Mal-MCA)$_6$ **33**. Plotted and fitted to first order kinetics (green line) and Y' equation with Mestrenova.

Time-Course Kinetics of Dex-(SH)$_7$

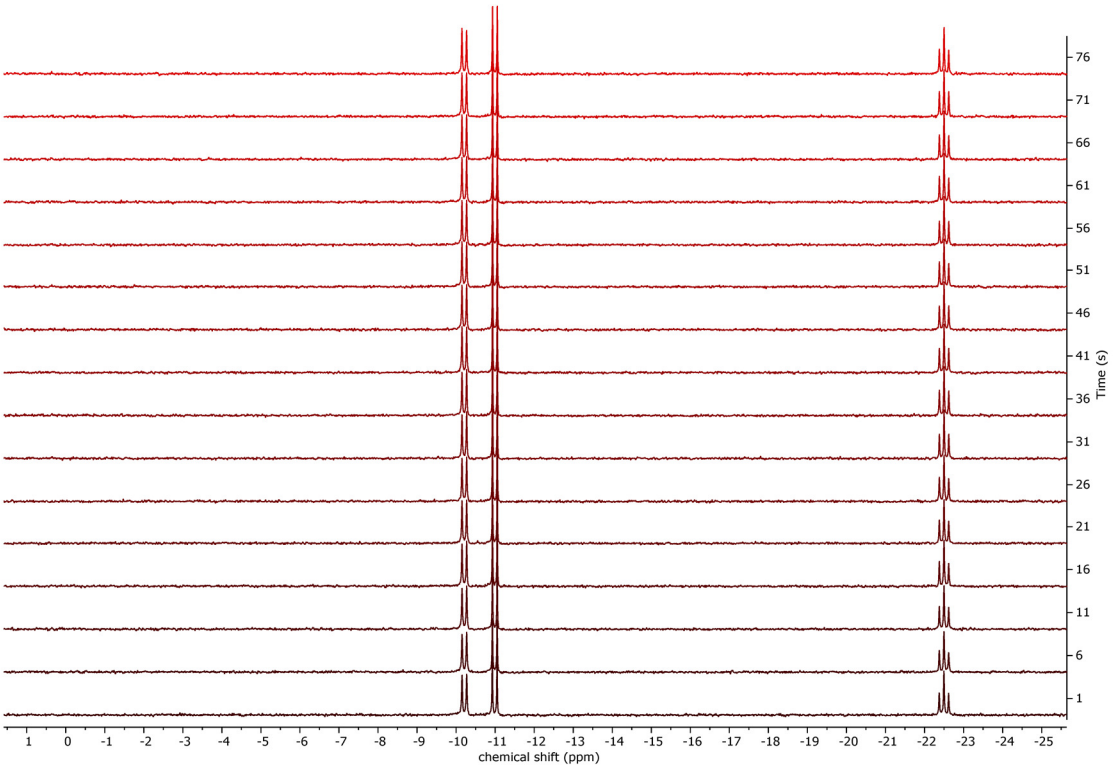

Figure 99: ^{31}P-NMR time-course kinetics of Dex-(SH)$_7$ **31**. No ATP cleavage is observed.

6.2.2 Electrospray Ionization Mass Spectra (ESI-MS)

Amino-modified Macrocyclic Polyamine NH_2-MCA

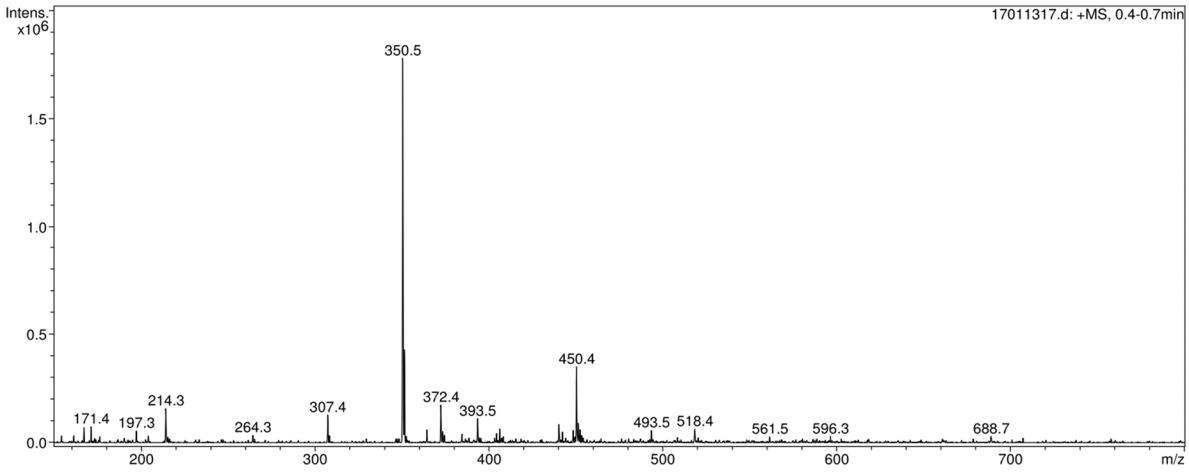

Figure 100: Mass spectrum of NH_2-MCA **13**.

BCN-modified Macrocyclic Polyamine BCN-MCA

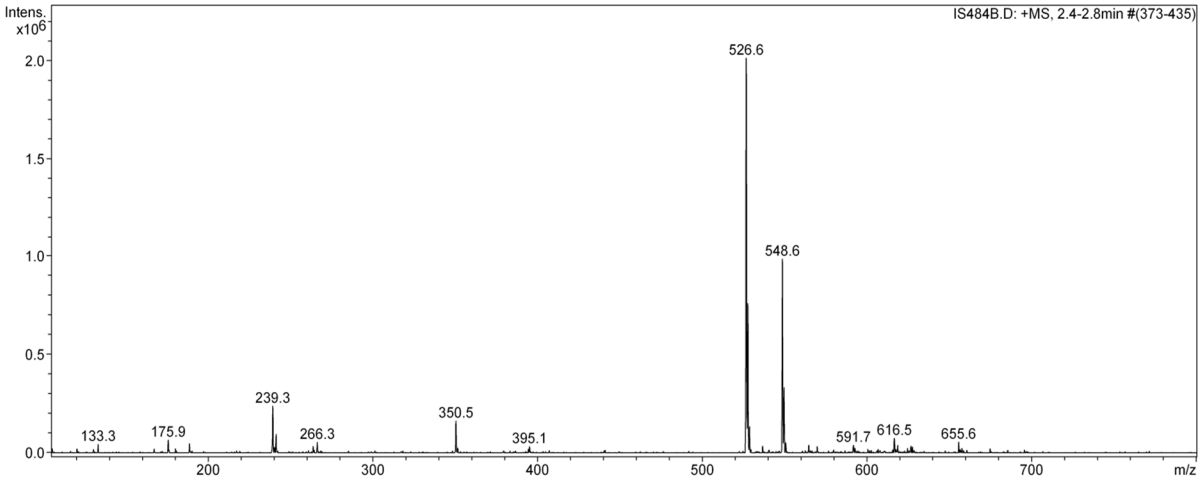

Figure 101: Mass spectrum of BCN-MCA **15**.

Mal-modified Macrocyclic Polyamine Mal-MCA

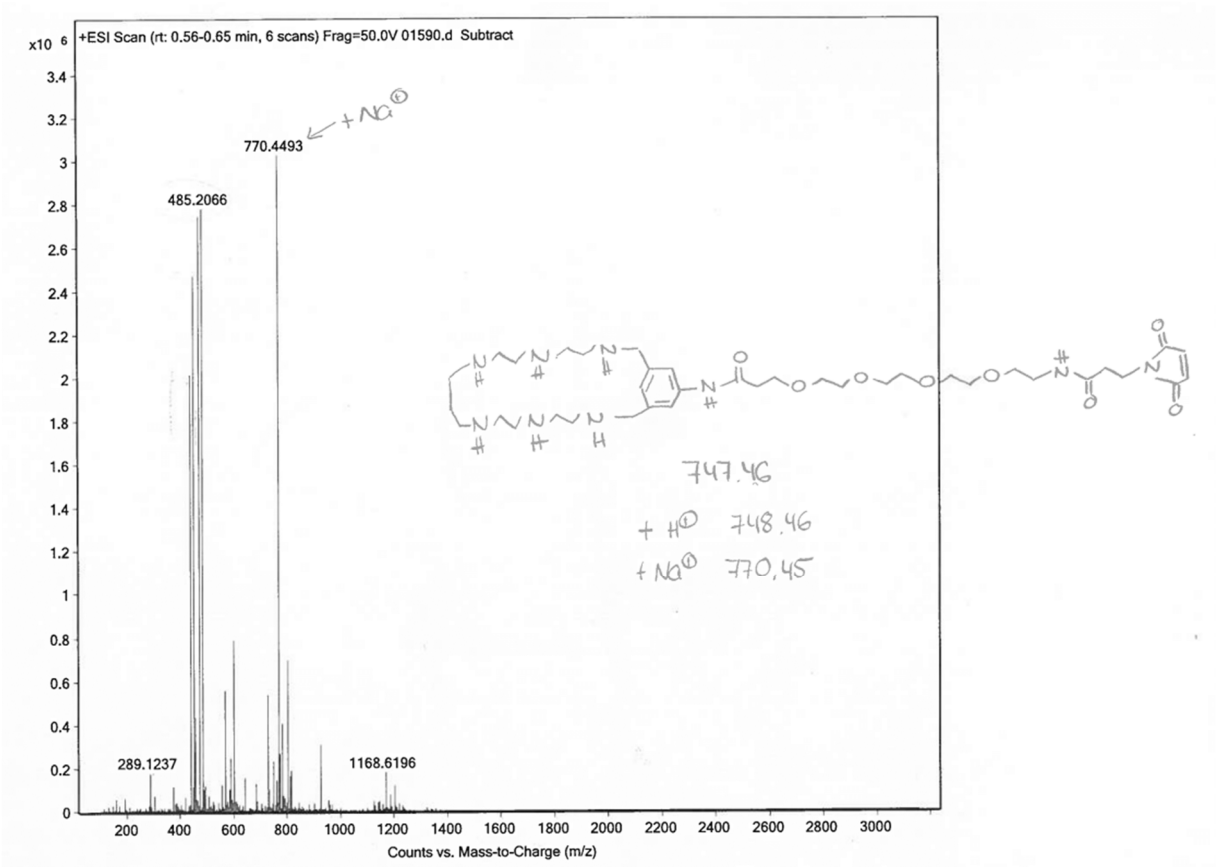

Figure 102: Mass spectrum of Mal-MCA **17**.

Hexapeptide Ac-HHHGGC-NH_2

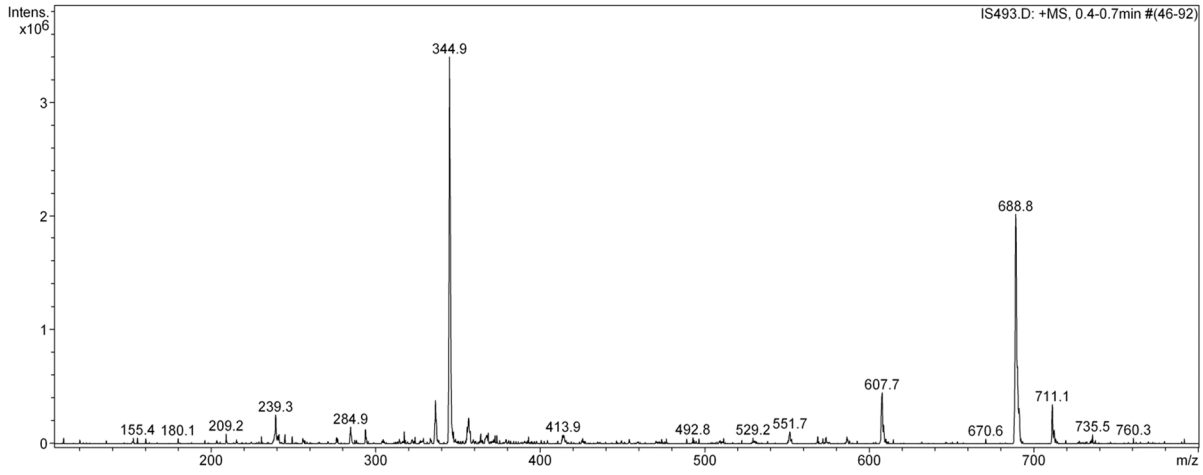

Figure 103: Mass spectrum of hexapeptide.

6.2.3 Graphs of Standard Curves

Aromatic Azide Content

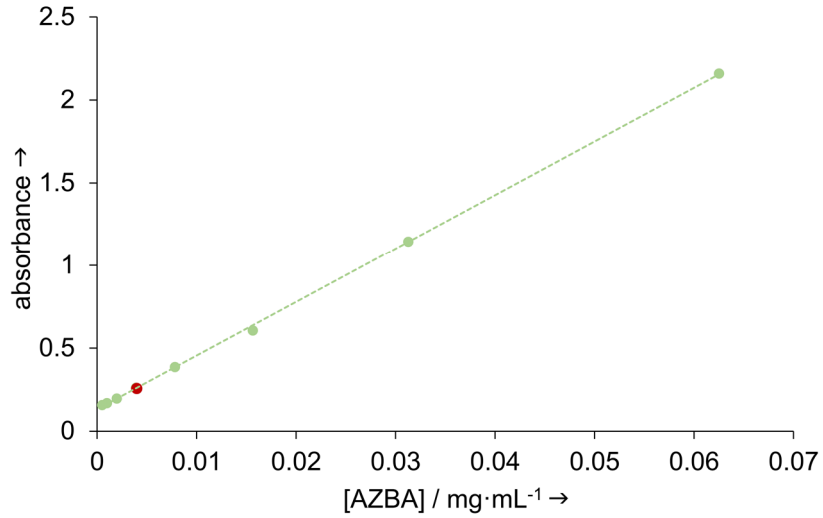

Figure 104: Standard curve (green line) of azidobenzoic acid **19** (green dots) and measured Dex-$(N_3)_9$ **20** sample at 280 nm to determine the amount of conjugated AZBA to the dextran backbone.

Ellman's Assay

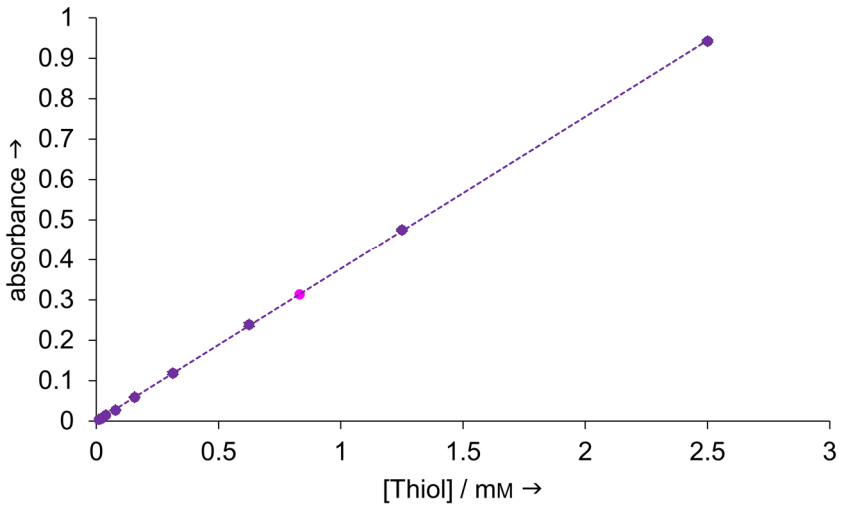

Figure 105: Standard curve (purple line) of acetyl cysteine (purple dots) and Dex-$(SH)_7$ **31** (pink dot) sample at 412 nm to determine the number of thiols per dextran backbone.

6.2.4 Esterase-like Activity of Pure Peptide

As described, the esterase-like activity of modified Cyt *c* compared to unmodified Cyt *c* was measured and it was possible to measure Michaelis-Menten kinetics for the system (**Figure 85**). For one substrate concentration (1.5 mM), the esterase-like activity of the pure peptide was measured in the same concentration as attached to the enzyme's surface (**Figure 106**). A higher esterase-like activity for the unconjugated peptide was observed which can be explained by a much higher diffusion of the small molecules in solution.

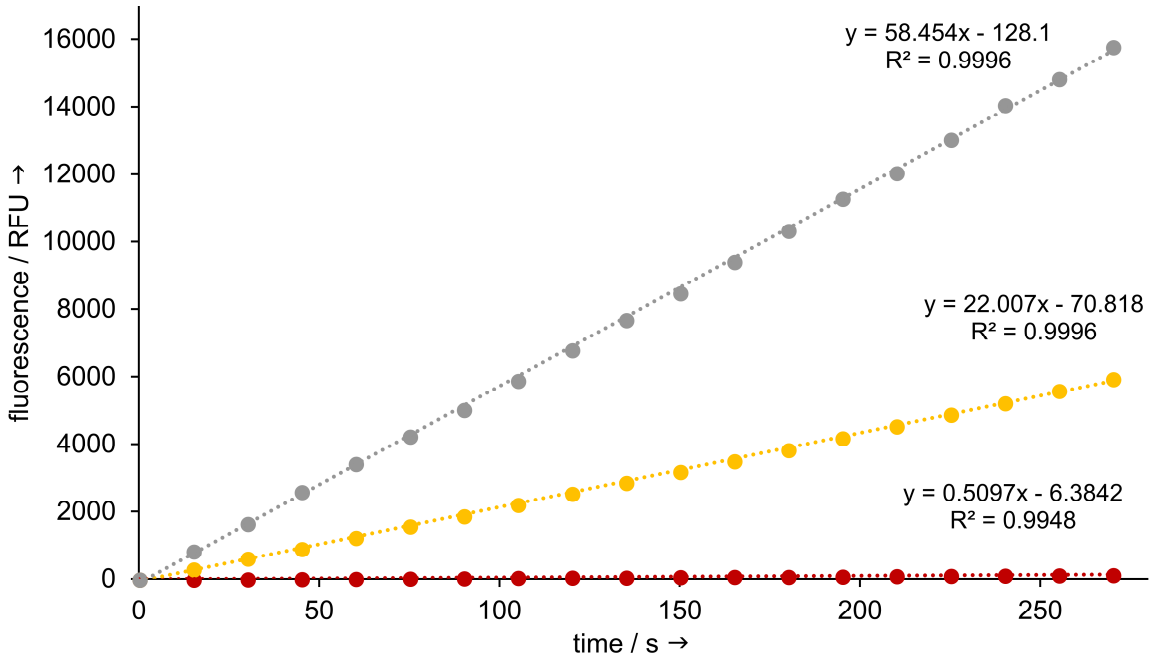

Figure 106: Comparison of esterase-like activity at one substrate concentration (1.5 mM) for unmodified Cyt *c* (dark red line), Cyt(CGGHHH)$_{14}$ (orange line) and pure peptide HHHGGC (grey line).

Literature

[1] J. M. Berg, J. L. Tymoczko, G. J. Gatto, L. Stryer, *Biochemistry*, Springer Spektrum, **2015**.
[2] J. S. Richardson, D. C. Richardson, N. B. Tweedy, K. M. Gernert, T. P. Quinn, M. H. Hecht, B. W. Erickson, Y. B. Yan, R. D. Mcclain, M. E. Donlan, M. C. Surles, *Biophys. J.* **1992**, *63*, 1186-1209.
[3] C. B. Anfinsen, *Science* **1973**, *181*, 223-230.
[4] R. L. Baldwin, G. D. Rose, *Trends Biochem. Sci.* **1999**, *24*, 26-33.
[5] C. Walsh, *Enzymatic reaction mechanisms*, WH Freeman, **1979**.
[6] O. H. Hashim, N. A. Adnan, *Biochem. Mol. Biol. Edu.* **1994**, *22*, 93-94.
[7] L. C. Blasiak, F. H. Vaillancourt, C. T. Walsh, C. L. Drennan, *Nature* **2006**, *440*, 368-371.
[8] C. K. Brown, K. Madauss, W. Lian, M. R. Beck, W. D. Tolbert, D. W. Rodgers, *PNAS* **2001**, *98*, 3127-3132.
[9] L. Pauling, *Nature* **1948**, *161*, 707-709.
[10] G. E. Lienhard, *Science* **1973**, *180*, 149-154.
[11] W. D. Riley, E. E. Snell, *Biochemistry* **1968**, *7*, 3520-3528.
[12] D. M. Quinn, *Chem. Rev.* **1987**, *87*, 955-979.
[13] M. W. Makinen, L. C. Kuo, J. J. Dymowski, S. Jaffer, *J. Biol. Chem.* **1979**, *254*, 356-366.
[14] H. Yan, M. D. Tsai, *Adv. Enzymol. Relat. Areas Mol. Biol.* **1999**, *73*, 103-134.
[15] E. C. Webb, C. o. E. I. U. o. Biochemistry, *Report of the Commission on Enzymes of the International Union of Biochemistry*, Elsevier, **1964**.
[16] H. Bisswanger, *Enzyme kinetics: principles and methods*, John Wiley & Sons, **2017**.
[17] L. Michaelis, M. Menten, *Biochem. Z.* **1913**, *49*, 333-369.
[18] L. Michaelis, M. L. Menten, K. A. Johnson, R. S. Goody, *Biochemistry* **2011**, *50*, 8264-8269.
[19] G. E. Briggs, J. B. S. Haldane, *Biochem. J.* **1925**, *19*, 338-339.
[20] S. J. Benkovic, S. Hammes-Schiffer, *Science* **2003**, *301*, 1196-1202.
[21] A. Zaks, D. R. Dodds, *Drug Discov. Today* **1997**, *2*, 513-531.
[22] A. J. Straathof, S. Panke, A. Schmid, *Curr. Opin. Biotechnol.* **2002**, *13*, 548-556.
[23] O. Kirk, T. V. Borchert, C. C. Fuglsang, *Curr. Opin. Biotechnol.* **2002**, *13*, 345-351.
[24] C. Kuraishi, K. Yamazaki, Y. Susa, *Food Reviews International* **2001**, *17*, 221-246.
[25] D. Aaslyng, E. Gormsen, H. Malmos, *J. Chem. Technol. Biotechnol.* **1991**, *50*, 321-330.
[26] N. Duran, M. Duran, *Color. Technol.* **2000**, *30*, 41-44.
[27] L. Pasteur, *Mémoire sur la fermentation applée lactique. Mémoire sur la fermentation alcoolique*, Mallet-Bachelier, **1857**.
[28] A. Schmid, J. S. Dordick, B. Hauer, A. Kiener, M. Wubbolts, B. Witholt, *Nature* **2001**, *409*, 258-268.
[29] M. Muller, *Angew. Chem. Int. Ed.* **2005**, *44*, 362-365.
[30] J. A. Tobert, *Nat. Rev. Drug Discov.* **2003**, *2*, 517-526.
[31] H. Stark, *Pharmazie in unserer Zeit* **2003**, *32*, 464-470.
[32] R. DiCosimo, J. McAuliffe, A. J. Poulose, G. Bohlmann, *Chem. Soc. Rev.* **2013**, *42*, 6437-6474.
[33] M. K. Bhat, S. Bhat, *Biotechnol. Adv.* **1997**, *15*, 583-620.
[34] A. Liese, L. Hilterhaus, *Chem. Soc. Rev.* **2013**, *42*, 6236-6249.
[35] Q. K. Beg, M. Kapoor, L. Mahajan, G. S. Hoondal, *Appl. Microbiol. Biotechnol.* **2001**, *56*, 326-338.
[36] S. B. Kent, *Chem. Soc. Rev.* **2009**, *38*, 338-351.
[37] B. L. Nilsson, M. B. Soellner, R. T. Raines, *Annu. Rev. Biophys. Biomol. Struct.* **2005**, *34*, 91-118.
[38] E. Kuah, S. Toh, J. Yee, Q. Ma, Z. Gao, *Chem. Eur. J.* **2016**, *22*, 8404-8430.
[39] X. Y. Wang, Y. H. Hu, H. Wei, *Inorg. Chem. Front.* **2016**, *3*, 41-60.
[40] H. Wei, E. Wang, *Chem. Soc. Rev.* **2013**, *42*, 6060-6093.
[41] N. A. Kotov, *Science* **2010**, *330*, 188-189.
[42] F. Manea, F. B. Houillon, L. Pasquato, P. Scrimin, *Angew. Chem. Int. Ed.* **2004**, *43*, 6165-6169.
[43] R. Salvio, A. Cincotti, *RSC Adv.* **2014**, *4*, 28678-28682.
[44] Y. Lin, J. Ren, X. Qu, *Adv. Mater.* **2014**, *26*, 4200-4217.

[45] M. Comotti, C. Della Pina, R. Matarrese, M. Rossi, *Angew. Chem. Int. Ed.* **2004**, *116*, 5936-5939.
[46] K. Qu, P. Shi, J. Ren, X. Qu, *Chem. Eur. J.* **2014**, *20*, 7501-7506.
[47] F. Natalio, R. Andre, A. F. Hartog, B. Stoll, K. P. Jochum, R. Wever, W. Tremel, *Nat. Nanotechnol.* **2012**, *7*, 530-535.
[48] L. Artiglia, S. Agnoli, M. C. Paganini, M. Cattelan, G. Granozzi, *ACS Appl. Mater. Inter.* **2014**, *6*, 20130-20136.
[49] H. Liang, F. Lin, Z. Zhang, B. Liu, S. Jiang, Q. Yuan, J. Liu, *ACS Appl. Mater. Inter.* **2017**, *9*, 1352-1360.
[50] L. Gao, J. Zhuang, L. Nie, J. Zhang, Y. Zhang, N. Gu, T. Wang, J. Feng, D. Yang, S. Perrett, X. Yan, *Nat. Nanotechnol.* **2007**, *2*, 577-583.
[51] L. Gao, K. Fan, X. Yan, *Theranostics* **2017**, *7*, 3207-3227.
[52] A. Hu, G. T. Yee, W. Lin, *J. Am. Chem. Soc.* **2005**, *127*, 12486-12487.
[53] K. Fan, C. Cao, Y. Pan, D. Lu, D. Yang, J. Feng, L. Song, M. Liang, X. Yan, *Nat. Nanotechnol.* **2012**, *7*, 459-464.
[54] I. M. Okhapkin, L. M. Bronstein, E. E. Makhaeva, V. G. Matveeva, E. M. Sulman, M. G. Sulman, A. R. Khokhlov, *Macromolecules* **2004**, *37*, 7879-7883.
[55] F. Menger, A. Eliseev, V. Migulin, *J. Org. Chem.* **1995**, *60*, 6666-6667.
[56] F. M. Menger, J. Ding, V. Barragan, *J. Org. Chem.* **1998**, *63*, 7578-7579.
[57] R. Skouta, S. Wei, R. Breslow, *J. Am. Chem. Soc.* **2009**, *131*, 15604-15605.
[58] E. Buhleier, W. Wehner, F. Vogtle, *Synthesis* **1978**, *1978*, 155-158.
[59] C. J. Hawker, J. M. J. Frechet, *J. Am. Chem. Soc.* **1990**, *112*, 7638-7647.
[60] H. Brunner, *J. Organomet. Chem.* **1995**, *500*, 39-46.
[61] L. Liu, R. Breslow, *J. Am. Chem. Soc.* **2003**, *125*, 12110-12111.
[62] T. Habicher, F. Diederich, V. Gramlich, *Helv. Chim. Acta* **1999**, *82*, 1066-1095.
[63] D. A. Tomalia, H. Baker, J. Dewald, M. Hall, G. Kallos, S. Martin, J. Roeck, J. Ryder, P. Smith, *Polym. J.* **1985**, *17*, 117-132.
[64] L. Wang, Y. Cui, S. Chen, G. Wang, D. Gao, Y. Liu, Q. Luo, Z. Liu, X. Zhang, *Mater. Sci. Eng., C* **2017**, *78*, 315-323.
[65] H. Wariishi, S.-i. Tsutsumi, T. Yamanaka, K. Uezu, M. Goto, S. Furusaki, H. Tanaka, in *Oxidative Delignification Chemistry, Vol. 785*, American Chemical Society, **2001**, pp. 226-234.
[66] L. A. Baker, L. Sun, R. M. Crooks, *Bull. Korean Chem. Soc.* **2002**, *23*, 647-654.
[67] A. Esposito, E. Delort, D. Lagnoux, F. Djojo, J. L. Reymond, *Angew. Chem. Int. Ed.* **2003**, *42*, 1381-1383.
[68] C. Douat-Casassus, T. Darbre, J.-L. Reymond, *J. Am. Chem. Soc.* **2004**, *126*, 7817-7826.
[69] T. Darbre, J. L. Reymond, *Acc. Chem. Res.* **2006**, *39*, 925-934.
[70] T. Darbre, J.-L. Reymond, *Chimica oggi/Chemistry today* **2007**, *25*, 25-27.
[71] S. Javor, J. L. Reymond, *Isr. J. Chem.* **2009**, *49*, 129-136.
[72] E. Delort, N.-Q. Nguyen-Trung, T. Darbre, J.-L. Reymond, *J. Org. Chem.* **2006**, *71*, 4468-4480.
[73] E. Delort, T. Darbre, J.-L. Reymond, *J. Am. Chem. Soc.* **2004**, *126*, 15642-15643.
[74] P. Sommer, V. S. Fluxa, T. Darbre, J. L. Reymond, *ChemBioChem* **2009**, *10*, 1527-1536.
[75] J. Kofoed, J. L. Reymond, *Curr. Opin. Biotechnol.* **2005**, *9*, 656-664.
[76] H. Gao, *Macromol. Rapid Commun.* **2012**, *33*, 722-734.
[77] M. Jikei, M.-a. Kakimoto, *Prog. Polym. Sci.* **2001**, *26*, 1233-1285.
[78] C. Gao, D. Yan, *Prog. Polym. Sci.* **2004**, *29*, 183-275.
[79] J. M. Ren, T. G. McKenzie, Q. Fu, E. H. H. Wong, J. Xu, Z. An, S. Shanmugam, T. P. Davis, C. Boyer, G. G. Qiao, *Chem. Rev.* **2016**, *116*, 6743-6836.
[80] B. Helms, S. J. Guillaudeu, Y. Xie, M. McMurdo, C. J. Hawker, J. M. J. Fréchet, *Angew. Chem. Int. Ed.* **2005**, *44*, 6384-6387.
[81] Y. Chi, S. T. Scroggins, J. M. J. Fréchet, *J. Am. Chem. Soc.* **2008**, *130*, 6322-6323.
[82] V. Rodionov, H. Gao, S. Scroggins, D. A. Unruh, A.-J. Avestro, J. M. J. Fréchet, *J. Am. Chem. Soc.* **2010**, *132*, 2570-2572.

[83] T. Terashima, M. Kamigaito, K.-Y. Baek, T. Ando, M. Sawamoto, *J. Am. Chem. Soc.* **2003**, *125*, 5288-5289.
[84] A. M. Hanlon, C. K. Lyon, E. B. Berda, *Macromolecules* **2016**, *49*, 2-14.
[85] H. Rothfuss, N. D. Knofel, P. W. Roesky, C. Barner-Kowollik, *J. Am. Chem. Soc.* **2018**, *140*, 5875-5881.
[86] J. Rubio-Cervilla, E. González, J. Pomposo, *Nanomaterials* **2017**, *7*, 341.
[87] J. He, L. Tremblay, S. Lacelle, Y. Zhao, *Soft Matter* **2011**, *7*, 2380-2386.
[88] E. Huerta, P. J. M. Stals, E. W. Meijer, A. R. A. Palmans, *Angew. Chem. Int. Ed.* **2013**, *52*, 2906-2910.
[89] Y. Liu, S. Pujals, P. J. M. Stals, T. Paulöhrl, S. I. Presolski, E. W. Meijer, L. Albertazzi, A. R. A. Palmans, *J. Am. Chem. Soc.* **2018**, *140*, 3423-3433.
[90] C. Tooley, S. Pazicni, E. Berda, *Polym. Chem.* **2015**, *6*, 7646-7651.
[91] S. Thanneeru, S. S. Duay, L. Jin, Y. Fu, A. M. Angeles-Boza, J. He, *ACS Macro Lett.* **2017**, *6*, 652-656.
[92] M. Raynal, P. Ballester, A. Vidal-Ferran, P. W. N. M. van Leeuwen, *Chem. Soc. Rev.* **2014**, *43*, 1734-1787.
[93] T. Wang, X. Fan, C. Hou, J. Liu, *Curr. Opin. Struc. Biol.* **2018**, *51*, 19-27.
[94] M. J. Wiester, P. A. Ulmann, C. A. Mirkin, *Angew. Chem. Int. Ed.* **2011**, *50*, 114-137.
[95] R. Breslow, *Acc. Chem. Res.* **1995**, *28*, 146-153.
[96] J. Meeuwissen, J. N. Reek, *Nat. Chem.* **2010**, *2*, 615.
[97] Z. Dong, Q. Luo, J. Liu, *Chem. Soc. Rev.* **2012**, *41*, 7890-7908.
[98] J. Zhou, H. Ritter, *Polym. Chem.* **2010**, *1*, 1552-1559.
[99] L. Marinescu, M. Bols, *Trends Glycosci. Glyc.* **2009**, *21*, 309-323.
[100] R. Villalonga, R. Cao, A. Fragoso, *Chem. Rev.* **2007**, *107*, 3088-3116.
[101] R. Breslow, S. D. Dong, *Chem. Rev.* **1998**, *98*, 1997-2012.
[102] R. Breslow, L. E. Overman, *J. Am. Chem. Soc.* **1970**, *92*, 1075-1077.
[103] R. Breslow, J. B. Doherty, G. Guillot, C. Lipsey, *J. Am. Chem. Soc.* **1978**, *100*, 3227-3229.
[104] R. Breslow, P. Campbell, *J. Am. Chem. Soc.* **1969**, *91*, 3085-3085.
[105] Y. H. Zhou, M. Zhao, Z. W. Mao, L. N. Ji, *Chem. Eur. J.* **2008**, *14*, 7193-7201.
[106] L. G. Marinescu, M. Bols, *Angew. Chem. Int. Ed.* **2006**, *45*, 4590-4593.
[107] L. Marinescu, M. Mølbach, C. Rousseau, M. Bols, *J. Am. Chem. Soc.* **2005**, *127*, 17578-17579.
[108] Z.-X. Zhang, X. Liu, F. J. Xu, X. J. Loh, E.-T. Kang, K.-G. Neoh, J. Li, *Macromolecules* **2008**, *41*, 5967-5970.
[109] S. Yu, Y. Yin, J. Zhu, X. Huang, Q. Luo, J. Xu, J. Shen, J. Liu, *Soft Matter* **2010**, *6*, 5342-5350.
[110] D. Fiedler, R. G. Bergman, K. N. Raymond, *Angewandte Chemie* **2004**, *116*, 6916-6919.
[111] Z. Liu, X. Sun, N. Nakayama-Ratchford, H. Dai, *ACS Nano* **2007**, *1*, 50-56.
[112] M. Ooe, M. Murata, T. Mizugaki, K. Ebitani, K. Kaneda, *J. Am. Chem. Soc.* **2004**, *126*, 1604-1605.
[113] A. J. Kirby, F. Hollfelder, *From enzyme models to model enzymes*, Royal Society of Chemistry, **2009**.
[114] D. W. Bruce, J. W. Steed, P. A. Gale, *Supramolecular Chemistry: From Molecules to Nanomaterials*, London: John Wiley & Sons, **2012**.
[115] L. J. Childs, J. Malina, B. E. Rolfsnes, M. Pascu, M. J. Prieto, M. J. Broome, P. M. Rodger, E. Sletten, V. Moreno, A. Rodger, *Chem. Eur. J.* **2006**, *12*, 4919-4927.
[116] A. Rioz-Martínez, J. Oelerich, N. Ségaud, G. Roelfes, *Angew. Chem. Int. Ed.* **2016**, *55*, 14136-14140.
[117] D. M. Kaphan, F. D. Toste, R. G. Bergman, K. N. Raymond, *J. Am. Chem. Soc.* **2015**, *137*, 9202-9205.
[118] K. Yan, M. Fujita, *Science* **2015**, *350*, 1165-1166.
[119] R. Mathieu, N. Hajime, Z. Xiaodong, *Curr. Protein Pept. Sc.* **2004**, *5*, 89-105.
[120] K. Lohmann, *Naturwissenschaften* **1928**, *16*, 298-298.
[121] N. V. C. College, *Vol. 2018*, Northern Virginia Community College, https://courses.lumenlearning.com/suny-fitness/chapter/muscle-fiber-contraction-and-relaxation/, **2018**.
[122] I. Rayment, *J. Biol. Chem.* **1996**, *271*, 15850-15853.

[123] D. L. Miller, F. Westheimer, *J. Am. Chem. Soc.* **1966**, *88*, 1507-1511.
[124] S. Benkovic, K. Schray, in *The Enzymes, Vol. 8*, Elsevier, **1973**, pp. 201-238.
[125] F. Ramirez, J. Marecek, *Pure Appl. Chem.* **1980**, *52*, 2213-2227.
[126] S. Meyerson, E. S. Kuhn, F. Ramirez, J. F. Marecek, *J. Am. Chem. Soc.* **1982**, *104*, 7231-7239.
[127] T. C. Bruice, S. J. Benkovic, *Bioorganic mechanisms*, WA Benjamin New York, **1966**.
[128] H. Sigel, *Metal Ions in Biological Systems, Vol. 15*, CRC press, **1983**.
[129] M. Tetas, J. M. Lowenstein, *Biochemistry* **1963**, *2*, 350-357.
[130] S. Suzuki, T. Higashiyama, A. Nakahara, *Bioinorganic chemistry* **1978**, *8*, 277-289.
[131] M. Hediger, R. M. Milburn, *J. Inorg. Biochem.* **1982**, *16*, 165-182.
[132] C. Nakai, W. Glinsmann, *Biochemistry* **1977**, *16*, 5636-5641.
[133] S. Suzuki, T. Higashiyama, A. Nakahara, *Bioorg. Chem.* **1973**, *2*, 145-154.
[134] B. Dietrich, M. W. Hosseini, J. M. Lehn, R. B. Sessions, *J. Am. Chem. Soc.* **1981**, *103*, 1282-1283.
[135] E. Kimura, M. Kodama, T. Yatsunami, *J. Am. Chem. Soc.* **1982**, *104*, 3182-3187.
[136] M. W. Hosseini, J.-M. Lehn, M. P. Mertes, *Helv. Chim. Acta* **1983**, *66*, 2454-2466.
[137] M. W. Hosseini, J. M. Lehn, L. Maggiora, K. B. Mertes, M. P. Mertes, *J. Am. Chem. Soc.* **1987**, *109*, 537-544.
[138] M. W. Hosseini, J. M. Lehn, *J. Am. Chem. Soc.* **1987**, *109*, 7047-7058.
[139] M. W. Hosseini, J. M. Lehn, K. C. Jones, K. E. Plute, K. B. Mertes, M. P. Mertes, *J. Am. Chem. Soc.* **1989**, *111*, 6330-6335.
[140] M. P. Mertes, K. B. Mertes, *Acc. Chem. Res.* **1990**, *23*, 413-418.
[141] A. Bencini, A. Bianchi, E. Garcia-Espana, E. C. Scott, L. Morales, B. Wang, T. Deffo, F. Takusagawa, M. P. Mertes, K. B. Mertes, *Bioorg. Chem.* **1992**, *20*, 8-29.
[142] M. W. Hosseini, A. J. Blacker, J. M. Lehn, *J. Am. Chem. Soc.* **1990**, *112*, 3896-3904.
[143] H. Fenniri, M. W. Hosseini, J. M. Lehn, *Helv. Chim. Acta* **1997**, *80*, 786-803.
[144] J. A. Aguilar, A. B. Descalzo, P. Díaz, V. Fusi, E. García-España, S. V. Luis, M. Micheloni, J. A. Ramírez, P. Romani, C. Soriano, *J. Chem. Soc., Perkin Trans. 2* **2000**, 1187-1192.
[145] R. Salvio, A. Casnati, L. Mandolini, F. Sansone, R. Ungaro, *Org. Biomol. Chem.* **2012**, *10*, 8941-8943.
[146] B. Frydman, A. V. Blokhin, S. Brummel, G. Wilding, Y. Maxuitenko, A. Sarkar, S. Bhattacharya, D. Church, V. K. Reddy, J. A. Kink, L. J. Marton, A. Valasinas, H. S. Basu, *J. Med. Chem.* **2003**, *46*, 4586-4600.
[147] K. Popaj, M. Hesse, *Helv. Chim. Acta* **2001**, *84*, 180-186.
[148] B. Frydman, S. Bhattacharya, A. Sarkar, K. Drandarov, S. Chesnov, A. Guggisberg, K. Popaj, S. Sergeyev, A. Yurdakul, M. Hesse, H. S. Basu, L. J. Marton, *J. Med. Chem.* **2004**, *47*, 1051-1059.
[149] M. G. Vander Heiden, L. C. Cantley, C. B. Thompson, *Science* **2009**, *324*, 1029-1033.
[150] S. Altenhofer, I. Witte, J. F. Teiber, P. Wilgenbus, A. Pautz, H. Li, A. Daiber, H. Witan, A. M. Clement, U. Forstermann, S. Horke, *J. Biol. Chem.* **2010**, *285*, 24398-24403.
[151] P. F. Hall, *J. Steroid Biochem. Mol. Biol.* **1991**, *40*, 527-532.
[152] K. Kirschner, A. N. Lane, A. W. M. Strasser, *Biochemistry* **1991**, *30*, 472-478.
[153] A. N. Lane, C. H. Paul, K. Kirschner, *EMBO J.* **1984**, *3*, 279-287.
[154] M. F. Dunn, D. Niks, H. Ngo, T. R. Barends, I. Schlichting, *Trends Biochem. Sci.* **2008**, *33*, 254-264.
[155] C. C. Hyde, S. A. Ahmed, E. A. Padlan, E. W. Miles, D. R. Davies, *J. Biol. Chem.* **1988**, *263*, 17857-17871.
[156] I. Wheeldon, S. D. Minteer, S. Banta, S. C. Barton, P. Atanassov, M. Sigman, *Nat. Chem.* **2016**, *8*, 299.
[157] B. K. Burgess, D. J. Lowe, *Chem. Rev.* **1996**, *96*, 2983-3012.
[158] V. K. Shah, G. Stacey, W. J. Brill, *J. Biol. Chem.* **1983**, *258*, 12064-12068.
[159] A. Witkowski, V. S. Rangan, Z. I. Randhawa, C. M. Amy, S. Smith, *Eur. J. Biochem.* **1991**, *198*, 571-579.
[160] J. K. Stoops, N. Singh, S. J. Wakil, *J. Biol. Chem.* **1990**, *265*, 16971-16977.
[161] N. Singh, S. J. Wakil, J. K. Stoops, *Biochemistry* **1985**, *24*, 6598-6602.
[162] I. B. Lomakin, Y. Xiong, T. A. Steitz, *Cell* **2007**, *129*, 319-332.

[163] P. Gipson, D. J. Mills, R. Wouts, M. Grininger, J. Vonck, W. Kuhlbrandt, *PNAS* **2010**, *107*, 9164-9169.
[164] D. N. Wilson, J. H. Doudna Cate, *Cold Spring Harb. Perspect. Biol.* **2012**, *4*, 1-17.
[165] L. Hoopes, *Nat. Edu.* **2008**, *1*, 160.
[166] J. A. Doudna, E. Charpentier, *Science* **2014**, *346*, 1258096.
[167] P. D. Hsu, E. S. Lander, F. Zhang, *Cell* **2014**, *157*, 1262-1278.
[168] R. Sorek, V. Kunin, P. Hugenholtz, *Nat. Rev. Microbiol.* **2008**, *6*, 181-186.
[169] M. Jinek, F. Jiang, D. W. Taylor, S. H. Sternberg, E. Kaya, E. Ma, C. Anders, M. Hauer, K. Zhou, S. Lin, M. Kaplan, A. T. Iavarone, E. Charpentier, E. Nogales, J. A. Doudna, *Science* **2014**, *343*, 1247997.
[170] E. Ricca, B. Brucher, J. H. Schrittwieser, *Adv. Synth. Catal.* **2011**, *353*, 2239-2262.
[171] L. F. Tietze, U. Beifuss, *Angew. Chem. Int. Ed.* **1993**, *32*, 131-163.
[172] T. Matsuda, R. Yamanaka, K. Nakamura, *Tetrahedron-Asymmetr.* **2009**, *20*, 513-557.
[173] C. K. Savile, J. M. Janey, E. C. Mundorff, J. C. Moore, S. Tam, W. R. Jarvis, J. C. Colbeck, A. Krebber, F. J. Fleitz, J. Brands, P. N. Devine, G. W. Huisman, G. J. Hughes, *Science* **2010**, *329*, 305-359.
[174] A. S. Bommarius, M. Schwarm, K. Drauz, *J. Mol. Catal. B: Enzym.* **1998**, *5*, 1-11.
[175] J. Ovadi, P. A. Srere, *Cell Biochem. Funct.* **1996**, *14*, 249-258.
[176] U. Hanefeld, L. Gardossi, E. Magner, *Chem. Soc. Rev.* **2009**, *38*, 453-468.
[177] F. Jia, B. Narasimhan, S. Mallapragada, *Biotechnol. Bioeng.* **2014**, *111*, 209-222.
[178] C. Mateo, J. M. Palomo, G. Fernandez-Lorente, J. M. Guisan, R. Fernandez-Lafuente, *Enzyme Microb. Tech.* **2007**, *40*, 1451-1463.
[179] K. Mosbach, B. Mattiasson, E. Hemmer, D. Holme, A. Lamvik, E. Sunde, N. A. Sørensen, *Acta Chem. Scand.* **1970**, *24*, 2093-2100.
[180] S. Schoffelen, J. C. M. van Hest, *Soft Matter* **2012**, *8*, 1736-1746.
[181] A. Grotzky, T. Nauser, H. Erdogan, A. D. Schluter, P. Walde, *J. Am. Chem. Soc.* **2012**, *134*, 11392-11395.
[182] A. Grotzky, Y. Manaka, T. Kojima, P. Walde, *Biomacromolecules* **2011**, *12*, 134-144.
[183] R. Childs, W. G. Bardsley, *Biochem. J.* **1975**, *145*, 93-103.
[184] L. Babich, A. F. Hartog, L. J. van Hemert, F. P. Rutjes, R. Wever, *ChemSusChem* **2012**, *5*, 2348-2353.
[185] K. Yang, N. S. Xu, W. W. Su, *J. Biotechnol.* **2010**, *148*, 119-127.
[186] Y. Zhang, F. Gao, S. P. Zhang, Z. G. Su, G. H. Ma, P. Wang, *Bioresour. Technol.* **2011**, *102*, 1837-1843.
[187] K. Hernandez, R. Fernandez-Lafuente, *Enzyme Microb. Tech.* **2011**, *48*, 107-122.
[188] Z. Liu, J. Zhang, X. Chen, P. G. Wang, *ChemBioChem* **2002**, *3*, 348-355.
[189] D. Wasserberg, J. Cabanas-Danes, J. Prangsma, S. O'Mahony, P. A. Cazade, E. Tromp, C. Blum, D. Thompson, J. Huskens, V. Subramaniam, P. Jonkheijm, *ACS Nano* **2017**, *11*, 9068-9083.
[190] I. Rootman, M. de Villiers, L. A. Brand, E. Strauss, *ChemCatChem* **2010**, *2*, 1239-1251.
[191] M. C. van Oers, F. P. Rutjes, J. C. van Hest, *Curr. Opin. Biotechnol.* **2014**, *28*, 10-16.
[192] L. Betancor, C. Berne, H. R. Luckarift, J. C. Spain, *Chem. Commun.* **2006**, 3640-3642.
[193] H. J. Choi, C. D. Montemagno, *Nano Lett.* **2005**, *5*, 2538-2542.
[194] D. P. Patterson, B. Schwarz, R. S. Waters, T. Gedeon, T. Douglas, *ACS Chem. Biol.* **2014**, *9*, 359-365.
[195] U. Roessl, J. Nahalka, B. Nidetzky, *Biotechnol. Lett.* **2010**, *32*, 341-350.
[196] R. Schoevaart, M. W. Wolbers, M. Golubovic, M. Ottens, A. P. Kieboom, F. van Rantwijk, L. A. van der Wielen, R. A. Sheldon, *Biotechnol. Bioeng.* **2004**, *87*, 754-762.
[197] R. A. Sheldon, *Org. Process Res. Dev.* **2011**, *15*, 213-223.
[198] L. T. Nguyen, K. L. Yang, *Enzyme Microb. Tech.* **2017**, *100*, 52-59.
[199] T. Farrugia, A. W. Perriman, K. P. Sharma, S. Mann, *Chem. Commun.* **2017**, *53*, 2094-2097.
[200] S. Fornera, P. Kuhn, D. Lombardi, A. D. Schlüter, P. S. Dittrich, P. Walde, *ChemPlusChem* **2012**, *77*, 98-101.
[201] A. Chmura, S. Rustler, M. Paravidino, F. van Rantwijk, A. Stolz, R. A. Sheldon, *Tetrahedron-Asymmetr.* **2013**, *24*, 1225-1232.

[202] R. A. Scism, B. O. Bachmann, *ChemBioChem* **2010**, *11*, 67-70.
[203] E. Basle, N. Joubert, M. Pucheault, *Chem. Biol.* **2010**, *17*, 213-227.
[204] N. S. Hatzakis, H. Engelkamp, K. Velonia, J. Hofkens, P. C. M. Christianen, A. Svendsen, S. A. Patkar, J. Vind, J. C. Maan, A. E. Rowan, R. J. M. Nolte, *Chem. Commun.* **2006**, 2012-2014.
[205] J. Xiao, T. J. Tolbert, *Organic letters* **2009**, *11*, 4144-4147.
[206] K. L. Heredia, G. N. Grover, L. Tao, H. D. Maynard, *Macromolecules* **2009**, *42*, 2360-2367.
[207] L. Bulow, K. Mosbach, *Trends Biotechnol.* **1991**, *9*, 226-231.
[208] C. Lindbladh, M. Rault, C. Hagglund, W. C. Small, K. Mosbach, L. Bulow, C. Evans, P. A. Srere, *Biochemistry* **1994**, *33*, 11692-11698.
[209] L. Iturrate, I. Sanchez-Moreno, I. Oroz-Guinea, J. Perez-Gil, E. Garcia-Junceda, *Chemistry* **2010**, *16*, 4018-4030.
[210] D. I. Colpa, N. Lončar, M. Schmidt, M. W. Fraaije, *ChemBioChem* **2017**, *18*, 2226-2230.
[211] R. Mehvar, *J. Control. Release* **2000**, *69*, 1-25.
[212] J. D. Paull, *Dev. Biol. Stand.* **1987**, *67*, 133-138.
[213] H. Otsuka, Y. Nagasaki, K. Kataoka, *Adv. Drug Delivery Rev.* **2012**, *64*, 246-255.
[214] D. Zaramella, P. Scrimin, L. J. Prins, *J. Am. Chem. Soc.* **2012**, *134*, 8396-8399.
[215] M. O. Guler, S. I. Stupp, *J. Am. Chem. Soc.* **2007**, *129*, 12082-12083.
[216] F. Schneider, *Angew. Chem. Int. Ed.* **1978**, *90*, 616-625.
[217] G. T. Hermanson, *Bioconjugate techniques*, Academic press, **2013**.
[218] Y. Méndez, J. Chang, A. R. Humpierre, A. Zanuy, R. Garrido, A. V. Vasco, J. Pedroso, D. Santana, L. M. Rodríguez, D. García-Rivera, Y. Valdés, V. Vérez-Bencomo, D. G. Rivera, *Chem. Sci.* **2018**, *9*, 2581-2588.
[219] S. Kalkhof, A. Sinz, *Anal. Biolanal. Chem.* **2008**, *392*, 305-312.
[220] V. R. Pattabiraman, J. W. Bode, *Nature* **2011**, *480*, 471-479.
[221] E. M. Sletten, C. R. Bertozzi, *Angew. Chem. Int. Ed.* **2009**, *48*, 6974-6998.
[222] C. R. Bertozzi, *Acc. Chem. Res.* **2011**, *44*, 651-673.
[223] J. C. Jewett, C. R. Bertozzi, *Chem. Soc. Rev.* **2010**, *39*, 1272-1279.
[224] E. M. Sletten, C. R. Bertozzi, *Acc. Chem. Res.* **2011**, *44*, 666-676.
[225] A. F. Trindade, R. F. Frade, E. M. Macoas, C. Graca, C. A. Rodrigues, J. M. Martinho, C. A. Afonso, *Org. Biomol. Chem.* **2014**, *12*, 3181-3190.
[226] D. G. Smyth, O. O. Blumenfeld, W. Konigsberg, *Biochem. J.* **1964**, *91*, 589-595.
[227] C. F. Brewer, J. P. Riehm, *Anal. Biochem.* **1967**, *18*, 248-255.
[228] G. Thumshirn, U. Hersel, S. L. Goodman, H. Kessler, *Chem. Eur. J.* **2003**, *9*, 2717-2725.
[229] M. Colombo, A. Bianchi, *Molecules* **2010**, *15*, 178-197.
[230] A. Dirksen, T. M. Hackeng, P. E. Dawson, *Angew. Chem. Int. Ed.* **2006**, *45*, 7581-7584.
[231] J. J. Kohler, *ChemBioChem* **2009**, *10*, 2147-2150.
[232] E. H. Lempens, B. A. Helms, M. Merkx, E. Meijer, *ChemBioChem* **2009**, *10*, 658-662.
[233] M. W. Hosseini, J. M. Lehn, L. Maggiora, K. B. Mertes, M. P. Mertes, *J. Am. Chem. Soc.* **1987**, *109*, 537-544.
[234] I. Schmid, Johannes Gutenberg-University Mainz, **2013**.
[235] A. Bencini, M. I. Burguete, E. Garcia-Espana, S. V. Luis, J. F. Miravet, C. Soriano, *J. Org. Chem.* **1993**, *58*, 4749-4753.
[236] C. A. Ilioudis, J. W. Steed, *Org. Biomol. Chem.* **2005**, *3*, 2935-2945.
[237] H. Schumann, U. A. Bottgef, K. Zietzke, H. Hemling, G. Kociok-Kohn, J. Pickardt, F. Ekkehardt Hahnb, A. Zschunke, B. Schiefnef, H. Gries, B. Radiichel, J. Platzeke, *Chem. Ber.* **1997**, *130*, 267-277.
[238] R. S. Macomber, *A complete introduction to modern NMR spectroscopy*, Wiley New York, **1998**.
[239] J. Stothers, *Carbon-13 NMR Spectroscopy: Organic Chemistry, A Series of Monographs, Vol. 24*, Elsevier, **2012**.
[240] H.-O. Kalinowski, S. Berger, S. Braun, *Carbon-13 NMR spectroscopy*, **1988**.
[241] P. G. Wuts, T. W. Greene, *Greene's protective groups in organic synthesis*, John Wiley & Sons, **2006**.
[242] C. Jiang, L. Yang, W. T. Wu, Q. L. Guo, Q. D. You, *Biorg. Med. Chem.* **2011**, *19*, 5612-5627.
[243] R. Erez, D. Shabat, *Org. Biomol. Chem.* **2008**, *6*, 2669-2672.

[244] K. G. E. Fanghänel, H. Schmidt, P. Metz, *Organikum*, Wiley-VCH, **2001**.
[245] M. W. Easson, F. R. Fronczek, T. J. Jensen, M. G. Vicente, *Biorg. Med. Chem.* **2008**, *16*, 3191-3208.
[246] K. D. Karlin, M. S. Nasir, B. I. Cohen, R. W. Cruse, S. Kaderli, A. D. Zuberbuehler, *J. Am. Chem. Soc.* **1994**, *116*, 1324-1336.
[247] B. P. Morgan, A. Muci, P. P. Lu, X. Qian, T. Tochimoto, W. W. Smith, M. Garard, E. Kraynack, S. Collibee, I. Suehiro, A. Tomasi, S. C. Valdez, W. Wang, H. Jiang, J. Hartman, H. M. Rodriguez, R. Kawas, S. Sylvester, K. A. Elias, G. Godinez, K. Lee, R. Anderson, S. Sueoka, D. Xu, Z. Wang, N. Djordjevic, F. I. Malik, D. J. Morgans, Jr., *ACS Med. Chem. Lett.* **2010**, *1*, 472-477.
[248] R. S. Compagnone, H. Rapoport, *J. Org. Chem.* **1986**, *51*, 1713-1719.
[249] R. P. Temming, L. Eggermont, M. B. van Eldijk, J. C. van Hest, F. L. van Delft, *Org. Biomol. Chem.* **2013**, *11*, 2772-2779.
[250] D. Arora, N. Sharma, V. Sharma, V. Abrol, R. Shankar, S. Jaglan, *Appl. Microbiol. Biotechnol.* **2016**, *100*, 2603-2015.
[251] L. Pasteur, *Bull. Soc. Chim. Paris* **1861**, *11*, 30-31.
[252] P. Van Tieghem, *Ann. Sci. Nat. Bot. Biol. Veg* **1878**, *7*, 180-203.
[253] A. Jeanes, W. C. Haynes, C. Wilham, J. C. Rankin, E. Melvin, M. J. Austin, J. Cluskey, B. Fisher, H. Tsuchiya, C. Rist, *J. Am. Chem. Soc.* **1954**, *76*, 5041-5052.
[254] L.-O. Lamke, S.-O. Liljedahl, *Resuscitation* **1976**, *5*, 93-101.
[255] M. Yalpani, *Polysaccharides: syntheses, modifications and structure/property relations, Vol. 36*, Elsevier, **2013**.
[256] V. T. Bhat, N. R. James, A. Jayakrishnan, *Polym. Int.* **2008**, *57*, 124-132.
[257] A. Jeanes, C. A. Wilham, *J. Am. Chem. Soc.* **1950**, *72*, 2655-2657.
[258] J. C. Rankin, A. Jeanes, *J. Am. Chem. Soc.* **1954**, *76*, 4435-4441.
[259] J. L. Cohen, S. Schubert, P. R. Wich, L. Cui, J. A. Cohen, J. L. Mynar, J. M. Frechet, *Bioconjugate Chem.* **2011**, *22*, 1056-1065.
[260] A. N. Lukyanov, R. M. Sawant, W. C. Hartner, V. P. Torchilin, *J. Biomater. Sci., Polym. Ed.* **2004**, *15*, 621-630.
[261] J. M. Harris, *Poly (ethylene glycol) chemistry: biotechnical and biomedical applications*, Springer Science & Business Media, **2013**.
[262] R. Gref, M. Lück, P. Quellec, M. Marchand, E. Dellacherie, S. Harnisch, T. Blunk, R. Müller, *Colloids Surf., A* **2000**, *18*, 301-313.
[263] P. Calvo, B. Gouritin, H. Chacun, D. Desmaele, J. D'Angelo, J. P. Noel, D. Georgin, E. Fattal, J. P. Andreux, P. Couvreur, *Pharm. Res.* **2001**, *18*, 1157-1166.
[264] T. L. Schlick, Z. Ding, E. W. Kovacs, M. B. Francis, *J. Am. Chem. Soc.* **2005**, *127*, 3718-3723.
[265] O. Mitsunobu, M. Yamada, T. Mukaiyama, *Bull. Chem. Soc. Jpn.* **1967**, *40*, 935-939.
[266] G. H. Lathe, Ruthven, C.R.J., *Biochem. J.* **1955**, *62*, 665-674.
[267] J. C. Moore, *J. Polym. Sci., Part A: Polym. Chem.* **1964**, *2*, 835-843.
[268] H. Sawada, N. Shimura, F. Hosokawa, N. Shibata, Y. Ikuhara, *Microscopy* **2015**, *64*, 213-217.
[269] Q. Huang, B. Yang, H. Liu, Y. Zhao, J. Du, *Polym. Chem.* **2015**, *6*, 886-890.
[270] C. Hiemstra, L. J. Aa, Z. Zhong, P. J. Dijkstra, J. Feijen, *Biomacromolecules* **2007**, *8*, 1548-1556.
[271] J. C. Ramirez, M. Sanchezchaves, F. Arranz, *Angew. Makromol. Chem.* **1995**, *225*, 123-130.
[272] A. M. Striegel, *Carbohydr. Polym.* **1997**, *34*, 267-274.
[273] J. Sedlak, R. H. Lindsay, *Anal. Biochem.* **1968**, *25*, 192-205.
[274] A. Borrmann, S. Milles, T. Plass, J. Dommerholt, J. M. Verkade, M. Wiessler, C. Schultz, J. C. van Hest, F. L. van Delft, E. A. Lemke, *ChemBioChem* **2012**, *13*, 2094-2099.
[275] M. B. van Eldijk, F. C. Smits, N. Vermue, M. F. Debets, S. Schoffelen, J. C. van Hest, *Biomacromolecules* **2014**, *15*, 2751-2759.
[276] E. Oude Blenke, G. Klaasse, H. Merten, A. Pluckthun, E. Mastrobattista, N. I. Martin, *J. Control. Release* **2015**, *202*, 14-20.
[277] T. Mosmann, *J. Immunol. Methods* **1983**, *65*, 55-63.
[278] D. G. Gorenstein, *Phosphorous-31 NMR: Principles and applications*, Academic Press, **2012**.

[279] C. Bazzicalupi, A. Bianchi, C. Giorgi, M. Savastano, F. Morales-Lara, *Chem. Commun.* **2015**, *51*, 3907-3910.
[280] E. A. Barnard, W. D. Stein, in *Adv. Enzymol. Relat. Areas Mol. Biol.*, John Wiley & Sons, Inc., **2006**, pp. 51-110.
[281] L. Pasquato, F. Rancan, P. Scrimin, F. Mancin, C. Frigeri, *Chem. Commun.* **2000**, 2253-2254.
[282] P. Pengo, S. Polizzi, L. Pasquato, P. Scrimin, *J. Am. Chem. Soc.* **2005**, *127*, 1616-1617.
[283] N. Singh, M. P. Conte, R. V. Ulijn, J. F. Miravet, B. Escuder, *Chem. Commun.* **2015**, *51*, 13213-13216.
[284] M. C. Cleij, W. Drenth, R. J. M. Nolte, *J. Org. Chem.* **1991**, *56*, 3883-3891.
[285] D. J. Bell, H. Gutfreund, B. S. Hartley, C. Rimington, *Annu. Rep. Prog. Chem.* **1954**, *51*, 295-334.
[286] E. Anslyn, R. Breslow, *J. Am. Chem. Soc.* **1989**, *111*, 5972-5973.
[287] F. Schneider, *Angew. Chem. Int. Ed.* **1978**, *17*, 583-592.
[288] D. J. Mikolajczak, J. L. Heier, B. Schade, B. Koksch, *Biomacromolecules* **2017**, *18*, 3557-3562.
[289] M. P. Barnes, W. C. Shen, *Int. J. Pharm.* **2009**, *369*, 79-84.
[290] G. T. Hermanson, in *Bioconjugate Techniques (Third edition)*, Academic Press, Boston, **2013**, pp. 127-228.
[291] G. W. Bushnell, G. V. Louie, G. D. Brayer, *J. Mol. Biol.* **1990**, *214*, 585-595.
[292] Y. P. Myer, A. F. Saturno, B. C. Verma, A. Pande, *J. Biol. Chem.* **1979**, *254*, 11202-11207.
[293] R. Vazquez-Duhalt, *J. Mol. Catal. B: Enzym.* **1999**, *7*, 241-249.
[294] S. Yoshitake, Y. Yamada, E. Ishikawa, R. Masseyeff, *Eur. J. Biochem.* **1979**, *101*, 395-399.
[295] J. A. Burns, J. C. Butler, J. Moran, G. M. Whitesides, *J. Org. Chem.* **1991**, *56*, 2648-2650.
[296] M. Henkel, N. Rockendorf, A. Frey, *Bioconjugate Chem.* **2016**, *27*, 2260-2265.
[297] U. K. Laemmli, *Nature* **1970**, *227*, 680-685.
[298] F. Hillenkamp, M. Karas, R. C. Beavis, B. T. Chait, *Anal. Chem.* **1991**, *63*, 1193-1203.
[299] A. F. Habeeb, *Anal. Biochem.* **1966**, *14*, 328-336.
[300] R. B. Sashidhar, A. K. Capoor, D. Ramana, *J. Immunol. Methods* **1994**, *167*, 121-127.
[301] B. Lorber, F. Fischer, M. Bailly, H. Roy, D. Kern, *Biochem. Mol. Biol. Edu.* **2012**, *40*, 372-382.
[302] F. Marken, C. A. Paddon, D. Asogan, *Electrochem. Commun.* **2002**, *4*, 62-66.
[303] G. Wang, J.-J. Xu, H.-Y. Chen, *Electrochem. Commun.* **2002**, *4*, 506-509.
[304] N. J. Greenfield, *Nat. Protoc.* **2006**, *1*, 2876-2890.
[305] G. Holzwarth, P. Doty, *J. Am. Chem. Soc.* **1965**, *87*, 218-228.
[306] L. Whitmore, B. A. Wallace, *Nucleic Acids Res.* **2004**, *32*, 668-673.
[307] L. Whitmore, B. A. Wallace, *Biopolymers* **2008**, *89*, 392-400.
[308] N. Sreerama, R. W. Woody, *Anal. Biochem.* **2000**, *287*, 252-260.
[309] W. R. Fisher, H. Taniuchi, C. B. Anfinsen, *J. Biol. Chem.* **1973**, *248*, 3188-3195.
[310] I. S. Isaac, J. H. Dawson, *Essays Biochem.* **1999**, *34*, 51-69.
[311] N. H. Kim, M. S. Jeong, S. Y. Choi, J. H. Kang, *Bull. Korean Chem. Soc.* **2004**, *25*, 1889-1892.
[312] D. A. S. Grahame, B. C. Bryksa, R. Y. Yada, in *Improving and Tailoring Enzymes for Food Quality and Functionality*, Woodhead Publishing, **2015**, pp. 11-55.
[313] I. M. Roberts, *Lipids* **1985**, *20*, 243-247.
[314] M. Vaneechoutte, G. Verschraegen, G. Claeys, P. Flamen, *J. Clin. Microbiol.* **1988**, *26*, 1227-1228.
[315] M. S. Izquierdo, R. J. Henderson, *Fish Physiol. Biochem.* **1998**, *19*, 153-162.
[316] G. Gulseren, M. A. Khalily, A. B. Tekinay, M. O. Guler, *J. Mater. Chem.* **2016**, *4*, 4605-4611.
[317] B. Paital, *Biomed. Res. Int.* **2014**, 1-8.
[318] G. G. Guilbault, P. J. Brignac, M. Zimmer, *Anal. Chem.* **1968**, *40*, 190-196.
[319] H. Corrodi, B. Werdinius, *Acta Chem. Scand.* **1965**, *19*, 1854-1858.
[320] L. Callewaert, C. W. Michiels, *J. Biosci.* **2010**, *35*, 127-160.
[321] H. Stapelfeldt, C. E. Olsen, L. H. Skibsted, *J. Agric. Food. Chem.* **1999**, *47*, 3986-3990.
[322] S. G. Hambling, A. McAlpine, L. Sawyer, *Adv. Dairy Chem.* **1992**, *1*, 141-190.
[323] A. Fiocchi, J. Brozek, H. Schünemann, S. L. Bahna, A. von Berg, K. Beyer, M. Bozzola, J. Bradsher, E. Compalati, M. Ebisawa, *W. All. Org. J.* **2010**, *3*, 57-161.
[324] G. A. Kimmich, J. Randles, J. S. Brand, *Anal. Biochem.* **1975**, *69*, 187-206.
[325] H. E. Gottlieb, V. Kotlyar, A. Nudelman, *J. Org. Chem.* **1997**, *62*, 7512-7515.

[326] A. D. Duong, S. Sharma, K. J. Peine, G. Gupta, A. R. Satoskar, E. M. Bachelder, B. E. Wyslouzil, K. M. Ainslie, *Mol. Pharm.* **2013**, *10*, 1045-1055.
[327] A. K. Covington, M. Paabo, R. A. Robinson, R. G. Bates, *Anal. Chem.* **1968**, *40*, 700-706.
[328] P. Ahlers, H. Frisch, P. Besenius, *Polym. Chem.* **2015**, *6*, 7245-7250.
[329] Y. F. Zhang, Q. Wang, H. Hess, *ACS Catal.* **2017**, *7*, 2047-2051.

Curriculum Vitae

List of Publications

Scientific Papers

Schmid, I., Scherger, M., Wich, P.R., "Modification of Cytochrome *c* with Catalytically Active Peptides for Dual Enzymatic Functionality", *ChemCatChem*, **2018**, *submitted.*

Schmid, I., Mackiol, T., Lantzberg, B., Wich, P.R., "Artificial ATPase based on a dextran bioconjugate", *Bioconjugate Chem,* **2018**, *in preparation.*

Breitenbach, B., **Schmid, I.**, Wich, P.R., "Amphiphilic polysaccharide block copolymers for pH- responsive micellar nanoparticles", *Biomacromolecules*, **2017**, *18* (9), 2839-2848.

Previti, S., Ettari, R., Cosconati, S., Amendola, G., Chouchene, K., Wagner, A., Hellmich, U. A., Ulrich, K., Krauth-Siegel, L. R., **Schmid, I.**, Wich, P. R., Schirmeister, T., Gut, J., Rosenthal, P. J., Grasso, S., Zappalà, M., "Development of Novel Peptide-Based Michael Acceptors Targeting Rhodesain and Falcipain-2 for the Treatment of Neglected Tropical Diseases (NTDs)", *Journal of Medicinal Chemistry*, **2017**, *60*, 6911-6923.

Editorial Contributions

Schmid, I., Radi, L.: Auf dem Sprung zum Apotheker, Pharmazeutische Zeitung (2016), Nr. 17, S.40.

Schmid, I., Radi, L.: Feierliche Zeugnisübergabe, Pharmazeutische Zeitung (2016), Nr. 45, S.50.

Books

Assistance in: T. Schirmeister, C. Schmuck, P. R. Wich (Hg.), Organische Chemie, Beyer/Walter, *Hirzel Verlag*, 2015, 25th edition, entirely new edited